

Understanding Invasions — From the Genetic Basis to the
Ecological Dynamics of Spreading Populations

Dissertation

zur

**Erlangung der naturwissenschaftlichen Doktorwürde
(Dr. sc. nat.)**

vorgelegt der

Mathematisch-naturwissenschaftlichen Fakultät

der

Universität Zürich

von

Felix Elke Moerman

aus

Belgien

Promotionskommission

Prof. Dr. Florian Altermatt (Leitung der Dissertation, Vorsitz)

Prof. Dr. Andreas Wagner

Dr. Emanuel A. Fronhofer

Prof. Dr. Rolf Kümmerli

Prof. Dr. Hanna Kokko

Zürich, 2021

Abstract

Human activities are increasingly disrupting the spatial distribution of species, either by introducing species in new regions (invasions) or by forcing them to actively move due to changing climate conditions (range shifts and expansions). Whereas the ecological impacts of invasions and range shifts have been studied for some time, it is only more recently that biologists have started investigating the evolutionary forces that act during range expansions. Empirical and experimental studies in the last two decades have demonstrated that selection during range expansions leads to rapid evolution of dispersal behaviour, life-history traits, and adaptation to the local environment. Experimental studies have proven to be an especially powerful approach to investigate range expansion, because they allow a careful control of experimental conditions, as well as to distinguish clearly which evolutionary changes are due to selection and which are due to genetic drift. In this thesis, I investigated how the presence of new environments (abiotic or biotic), different reproductive modes, and the magnitude of gene flow affect the evolution of populations during range expansions, using a series of experiments with the protist model species *Tetrahymena thermophila*.

In a first experiment (**Chapter 1**), I investigated how populations in a range core adapt to a new abiotic stressor (pH-stress), by subjecting several different clonal populations of *T. thermophila* to high population densities in the presence or absence of

pH-stress. I found that a combination of pH-stress and high population densities led to a maximization of density-dependent population growth under the density conditions experienced during evolution. This maximization of density-dependent growth resulted in a convergence of life-history strategy between all clonal populations.

In a second collaborative project (**Chapter 2**), I investigated co-evolution between populations of the predator *T. thermophila* and seven of its bacterial prey species. Here, I found that evolution of the prey species resulted in an average decrease of predator growth. However, predator evolution also led to a shift in behavioural and morphological traits of the predator. Co-evolved predators were on average larger, and swam faster and in straighter trajectories. These evolutionary changes of the predator are likely adaptations that help capturing and ingesting prey.

In the third experiment (**Chapter 3**), I investigated whether gene swamping alters evolution of *T. thermophila* during experimental range expansions. To do so, I controlled the presence/absence of a pH-gradient during range expansion, reproductive mode (asexual/sexual), and gene flow from the range core to the range edge. I found that gene swamping does indeed limit adaptation during range expansion. However, contrary to theoretical predictions, I observed a gene swamping effect both in the presence and in the absence of a pH-gradient. The presence of a gene swamping effect in the absence of a pH-gradient likely stems from the evolution of life-history traits during range expansion.

Lastly, in **Chapter 4**, I investigated the genetic basis of adaptations during range expansion. I sequenced the genome of evolved populations from the third experiment, and investigated how the presence/absence of a pH-gradient, the reproductive mode, and gene flow alter the speed of genetic evolution during range expansion. Additionally, I identified genes that were under selection in general during range expansions, and

genes that were under selection due to the presence of a pH-gradient. I found that sexual reproduction increased the number of *de novo* mutations that rose to a measurable frequency. The number of variants that changed in allele frequency from standing genetic variation, in contrast, depended on the mode of reproduction as well as on gene flow and on the presence of a pH-gradient. I found that evolution during range expansions led to selection on genes coding for membrane proteins, as well as on genes linked to cell division and DNA repair. The presence of a pH-gradient led to selection on genes associated with ion transport and ion binding, as well as on oxidoreductase reactions.

Finally, I conclude this thesis with a brief discussion on the overarching results of the four chapters, as well as potential avenues for future research. I discuss the need for explicitly integrating life-history conditions in eco-evolutionary studies of range expansion dynamics, how pushed and pulled wave dynamics may alter predictions for gene swamping, the importance of biotic interactions during range expansions, and the need for more integrated and diverse genetic approaches for studying range expansions.

Preface

This thesis is composed from original research conducted by the author and in collaboration with the listed co-authors in each chapter. The contributions of all authors, as well as technical assistance by technicians, are described and acknowledged at the end of each chapter.

A version of Chapter 1 was published in the journal *Evolution* as

F. Moerman, A. Arquint, S. Merkli, A. Wagner, F. Altermatt, and E. A. Fronhofer, “Evolution under pH stress and high population densities leads to increased density-dependent fitness in the protist *Tetrahymena thermophila*,” *Evolution*, vol. 74, no. 3, pp. 573–586, 2020, doi: 10.1111/evo.13921.

The manuscript was reformatted for Chapter 1 and minor typographic errors were corrected. The appropriate license (number 4939020498970) has been acquired from John Wiley and Sons to reproduce the publication in this thesis.

A version of Chapter 2 was published in the journal *Proceedings of the Royal Society B: Biological Sciences* as

J. Cairns, F. Moerman, E. A. Fronhofer, F. Altermatt, and T. Hiltunen, “Evolution in interacting species alters predator life-history traits, behaviour and morphology in experimental microbial communities,” *Proc. R. Soc. B-Biol. Sci.*, vol. 287, no. 1928, p. 20200652, Jun. 2020, doi: 10.1098/rspb.2020.0652.

The manuscript was reformatted for Chapter 2 and minor typographic errors were corrected. Permission has been acquired from Royal Society Publishing to reproduce the publication in this thesis.

A version of Chapter 3 was published in the journal *Biology Letters* as

F. Moerman, E. A. Fronhofer, A. Wagner, and F. Altermatt, “Gene swamping alters evolution during range expansions in the protist *Tetrahymena thermophila*,” *Biol. Lett.*, vol. 16, no. 6, p. 20200244, Jun. 2020, doi: 10.1098/rsbl.2020.0244.

The manuscript was reformatted for Chapter 3 and minor typographic errors were corrected. Permission has been acquired from Royal Society Publishing to reproduce the publication in this thesis.

Chapter 4 is in preparation for publication, with submission foreseen by the end of 2020. The tentative record for the manuscript in preparation is:

F. Moerman, E. A. Fronhofer, F. Altermatt and A. Wagner, “Selection on growth rate and local adaptation drive genetic adaptation during range expansions in the protist *Tetrahymena thermophila*,” *In prep.*

Contents

Abstract	2
Preface	5
Contents	7
Introduction	15
General introduction	15
Range shifts and invasions in the Anthropocene	15
Evolution during range expansions	18
Box 1: Cane toads in Australia — the poster child of invasive species	19
Gene swamping and the role of sex during range expansions	23
Box 2: Invasion in European catchments — the spread of the Killer Shrimp	25
<i>Tetrahymena thermophila</i> as a model system for studying range expan- sions	26
Structure of the PhD thesis	29
Objectives	29
Thesis outline	29

Chapter 1: Evolution under pH stress and high population densities leads to increased density-dependent fitness in the protist <i>Tetrahymena thermophila</i>	33
Abstract	33
Introduction	34
Material and methods	38
Experiment	38
Statistical analyses	42
Results	46
Evolution of life-history traits	47
Variation and covariation in r_0 and α	50
Density-dependent fitness	54
Discussion	56
Author contributions	61
Acknowledgements	61
Data accessibility statement	61
 Chapter 2: Evolution in interacting species alters predator life-history traits, behaviour and morphology in experimental microbial communities	 62
Abstract	62
Introduction	63
Material and Methods	66
Strains and culture conditions	66
Predator-prey evolutionary experiment	69
Sample collection and preparation	70
Physiological measurements	71

Bacterial density measurements	72
Ciliate density and trait measurements	72
Data analysis	73
Results	76
Discussion	83
Author contributions	87
Acknowledgements	87
Data accessibility statement	87

Chapter 3: Gene swamping alters evolution during range expansions in the protist *Tetrahymena thermophila* 88

Abstract	88
Introduction	89
Material and methods	91
Study organism	91
Experiment	92
Beverton-Holt model fitting	95
Statistical analyses	96
Results	97
Discussion	100
Author contributions	103
Acknowledgements	103
Data accessibility statement	103

Chapter 4: Selection on growth rate and local adaptation drive genetic adaptation during range expansions in the protist *Tetrahymena thermophila* 104

Abstract	104
Introduction	105
Material and methods	109
Study organism and experimental populations	109
Experimental evolution	111
Common garden and growth assessment	113
Sequencing and identification of variants	115
Statistical analyses	122
Results	128
Gene swamping alters fitness changes	128
Reproduction and gene flow alter allele frequency change.	132
Frequencies of <i>de novo</i> mutations change most strongly in sexually re- producing populations.	138
Genes involved in adaptive evolution through allele frequency changes.	141
Changes in standing variation associated with general adaptation in- volve transmembrane proteins and kinase domains.	142
Gradient-specific changes in allele frequency are associated with ion balance.	143
General adaptation preferentially affects genes involved in DNA repair and gene expression.	144
Discussion	146
The role of sexual recombination on genetic changes during range ex- pansions	146
Genes under selection during range expansions	149
Limitations and concluding remarks	151

Acknowledgements	152
Data availability statement	153
Author contributions	153
Discussion and conclusions	154
Summary of the main results	154
Integrating demographic conditions and life-history strategy in eco-evolutionary research	156
Biotic interactions may strongly affect success of invaders	158
Gene swamping: natural occurrences and the influence of pushed versus pulled waves	160
Towards an integrative view of molecular adaptation in expanding populations	162
Towards an integrative view of molecular adaptation in expanding populations	162
Concluding remarks	164
Acknowledgements	166
Bibliography	168
Curriculum Vitae	207
Publication list	210
S.1 Supplementary Material of Chapter 1	212
Supplementary Material of Chapter 1	212
S.1.1 Relationship between HCl and pH	212
S.1.2 PCA plot showing genotype differences	214

S.1.3 Video analysis script	215
S.1.4 Model priors for fitting Bayesian evolution models	219
S.1.4.1 Models for r_0	219
S.1.4.2 Models for K	219
S.1.4.3 Models for α	219
S.1.5 Correlation r_0 - α	220
S.1.5.1 Model code	220
S.1.5.2 Correlation test for individual groups	221
S.1.6 Density regulation functions	223
S.1.7 Model construction tables	224
S.1.8 Relative importance tables	227
S.1.9 Density-dependent fitness of the NpH populations	229
S.1.10 Population growth assessment: raw data and posterior predictions	232
S.2 Supplementary Material of Chapter 2	236
S.3 Supplementary Material of Chapter 3	269
S.3.1 Experimental design	269
S.3.1.1 Treatment groups	269
S.3.1.2 Extended methodology experimental evolution	270
S.3.1.3 Experimental handling	273
S.3.2 Video analysis script	275
S.3.3 Beverton-Holt model fitting	279
S.3.4 Additional results	279
S.3.4.1 Model comparison and summary table local adaptation test	279
S.3.4.2 Expansion rate	281

S.3.4.3	Density dynamics during range expansion	283
S.3.4.4	Adaptation test raw evolution data	285
S.3.4.5	Evolution test over whole pH range	288
S.3.4.6	Survival probability	290
S.3.4.7	Morphology: cell size	292
S.3.4.8	Morphology: cell elongation	295
S.3.4.9	Movement: cell speed	298
S.3.4.10	Movement: cell turning	301
S.3.4.11	Dispersal rates	304
S.4	Supplementary Material of Chapter 4	306
S.4.1	Video analysis script and parameters	306
S.4.2	Visual representation of experimental evolution phase	309
S.4.3	Nuclear separation media reagents	311
S.4.4	Read mapping statistics	312
S.4.5	Coverage statistics	314
S.4.6	Derived alleles in sequenced populations	315
S.4.7	Principle component analysis on standing genetic variation	317
S.4.8	Intrinsic growth rate of populations	318
S.4.9	Gene ontology Classification	319
S.4.10	Model summary and Anova tables	351
S.4.10.1	Genetic changes on standing genetic variation	351
S.4.10.2	Genetic changes through <i>De novo mutation</i>	353
S.4.10.3	Fitness changes: evolution of population growth rate	353

S.4.11	Association between genetic change through <i>de novo</i> mutation and fitness change.	355
S.4.12	Genes involved in adaptive evolution through genetic change on standing variation	356
S.4.12.1	Analysis of genetic changes on standing variation: general adaptation	356
S.4.12.2	Analysis of genetic changes on standing variation: gradient-specific adaptation	358
S.4.13	Genes involved in adaptive evolution through <i>de novo</i> mutation.	380
S.4.13.1	Analysis of <i>de novo</i> mutations: general adaptations	380
S.4.13.2	Analysis of <i>de novo</i> mutations: gradient-specific adaptations	384
S.4.14	Cochran-Mantel-Haenszel test	388
S.4.14.1	Pairing of populations	388

Introduction

General introduction

Range shifts and invasions in the Anthropocene

Ecologists and evolutionary biologists have always been interested in what determines or limits the spatial distribution of species. Already in the Victorian age, biologists like Charles Darwin and Alfred Russel Wallace were fascinated by the diversity of life across the world, describing their findings on the distribution and spread of species (Darwin, 1869; Wallace, 1876). Whereas this early work was largely descriptive, research later moved towards understanding the fundamental processes that led to observed patterns in species ranges and distributions. This shift towards a more systematic understanding of species ranges and distributions was spearheaded by foundational researchers like John Gordon Skellam, Robert MacArthur and Charles Elton.

Skellam's seminal work on the expansion of populations (Skellam, 1951) elucidated the dynamics of single populations that were spreading through space. In this theoretical work, Skellam provided the groundwork to understand how the spread of populations follows almost universally a wave-like pattern, where the speed of the expanding wave is driven by the dispersal ability of individuals and the growth rate of the population

(Skellam, 1951). Through his work, Skellam thus laid the mathematical basis for future work on the study of expanding populations (see for example Kot et al., 1996; Sakai et al., 2001; Cantrell and Cosner, 2004), by developing an intuitive and general model to describe the spreading of populations. Charles Elton expanded on this knowledge, by moving from the theoretical to the empirical realm and studying invasions of animals in nature (Elton, 1958). With his work, Elton not only advanced the understanding of the fundamental dynamics governing the spread of invading populations, but also discussed the severe consequences that invasions of non-native species can have by disrupting local biodiversity during invasions. Even to this date, Elton's work still profoundly shapes the field of invasion biology (Williamson and Griffiths, 1996; Ricciardi and MacIsaac, 2008; Richardson, 2011). Finally, MacArthur's theory of island biogeography (MacArthur and Wilson, 1967; Brown and Lomolino, 2000; Whittaker et al., 2008; Losos and Ricklefs, 2009) provided a framework to investigate how invasions and extinctions on longer timescales determine the expected biodiversity on landmasses, thus fully extending the systematic study of species distributions from the population level to the community level.

In recent decades, efforts to understand and predict species distributions have gained a renewed interest, because anthropogenic disturbances are increasingly impacting the natural world. Invasion by non-native species have been shown to be one of the most important threats to biodiversity (Intergovernmental Science-Policy Platform on Biodiversity and Ecosystem Services, 2019). Such a loss of biodiversity may negatively affect functions and services provided by ecosystems (Singh, 2002; Srivastava and Vellend, 2005; Harrison et al., 2014). Therefore it is important that we thoroughly understand how human activities may affect species distributions, and what the consequences of these disruptions are. Anthropogenic disruption of species distributions happens primar-

ily in two distinct ways:

Firstly, anthropogenic activities can lead to changes in the abiotic environment which may negatively affect species. For example, industrial and agricultural activities led to the formation of acid rains and the run-off of pesticides, respectively, which both negatively affected many species (Likens and Bormann, 1974; Likens et al., 1996; DeLorenzo et al., 2001; Burns et al., 2016; Sánchez-Bayo and Wyckhuys, 2019). Such a decline in environmental conditions may force species to either adapt to the environmental stress, or to disperse to a different location. This dispersal response due to changing abiotic conditions is perhaps best exemplified by the increase in anthropogenic carbon dioxide emissions. As a consequence of these increased emissions, temperatures have been gradually rising, and climate conditions (for example precipitation patterns) have changed. These changes in climatic conditions have led to range shifts when many species track their optimal climate niche, a behaviour that has been observed across many taxonomic groups, including plants, arthropods and birds (Hill et al., 1999; Parmesan et al., 1999; Parmesan, 2006; Chen et al., 2011). As a consequence, many species are either shifting their range polewards or upwards in altitude along mountain ranges.

Secondly, humans are increasingly altering the distribution of species by distorting existing dispersal trajectories (human-altered dispersal, for example due to habitat fragmentation) or by creating new long-distance dispersal trajectories through accidental or intentional introductions (human-vectored dispersal; reviewed in Bullock et al., 2018). Human-vectored dispersal in particular, where humans introduce species to distant regions or even new continents can severely impact species distributions. As in the past already pointed out by Elton (1958), introductions to new environments or continents regularly lead to strong invasiveness of the introduced species. Mounting evidence

demonstrates how severely invasive species across taxonomic domains and continents can affect the habitats they invade (for the Management of Noxious and Exotic Weeds and Westbrooks, 1998; Frenot et al., 2005; Gozlan et al., 2010).

Although one might assume that species invasions and range expansions would lead to a net increase in local biodiversity, the opposite is often true. Especially in the case of invasions to completely new areas, the invading species typically lack natural enemies in the area of introduction. Consequently, these invading species may outcompete local species or disrupt ecological communities, resulting in a loss of biodiversity (Grosholz, 2002; Sanders et al., 2003; David et al., 2017). Such disruption of the local community can in turn negatively affect ecosystem functions and services provided by local ecosystem, with negative ecological and economical consequences for nature and humans alike (Dukes and Mooney, 2004; Charles and Dukes, 2007; Pejchar and Mooney, 2009; Phillips et al., 2009, see also Box 2 for the case study of the amphipod *Dikerogammarus villosus*). Additionally, invasions and range expansions often lead to strong bottlenecks in the population, resulting in low genetic diversity (Excoffier et al., 2009; Chuang and Peterson, 2016). The loss of genetic diversity can similarly have a negative impact on ecological or ecosystem functions provided by species (Hughes et al., 2008).

Evolution during range expansions

Range expansions have been studied extensively from an ecological point of view. Only more recently have biologists started investigating the evolutionary changes that occur during range expansions. As described by the travelling wave model (Skellam, 1951; Giometto et al., 2014), the range expansion rate is driven by the dispersal ability of the

individuals and the growth rate of the population. Empirical studies of range expansions also showed that individuals at a range edge can differ phenotypically from the individuals in the range core, suggesting that rapid evolution may play an important role during range expansion. For example, in the case of the cane toad in Australia (see Box 1), individuals at the range edge are significantly larger and have longer limbs compared to individuals in the range core, which allowed them to move greater distances (Brown et al., 2007; Clarke et al., 2019). Additionally, toad populations at the range edge have higher growth rates than populations in the core (Phillips, 2009).

Box 1: Cane toads in Australia — the poster child of invasive species

The cane toad (*Rhinella marina*) is one of the most extensively studied invasive species, and often seen as the poster child for the problems that can arise from invasive species. Indigenous to Central and South America, the cane toad was introduced in Australia as a means for biocontrol of pests in sugarcane fields. However, after its introduction in 1935, the cane toad rapidly spread in the northern part of Australia, and is now present in a large area of the country (Phillips et al., 2007). This rapid spread of the cane toad was largely attributed to a lack of natural enemies in Australia. Because the cane toad is poisonous to most animals, some local predatory species even evolved to avoid the cane toad (Phillips and Shine, 2006). As a result, this species faces few risks from predation. Additionally, cane toads have negatively impacted both other anurans as well as invertebrate prey species (Greenlees et al., 2006; Crossland et al., 2008). Consequently, managing the threat of the invasive cane toad has become an important issue for nature management in Australia (Tingley et al., 2017), that remains partially unresolved until today.

Although these empirical observations provide strong indications of evolutionary changes during range expansions, the use of such field studies has two inherent limits. Firstly, because one observes an expanding population spreading in nature, there is usually no replication, which makes it hard to distinguish between evolution by natural selection and evolution by genetic drift. Drift may play an important role during range expansions, due to the low population densities at the range edge (Excoffier et al., 2009). Secondly, because changes in the landscape (for example changes in the abiotic environment, new biotic interactions) may result in additional selection pressures aside from selection due to the range expansion process itself, disentangling which evolutionary changes stem from selection purely due to the spatial process of range expansion, and which stem from selection due to changes in the environment may be difficult. Therefore, some of the observed evolutionary changes may be specific to this range expansion, and not generally the case for all range expansions. Theoretical and experimental studies can help alleviate these restrictions. Consequently, increasing efforts have been undertaken to study range expansions using experimental and theoretical methods, to investigate which evolutionary responses can be expected during range expansions.

Theoretical work indicates that observed changes in dispersal during range expansions stem from spatial sorting and assortative mating (Shine et al., 2011; Perkins et al., 2013). Theory predicts that during range expansions, individuals will sort according to dispersal ability, with highly dispersive individuals occurring preferentially at the range edge, and less dispersive individuals remaining close to the range core (spatial sorting). Subsequently, individuals mate with conspecifics which are similar in dispersal ability (assortative mating). The repetition of these two processes during range expansions is predicted to lead to continuous evolution of increased dispersal ability at the range edge, and decreased dispersal ability in the range core. Indeed, several experimental

studies have demonstrated that changes in dispersal ability occur during range expansions (Fronhofer and Altermatt, 2015; Williams et al., 2016; Weiss-Lehman et al., 2017; Ochocki and Miller, 2017).

Theoretical work also indicates that observed changes in growth rate stem from the population densities that individuals at the range edge experience during range expansions (Burton et al., 2010; Phillips et al., 2010). Populations in a range core typically experience continuously high population densities, and are therefore subject to strong selection for competitive ability. In contrast, populations at the range edge are released from these high population densities by moving beyond the species range. Individuals at the range edge that reproduce quickly are likely to be successful because they can colonize this new space. Therefore, populations at a range edge are under selection for increased growth rate. Because competitive ability and growth rate often trade-off with each other (Luckinbill, 1978; Mueller and Ayala, 1981; Andrews and Rouse, 1982; Mueller et al., 1991; Joshi et al., 2001), populations at the range edge become less competitive compared to their conspecifics in the range core. This prediction for evolution of increased growth rate at the range edge has been verified in experimental studies (Fronhofer and Altermatt, 2015; Ochocki et al., 2020).

It is important to note that the traits governing dispersal ability and growth rate are both driving the range expansion process (Skellam, 1951; Giometto et al., 2014), and are themselves under selection during range expansions (Burton et al., 2010; Phillips et al., 2010; Shine et al., 2011). Therefore, evolution during range expansions may in turn alter the range expansion process itself. This type of feedback between ecological processes (here range expansion) and evolution (here, change in dispersal ability and growth rate) can be classified as an eco-evolutionary process or feedback loop (Hendry, 2016; Govaert et al., 2019). During such eco-evolutionary feedback loops, ecological

conditions can induce evolution, which in turn can alter ecological conditions. Specifically in the case of range expansions, the range expansion process can lead to evolution of increased dispersal ability and population growth rate, which in turn will result in an acceleration of the range expansion process itself. Indeed, recent experimental studies have demonstrated that range expansion do indeed accelerate as they progress (Williams et al., 2016; Weiss-Lehman et al., 2017; Ochocki and Miller, 2017; Ochocki et al., 2020).

Experimental work during the last decade has demonstrated well how the spatial aspect of range expansion can drive the evolution of populations (Fronhofer and Altermatt, 2015; Williams et al., 2016; Weiss-Lehman et al., 2017; Ochocki and Miller, 2017). However, in the natural world environmental conditions often change in space. The presence of such environmental changes has the potential to complicate eco-evolutionary dynamics during range expansion. This is evidenced by empirical and experimental work, in which for example changing temperatures (Van Petegem et al., 2016; Giometto et al., 2018) or a new food source (Szűcs et al., 2017) affected evolutionary changes during range expansion. Not only can changes in the environment lead to additional selection pressures, but they may also change evolutionary changes on dispersal and population growth rate. For example, if organisms can sense the environmental conditions or the quality of their environment (see for example Giometto et al., 2015, 2017), environmental gradients may prevent selection on dispersal, because individuals will be deterred from moving towards the range edge (Fronhofer et al., 2017b). Another case where the presence of environmental gradients can alter evolution during range expansion, is when lower quality of the habitat at the range edge leads to a strong Allee effect, shifting range expansion dynamics from a pulled wave, where early dispersing individuals at the edge drive the range expansion process, to a

pushed wave, where the individuals behind the range edge drive the range expansion, and the population at a range edge needs to reach high population density before further expansion is possible (see for example Pachevsky and Levine, 2011). A pushed wave will therefore lead to a situation where populations at the range edge will experience increased population densities, and may hence not be able to escape competition.

When expanding populations face changing biotic rather than abiotic conditions (for example new prey species, competitors, or predators), evolutionary changes may be especially complex. This high complexity primarily stems from, two factors. First, the nature of the interaction between the invading and local species may strongly affect the evolutionary changes, as suggested by theory (Brooker et al., 2007; Van der Putten et al., 2010; Kubisch et al., 2014). Second, because both the invading species and the species with which it interacts are subject to evolution, one needs to consider co-evolutionary interactions between the two species. Recent experimental evidence demonstrates the importance of biotic interactions during range expansions and invasions (Nørgaard et al., 2019; Zilio et al., 2020). However, experimental evidence of the role that changing environmental conditions (be they biotic or abiotic) have on evolution during range expansions remains sparse. The combination of several and diverse selection pressures at a range edge — especially in presence of changing environmental conditions — may lead to complex evolutionary adaptations to cope with these novel conditions at the range edge.

Gene swamping and the role of sex during range expansions

One important mechanism by which populations adapt to novel conditions or complex selection pressures is sexual reproduction, which allows populations to reshuffle ge-

netic material (but, other mechanisms, such as mutation rate can also play an important role; Cobben et al., 2017). Theoretical work suggests that in well-adapted populations, sexual reproduction will decrease fitness by breaking up beneficial allele combinations (recombination load; Smith, 1978; Bell, 1982; Otto, 2009), but when populations need to adapt to changing conditions — as is the case for populations during range expansion, especially if abiotic or biotic conditions change in space — this reshuffling of genetic variation may be beneficial. The benefits of sexual reproduction for adapting to novel conditions have been demonstrated both in empirical work and in experimental work. Field studies of facultative sexually reproducing species have shown that species often reproduce asexually when environmental conditions are beneficial, but when environmental conditions deteriorate or when individuals perform badly in their current environment, they shift towards sexual reproduction (Schmeller et al., 2005; Arnold and Kunte, 2017). Similarly, several experimental studies have found that sexual reproduction can facilitate adaptation to novel conditions (Colegrave, 2002; McDonald et al., 2016; Petkovic and Colegrave, 2019). Additionally, further experiments showed that stressful conditions can lead to selection for increased rates of sexual reproduction (Becks and Agrawal, 2012; Luijckx et al., 2017).

These benefits of sex are predicted to be most effective when there is sufficient genetic variation present in the population (Lachapelle and Bell, 2012). Populations at a range edge are however often genetically depauperated (Excoffier et al., 2009; Chuang and Peterson, 2016) and may therefore benefit from sexual reproduction when there is an influx of genetic material. Indeed, several empirical studies have demonstrated that an introgression of locally adapted genes, for example by interbreeding with a closely related locally adapted species can facilitate adaptation of the invasive species, and consequently increase the success of invasion (Schmeller et al., 2005; Lavergne and Molof-

sky, 2007; Currat et al., 2008).

These predictions are contingent on the assumption that the introgressing genes are beneficial, and will therefore aid adaptation of the invading or expanding population. This assumption does not hold under all conditions. For example, the gene swamping hypothesis suggests that when populations expand their range into an environmental gradient, the population at the range edge may be subject to the influx of maladapted genes (Haldane and Ford, 1956; García-Ramos and Kirkpatrick, 1997; Kirkpatrick and Barton, 1997). Specifically, this hypothesis postulates that the increasing stress caused by an environmental gradient results in a gradient of population density, with high population densities in the range core and low densities at the range edge. This population density gradient may lead to asymmetric gene flow, with many individuals moving from the high density range core to the range edge, flooding the edge population with maladapted individuals. When populations rely on sex for reproduction, this would swamp the edge population with maladapted genes and limit the edge population in its adaptation to the local environment (Haldane and Ford, 1956; García-Ramos and Kirkpatrick, 1997; Kirkpatrick and Barton, 1997; Polechová and Barton, 2015; Polechová, 2018). Gene swamping can influence species distributions, and has even been argued to be a potential driver of stable range borders (Lenormand, 2002; Bridle and Vines, 2007; Gaston, 2009; Sexton et al., 2009). Yet despite these important predictions associated with the gene swamping hypothesis, this hypothesis has currently almost exclusively been studied theoretically (but for an important recent exception, see Bachmann et al., 2020).

Box 2: Invasion in European catchments — the spread of the Killer Shrimp

Another well studied invasive species is the amphipod *Dikerogammarus villosus*, also known by the slightly more sensational name of "Killer shrimp". *Dikerogammarus villosus* is native to the Ponto-Caspian region, but spread and invaded in several European river catchments, and continues to expand its range in these catchments. For example in the Rhine, this invasive amphipod has displaced several of its native allospecifics in certain parts of the river catchment (Van Den Brink et al., 1991; Kley and Maier, 2006; Leuven et al., 2009; Altermatt et al., 2014, 2016). Amphipods play an important role in the functioning of aquatic ecosystems by shredding leaf litter and thus making nutrients available for other aquatic organisms. Although native and invasive amphipods both perform this ecosystem function, experimental work has demonstrated that the invasive *D. villosus* has a lower biomass-adjusted leaf litter decomposition rate compared to its native competitor (Little and Altermatt, 2018). Consequently, a complete replacement of the native amphipods by the invasive species would likely result in a partial disruption of the ecosystem function (leaf litter decomposition) performed by these species.

***Tetrahymena thermophila* as a model system for studying range expansions**

The use of microbial and protist microcosms has become well-established in ecological and evolutionary research. Such systems have several distinct advantages because they allows the study of complex ecological and evolutionary phenomena in a very controlled experimental setting (Cadotte et al., 2005; Beyers and Odum, 2012; Altermatt

et al., 2015). Consequently, protist microcosms have been used to study ecological and evolutionary phenomena with varying complexity and research goals. This ranges from ecological and evolutionary dynamics in single species (Schtickzelle et al., 2009; Chaine et al., 2010; Hiltunen and Laakso, 2013; Pennekamp et al., 2014; Giometto et al., 2015; Fronhofer and Altermatt, 2015), to multi-species community dynamics (Gill and Hairston, 1972; Warren et al., 2003; Jacquet and Altermatt, 2020) and even meta-community and meta-ecosystem dynamics (Cadotte, 2006; Bell and Gonzalez, 2011; Altermatt et al., 2011; Altermatt and Holyoak, 2012; Harvey et al., 2020). Although the use of such microcosms has the advantage of allowing us to study ecological and evolutionary phenomena in a very controlled way, it should however also be noted that such systems are always a simplified abstraction of reality, and may not always account for the full complexity in natural systems.

Several protist species have also been used specifically for the study of range expansions, including *Euglena gracilis* (Giometto et al., 2017), *Paramecium caudatum* (Zilio et al., 2020), and species of the genus *Tetrahymena* (Giometto et al., 2014; Fronhofer and Altermatt, 2015). The use of protist microcosm systems for the study of range expansions, in comparison to other commonly used microcosm system with invertebrate animals (see for example Weiss-Lehman et al., 2017; Ochocki and Miller, 2017; Petegem et al., 2018; Ochocki et al., 2020), has the advantage that the short generation times allow to observe evolutionary changes within short times. Similarly, bacterial model system, which have even shorter generation times, are also commonly used for the study of range expansions (Hallatschek et al., 2007; Hallatschek and Nelson, 2010; Korolev et al., 2012; Gralka et al., 2016; Giometto et al., 2018). However, advancements in microscopy and automated video tracking in protist microcosms (Pennekamp et al., 2015; Altermatt et al., 2015) allow for the quantification of traits (e.g. movement

behaviour) on an individual level, something which is often more difficult to achieve in bacterial microcosms. Consequently, protist microcosms combine the best of two worlds, allowing to study range expansions in species with short generation times but with complex behaviour that can be easily measured on the individual level.

In this thesis, I performed several experiments to investigate how environmental changes and gene swamping affect evolution during range expansions of *Tetrahymena thermophila*. *Tetrahymena thermophila* is a freshwater protist that, like other protist species, is commonly used in evolutionary and ecological research (Schtickzelle et al., 2009; Altermatt et al., 2015; Collins, 2012; Fronhofer and Altermatt, 2015; Cairns et al., 2019). It is an ideal model species to study evolution during range expansion and the role of gene swamping for several reasons. Firstly, *T. thermophila* like many other protist species, it has a short life cycle (approximately 4 hours), which allows for evolution experiments within a relatively short time frame (Lynn and Doerder, 2012) and an active swimming behaviour. Secondly, the species has a distinct sexual and asexual reproductive cycle over which we have strict control (Lynn and Doerder, 2012; Ruehle et al., 2016), allowing us to influence its reproductive mode during experiments. Lastly, *T. thermophila* has a sequenced and annotated genome (Eisen et al., 2006), unlike for example *T. pyriformis*, a species of the genus *Tetrahymena* that has previously been used for the study of range expansions (Fronhofer and Altermatt, 2015). This allowed me to explore genomic evolution in this thesis.

Structure of the PhD thesis

Objectives

Range expansions and invasions may disrupt ecological communities and ecosystems (Phillips et al., 2009; Gross, 2018). To better anticipate the impact of the increasing number of human induced range expansions and invasions, it is therefore imperative that understand the eco-evolutionary responses of populations during range expansions. In this thesis, I asked how the presence of environmental changes as well as gene swamping alter evolution during range expansions. Because populations often encounter new environmental conditions during range expansions, I experimentally assessed how changes in the abiotic environment (changes in pH) and biotic environment (new prey species) affect evolution during range expansions. I also aimed to assess experimentally if gene swamping alters evolutionary changes during range expansion on a phenotypic and genetic level.

Thesis outline

To investigate how populations adapt to new environments, I performed two separate experiments, investigating adaptation to changing abiotic conditions (first experiment) and adaptation to changing biotic conditions (second experiment).

In the first experiment (described in **Chapter 1**), I investigated how established populations with high population densities (representing a range core) adapt to a changing abiotic environment. To do so, I performed an evolution experiment where populations of *T. thermophila* from four genetic backgrounds experienced either low pH, a common stressor in aquatic environments (Likens and Bormann, 1974; Likens et al., 1996;

Caldeira and Wickett, 2003; Raven et al., 2005; Zeebe et al., 2008; Burns et al., 2016) or neutral pH, whilst continuously experiencing high population densities. I assessed how life-history strategy (population growth rate and competitive ability) evolved under high population densities, in the presence or the absence of pH stress. I demonstrate in this chapter that high population densities affect the evolutionary trajectories of adapting populations, resulting in a maximization of population growth rate under the population densities which were experienced during the experiment. Overall, this led to a convergence of life-history strategy among the four genetic backgrounds when evolved under low pH conditions.

In the second experiment (discussed in **Chapter 2**), I investigated adaptation to a new biotic environment (i.e. new prey species). For this experiment, I also collaborated with Prof. Dr. Teppo Hiltunen and Dr. Johannes Cairns of the University of Helsinki, who had for two years co-evolved populations of the predator *T. thermophila* and seven of its bacterial prey species. I investigated how evolution of the predator and prey species altered the life-history traits (growth rate and competitive ability), morphology (size and elongation), and movement traits (movement speed and turning behaviour) of the predator species. To do so, I paired ancestral (naive) and evolved predators with ancestral and evolved prey in all four combinations. I subsequently measured the population growth rate and the behaviour of the predators. We found that evolution of the prey species typically had the strongest effect on predator performance, resulting in lower growth rates of predators when confronted with evolved prey compared to ancestral (naive) prey, independent of the evolutionary history of the predator. In contrast, changes in predator behaviour and morphology were mainly driven by evolutionary history of the predator, resulting in faster swimming, less turning, and larger cell sizes of evolved predators. These adaptations likely aid the predators in catching or ingesting

prey.

In the next two chapters, I investigated evolution during range expansions on a phenotypic level (Chapter 3) and on a genetic level (Chapter 4), specifically focussing on the role of gene swamping during range expansions.

In **Chapter 3**, I investigated how gene swamping altered adaptation during range expansion. I performed an evolution experiment using an established experimental method (Fronhofer and Altermatt, 2015). In this experiment, I subjected genetically diverse populations of *T. thermophila* to experimental range expansion in the presence and the absence of a pH-gradient. I controlled the reproductive mode of populations (asexual versus sexual reproduction) and long-distance gene flow from the range core to range edge (gene flow absent versus gene flow present) in a full factorial design. I then investigated how the pH-gradient, the reproductive mode, and long distance gene flow affected the evolution of population growth rate and range expansion dynamics (i.e. range expansion rate and population density). I demonstrate in this chapter that gene swamping (i.e. the interaction between reproductive mode and long-distance gene flow) altered adaptation. Specifically, I found that sexual reproduction aided adaptation in the absence of long-distance gene flow, but hindered adaptation when long-distance gene flow swamped the population at the range edge. Surprisingly, although theoretical predictions expect this gene swamping effect only in the presence of an abiotic gradient (Haldane and Ford, 1956; García-Ramos and Kirkpatrick, 1997; Kirkpatrick and Barton, 1997), I found it to be present both in the presence and in the absence of the pH gradient. I argue that this is due to the evolution of life-history traits during range expansions, which also results in a gradient in population density, similarly as in the case of an abiotic gradient.

Lastly, in **Chapter 4**, I analysed the genetic basis of adaptations during range ex-

pansion. To do so, I selected the most well adapted evolved populations from the experiment described in Chapter 3 (i.e. populations which showed the strongest increase in growth rate), and performed whole genome population sequencing. I then analysed genetic changes in these populations compared to the ancestral populations. Specifically, I investigated genetic changes both in terms of allele frequency changes on standing genetic variation, and in terms of *de novo* mutation. I assessed how the pH-gradient, the reproductive mode, and long-distance gene flow affect the number of variants that changed in allele frequency and the number of *de novo* mutations. Genetic changes can be associated with two kinds of selection, general selection during range expansion (associated with the process of range expansion and the general chemical environment), and gradient-specific selection, associated with the presence of a pH-gradient. I investigated which variants were associated with both kinds of selection, and identified protein-coding genes associated with these variants, to elucidate the functional nature of genetic adaptations during range expansions. I found that sexual reproduction increased the number of *de novo* variants that rose to detectable allele frequency, whereas the number of genetic changes from standing genetic variation depended on reproduction as well as gene flow and the presence of the pH-gradient. Additionally, I found that general selection during range expansion acted on genes associated with cell division, DNA repair and gene expression. Gradient specific selection, however, acted on genes involved in ion binding and transport, as well as in oxidoreductase reactions.

Finally, I conclude the thesis with a general discussion integrating the results of all chapters. I discuss how my findings relate to existing knowledge, where they corroborate existing predictions, and where I found results that indicated gaps in the existing knowledge. I then discuss potential directions of future research endeavours, to further elucidate the eco-evolutionary dynamics during range expansions.

Chapter 1: Evolution under pH stress and high population densities leads to increased density-dependent fitness in the protist *Tetrahymena thermophila*

Felix Moerman, Angelina Arquint, Stefanie Merkli, Andreas Wagner, Florian Altermatt and Emanuel A. Fronhofer

Evolution (2020) 74, 573–586. (doi:10.1111/evo.13921)

Abstract

Abiotic stress is a major force of selection that organisms are constantly facing. While the evolutionary effects of various stressors have been broadly studied, it is only more recently that the relevance of interactions between evolution and underlying ecological conditions, that is, eco-evolutionary feedbacks, have been highlighted. Here, we experimentally investigated how populations adapt to pH-stress under high population densities. Using the protist species *Tetrahymena thermophila*, we studied how four different

genotypes evolved in response to stressfully low pH conditions and high population densities. We found that genotypes underwent evolutionary changes, some shifting up and others shifting down their intrinsic rates of increase (r_0). Overall, evolution at low pH led to the convergence of r_0 and intraspecific competitive ability (α) across the four genotypes. Given the strong correlation between r_0 and α , we argue that this convergence was a consequence of selection for increased density-dependent fitness at low pH under the experienced high density conditions. Increased density-dependent fitness was either attained through increase in r_0 , or decrease of α , depending on the genetic background. In conclusion, we show that demography can influence the direction of evolution under abiotic stress.

Introduction

For many decades, biologists have studied the link between the abiotic environment and the distribution of species on earth, trying to understand why species occur in certain environments and not in others (Dunson and Travis, 1991; HilleRisLambers et al., 2012). Evolutionary biologists more specifically have studied the constraints and potential of species to adapt to their environment and how species respond when changes in their environment occur (Bijlsma and Loeschcke, 2005; Bridle and Vines, 2007). This encompasses research on adaptation to a multitude of abiotic stressors, including salt stress (Gunde-Cimerman et al., 2006; Flowers et al., 2010), heavy metal presence (Klerks and Weis, 1987; Shaw, 1994), thermal stress (Johnston et al., 1990; Angilletta, 2009, chapter 9) and stress associated with drought or the water regime (Lytle and Poff, 2004; Kooyers, 2015). Organisms can respond to such abiotic stress in several ways. They can respond through evolutionary adaptation, by evolving genotypes which match

the changed abiotic conditions (Kawecki and Ebert, 2004). They can also adapt through phenotypic plasticity, changing their phenotype to match the abiotic conditions (West-erberhard, 1989). When populations fail to either adapt quickly or to move away — to disperse (Clobert et al., 2001, part 1; Clobert et al., 2012, chapter 1-2) — these populations may be driven to extinction locally. In order to accurately predict local population dynamics and persistence in the context of evolutionary adaptations to abiotic change, it is necessary to understand the speed and direction of evolution in response to changing abiotic conditions, as well as to understand the constraints that such evolution faces.

The question of how populations can adapt through evolution to changing abiotic conditions has a long-standing history in empirical research, both in laboratory experiments as well as field studies (as reviewed in Kawecki and Ebert, 2004). Local adaptation has been recorded in response to different abiotic stressors, across different habitats, and in several taxonomic groups, including plants (Leimu and Fischer, 2008), fish (Fraser et al., 2011), and invertebrates (Sanford and Kelly, 2011). One important environmental impact of human activities is the acidification of natural waters and soils. In the past, acidification has strongly affected natural environments through acid rain (Likens and Bormann, 1974; Likens et al., 1996; Burns et al., 2016). It remains an important abiotic stressor because of the use of fossil fuels and ongoing anthropogenic increase in atmospheric carbon dioxide. Both lead to an acidification of water bodies, oceans in particular, (Caldeira and Wickett, 2003; Raven et al., 2005; Zeebe et al., 2008), with potentially severe consequences for organisms therein. Consequently, recent anthropogenic pressure on the natural environment has triggered increased efforts to understand if and how populations respond to human-induced climate shifts. Reviews of the literature showed that some species evolve to the changing climate, whereas others do not, at least not in the short term (Hoffmann and Sgro, 2011; Franks and Hoffmann,

2012). Ocean acidification has sparked efforts to understand how readily species can evolve to changing pH conditions (Kelly and Hofmann, 2013; Sunday et al., 2014).

Despite a growing body of work, evolution to pH stress is still less well studied experimentally, compared to many other stressors. Evolutionary changes caused by pH shifts have already been studied in the past, and this has typically been done comparatively or through translocation experiments along gradients or between locations differing in pH. For example Derry and Arnott (2007) and Hangartner et al. (2011) showed that copepods and frogs are locally adapted to the pH of their environment. Experimental evolution studies on adaptation to pH stress, although existing, are limited to only few systems that include bacterial model species (Hughes et al., 2007; Zhang et al., 2012; Gallet et al., 2014; Harden et al., 2015) and yeast (Fletcher et al., 2017). For example Gallet et al. (2014) demonstrate how the pH-niche under pH stress evolves through a transient broadening of the niche, followed by specialization. However, many of these studies are focused on adaptation to digestive tracts (Hughes et al., 2007; Harden et al., 2015) or oriented towards industrial application (Zhang et al., 2012; Fletcher et al., 2017). Although controlled experiments can help understand evolutionary adaptation to pH stress, they are still rare (Reusch and Boyd, 2013; Stillman and Paganini, 2015). In addition, existing experiments do not explore important factors that can affect adaptive evolution, such as demography.

Abiotic conditions will alter population performance, and hence also demography. Understanding how demographic conditions influence evolution, specifically the evolution of life-history traits, has led to an extensive body of theory and experiments (Stearns, 1977, 1992). This work has, for example, demonstrated the importance of density-dependent selection and life-history trade-offs between population growth and intraspecific competitive ability (competition-growth trade-offs; Luckinbill, 1978;

Mueller and Ayala, 1981; Andrews and Rouse, 1982; Mueller et al., 1991; Joshi et al., 2001). The eco-evolutionary interaction between demographic changes due to abiotic stress, that is, ecological conditions, and adaptation to abiotic conditions, remains less well understood.

Such eco-evolutionary feedbacks highlight that ecological conditions can alter evolutionary trajectories, and, conversely, that evolutionary change can impact ecological conditions (Pelletier et al., 2009; Hendry, 2016; Govaert et al., 2019). Whereas theoretical work has already incorporated the demographic context into evolutionary questions for some time (for a review, see Govaert et al., 2019), empirical work on adaptation to novel conditions still rarely includes the effect of demography on population performance or density explicitly (for some recent examples that do, see Michel et al., 2016; Nørgaard et al., 2019).

In our study, we experimentally explored how four distinct genotypes of the model protist species *Tetrahymena thermophila* evolve when being subjected to either a low pH treatment or a neutral pH treatment (control setting). We explicitly address the question of adaptation to low-pH stress in established populations with densities close to equilibrium. We quantify how evolution changes life-history strategies in four different genetic backgrounds and highlight the importance of trade-offs in life-history traits for understanding how populations adapt to abiotic stress under conditions of high population density, and assess if populations become more similar in life-history strategy.

We can expect directional selection leading to either a maximization of growth rate, or a maximization of competition related traits. When populations experience low competition, the fastest grower likely experiences a selective advantage, and hence we can expect evolution to lead to an increase in the average growth rate. In contrast, when competition is very high due to high population density, strong competitors will likely

be under positive selection. Depending on how abiotic stress alters the selection pressures, expected trends in evolution will change. If a stressful abiotic environment affects mostly growth, but does not influence competition, we might expect stronger selection for increased growth. In contrast, if a stressful abiotic environment mostly affects competition (for example, by limiting the amount of available food, or the uptake thereof), we would expect to see stronger selection for investment in competition related traits at lower population densities compared to the optimal abiotic environment.

Material and methods

Experiment

Study organism

We used the freshwater ciliate *Tetrahymena thermophila* as a model species. Due to its small body size, high population densities and short doubling time of ~ 4 h (Cassidy-Hanley, 2012; Collins, 2012), *T. thermophila* is well suited for both ecological and evolutionary experiments (e.g. Fjerdingstad et al., 2007; Collins, 2012; Coyne et al., 2012; Altermatt et al., 2015; Jacob et al., 2016). *T. thermophila* is characterized by a high mutation rate in the macronucleus (Brito et al., 2010). This high mutation rate, in combination with large population sizes (here, ranging from $\sim 1 \times 10^3$ cells/mL to 2×10^6 cells/mL), makes the species an ideal model system for adaptation experiments relying on mutation-driven evolution.

We used four clonal genotypes of *T. thermophila* obtained from the Tetrahymena Stock Center at Cornell University. These 4 genotypes are strain B2086.2 (henceforth called genotype 1; Research Resource Identifier TSC_SD00709), strain CU427.4

(genotype 2; Research Resource Identifier TSC_SD00715), strain CU428.2 (genotype 3; Research Resource Identifier TSC_SD00178) and strain SB3539 (genotype 4; Research Resource Identifier TSC_SD00660). We selected these strains because they differ strongly in both general life-history strategy and their response to pH stress (see Fig. S1.2 in Supplementary Information section S.1.2).

We maintained all cultures in axenic SSP medium consisting of proteose peptone, yeast extract and glucose (Cassidy-Hanley, 2012; Altermatt et al., 2015). To avoid bacterial or fungal contamination, we complemented the medium with 10 µg/mL Fungin, 250 µg/mL Penicillin and 250 µg/mL Streptomycin. We added these antibiotics at the start of all bioassays, at the start of the evolution experiment, and at every medium replacement during the evolution experiment (three times per week). At the beginning of the evolution experiment, we cryopreserved the ancestor genotypes in liquid nitrogen and later revived them for bioassays (following the protocol described by Cassidy-Hanley, 2012). Ancestors are from here on referred to as ANC. During the experiment, we maintained cultures at 30 °C, on a shaker rotating at 150 rpm.

Evolution experiment

We prepared 32 50 mL Falcon® tubes containing 20 mL of SSP medium with antibiotics. For each of the four genotypes, we inoculated eight tubes with 100 µL of high-density *T. thermophila* culture and let them grow for three days to ensure that populations were well established before starting the evolution experiment. After these three days, we divided the eight replicates of each genotype into two groups, a low pH treatment (from here on abbreviated as LpH) and a neutral pH treatment (hereafter called NpH). At day one of the experiment, we removed 10 mL of culture from all 32 replicate populations and replaced it with 10 mL of SSP medium with antibiotics for the

NpH treatment, and with 10 mL of pH-adjusted SSP medium with antibiotics for the LpH treatment. The pH of the pH-adjusted medium used for these 10 mL replacements was prepared by adding 1 M HCl solution to the medium until a pH of 4.5 was reached (1.6 mL of 1 M HCl per 100 mL of SSP medium, for the relationship between added HCl and pH, see Supporting Information section S.1.1). We repeated this regime of medium removal and replacement on every first, third and fifth day of the week for a total of six weeks. Consequently, the pH of the medium for LpH populations was gradually reduced over a period of two weeks, after which it was kept approximately stable at 4.5 for the remainder of the experiment.

Genotype revival and common garden conditions

In order to perform all population growth assays of evolved (LpH and NpH) and ancestral (ANC) populations at the same time, we revived the ancestor populations from liquid nitrogen storage. We transferred revived cells to SSP-medium with antibiotics for recovery. We then prepared a common garden treatment. We inoculated common garden cultures for the LpH, NpH and ANC populations (50 mL Falcon® tubes with 20 mL of SSP medium with antibiotics) with 100 µL culture and transferred them to a shaker for 72 h, in order to control for potential plastic or parental effects. This should ensure that any observed phenotypic changes are the result of either de novo mutations, or of highly stable epigenetic effects.

Population growth assessment

After culturing all populations in the same environment (common garden), we assessed population growth at low pH (pH 4.5) and neutral pH (pH 6.5) of the assay medium for the ANC (four genotypes, each replicated four times per assay medium pH treatment),

and evolved (LpH and NpH) populations (29 surviving populations per assay medium pH treatment) for a total of 90 cultures. We placed these cultures in an incubator, and grew them for seven days. Most populations reached equilibrium density well before the end of these seven days (between 20 and 100 hours after populations started growing; see also section S.1.10 in the Supporting Information), which allows us to obtain precise measurements of growth rates and population equilibrium densities.

Data collection and video analysis

We sampled populations both during the evolution experiment and during the population growth assessments, to quantify (i) population density during evolution, (ii) intrinsic rates of increase (r_0), and (iii) intraspecific competition coefficients (α) for the ANC, LpH and NpH populations. These r_0 and α estimates were obtained through fitting of a population growth model, as described below in the section "Population growth model fitting". During the evolution experiment, we sampled three times per week prior to medium replacement. For the population growth rate assessments of the evolved and ancestral populations, we sampled a total of 10 time-points over a course of the seven days, with more frequent sampling early in the growth phase (four times over two days) to adequately capture the population dynamics. For sampling and analysis, we followed a previously established method of video analysis to extract information on cell density and morphology of our evolved and ancestral populations, using the BEMOVI R package (Pennekamp et al., 2015).

Our population sampling method is adapted from well-established protocols (Fronhofer and Altermatt, 2015; Fronhofer et al., 2017b). Briefly, 200 μ L of culture was sampled from the population, and if cell density was too high for video analysis, diluted 1/10 or 1/100, because excessive cell density decreases the accuracy of cell recognition

during video analysis. We then transferred the culture to a system of microscope slides with fixed capacity, so that a standard volume (34.4 μL) of culture could be measured for all videos. Next, we took a 20 s video at 25 fps (total of 500 frames) using a Leica M165FC stereomicroscope with top-mounted Hamamatsu Orca Flash 4.0 camera. We analyzed our videos using the BEMOVI R package (Pennekamp et al., 2015) to extract the relevant information. Parameters used for video analysis can be found in the Supporting Information (section S.1.3).

Statistical analyses

All statistical analyses were performed using the R statistical software (version 3.5.1) with the ‘rstan’ (version 2.18.2) and ‘rethinking’ (version 1.5.2) packages (McElreath, 2015).

Population growth model fitting

In order to analyze population growth dynamics of ancestral and evolved populations, we fit a continuous-time version of the Beverton-Holt population growth model (Beverton and Holt, 1993). As recently discussed by Fronhofer et al. (2018, see also chapter 5 in Thieme 2003), using this model provides a better fit to microcosm data compared to less mechanistic models (for example an r - K population growth model, which captures the density-regulation of microcosms less well) and readily allows for a biological interpretation of its parameters. The Beverton-Holt model is given by the equation

$$\frac{dN}{dt} = \left(\frac{r_0 + d}{1 + \alpha N} - d \right) N \quad (1)$$

with the intraspecific competitive ability (α) being

$$\alpha = \frac{r_0}{Kd} \quad (2)$$

Here, N corresponds to population size, r_0 corresponds to the intrinsic rate of increase, α to the intraspecific competitive ability (hereafter referred to as competitive ability), and d to the death rate of individuals in the population. The K parameter in equation (2) represents the equilibrium population density. We adapted Bayesian statistical models from Rosenbaum et al. (2019) to estimate parameter values for r_0 , α , d , and K using the rstan package and trajectory matching, that is, assuming pure observation error (see <https://zenodo.org/record/2658131> for code). We chose vaguely informative priors, that is, we provided realistic mean estimates, but set standard deviation broad enough to not constrain the model too strongly, for the logarithmically (base e) transformed parameters with $\ln(r_0) \sim normal(-2.3, 1)$, $\ln(d) \sim normal(-2.3, 1)$ and $\ln(K) \sim normal(13.1, 1)$.

Analysis of parameter estimates r_0 , α , and K

In a next step, we analyzed the population growth parameter estimates to determine how our experimental treatments affected them. As intrinsic rates of increase (r_0) integrate birth and death rates and are more reliably estimated than its components (narrower posterior distributions), we here focussed on intrinsic rates of increase and excluded the death rate from further analyses (see also Tab. S1.10 for summarized posteriors).

To analyse the parameter estimates (r_0 , α , and K), we constructed separate linear models for each genotype, and fit logarithmically (\ln) transformed parameters r_0 , α and K as a function of a) the pH of the assay medium, b) general evolution across pH

treatments, that is, difference between ANC populations, on the one hand, and evolved populations, on the other hand, c) evolution to specific pH treatments (that is, differences between ANC, LpH and NpH) and d) interactions between pH of the medium and evolutionary changes. This resulted in 16 statistical models for each of the response variables and each of the four genotypes (see Tab. S1.3 in Supporting Information section S.1.7 for details). Information on priors can be found in the Supporting Information (section S.1.4). Following McElreath (2015, chapter 14), we did not only use our mean parameter estimates, but took their uncertainty into account by modelling both means and errors of the parameters obtained during Beverton-Holt model fitting.

We then compared the models using the deviance information criterion (DIC), a Bayesian implementation of the Akaike information criterion (Gelman et al., 2014) and averaged the posterior predictions of the 16 models based on DIC weights. Next, we calculated the relative importance (RI) of the explanatory variables by summing for each explanatory variable the respective model weights in which this variable is included.

Correlation between r_0 and α

In order to detect potential correlations between intrinsic rate of increase (r_0) and competitive ability (α), we performed a Bayesian correlation analysis using the logarithmically transformed estimates of r_0 and α and fitting a multivariate normal distribution. We again used both mean estimates and their errors to account for errors caused by population growth model fitting. To account for plastic effects associated with the pH of the assay medium, we performed the correlation analysis separately for low pH and neutral pH of the assay medium, while pooling the data for all four genotypes and treatments (ANC, LpH, and NpH). Pertinent computer code can be found in the Supporting Information (section S.1.5).

Variation in life-history traits

We asked whether evolutionary history altered between-genotype variation in life-history traits (r_0 , α and K) at low and neutral pH of the assay medium. We first calculated for each group (ANC, LpH and NpH) the mean of the natural logarithm of r_0 , α and K over all 4 genotypes, and subsequently calculated the absolute difference between this mean and the observed trait values (r_0 , α and K) of all replicate populations (logarithmically transformed). We then used Bayesian models to calculate whether these differences varied between the treatments (Evolved (general evolutionary change, difference between ANC and all evolved lines), LpH and NpH). To account for potential genotype effects, we also included both models with and without random effects per genotype (random genotype intercepts), leading to a total of 6 models per trait, as shown in Tab. S1.4 in the Supporting Information section S.1.7. After fitting the models, we compared the models using the Watanabe-Akaike information criterion (WAIC), a generalized form of the Akaike information criterion used for comparison of Bayesian statistical models (Gelman et al., 2014). We then calculated relative parameter importance using WAIC weights.

Density-dependent fitness calculation

To assess how the observed convergence in life-history strategy might have arisen, we calculated the population growth rate (r) for the LpH and for ANC populations over all observed population densities during the evolution experiment and integrated over these values to calculate a weighted density-dependent fitness estimate. We then used Bayesian models to fit these density-dependent fitness values as a function of a) population origin (ANC or LpH), b) centered intrinsic rate of increase (r_0), and c) an interaction

term between r_0 and population origin. Centered r_0 represents the intrinsic rate of increase, rescaled to have its mean at zero, and was calculated by subtracting the mean r_0 from all r_0 values. In this analysis, we also included a random intercept for the different genotypes (details in Tab. S1.5 in section S.1.7 of the Supporting Information). We fit all five models, starting from the intercept model to the full interaction model. Subsequently, we ranked these models using the WAIC criterion and calculated the relative importance of all explanatory variables based on WAIC weights. The corresponding analysis for the NpH populations can be found in Supporting information section S.1.9.

Results

We subjected replicate populations of four different genotypes to either low pH (LpH) conditions or neutral pH conditions (NpH), while keeping population densities high over the course of the evolution experiment. Fig. 1.1 shows the population densities as observed during the experiment. We then tested whether and how evolution changed life-history strategies in all four different genetic backgrounds. Fig. 1.2 shows the data and model predictions for changes in life-history traits. Next, we tested how life-history traits were correlated and how this may have constrained evolutionary changes. The correlation in life-history traits is depicted in Fig. 1.3. We then tested for changes in variation of life-history strategy between populations (shown in Fig. 1.4). Lastly, we tested how evolution of life-history strategies affected density-dependent fitness under the observed densities during the evolution experiment. Fig. 1.5 shows data and model predictions of density-dependent fitness under low pH conditions.

Evolution of life-history traits

During the 42 days of the evolution experiment, population densities ranged from approximately 1×10^3 cells/mL to 2×10^6 cells/mL (see Fig. 1.1) and fluctuated around the population equilibrium density due to stochastic variation in death and division rates. Observed densities varied strongly depending on treatment and genetic background. Out of 32 evolving populations, three went extinct during the experiment, all in the low pH treatment (one population each for genotype 1, 2 and 3).

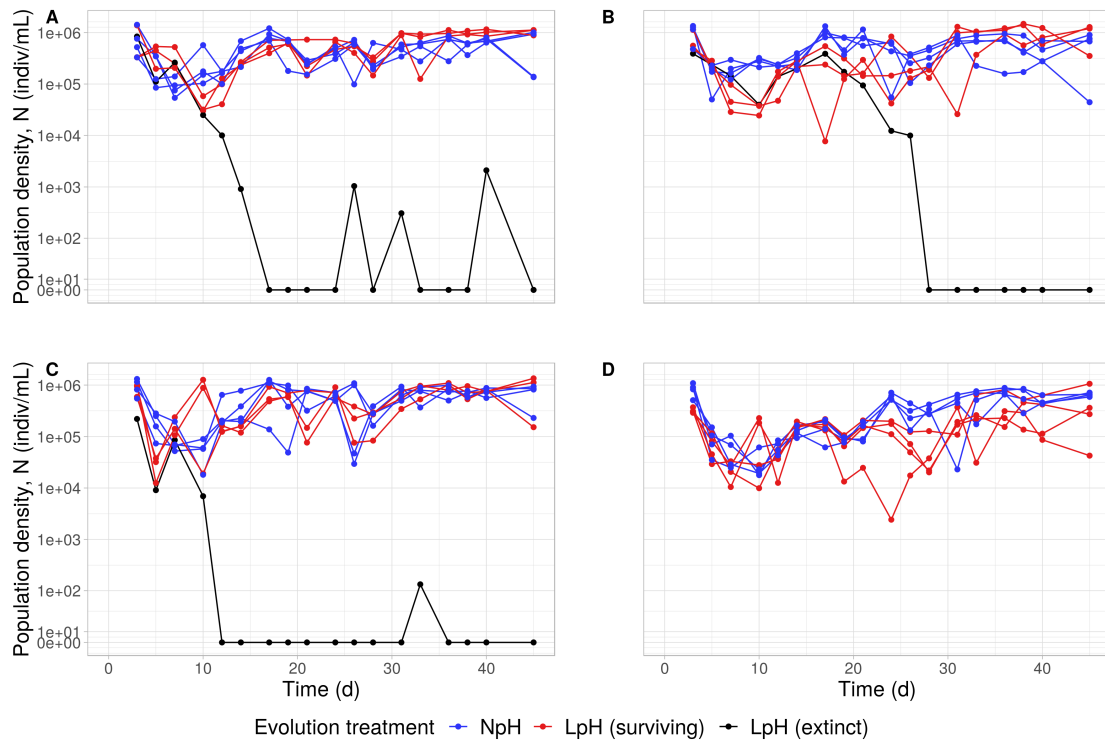


Figure 1.1: Density dynamics of the replicate populations over the course of the evolution experiment. The y-axis shows the population density (axis is pseudo-logarithmically transformed, to account for 0 values in the dataset), the x-axis the time since the beginning of the experiment in days. Each set of dots connected by a line represents data from a single replicate population. Red and blue symbols correspond to data from populations that survived to the end of the experiment from the LpH (populations evolved under low pH conditions) and NpH (populations evolved under neutral pH conditions) treatments, respectively. Black symbols correspond to data from LpH populations that went extinct. Panel A shows the density dynamics for genotype 1, panel B for genotype 2, panel C for genotype 3 and panel D for genotype 4.

After the experimental evolution phase, we found that all four genotypes showed strong plastic effects associated with the pH of the assay medium (see also Tab. S1.6 in the Supporting Information section S.1.8). Low pH of the assay medium consistently decreased intrinsic rate of increase (r_0), led to lower competitive ability (α), and, as a consequence of this decrease in α , to increased equilibrium population densities (K) as shown in Fig. 1.2. This effect of low pH was especially pronounced for r_0 and α , where

the relative importance values associated with pH of the medium were typically close to one for all four genotypes (see also Tab. S1.6 in the Supporting Information section S.1.8). The effect of low pH was less pronounced for the equilibrium population density (K), specifically for genotype 2.

We additionally found signatures of evolutionary change. These were less consistent than the plastic effects, that is, they differed between the genotypes. Evolution led to an increase in r_0 for genotypes 2 and 4 (Fig. 1.2B,D). However, for genotype 2 this increase only occurred in the LpH populations. For genotype 4 we mostly observed a general change in all evolving populations and only to a lesser degree specific changes in the LpH and NpH treatments.

LpH led to increased equilibrium population density (K) for genotype 1 and genotype 4 (Fig. 1.2E, H), and a decreased equilibrium population density (K) for genotype 3 (Fig. 1.2G). As equilibrium density is an emergent trait, the changes in K were driven both by the changes in r_0 described above and by changes in α . Evolution led to lower competitive ability (α) for LpH genotype 1 populations (Fig. 1.2I), to increased competitive ability (α) for evolved genotype 2 populations (Fig. 1.2J), to no clear change for genotype 3 (Fig. 1.2K), and to increased competitive ability (α) for evolved and especially NpH for genotype 4 populations (Fig. 1.2L). Overall, we detected evolutionary changes in all traits (r_0 , α and K), although direction and strength of change strongly differed between genotypes.

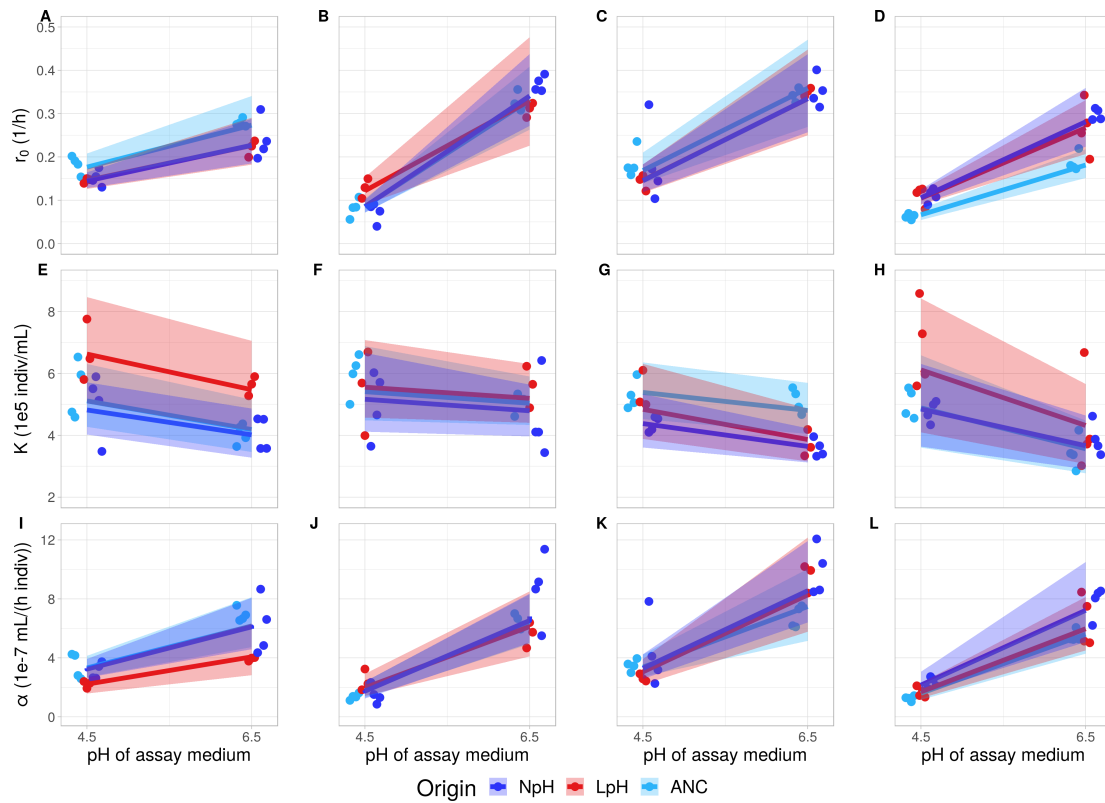


Figure 1.2: Evolutionary trends in intrinsic rate of increase (r_0 ; A-D), equilibrium population density (K ; E-H) and competitive ability (α ; I-L) for the 4 different genotypes. Each circle represents an estimate of r_0 , K or α (posterior means) from the Beverton-Holt model for one replicate population. Lines and shaded areas represent the averaged posterior model predictions based on DIC weights (means and 95 % probability interval). Light blue = ANC (ancestor populations), dark blue = NpH (populations evolved under neutral pH conditions), red = LpH (populations evolved under low pH conditions).

Variation and covariation in r_0 and α

The intrinsic rate of increase (r_0) and competitive ability (α) were positively correlated both at low pH and neutral pH of the assay medium (Fig. 1.3). However, the correlation was markedly stronger at low pH ($R^2 = 0.95$) than at neutral pH ($R^2 = 0.61$). Variation in these two quantities was also larger at low pH compared to neutral pH (Fig. 1.3).

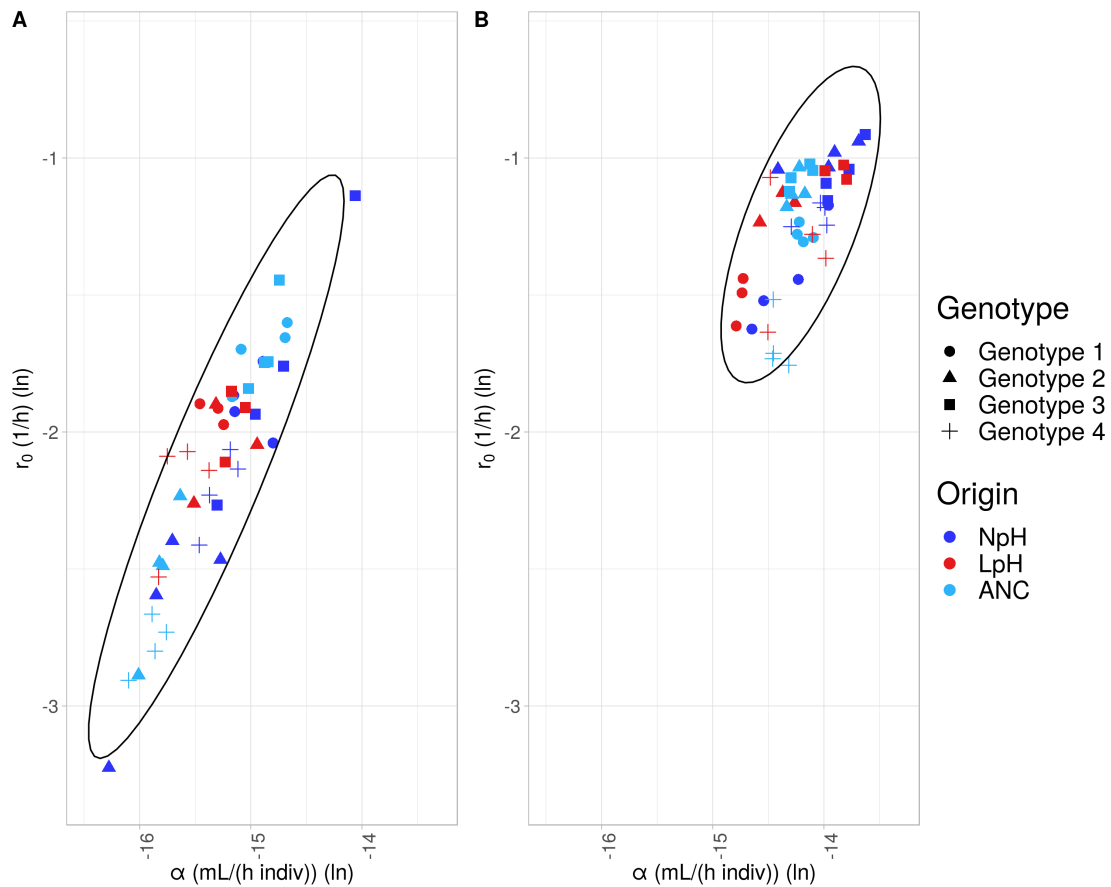


Figure 1.3: Correlation between the intrinsic rate of increase (r_0) and competitive ability (α) at low pH (A), and at neutral pH (B) of the assay medium. Symbols represent the different genotypes (see legend); Light blue = ANC (ancestor populations), dark blue = NpH (populations evolved under neutral pH conditions), red = LpH (populations evolved under low pH conditions). Ellipses represents 95% probability intervals.

At a low pH of the assay medium, r_0 and α showed lower variation for the LpH populations compared to the ANC and NpH populations (Fig. 1.4 panels A-B and I-J; see also Tab. S1.7 in Supporting Information section S.1.8). We did not detect differences in terms of equilibrium population density (K). At a neutral pH of the assay medium, we did not detect differences in variation for the intrinsic rate of increase (r_0), slightly more variation in equilibrium population density (K), and strongly higher variation in

competitive ability (α) of both the LpH and NpH populations compared to the ANC. Note that despite the high relative importance of the evolution variables (Evolved (general evolutionary change), LpH and NpH) for r_0 at neutral pH, the effect size associated with these variables was close to zero. The high relative importance stems from the differences in how the different genotypes responded to the pH treatments, which was captured in the random effects (Fig. 1.4 panels C-D and K-L). In summary, we found a correlation between r_0 and α both at low and neutral pH and found that LpH populations converged in life-history strategy, in the sense that LpH populations became more similar in life-history strategy compared to the ANC populations.

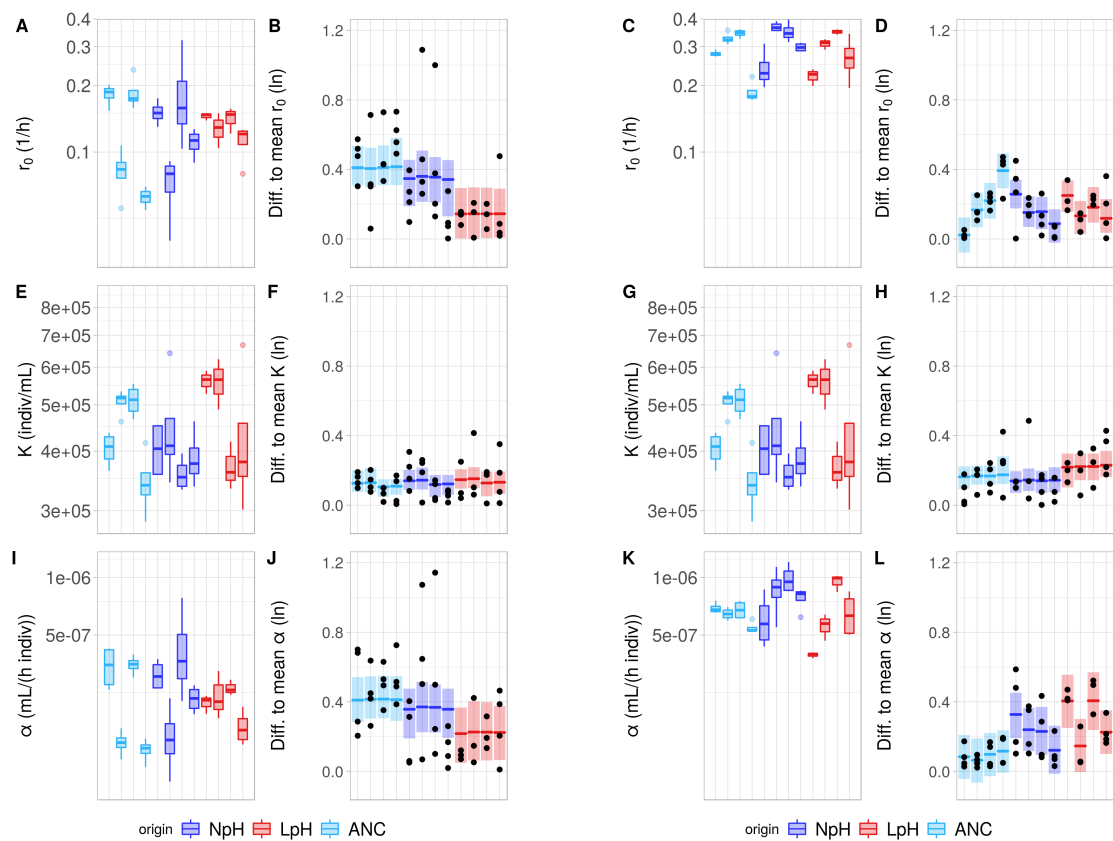


Figure 1.4: Left half of the figure (panels A,B,E,F,I,J) shows data for growth curves measured at low pH of the assay medium, right half (panels C,D,G,H,K,L) for growth curves measured at neutral pH of the assay medium. Traits shown are intrinsic rate of increase (r_0 ; A-D), carrying capacity (K ; E-H) and competitive ability (α ; I-L). Panels A, C, E, G, I and K show r_0 , K and α estimates (1 box plot is 1 genotype). Panels B, D, F, H, J and L show averaged model predictions (mean and 95 % probability interval) of difference between r_0 , K and α estimates and mean per treatment (ANC, LpH or NpH; boxes) and individual datapoints (black dots). Light blue = ANC (ancestor populations), dark blue = NpH (populations evolved under neutral pH conditions), red = LpH (populations evolved under low pH conditions).

Density-dependent fitness

While the evolutionary shifts of the individual population growth parameters were highly variable as described above, we found that under low pH of the assay medium these different changes led to an increase in the overall density-dependent fitness of the LpH populations compared to the ANC population (see also Tab. S1.8 in the Supporting Information section S.1.8). No such increase in density-dependent fitness was observed for the NpH population compared to the ANC populations (see also Supporting information section S.1.9). In both the ANC and LpH populations, density-dependent fitness increased with the intrinsic rate of increase (r_0). The smaller range of r_0 - and α -values for the LpH population (Fig. 1.5 C and Fig. 1.4 panels A,B and I,J) shows the convergence of r_0 discussed above. As exemplified in Fig. 1.5A-B, density-dependent fitness can increase whether r_0 increases or decreases due to correlated changes in competitive ability (α). In ancestral populations where the intrinsic rate of increase (r_0) was initially high (Fig. 1.5A), competitive ability (α) was also high due to the strong correlation between α and r_0 . Consequently density regulation acted strongly in these populations, leading to very slow population growth (r) under high density conditions. Given that densities were typically high during the evolution experiment (Fig. 1.1; Fig. 1.5A), lowering r_0 allowed for increased growth at higher densities and hence an increase in density-dependent fitness. If r_0 was initially very low (Fig. 1.5B), density regulation did not act very strongly, because competitive ability (α) was also very low, and as a population's intrinsic rate of increase (r_0) became higher, the population's fitness increased for all density values, leading to an increase in density-dependent fitness as well. In essence, we found that the observed convergence in life-history traits led to an average increase in density-dependent fitness at low pH for the LpH populations.

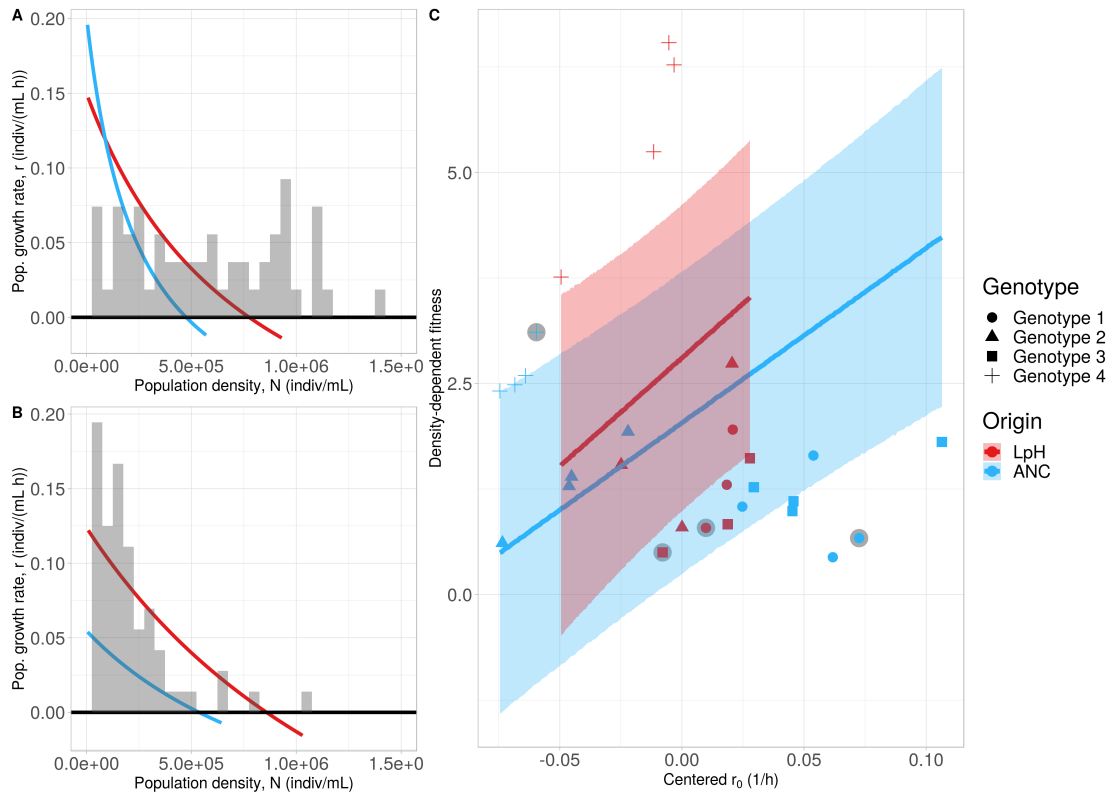


Figure 1.5: Density regulation functions for selected populations where the intrinsic rate of increase (r_0) evolved to decrease (panel A – genotype 1) or increase (panel B – genotype 4) in LpH populations (populations evolved under low pH conditions). Light blue lines show the density regulation functions for the ANC populations (ancestral populations), red lines for the LpH populations. Grey bars show a histogram of the observed population densities during the evolution experiment for the corresponding genotype. C) Density-dependent fitness depending on the (centered) intrinsic rate of increase (r_0). Symbols correspond to data from LpH (red) or ANC (blue) populations (shape represents genotype, see legend). Symbols surrounded by a grey disc represent the example populations of panels A-B. Lines and shaded areas represent the weighted posterior predictions and the 95% probability intervals for the four genotypes. A visual representation of the density regulation function of all replicate populations can be found in the Supporting Information Fig. S1.4 in section S.1.6.

Discussion

In this experiment, we investigated the evolutionary response of the model protist *Tetrahymena thermophila* to pH stress under high population densities. Instead of maximizing the intrinsic rate of increase (r_0) we found that evolution of four different genotypes under low pH and high population density led to a convergence of life-history strategy, that is, genotypes became more similar in life-history strategy (see below). This observation stems, on the one hand, from the high population density (demography) the populations experienced during our experiment, and, on the other hand, from the genetic architecture of life-history traits, where we found that intrinsic rate of increase (r_0) and competitive ability (α) were positively correlated, especially under stressful conditions.

Evolution can help populations adapt to changing environments (Kawecki and Ebert, 2004). Depending on the rate and severity of such change, populations need to respond quickly, as they may otherwise be driven to extinction. Past experiments have demonstrated that evolution can lead to adaptation to an abiotic stressor within few generations (Bell and Gonzalez, 2011; Padfield et al., 2016; Harmand et al., 2018). However, evidence from experimental evolution of such adaptation to pH stress remains relatively limited in many species, and is still more commonly studied using comparative work (Reusch and Boyd, 2013; Stillman and Paganini, 2015, with the notable exception of bacterial evolution experiments, as discussed above). Our results show that populations of the freshwater protist *T. thermophila* can adapt to such stress, even under conditions of strong competition due to high population densities.

Whereas our finding that evolution can alter population performance under abiotic stress agrees with the existing literature (Leimu and Fischer, 2008; Fraser et al., 2011; Kelly and Hofmann, 2013), our results on the direction of evolution were less expected.

Specifically, the observed evolutionary changes in the intrinsic rates of increase (r_0 , Fig. 1.2) showed opposite directions depending on the genetic background. Many evolution experiments are conducted by serially transferring populations into fresh medium (for examples see Lenski and Travisano, 1994; Bell and Gonzalez, 2011; Bono et al., 2017). In such experiments, population densities are low during much of the period of evolution, or at least a distinct phase of selection happens under low density conditions. Under these demographic condition, selection mainly acts on the intrinsic rate of increase (r_0) to maximize fitness (Mueller and Ayala, 1981). In contrast, although we use a similar approach of propagating our populations in this experiment, population densities were kept much higher (always above 50 % of population equilibrium density), leading to strongly different demographic conditions. A growing body of work on eco-evolutionary dynamics and feedbacks (Pelletier et al., 2009; Hendry, 2016) shows that it is important to consider the ecological context, here, the demographic conditions, under which evolution occurs.

This ecological context may affect how selection acts and thus alter evolutionary trajectories. Our results show that when populations evolve under high population densities, we do not find generally increased intrinsic rates of increase (r_0). We suggest that this pattern is driven by the combination of genetic architecture, that is, the linkage between intrinsic rate of increase (r_0) and competitive ability (α), constraining evolutionary trajectories (Fig. 1.3), and by selection for maximizing fitness under pH stress (abiotic conditions) and high population density (biotic factor). Firstly, evolution is constrained in the sense that the intrinsic rate of increase (r_0) is positively correlated with competitive ability (α ; see also Mueller and Ayala, 1981; Reznick et al., 2002; Fronhofer et al., 2018, for a different view see Joshi et al. 2001). This implies that fast growing genotypes will compete more strongly within the population than slow grow-

ing genotypes for available resources when densities increase, which is expected to slow down population growth rate at higher densities.

This slowdown in population growth rate (r) can clearly be seen in Fig. 1.5 (and Fig. S1.4 in the Supporting Information section S.1.6), where genotypes that show initially a high intrinsic rate of increase (r_0 ; high intercept) also show a strong density-dependent decrease in population growth rate (strong curvature). In contrast, populations with lower r_0 show less steep declines in population growth rate. Secondly, since stress associated with low pH strongly decreased population growth rates, LpH populations experienced more difficulty to recover in population size after each medium replacement event compared to NpH populations, and hence were subject to stronger selection for increased population growth. Given that the demographic conditions were such that populations had to grow starting from 50 % of the equilibrium population density, we expect selection to lead to a maximization of population growth rate (r) under these specific densities experienced during evolution, that is, a maximization of density-dependent fitness (as shown in Fig. 1.5C).

Of course, populations may sometimes undergo quasi density-independent growth, for example during range shifts or repeated colonization and extinction events. However, whenever densities are high, growth will be density-dependent. This will often be the case in established populations, which are expected to fluctuate around their equilibrium population density. For example, environmental shifts (acid rain or temperature shifts, for instance) could lead to local changes affecting already well-established populations. As shown in our experiment, adaptation to abiotic stress under such demographic conditions can strongly affect trajectories of evolution, leading to complex evolutionary changes when populations simultaneously need to adapt to abiotic and biotic stress. In addition, as in our experiment, the direction of the evolutionary trajectory may

depend on the starting conditions, and populations with different genetic backgrounds may evolve differently. We speculate here that under these high population density conditions, we can observe convergent evolution in life-history strategy, whereas under low population density conditions, we may instead expect parallel evolution where all populations shift their intrinsic rate of increase (r_0) upwards at low pH. The term convergent evolution has however been defined multiple times (as discussed in Wood et al., 2005; Bolnick et al., 2018; Blount et al., 2018). We here follow the geometric argumentation in Bolnick et al. (2018). We thus define and will use the following terminology to describe evolutionary responses as follows: 1) Convergent evolution occurs when different populations develop more similar phenotypes during evolution, 2) divergent evolution implies that different populations develop more distinct phenotypes during evolution) and 3) parallel evolution occurs when different populations undergo phenotypic changes in the same direction during evolution. We should however also note that our results suggest that within genotypes, evolution happened in parallel, as all replicate populations underwent directional evolution towards either increased or decreased intrinsic rate of increase (r_0), although over all genotypes, we observed convergence to a strategy that optimized the density-dependent fitness of populations.

In agreement with our observation that evolution in response to low pH may be variable, recent work has found no clear consensus on the effect of acidification on species growth rates (Kelly and Hofmann, 2013; Gattuso and Hansson, 2011, chapter 6-7). Also, shorter-term ecological experiments, despite showing a clear positive effect on photosynthesis, found that different species showed strongly differing changes in growth rates to acidification (Gattuso and Hansson, 2011, chapter 6). Similarly, longer-term evolution experiments have demonstrated that intrinsic rate of increase can either increase (Lohbeck et al., 2012; Schlüter et al., 2014) or not (Collins and Bell, 2004)

for populations evolved under conditions of increased CO₂. On a speculative note, our experiment suggests that demographic conditions may be a potential explanatory factor for such divergent results. Taking into account the demographic context and other potentially confounding eco-evolutionary interactions may help to clarify these factors in future work.

In conclusion, we found that demography affected adaptation to low pH in the protist *T. thermophila*, leading to a convergence in life-history strategies and increased high-density fitness. Our work shows that taking into account demography may be key to understanding evolutionary trajectories. In an eco-evolutionary context, quantifying density-regulation functions, that is, population growth rates as a function of population density, may be a useful way forward. Furthermore, although we observe convergent evolution in life-history strategy on a phenotypic level, it remains unclear whether this evolution is also convergent on a genetic level. As noted by Wood et al. (2005), when the genetic basis of traits is simple, convergent evolution often also has a genetic basis, but when the genetic basis is more complex, there are typically multiple paths available leading to similar phenotypic changes. An interesting avenue for future research could be to further study how the observed trade-off between intrinsic rate of increase (r_0) and intraspecific competitive ability (α) translate to the genetic level, as we see a clear trade-off between these traits, that seems phenotypically rather constrained. If such a trade-off also exists on a genetic level, understanding this link may yield new expectations concerning convergent and parallel evolution of populations, both in presence and absence of abiotic and biotic stress.

Author contributions

FM, FA and EAF designed the experiment. FM, AA and SM performed the experimental work. Statistical analyses were done by FM and EAF. FM, FA, AW and EAF interpreted the results. FM, FA and EAF wrote the first version of the manuscript and all authors commented the final version.

Acknowledgements

The authors thank Samuel Hürlemann for help with laboratory work. Funding is from the URPP Evolution in Action and the Swiss National Science Foundation, Grant No PP00P3_179089. This is publication ISEM-2019-284 of the Institut des Sciences de l'Evolution – Montpellier. We would also like to acknowledge support by Swiss National Science Foundation grant 31003A_172887 and by European Research Council Advanced Grant No. 739874. We would like to thank the editorial staff of Evolution and the two referees for the helpful and constructive comments on a previous version of this manuscript.

Data accessibility statement

All data has been made available on Dryad Digital Repository (<https://doi.org/10.5061/dryad.mpg4f4qvg>).

Chapter 2: Evolution in interacting species alters predator life-history traits, behaviour and morphology in experimental microbial communities

Johannes Cairns, Felix Moerman, Emanuel A. Fronhofer, Florian Altermatt and Teppo Hiltunen

Proc. R. Soc. B-Biol. Sci. (2020), 287, 20200652. (doi:10.1098/rspb.2020.0652)

Abstract

Predator–prey interactions heavily influence the dynamics of many ecosystems. An increasing body of evidence suggests that rapid evolution and coevolution can alter these interactions, with important ecological implications, by acting on traits determining fitness, including reproduction, anti-predatory defence and foraging efficiency. However, most studies to date have focused only on evolution in the prey species, and the pred-

ator traits in (co)evolving systems remain poorly understood. Here, we investigated changes in predator traits after approximately 600 generations in a predator–prey (ciliate–bacteria) evolutionary experiment. Predators independently evolved on seven different prey species, allowing generalization of the predator’s evolutionary response. We used highly resolved automated image analysis to quantify changes in predator life history, morphology and behaviour. Consistent with previous studies, we found that prey evolution impaired growth of the predator, although the effect depended on the prey species. By contrast, predator evolution did not cause a clear increase in predator growth when feeding on ancestral prey. However, predator evolution affected morphology and behaviour, increasing size, as well as speed and directionality of movement, which have all been linked to higher prey search efficiency. These results show that in (co)evolving systems, predator adaptation can occur in traits relevant to foraging efficiency without translating into an increased ability of the predator to grow on the ancestral prey type.

Introduction

Predator–prey interactions are ubiquitous across ecosystems. Predation has been widely studied at an ecological level (Lotka, 1925; Volterra, 1928; Rosenzweig and MacArthur, 1963), and recent research also shows that this interaction can be strongly altered by rapid evolution of anti-predatory defence in the prey (Yoshida et al., 2003) as well as by counter-adaptations in the predator (Brodie and Brodie, 1999; Motychak et al., 1999; Hiltunen and Becks, 2014), even though selection may be asymmetric, resulting in slower evolutionary change for the predator (Dawkins et al., 1979). Moreover, owing to population growth–defence trade-offs, rapid evolution of the prey and adaptation to predation can result in frequency-dependent selection of defended and undefended prey

types as a function of predator population size (Meyer et al., 2006; Haafke et al., 2016; van Velzen and Gaedke, 2017), an example of eco-evolutionary feedback dynamics. Common to this spectrum of evolutionary, coevolutionary and eco-evolutionary dynamics is that these dynamics are all driven by natural selection acting on fitness-relevant traits.

Predation can be described by three main phases, namely prey search, capture and ingestion (Matz and Kjelleberg, 2005). These three phases are shaped by key traits in predator–prey systems, including those influencing offence and defence level, and all these traits can be subject to evolutionary change (Abrams, 2000). The offence level is determined by sensory faculties and speed enabling location and capture of prey, and defence level by the capacity for predator avoidance and escape prior to ingestion as well as physico-chemical obstruction of ingestion and digestion (Matz and Kjelleberg, 2005). Adaptations in defence and offence, in turn, combined with associated trade-offs, modulate the reproduction (i.e. life-history traits) of both parties (Huang et al., 2017). Examples abound of the study of the different phases of predation, and adaptation in both predator and prey life-history traits. For example, the timing and population dynamics of many insectivorous bird species are tightly coupled to the dynamics of their prey insect species (Visser et al., 2012). Olive baboon sleeping site choice and behaviour (sharing sleeping sites between multiple baboon groups) in Kenya were recently linked to decreased contact and capture rate by leopards (Bidner et al., 2018). Coevolution has been hypothesized to occur between northern Pacific rattlesnakes and California ground squirrels whereby venom resistance in squirrels is matched by increased venom effectiveness in rattlesnakes based on field data supportive of local adaptation of the traits (Holding et al., 2016).

The empirical examples of evolving predator–prey interactions described above can-

not be used to experimentally investigate (co)evolution in predator–prey systems owing to the long generation times of the species. By contrast, microbial systems offer a unique opportunity to study predator–prey dynamics, as they include efficient (high prey capture rate) predators and allow for high replication as well as experimental approaches capturing both ecological and evolutionary dynamics. Microbial predator–prey systems show many key characteristics found also in other predator–prey systems, such as offence by speed (Visser, 2007) and defence by avoidance of detection (Wildschutte et al., 2004), escape (Matz and Jürgens, 2005) or physico-chemical obstruction of ingestion or digestion (for an overview, see Matz and Kjelleberg 2005). Defence level has also been demonstrated to evolve in controlled set-ups (Lurling and Beekman, 2006; Meyer and Kassen, 2007). However, to our knowledge, there exist little to no empirical studies examining offence mechanisms subject to rapid evolution in microbial predator–prey systems.

Here, we employed an experimental evolution approach to test the influence of approximately 600 generations of predator–prey interaction on predator traits, using a microbial (ciliate–bacteria) model system. Since predator–prey dynamics are characterized by the intrinsically linked dynamics of both interaction partners, we inspected the influence of both prey and predator evolution on predator traits. To find general patterns in predator traits independently of any specific prey species, as most predators have multiple prey species (Closs et al., 1999), we used seven different prey species that were all separately evolved with the predator. We expected rapid evolution of anti-predatory defence in the prey to cause impairment of predator growth (Hiltunen and Becks, 2014; Huang et al., 2017). We expected predator evolution to be weaker, in line with the life–dinner principle (Dawkins et al., 1979; Vermeij, 1994) positing that the prey experiences stronger selection pressure since its survival (life) directly depends

on defence, while the predator can afford a certain measure of unsuccessful prey encounters (dinner postponement). Asymmetric selection can result in dynamics other than classic arms race dynamics such as frequency-dependent cycling of traits (Brodie and Brodie, 1999), which have also been observed in microbial predator–prey systems (Meyer and Kassen, 2007). Nevertheless, instead of escalation where predators alone impose selection pressure, we expected to also observe predator evolution, since coevolution has been demonstrated to occur in bacteria–ciliate systems, in line with the Red Queen hypothesis (Gallet et al., 2009; Hiltunen and Becks, 2014; Huang et al., 2017).

Material and methods

We studied the evolutionary dynamics of one focal predator species (the ciliate *Tetrahymena thermophila*) and seven of its bacterial prey species in all seven combinations of predator–prey species communities, as well as dynamics in prey species populations only. We ran predator–prey evolutionary experiments over approximately 600 predator generations, and assessed evolutionary effects on life-history, morphology and behaviour using common garden experiments.

Strains and culture conditions

The seven prey species used in this study are listed in table 2.1. In addition to four taxa previously used as models in predator–prey studies, three strains were chosen based on representing genera associated with ciliate predators in natural habitats or potentially exhibiting different anti-predatory defence mechanisms (table 2.1). Since each strain represent a single genus, strains are referred to by their genus names in the text.

strain ^a	Rationale for selection
<i>Escherichia coli</i> ATCC 11303	model prey (Hiltunen et al., 2017)
<i>Janthinobacterium lividum</i> HAMBI 1919	pre-/post-ingestion defence: toxin release (Matz and Kjelleberg, 2005)
<i>Sphingomonas capsulata</i> HAMBI 103	model prey (Hiltunen and Laakso, 2013)
<i>Brevundimonas diminuta</i> HAMBI 18	realistic habitat (Becks et al., 2005)
<i>Pseudomonas fluorescens</i> SBW25 (Bailey et al., 1995)	model prey (Hiltunen et al., 2018)
<i>Comamonas testosteroni</i> HAMBI 403	pre-ingestion defence: oversize (Matz and Kjelleberg, 2005)
<i>Serratia marcescens</i> ATCC 13880	model prey (Hiltunen and Laakso, 2013)

Table 2.1: Bacterial strains used in this study. ^a ATCC, American Type Culture Collection; HAMBI, HAMBI mBRC, Microbial Domain Biological Resource Centre HAMBI, University of Helsinki, Finland.

We used a single strain of the asexually reproducing ciliate *T. thermophila* 1630/1U (CCAP; Ketola et al., 2004) as a generalist predator capable of consuming all the prey species. *Tetrahymena thermophila* is a ciliate species characterized by a facultative sexual reproductive cycle and nuclear dualism, where the cells contain a small diploid non-expressed germline nucleus (micronucleus) and a larger highly polyploid somatic nucleus (macronucleus), derived from the micronucleus after sexual reproduction (Ruehle et al., 2016). Only the macronuclear DNA is expressed and hence determines the phenotypic characteristics of *Tetrahymena* cells (Ruehle et al., 2016).

The micronucleus is only relevant for sexual reproduction. The species can be maintained either under settings of recurrent sexual reproduction, or as asexual lineages only. The *Tetrahymena* strain used in our experiment had been maintained in serial propagation for many years before the experiments. Sexual reproduction only occurs when induced by starvation (Lynn and Doerder, 2012), and because this was not the case during its long-term maintenance, the strain only underwent asexual reproduction. During asexual reproduction, micronuclei and macronuclei divide independently from each other (Ruehle et al., 2016). It has been noted that, when cultured for a long time asexually, the micronuclei can degrade (Cassidy-Hanley, 2012) and have subsequent negative effects on the genotype's fitness during a possible sexual reproduction, or even lead to genotypes losing their ability to reproduce sexually. However, given that micronuclei are never expressed and only play a role in sexual reproduction (Ruehle et al., 2016), and also given that we do not induce or study the genotype's ability to reproduce sexually, this possible degradation of the micronucleus does not have consequences on fitness as measured in our setting. We also note that it is a common practice to use *Tetrahymena* cell lines with non-functional micronuclei, as described in the standard handbook for *Tetrahymena* cell biology work (Cassidy-Hanley, 2012). In all of these cases, the serial propagation is not problematic as long as one is not inducing sexual reproduction. Hence, any evolution observed at the predator level in this experiment stems from either mutations or selection on existing variation in the macronuclear DNA. Furthermore, as the macronucleus is highly polyploid ($n = 45$), and chromosomes divide randomly during asexual reproduction (Ruehle et al., 2016), cells are relatively buffered to the effects of single maladaptive mutations, and can undergo relatively rapid purging of maladaptive mutations or selection for increased copies of adaptive mutations. This, together with the absence of sexual reproduction, which can

be affected by serial propagation (Cassidy-Hanley, 2012), makes it highly unlikely that the serial propagation set-up in the experiment would itself strongly influence the evolutionary dynamics of the predator.

Prior to the experiments, all bacterial stocks were kept at -80°C and ciliate stocks were cultured axenically in proteose peptone yeast extract (PPY) medium containing 20 g of proteose peptone and 2.5 g of yeast extract in 1 L of deionized water. During the evolutionary experiment, cultures were kept at 28°C ($\pm 0.1^{\circ}\text{C}$) with shaking at 50 r.p.m.

Predator-prey evolutionary experiment

The evolutionary experiment was started using a small aliquot (20 μL) of a 48 h bacterial culture started from a single colony and 10 000 ciliate cells (approx. 1700 cells mL^{-1}) from an axenic culture. Each bacterial strain was cultured alone and together with the ciliate predator (three replicates each, with the exception of six replicates for *Comamonas*) in batch cultures of 20 mL glass vials containing 6 mL of 5 % King's B (KB) medium, with 1 % weekly transfer to fresh medium.

Every four transfers (28 days), bacterial and predator densities were estimated using optical density (1 mL sample at 600 nm wavelength) as a proxy for bacterial biomass and direct ciliate counts ($5 \times 0.5 \mu\text{L}$ droplets using light microscopy) as used in this context and described previously (Cairns et al., 2016; Hiltunen et al., 2018; Cairns et al., 2018), and samples were freeze-stored with glycerol at -20°C for later analysis. Since predators do not survive freeze-storage in these conditions, at time points 52 and 89 weeks, predator cultures were made axenic by transferring 400 μL into 100 mL of PPY medium containing an antibiotic cocktail (42, 50, 50 and 33 $\mu\text{g mL}^{-1}$ of kanamycin, rifampicin,

streptomycin and tetracycline, respectively) and stored in liquid nitrogen. Axenicity was controlled for by plating on agar plates containing 50 % PPY medium, on which all the experimental bacterial strains grow. The liquid nitrogen storage protocol was modified from a previously used protocol (Cassidy-Hanley, 2012) and included starving a dense ciliate culture in 10 mM Tris-HCl solution (pH 7) for 2–3 days, centrifugation (1700g, 8 min, 4 °C), resuspension of the pellet in 1 mL of leftover supernatant and the addition of 4 mL of sterile 10 % dimethyl sulfoxide (DMSO). The resultant solution was transferred to cryotubes in 0.3 mL lots, and frozen in a $-20\text{ }^{\circ}\text{C}$ freezer at a rate of $-1\text{ }^{\circ}\text{C min}^{-1}$ using a Mr Frosty™ Freezing Container (Thermo Scientific) for cell preservation before transferring to liquid nitrogen.

Sample collection and preparation

We isolated the populations for the current experiment at time point 89 weeks (approx. 20 months). With the minimal assumption that populations multiply by 100-fold (dilution rate) until reaching the stationary phase, each weekly transfer interval represents 6.64 generations for both prey and predator (Lenski et al., 1991), constituting a total minimum of approximately 600 generations. Community dynamics are shown in Supporting Information figures S1 and S2 and demonstrate clear differences in population size between different prey species.

Bacteria were restored from freeze-storage by transferring 20 μL into 5 mL of 5 % KB medium and culturing for 72 h. Predators were restored from liquid nitrogen by thawing cryotubes in a $42\text{ }^{\circ}\text{C}$ water bath for 15 s, followed by the addition of 1 mL of $42\text{ }^{\circ}\text{C}$ PPY medium. The cryotube contents were then transferred to a Petri dish containing PPY medium at room temperature. Upon reaching a high density (approx. 48 h),

predators were transferred to 100 mL of PPY medium and cultured to a high density (approx. 7 days). To ensure that the antibiotic treatment or the liquid nitrogen storage and revival procedures do not contribute to potential differences between the ancestral predator and evolved predator lines, the axenic ancestral predator was subjected to identical procedures and was revived at the same time as the evolved lines. These culturing steps representing over 10 generations should remove the influence of non-genetic changes in predator traits caused by phenotypic plasticity (Fronhofer and Altermatt, 2015).

Physiological measurements

To test bacterial and ciliate performance and traits, we used a combination of automated video analysis, optical density measurements and flow cytometry. To separate evolutionary responses at the predator and prey level, we tested performance of both evolved and ancestral bacteria with evolved and ancestral ciliates for all evolved lines reciprocally. To do so, we prepared 12 50 mL Falcon® tubes by adding 20 mL of 5 % KB medium. Three of these were inoculated with ancestral bacteria and ancestral ciliates, three with ancestral bacteria and evolved ciliates, three with evolved bacteria and ancestral ciliates and the remaining three with evolved bacteria and evolved ciliates. We placed the Falcon® tubes in a 28 °C incubator, rotating on a shaker at 120 r.p.m. After inoculation, the samples were left to grow for a period of 12 days, to allow populations to grow to equilibrium density. Over the course of these 12 days, we took a total of 10 samples from each culture for analysing population density dynamics of bacteria and ciliates, and morphological and behavioural metrics for the ciliates. We sampled cultures by gently shaking the culture, to ensure it was well mixed and subsequently pipetting out 200 µL from the mixed culture.

Bacterial density measurements

Bacterial density was determined both through measurement of optical density and through flow cytometry. Flow cytometric analyses were based on established protocols (Hammes and Egli, 2005; Hammes et al., 2008) that facilitate distinction between living bacterial cells and background signals (e.g. dead cells or abiotic matter). For flow cytometry, we sampled 50 μL of all cultures, diluted the samples 1:1000 using filtered Evian water and transferred 180 μL of the diluted samples to a 96-well-plate. We then added 20 μL of SybrGreen to stain the cells and measured bacterial cell counts using a BD Accuri™ C6 flow cytometer. As the inner diameter of the needle from the flow cytometer was 20 μm , and hence smaller than typical ciliate cell sizes, it is highly unlikely that ciliate cells were accidentally measured during flow cytometry. Also, given that bacterial densities were typically between one and five orders of magnitude larger than ciliate densities, even an occasional measurement of ciliate cells would have a negligible effect on bacterial density estimates. The full protocol can be found in the Supporting Information. For optical density measurement, we sampled 50 μL of all cultures, diluted 1:10 using filtered Evian water, and measured absorbance at 600 nm using a SpectroMax 190 plate reader.

Ciliate density and trait measurements

For measuring ciliate density, we performed video analysis (Altermatt et al., 2015) using the BEMOVI R-package (Pennekamp et al., 2015). We followed a previously established method (Fronhofer et al., 2017b) where we took a 20 s video (25 frames/s, 500 frames) of a standardized volume using a Leica M165FC stereomicroscope with circular lighting and mounted Hamamatsu Orca Flash 4.0 camera. We then analysed the

videos using BEMOVI (Pennekamp and Schtickzelle, 2013; Pennekamp et al., 2015), which returns information on the cell density, morphological traits (longest and shortest cell axis length) and movement metrics (gross speed and net speed of cells, as well as turning angle distribution). The video analysis script, including used parameter values, can be found in the Supporting Information.

Data analysis

All statistical analyses were done using the R statistical software (v. 3.5.1; R Core Team, 2017). To obtain the reported F- and p-values for predator traits, we performed ANOVA for the best linear models constructed for the different traits as described below.

Predator trait space

To visualize whether the full set of trait data displayed structure depending on the evolutionary history of the predator and prey species, t-distributed stochastic neighbour embedding (t-SNE) was performed for each prey species separately using the Rtsne package (Krijthe, 2015) with a perplexity parameter of 3 owing to small sample size.

Beverton-Holt model fitting

For analysing the population growth dynamics of the ciliates, we implemented the Beverton–Holt population growth model (Beverton and Holt, 1993, Supporting Information, figure S3) using a Bayesian framework in RStan (Stan Development Team, 2018), following methods used by the authors in Fronhofer et al. (2018); Rosenbaum et al. (2019). This function has the form of

$$\frac{dN}{dt} = \left(\frac{r_0 + d}{1 + \alpha N} - d \right) N, \quad (3)$$

with r_0 being the intrinsic rate of increase, α the intraspecific competitive ability and d being the death rate in the population. Model code for fitting this function can be found in a Github repository (doi:10.5281/zenodo.2658131). For fitting this model, we needed to provide prior information for r_0 , d and equilibrium density K . The intraspecific competitive ability α was later derived from the other parameter values as

$$\alpha = \frac{r_0}{Kd} \quad (4)$$

The priors (lognormal distribution) of the model were chosen in such a way that the mean estimates lay close to the overall observed means, but were broad enough so the model was not constrained too strongly:

- equilibrium population density K : $\ln(K) \sim normal(9.21, 0.5)$,
- intrinsic rate of increase r_0 : $\ln(r_0) \sim normal(-2.3, 0.5)$,
- rate of mortality d : $\ln(d) \sim normal(-2.3, 0.5)$.

Models were run with a warm-up of 2000 iterations and a chain length of 8000 iterations.

Life-history trait analysis

We analysed the estimates of the life-history traits obtained from the Beverton–Holt model fit (r_0 , α and K) using linear models and model selection. We first constructed a full model with life-history traits being a function of bacterial evolutionary history

(evolved/ancestor), ciliate evolutionary history (evolved/ancestor) and bacterial species (seven species factors) in a full interaction model. Next, we used automated bidirectional model selection using the step function (stats package v.3.5.1) to find the best model. To avoid bias due to starting point, we fitted the model starting from both the intercept model and the full model, and if model selection resulted in different models, we used sample-size adjusted Akaike Information Criterion (AICc) comparison (MuMIn R-package, v.1.42.1; Bartoń 2009) to select the model with the smallest AICc value.

Morphological and behavioural trait analysis

Morphological and behavioural data were available for every time point during the growth curve, and since we know these traits can be plastically strongly affected by density (Fronhofer et al., 2015, 2017a), we had to take density into account in the model. We hence separated the analysis into two steps: first, we identified key points in the growth curves (early phase, mid-log phase and equilibrium density phase) and analysed the traits for these particular points. Secondly, we fitted models over all data, but taking bacterial (using flow cytometry data) and ciliate densities into account as covariates in the statistical analysis.

We defined the early phase as the second time point in the time series, equilibrium density phase as the first time point where density was larger than 99 % of K , or alternatively the highest density, and the mid-log phase as the point between the early and equilibrium density phase where density was closest to 50 % of K . We then created statistical models for the traits (major cell axis size, gross speed of cells and turning angle distribution) as a function of bacterial evolutionary history (evolved/ancestor), ciliate evolutionary history (evolved/ancestor) and bacterial species (seven species factors),

including a full interaction for the data at the particular time point. Next, we used automated bidirectional model selection to find the best-fitting model. This was done separately for all three phases (early, mid-log and equilibrium density phases). We again performed model selection starting from both the intercept model and full model, and compared the two models using AICc comparison to identify the best model.

We then created models using all the data, where we fitted major cell axis size, gross speed and turning angle distribution as a function of bacterial evolutionary history (evolved/ancestor), ciliate evolutionary history (evolved/ancestor) and bacterial species (seven species factors), ciliate population density (ln-transformed, continuous) and bacterial population density (ln-transformed, continuous), including a full interaction. For turning angle, we also did a \log_{10} transformation of the turning angle distributions, as fitting the model on untransformed data leads to a strong deviation on the qqplot. Next, we used automated bidirectional model selection using the step function starting from intercept model and full model, and compared the two models using AICc comparison to select the best model.

Results

The t-SNE maps (figure 2.1) showed that the evolutionary history of the predator and prey species frequently resulted in predator divergence in trait space. Importantly, this divergence evolved from a single ancestral predator population, which was subjected to co-culture with different prey species. The full results for all statistical analyses presented below to assess this divergence in detail are available in the Supporting Information.

Prey evolution drove changes in the life-history traits of the predator, including

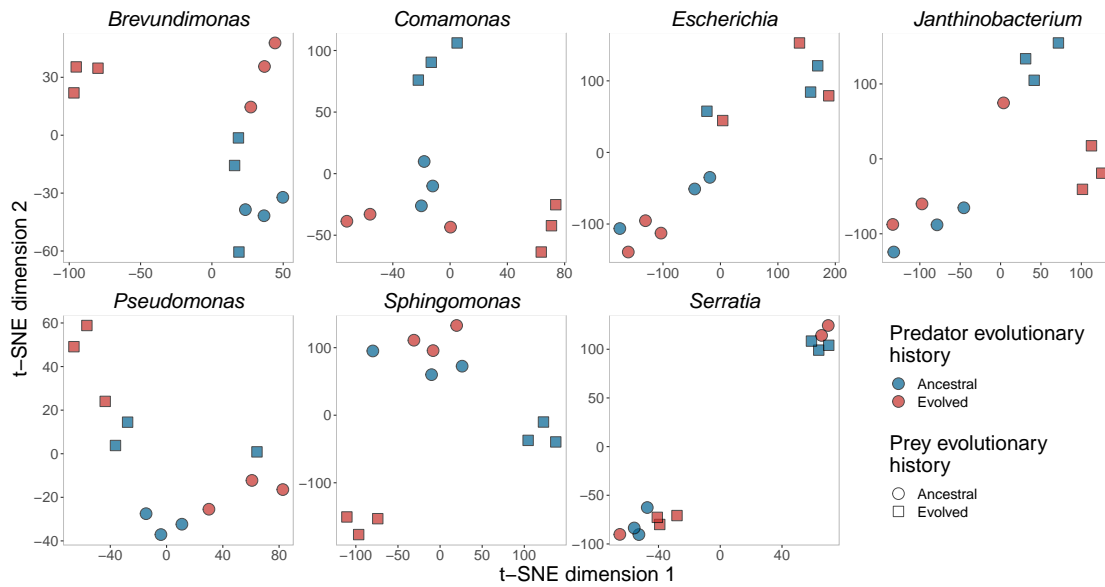


Figure 2.1: t-SNE map of contribution of predator and prey evolutionary history to predator divergence in trait space. The traits included in the analysis encompass life history (intrinsic growth rate, equilibrium density and competitive ability), morphology (cell size and biovolume) and behavior (speed and cell turning angle distribution).

intrinsic rate of increase (r_0), equilibrium density (K) and competitive ability (α), although the presence and strength of the effect depended on the bacterial species (ANOVA, r_0 : prey evolution $F_{1,78} = 15.32$, $p < 0.001$; prey evolution \times prey species $F_{6,78} = 9.03$, $p < 0.001$; K : prey evolution \times prey species $F_{6,80} = 13.7$, $p < 0.001$; α : prey evolution $F_{1,78} = 4.79$, $p = 0.031$; prey evolution \times prey species $F_{6,78} = 5.40$, $p < 0.001$; Supporting Information, tables S1–S3 and S7–S9; figure 2.2). The intrinsic rate of increase of ciliates (r_0) was generally lower in the presence of evolved bacterial prey compared with ancestral prey, with the notable exception of *Serratia*, where intrinsic rate of increase was higher in the presence of evolved prey (table 2.2 and figure 2.2). For three species (*Brevundimonas*, *Janthinobacterium* and *Pseudomonas*), evolved predators had a higher intrinsic rate of increase (r_0) on evolved prey compared with ancestral prey (figure 2.2). Changes in population equilibrium density (K) were highly depend-

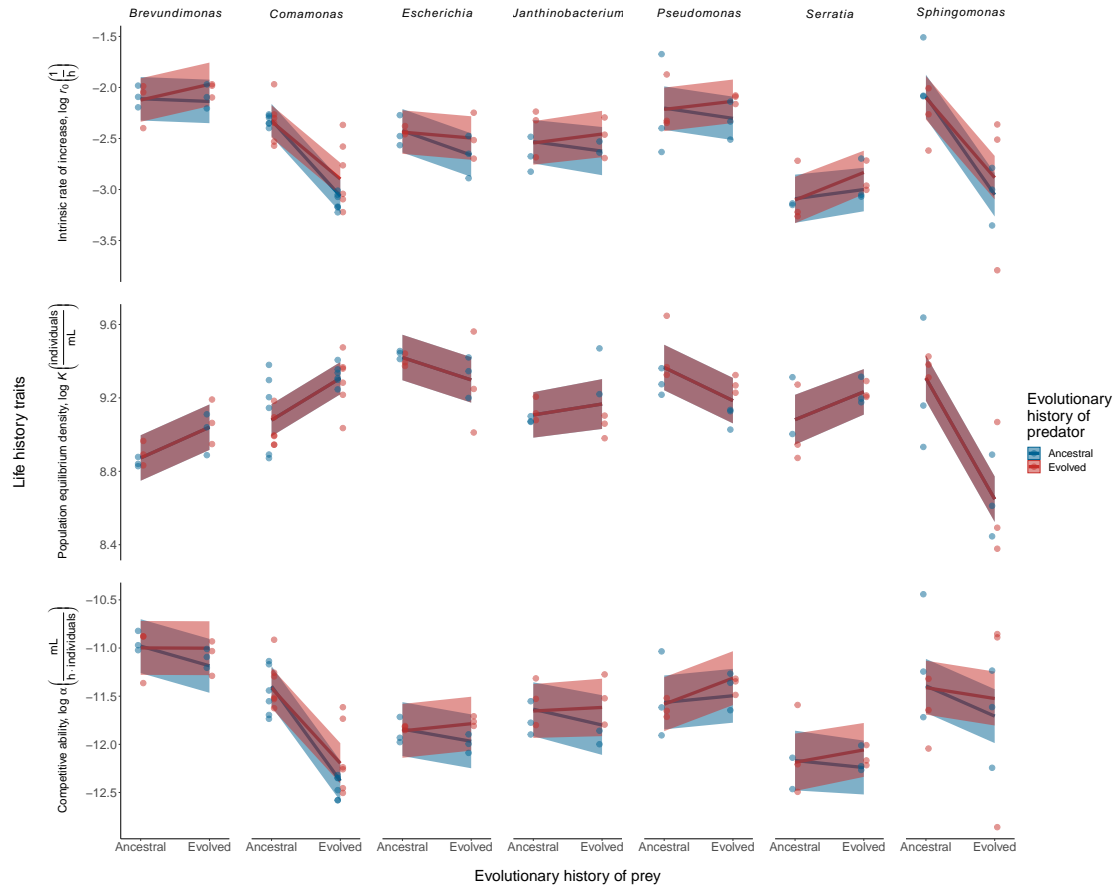


Figure 2.2: Reaction norms showing effect of evolving predator-prey interaction on life-history traits of predator (data points with linear model estimate $\pm 95\%$ confidence intervals.; $N = 3$ except 6 for *Comamonas*). The life-history traits for predators are parameters of Beverton-Holt continuous-time population models fitted to data, and include intrinsic growth rate (r_0), equilibrium density (K) and competitive ability (α). The reaction norms for predators (one strain of the ciliate *Tetrahymena thermophila*) feeding on ancestral or evolved prey (seven bacterial strains indicated by genus name) are depicted separately for ancestral and evolved predators (color coding). Predators evolved with a particular prey taxon have always been coupled with ancestral or evolved populations of the same taxon, while the ancestral predator is the same for all prey taxa.

ent on species, with four species (*Brevundimonas*, *Comamonas*, *Janthinobacterium* and *Serratia*) showing higher population equilibrium density in the presence of evolved prey compared with ancestral prey, and the remaining three (*Escherichia*, *Pseudomonas* and *Sphingomonas*) showing decreased population equilibrium density in the presence of evolved prey compared with ancestral prey. Competitive ability (α) typically decreased in the presence of evolved prey compared with ancestral prey, with the exception of *Pseudomonas*, where competitive ability was higher in the presence of evolved bacteria compared with ancestral bacteria. Notably, for *Escherichia*, *Janthinobacterium* and *Serratia*, the competitive ability (α) of evolved predators was higher in the presence of evolved prey compared with ancestral prey (figure 2.2).

In contrast with life-history traits, which were affected by prey evolution alone, morphological and behavioural traits of the predator were affected by predator evolution (figure 2.3). However, the effect size of predator evolution was also strongly dependent on predator density (for the movement metrics gross speed and turning angles) or both predator and prey density (for the biovolume metric cell size). Evolved predators were slightly but significantly larger than ancestral predators (ANOVA: predator evolution $F_{1,767} = 7.87$, $p = 0.005$). Although there was a significant effect indicating that this was modulated by the evolutionary history of the prey (ANOVA: prey evolution $F_{1,767} = 4.85$, $p = 0.033$), the associated effect size was much smaller than predator evolution. On average, evolved predators were 39.12 μm larger than ancestral predators, and predators were on average 1.629 μm smaller in the presence of evolved prey compared with ancestral prey. The effect of predator evolution also depended strongly on prey densities (ANOVA: log prey density \times predator evolution $F_{1,767} = 6.87$, $p = 0.009$; figure 2.3). The strongest differences in cell size between ancestral and evolved predators were observed at low prey densities (cell sizes 1.2–1.3 times larger for evolved compared with

ancestral ciliates), whereas the effects were negligible at high prey densities (approximately equal size for evolved and ancestral ciliates; Supporting Information, tables S4 and S10 and figures S4–S6; figure 2.3).

Prey species	Predator evolution	r_0 -ratio	K -ratio	α -ratio
<i>Escherichia</i>	ancestor	0.788	0.885	0.881
<i>Escherichia</i>	evolved	0.943	0.885	1.08
<i>Janthinobacterium</i>	ancestor	0.912	1.06	0.849
<i>Janthinobacterium</i>	evolved	1.09	1.06	1.04
<i>Sphingomonas</i>	ancestor	0.381	0.517	0.730
<i>Sphingomonas</i>	evolved	0.457	0.517	0.893
<i>Brevundimonas</i>	ancestor	0.974	1.18	0.815
<i>Brevundimonas</i>	evolved	1.17	1.18	0.997
<i>Pseudomonas</i>	ancestor	0.904	0.835	1.07
<i>Pseudomonas</i>	evolved	1.08	0.835	1.31
<i>Comamonas</i>	ancestor	0.475	1.26	0.374
<i>Comamonas</i>	evolved	0.569	1.26	0.457
<i>Serratia</i>	ancestor	1.09	1.16	0.930
<i>Serratia</i>	evolved	1.31	1.16	1.14

Table 2.2: Predicted change in intrinsic rate of growth (r_0), population equilibrium density (K) and competitive ability (α) in the presence of evolved bacteria compared with ancestral bacteria according to the linear models. The r_0 -, K - and α -ratios are calculated as the predicted trait value (r_0 , K or α) in the presence of evolved bacteria divided by the predicted trait value in the presence of ancestral bacteria. Note that for the K -ratio, since predator evolution is excluded during model selection, predictions for ancestral and evolved predators are identical.

The gross movement speed of predators depended on the interplay between predator

density and predator or prey evolutionary history. Evolved predators had, on average, up to 1.25 times higher speed compared to ancestral predators. However, this effect occurred for evolved predators at high predator densities, whereas at low predator densities, movement speed was approximately similar for ancestral and evolved ciliates (ANOVA: predator density $F_{1,763} = 116.20$, $p < 0.001$; predator evolution $F_{1,763} = 1.90$, $p = 0.239$; predator evolution \times predator density $F_{1,763} = 4.36$, $p = 0.037$; figure 2.3). This effect was partially counteracted by prey evolution by driving speed to a lower rate at increasing predator densities (ANOVA: prey evolution $F_{1,763} = 2.17$, $p = 0.141$; prey evolution \times predator density $F_{1,763} = 5.46$, $p = 0.020$). The movement speed of ciliate cells was also dependent on the identity of the prey species, with ciliates moving slower when subjected to three particular prey species (*Janthinobacterium*, *Pseudomonas* and *Serratia*; ANOVA: prey evolution $F_{6,763} = 9.11$, $p < 0.001$; Supporting Information, tables S5 and S11 and figure S7). Finally, predator evolution altered cell turning angle distributions across prey species such that evolved predator lines moved in straighter trajectories (ANOVA: predator evolution $F_{1,56} = 10.15$, $p = 0.001$). This effect was again highly dependent on predator population size, with evolved predators turning at approximately 0.92 times the turning rate of ancestral predators at low predator density, but turning equally as much at high predator density (ANOVA: predator density $F_{1,763} = 33.90$, $p < 0.001$; predator evolution \times predator density $F_{1,763} = 5.44$, $p = 0.02$; figure 2.3). The effect of predator population size was also dependent on prey species, such that for three prey species (*Janthinobacterium*, *Pseudomonas* and *Serratia*), evolved predators moved even straighter (less turning) at higher predator densities (ANOVA: predator density \times prey species $F_{1,763} = 6.76$, $p < 0.001$; Supporting Information, tables S6 and S12 and figures S8–S10).

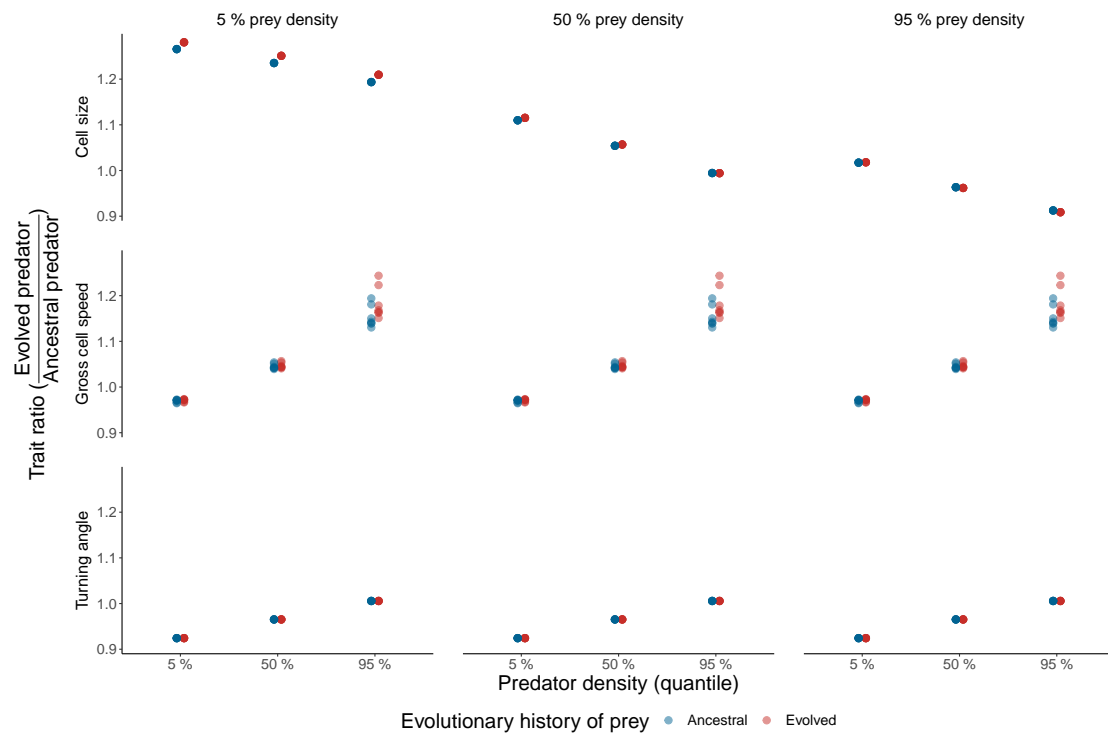


Figure 2.3: Ratios of the predicted trait values of the linear models (cell size, gross cell speed and turning angles) for the evolved predator divided by the ancestral predator at different prey densities (5 %, 50 % and 95 % quantiles) and predator densities (5 %, 50 % and 95 % quantiles). Ratios represent how ciliate traits differ between evolved and ancestral ciliates, with values of one meaning evolved and ancestral ciliates are identical, values larger than one meaning higher trait values for evolved strains, and values smaller than one higher trait values for ancestral ciliates.

Discussion

We quantified the contribution of predator and prey evolution to predator trait change across seven different prey species in a 20-month (approx. 600 predator generations) co-culture experiment. Prey evolution frequently led to changes in predator life-history traits, decreasing intrinsic growth rate, equilibrium density or competitive ability, while not affecting morphological or behavioural traits in the predator. Interestingly, the strength of the effect and the life-history trait affected depended on the prey species. These results may be influenced by different growth dynamics, defence levels or defence mechanisms of the different prey species (table 2.1; Supporting Information, figures S1 and S2; Matz and Kjelleberg, 2005).

For two of the predator life-history traits, intrinsic rate of increase (r_0) and competitive ability (α), the trait was impaired, with evolved compared with ancestral prey in all except for two cases (*Serratia* for r_0 and *Pseudomonas* for α). This could be caused by any mechanism of prey defence evolution decreasing effective prey population size or increasing prey handling time, including cell aggregation of bacterial prey, frequently shown under ciliate predation (Hall et al., 2008; Friman et al., 2014). While a similar result was also observed for population equilibrium density (K) with three prey species (*Escherichia*, *Pseudomonas* and *Sphingomonas*), intriguingly, the remaining four prey species (*Brevundimonas*, *Comamonas*, *Janthinobacterium* and *Serratia*) showed higher K in the presence of evolved compared with ancestral prey. This counterintuitive result may be caused by resource use evolution, which can occur rapidly in bacterial evolutionary experiments (Lenski et al., 1991) but differ in magnitude between bacterial (i.e. prey) species. In this situation, a sufficient increase in prey population size could sustain a higher predator population size despite anti-predatory defence evolution.

Consistent with the Red Queen hypothesis, evolved predators displayed both behavioural and morphological changes linked to prey foraging efficiency. Increased swimming speed and body size were observed for evolved predators with certain prey species, and predators evolved to swim in straighter trajectories across the different prey species. Increased swimming speed and decreased cell turning (i.e. moving in straighter trajectories) have both been linked to prey search efficiency (Crawford, 1992; Zollner and Lima, 1999; Visser, 2007), and in line with this, ciliates have been shown to display decreased cell turning and increased speed at low food concentrations (Buskey and Stoecker, 1988). The role of increased body size is less clear but may also be related to increased prey search efficiency since swimming speed can be a function of body size (Crawford, 1992; Visser, 2007). All these evolutionary trait changes in the predator are consistent with being adaptations to decreased food availability owing to anti-predatory defence evolution in the prey species.

Interestingly, against our expectation based on the Red Queen hypothesis, we did not find detectable levels of adaptation in predator life-history traits when prey-evolved predators fed on their respective ancestral prey species. This could be indicative of asymmetry of selection (Brodie and Brodie, 1999; Meyer and Kassen, 2007) such that predators experience weaker selection pressure compared with prey owing to the life-dinner principle (Dawkins et al., 1979), whereby prey species rely on adaptation (needed to stay alive) more strongly than predators (needed to increase energy uptake). Asymmetric evolutionary change for ciliate predators could also result from smaller population size (in the order of $1 \times 10^4 \text{ mL}^{-1}$ for ciliates compared to $1 \times 10^8 \text{ mL}^{-1}$), larger genome size (greater than 100 Mb for *T. thermophila* compared to less than 10 Mb for bacteria) or more complex genomic architecture limiting adaptive mutation supply compared with the bacterial prey (Eisen et al., 2006).

There are two ways asymmetric selection could account for our unexpected result regarding the lack of evolution in ciliate life-history traits. First, the offence-related traits (morphology and behaviour) where predator evolution was observed may simply not have improved sufficiently to be detectable as increased predator growth on ancestral prey using our methods. Although the culture conditions were mostly identical between the serial passage experiment and ciliate physiology measurements (same culture medium, temperature, covering 7-day time span representing serial passage culture cycle), it is also possible that minor differences in experimental conditions (different culture vials, volumes and shaking parameters) or the revival of ciliates from liquid nitrogen storage could have introduced noise in the data, masking ciliate evolution in life-history traits. Second, rapid evolution in the prey species may have changed basic features of the prey population early on in the experiment, such as causing cell aggregation, which is widely documented to evolve rapidly in similar setups (Lurling and Beekman, 2006; Meyer and Kassen, 2007; Hall et al., 2008; Friman et al., 2014). An improved ability of the predator to feed on defended prey with altered characteristics may not allow for an improved ability to also feed on ancestral prey. For instance, higher speed and directionality of movement may be useful when feeding on unevenly distributed prey aggregates while not causing a benefit when feeding on prey as homogeneously distributed single cells (food being always closely available). Alternatively, as a more complex explanation, a steepening growth–offence trade-off during coevolution (Huang et al., 2017) could cause stunted growth in coevolved high-offence-level predators, which may, therefore, only display a net fitness improvement against prey in a recent evolutionary state. Since our sample material represents a snapshot from the endpoint of a long-term (co)evolutionary experiment, further experiments would be needed to assess the dynamics of predator trait change over time to test these hypotheses.

Our findings have implications for interpreting data from (co)evolving predator–prey systems. First, the pronounced impairment of predator growth traits upon prey evolution together with the lack of clear improvements in the ability of evolved predators to feed on ancestral prey types support the asymmetric selection hypothesis. Second, the occurrence of predator evolution in other key traits for predator–prey interaction despite this suggests that tracking ecological changes alone may result in an underestimation of predator evolution (Cairns et al., 2019; Kaitala et al., 2020). A deeper understanding of predator–prey evolutionary dynamics is, therefore, likely to critically depend on the identification and examination of key traits for the interaction, preferably over time and including both interaction partners.

Author contributions

J.C. and T.H. designed the coevolutionary experiment. J.C. performed and managed the experiment and wrote the draft manuscript. F.M., E.A.F. and F.A. designed and performed physiological measurements. F.M. and J.C. analysed data. All authors interpreted results and participated in improving the manuscript.

Acknowledgements

This work was funded by the Academy of Finland (T.H.; project no. 106993), the University Research Priority Program (URPP) ‘Evolution in Action’ of the University of Zurich and the Swiss National Science Foundation (grant no. PP00P3_179089, to F.A.) and the Jenny and Antti Wihuri Foundation (grant no. 00190040, to J.C.). We thank Veera Partanen for technical help with maintaining the coevolutionary experiment and reviving samples for the physiological measurements. We thank Samuel Hürlemann for help during the laboratory work. We thank two reviewers for constructive comments on a previous version of the manuscript. This is publication ISEM-2020-16 of the Institut des Sciences de l’Evolution–Montpellier.

Data accessibility statement

All code and pre-processed data needed to reproduce the ecological and evolutionary analyses are available from the Dryad Digital Repository: <https://doi.org/10.5061/dryad.08kpr4zr> (Cairns et al., 2020).

Chapter 3: Gene swamping alters evolution during range expansions in the protist *Tetrahymena thermophila*

Felix Moerman, Emanuel A. Fronhofer, Andreas Wagner and Florian Altermatt

Biol. Lett. (2020), 16, 20200244. (doi:10.1098/rsbl.2020.0244)

Abstract

At species' range edges, individuals often face novel environmental conditions that may limit range expansion until populations adapt. The potential to adapt depends on genetic variation upon which selection can act. However, populations at species' range edges are often genetically depauperate. One mechanism increasing genetic variation is reshuffling existing variation through sex. Sex, however, can potentially limit adaptation by breaking up existing beneficial allele combinations (recombination load). The gene swamping hypothesis predicts this is specifically the case when populations expand along an abiotic gradient and asymmetric dispersal leads to numerous maladapted dispersers from the range core swamping the range edge. We used the ciliate *Tetra-*

hymena thermophila as a model for testing the gene swamping hypothesis. We performed replicated range expansions in landscapes with or without an pH-gradient, while simultaneously manipulating the occurrence of gene flow and sexual versus asexual reproduction. We show that sex accelerated evolution of local adaptation in the absence of gene flow, but hindered it in the presence of gene flow. However, sex affected adaptation independently of the pH-gradient, indicating that both abiotic gradients and the biotic gradient in population density lead to gene swamping. Overall, our results show that gene swamping alters adaptation in life-history strategies.

Introduction

Individuals living at the edge of a species' range face different conditions compared to those in the core region. Selection pressures differ, and often the individuals at the edge represent only a small subset of a species' genetic variation (Chuang and Peterson, 2016). The potential of a population to spread depends on the capacity to disperse and the ability to grow in the local abiotic environment (Skellam, 1951). Consequently, when populations expand their range, they experience strong selection due to the range expansion itself, and are also affected by concurrently changing environmental conditions.

During range expansions, populations can undergo rapid evolution, as demonstrated by recent comparative and experimental work (Chuang and Peterson, 2016), showing evolution of increased dispersal (Simmons and Thomas, 2004; Fronhofer and Altermatt, 2015; Ochocki and Miller, 2017; Weiss-Lehman et al., 2017), r-selected life-history strategies (Therry et al., 2014; Phillips et al., 2010), and adaptation to abiotic conditions (Van Petegem et al., 2016; Szűcs et al., 2017). Expanding into previously uninhabited

space allows populations to escape intraspecific competition. Consequently, evolving in response to multiple selective pressures can potentially lead to substantial benefits, despite the challenges involved (Brook and Bradshaw, 2006; Phillips et al., 2010).

A major modulator of evolution is sex. Sex allows populations to reshuffle existing genetic variation (Smith, 1978; Bell, 1982; Kondrashov, 1993; Otto and Lenormand, 2002). Theoretical work suggests that sex would typically lead to offspring with lower fitness, by breaking up advantageous allele combinations (recombination load), and hence an advantage for asexual reproduction (Otto, 2009). However, populations during range expansion experience strong stochasticity due to repeated founder events, leading to maladaptive mutations becoming fixed and surfing along at the range edge (expansion load; Klopstein et al., 2006; Excoffier et al., 2009). Sex can strongly reduce these negative effects of expansion load, thus making it advantageous (Excoffier et al., 2009; Keller and Taylor, 2010; Peischl et al., 2015).

If populations face strong abiotic stressors or heterogeneous environments, sex may also facilitate adaptation (Becks and Agrawal, 2010; Luijckx et al., 2017; Lachapelle and Colegrave, 2017). Given that some experimental work found stronger benefits of sex if genetic variation is sufficiently high (Lachapelle and Bell, 2012), we expect that sex is only favoured at the range edge when genetic variation is bolstered through gene flow from the high diversity core, because populations at a range edge are genetically depauperated due to repeated founder events (Hallatschek et al., 2007; Chuang and Peterson, 2016). However, theory on gene swamping predicts the opposite (Haldane and Ford, 1956; García-Ramos and Kirkpatrick, 1997; Kirkpatrick and Barton, 1997). As individuals bolstering the gene pool will be maladapted to the abiotic conditions at the range edge, sex may hinder adaptation when there is too much gene flow from the range core to the range edge (Haldane and Ford, 1956; García-Ramos and Kirkpatrick,

1997; Kirkpatrick and Barton, 1997; Polechová and Barton, 2015; Polechová, 2018). Under such conditions, reproducing sexually would swamp the gene pool at the range edge with maladapted genes. This could prevent the population from adapting to the abiotic environment at the range edge, and hence slow down and even halt range expansion, leading to stable range borders (García-Ramos and Kirkpatrick, 1997; Kirkpatrick and Barton, 1997). In contrast, when drift strongly reduces adaptive variation, gene flow may positively affect adaptation by counteracting the effects of drift (Polechová and Barton, 2015; Polechová, 2018). Despite extensive theory on gene swamping, surprisingly little empirical and experimental work exists (reviewed in Lenormand, 2002; Bridle and Vines, 2007; Gaston, 2009; Sexton et al., 2009).

Here, we experimentally tested the gene swamping hypothesis using the ciliate *Tetrahymena thermophila*. We assessed how reproduction (asexual or sexual) and gene flow (i.e., dispersal from the range core to the range edge) altered evolutionary adaptation during range expansions in landscapes with or without a gradient in pH. We found a distinct signal of gene swamping, where sex facilitated or hindered adaptation depending on the presence or absence of gene flow.

Material and methods

Study organism

Tetrahymena thermophila is a freshwater ciliate commonly used in ecological and evolutionary experiments (Collins, 2012; Altermatt et al., 2015; Jacob et al., 2015; Fronhofer et al., 2017a; Scheuerl Thomas et al., 2019; Cairns et al., 2019). We used four phenotypically divergent (Moerman et al., 2020a) clonal strains of *T. thermophila* ob-

tained from the Tetrahymena Stock Center: strain B2086.2 (Research Resource Identifier TSC_SD00709), strain CU427.4 (TSC_SD00715), strain CU428.2 (TSC_SD00178) and strain SB3539 (TSC_SD00660).

Experiment

Microcosms

We performed all evolution experiments and all bioassays in a 20 °C climate-controlled room. Following an established method (Fronhofer and Altermatt, 2015), we experimentally emulated an expanding range front with two-patch landscapes, which consisted of two 25 mL Sarstedt tubes connected by an 8 cm long silicone tube (inner diameter 4 mm). See also Supplementary Material figure S3.1.

We prepared 40 two-patch landscapes, and filled patches of each landscape with 15 mL modified Neff-medium (Cassidy-Hanley, 2012). We complemented the medium for experimental evolution and bioassays with 10 $\mu\text{g mL}^{-1}$ Fungin and 100 $\mu\text{g mL}^{-1}$ Ampicillin to prevent bacterial and fungal contamination. We then inoculated one patch of each two-patch landscape with 200 μL of ancestor culture (50 μL from each of the four ancestral strains). This allowed adaptation through clonal selection and *de novo* mutation (Brito et al., 2010) in populations designated for asexual reproduction, as well as recombination (Lynn and Doerder, 2012) in populations designated for sexual reproduction.

Treatment groups

We designed a full factorial experiment that tested the effect of 1) abiotic conditions, with two treatment levels (“Uniform”: pH always 6.5, “Gradient”: pH starts at 6.5 and

then gradually decreases), 2) reproduction, with two treatment levels (“Asexual”: pure asexual reproduction, “Sexual”: asexual and sexual reproduction) and 3) gene flow, with two treatment levels (“Absent”: no gene flow; “Present”: gene flow from the range core to range edge). We evolved five replicate populations per treatment, for a total of 40 evolving populations.

Experimental evolution

We performed a range expansion experiment that lasted ten weeks, in which we repeated the same procedure cycle every 14 days. This cycle consisted of three dispersal events (on days 1, 3 and 5). These events were followed by a gene flow and sexual reproduction event or the appropriate controls depending on the treatment groups (on day 8), and subsequently an additional two dispersal events (on days 10 and 12).

We initiated dispersal by opening the clamps in the two-patch landscapes for one hour, which allowed cells to disperse from their original (home) patch to the target patch. After dispersal, we prepared 40 new two-patch landscapes. If population density was measurable (≥ 1 cell observed during video analysis, see below) in the target patch, we transferred the content of the target patch to a new two-patch landscape. If no measurable dispersal occurred, we transferred the content of the home patch to the new two-patch landscape.

In treatment groups designated for gene flow to occur, we emulated long-distance gene flow (from the range core to the edge, following theoretical predictions, García-Ramos and Kirkpatrick, 1997; Kirkpatrick and Barton, 1997), by transferring 1.5 mL of culture from the core population to the range front.

To control reproduction, we transferred all populations to a starvation medium, because *T. thermophila* only mates when starved (Lynn and Doerder, 2012). We incubated

the starvation cultures on a shaker rotating at 120 rpm. After 36 hours, we placed the populations designated for sexual reproduction off the shaker, but kept populations designated for asexual reproduction on the shaker, because the shaking movement prevents cells from mating. We left cells to mate overnight, after which we transferred populations to new two-patch landscapes. For a more extensive technical description, see Supplementary Material section S.3.1.2.

Common garden

After experimental evolution, we sampled 100 μ L of culture from all surviving populations, and transferred this sample to 25 mL Sarstedt tubes containing 15 mL Neff-medium at pH 6.5. We maintained these populations in the common garden for 72 hours before starting bioassays, to reduce epigenetic and trans-generational effects.

Bioassays

We quantified the population growth rate of ancestral and evolved populations, after common garden cultivation, at eight different pH values (pH 6.5, 6.0, 5.5, 5.0, 4.5, 4.0, 3.5 and 3.0). Specifically, we prepared for every population Sarstedt tubes containing Neff-medium whose pH we had adjusted to the desired value using 1 M HCL, and inoculated this medium with 100 μ L of culture from the evolved or ancestral populations. We grew the resulting cultures for 12 days, sampling populations twice on the first two days, and once per day on all subsequent days. Every two days, we replaced 1 mL of culture with fresh medium to prevent population decline.

Sampling and video analysis

We measured population density and cell characteristics (morphology and movement) using an established method (Altermatt et al., 2015; Pennekamp et al., 2015). We sampled 200 μL of culture from every population, and diluted samples 10—100 fold in Neff-medium to ensure densities were similar, as excessive density prevents accurate video analysis. We then took 10 s videos (250 frames, 25 fps) using a Leica M165FC stereomicroscope and top-mounted Hamamatsu Orca Flash 4.0 camera. We analyzed videos using the BEMOVI R-package (Pennekamp et al., 2015, parameters in Supplementary Material section S.3.2).

Beverton-Holt model fitting

To analyze local adaptation, we assessed growth rates by fitting a continuous-time version of the Beverton-Holt model (Beverton and Holt, 1993), as this model is well-suited for microcosm data and facilitates biological interpretation of parameters (Thieme, 2003; Fronhofer et al., 2018). The Beverton-Holt model is given by the equation:

$$\frac{dN}{dt} = \left(\frac{r_0 + d}{1 + \alpha N} - d \right) N, \quad (5)$$

where the intraspecific competitive ability (α) is equal to

$$\alpha = \frac{r_0}{\widehat{N}d} \quad (6)$$

and r_0 is the intrinsic rate of increase, N the population size, α the intraspecific competitive ability, \widehat{N} the equilibrium population density and d the death rate of the population. We estimated the parameters using a Bayesian approach adapted from Rosenbaum et al.

(2019). For model code see <https://zenodo.org/record/2658131>

Statistical analysis

All statistical analyses were performed with the R language for statistical computing, version 3.5.1. We calculated local adaptation by assessing changes in the intrinsic rate of increase r_0 of evolved populations under the pH conditions they experienced during evolution, compared to the ancestor under the same pH conditions. This was done by dividing the r_0 estimates of evolved populations by the mean r_0 of the mixed ancestral populations (populations with the initial ancestral genotype mixture), and by subsequently calculating the logarithm (base 2) of this ratio (log-ratio response).

Next, we created linear models assessing the effect of reproduction, gene flow and abiotic conditions (explanatory variables) on range expansion distance (number of successful dispersal events) and local adaptation respectively. We additionally created a linear mixed model ('nlme'-package, version 3.1-137) to assess how population density during range expansion was influenced by the three treatments: reproduction, gene flow, abiotic conditions, as well as the covariate range expansion distance (the number of successful dispersal events). We included population ID as a random effect. We subsequently compared all possible models for these three response variables using the dredge function ('MuMin'-package, version 1.43.6) to select the model with lowest AICc (Akaike Information Criterion, corrected for small sample size; Hurvich and Tsai 1989) score for local adaptation and range expansion distance, and lowest BIC (Bayesian information criterion; Gelman et al. 2014) for population density. We report relative importance and model output. See Supplementary Material section S.3.4 for additional analyses on population survival and cell movement and morphology.

Results

Population densities (figure 3.1 panels A, B, E and F; Table 3.1) showed strong temporal variation in all replicates. Mean density decreased marginally for populations expanding into uniform abiotic conditions ($\chi^2_{1,746}=4.526$, $p=0.034$), whereas population density of populations expanding into a gradient decreased strongly ($\chi^2_{1,746}=108.258$, $p<0.0001$). Additionally, we observed that populations faced with a gradient showed significantly slower range expansion (figure 3.1 panels C, D, G and H; $F_{1,31}=141.4$, $p<0.0001$; table 3.2), and were more prone to go extinct, in the absence of gene flow (see Supplementary material section S.3.4.6).

Table 3.1: Type III ANOVA table of the best model for population density during range expansion according to BIC model comparison.

Model and explanatory variables	Degrees of freedom	χ^2-value	Pr ($>\chi^2$)
Abiotic conditions	1	0.044	0.833
Range expansion distance	1	4.526	0.034
Abiotic conditions \times position	1	108.258	$<.0001$

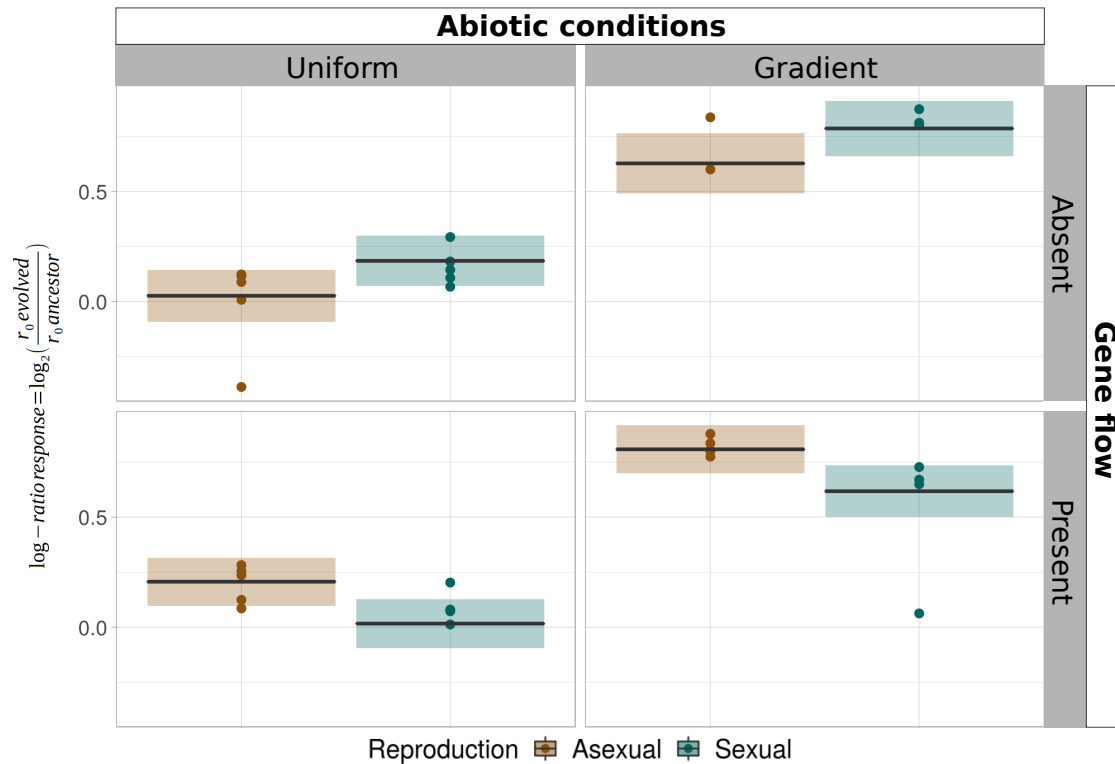


Figure 3.2: Local adaptation, measured as the evolution of intrinsic rate of increase r_0 in the abiotic conditions experienced during range expansion (uniform or gradient), compared to the ancestor population. The y-axis shows the change in r_0 compared to the ancestor (log-ratio response). Dots represent individual data points, black lines and shaded areas show the model predictions of the best model (mean and 95 %-confidence interval). Brown colours denote populations in treatment groups with asexual reproduction, green colours denote populations in treatment groups with sexual reproduction.

Table 3.2: Type III ANOVA table of the best model for local adaptation (evolution of intrinsic rate of increase r_0) and range expansion distance (total number of successful dispersal events) during range expansion according to AICc model comparison.

Model and explanatory variables	Degrees of freedom	F-value	Pr (>F)
Local adaptation			
Reproduction	1	3.96	0.056
Gene flow	1	5.55	0.025

Abiotic conditions	1	122.58	<0.0001
Reproduction×Gene flow	1	10.67	0.003
Residuals	29		
<hr/>			
Range expansion distance			
Abiotic conditions	1	141.4	<0.0001
Residuals	31		

Local adaptation (evolution of intrinsic rate of increase r_0 ; figure 3.2; table 3.2) increased only slightly for population expanding into uniform abiotic conditions, whereas populations that expanded into a gradient greatly increased local adaptation ($F_{1,29}=128.58$; $p<0.0001$). Although sexual reproduction ($F_{1,29}=3.96$; $p=0.056$) and the presence of gene flow ($F_{1,29}=5.55$; $p=0.025$) individually slightly increased local adaptation, their interaction strongly decreased local adaptation ($F_{1,29}=10.67$, $p=0.003$), with populations evolving lower intrinsic rates of increase either when reproduction was sexual and gene flow present, or with asexual reproduction but gene flow absent.

Discussion

We experimentally assessed the gene swamping hypothesis using replicated range expansions of the protist *Tetrahymena thermophila*. We experimentally manipulated abiotic conditions (uniform versus gradient), reproduction (asexual versus sexual) and gene flow (absent versus present). We demonstrated how sex interacts with gene flow, affecting local adaptation of organisms at the range edge (figure 3.2; table 3.2).

Populations undergoing range expansions face multiple selective pressures (Chuang and Peterson, 2016), and hence face a strong pressure to adapt. Theoretical predictions suggest that sex can be advantageous or disadvantageous during range expansion, depending on the context. Theory on gene swamping predicts that sex hinders adaptation during range expansions when populations undergo strong asymmetrical dispersal from a range core to a range edge (Haldane and Ford, 1956; García-Ramos and Kirkpatrick, 1997; Kirkpatrick and Barton, 1997). We showed here that the effect of sex is conditional on the presence of gene flow. Despite having only four distinct events of sexual reproduction in otherwise asexually reproducing populations, we found a beneficial effect of sex on local adaptation in the absence of gene flow. However, when gene flow was present and swamped the edge population with maladapted individuals, sex hindered adaptation. Surprisingly, while the gene swamping hypothesis predicts this pattern exclusively in the presence of abiotic gradients (Haldane and Ford, 1956; García-Ramos and Kirkpatrick, 1997; Kirkpatrick and Barton, 1997), we observed similar effects of gene swamping in the presence and absence of an abiotic gradient. We argue that gene swamping in the absence of an abiotic gradient could stem from evolving life-history strategies during range expansions. Range expanding populations are thought to exhibit a gradient of decreased density towards the range front, which translates to decreased competition and selection for fast reproduction (Burton et al., 2010). Hence, gene swamping may imply that individuals maladapted in life-history strategy interbreed with the population at the range edge. Consequently gene swamping affects adaptation during range expansions even without an abiotic gradient, leading to analogous changes in adaptation as for range expansions into abiotic gradients.

Although we show that gene swamping affects adaptation during range expansions, we could not detect effects of gene swamping on range expansion rates as described

by theory, despite population growth rate being a driving force behind expansion rate (Skellam, 1951; Giometto et al., 2014, 2017). This discrepancy could result from our experimental setup, where we used discrete landscapes connected through repeated dispersal events, rather than continuous dispersal. This setup may be insufficiently sensitive to detect signals in expansion rate. Alternatively, this setup may lead to pushed rather than pulled waves (see Pachevsky and Levine, 2011) which changes predictions. Under pulled waves, dispersers from the low-density range front drive further range expansion. In contrast, further spread in pulled waves will only be possible after the population at the front has grown sufficiently large. Although it is possible that the abiotic gradient leads to a pushed wave, for example by reducing survival during the dispersal stage, determining this with absolute certainty would require extensive dispersal measurements at a temporal resolution that we lack in this experiment. Testing the interaction between pushed/pulled waves and gene swamping would, however, be interesting, as pushed waves might be less susceptible to gene swamping, because the population density gradient from the range core to the range edge is less steep compared to pulled waves.

Author contributions

FM, EAF, AW and FA designed the experiment. FM performed experimental work and statistical analyses. FM, FA, AW and EAF interpreted the results. FM and FA wrote the first version of the manuscript and all authors commented on and approved of the final version. All authors are accountable for all aspects of this work.

Acknowledgements

We thank Samuel Hürlemann, Silvana Käser and Sarah Bratschi for help with laboratory work, and Lynn Govaert, Claire Jacquet and the three reviewers for their helpful comments. Funding is from the University of Zurich URPP Evolution in Action and the Swiss National Science Foundation, Grant No PP00P3_179089. This is publication ISEM-2020-119 of the Institut des Sciences de l'Evolution – Montpellier. We would also like to acknowledge support by Swiss National Science Foundation grant 31003A_172887 and European Research Council Advanced Grant No. 739874.

Data accessibility statement

Data is available from the Dryad Digital Repository (DOI: [10.5061/dryad.6wwpzgmtk](https://doi.org/10.5061/dryad.6wwpzgmtk); Moerman et al., 2019) and analysis scripts on Github (DOI: [10.5281/zenodo.3560982](https://doi.org/10.5281/zenodo.3560982); Moerman, 2019).

Chapter 4: Selection on growth rate and local adaptation drive genetic adaptation during range expansions in the protist *Tetrahymena thermophila*

Felix Moerman, Emanuel A. Fronhofer, Florian Altermatt and Andreas Wagner

Abstract

Mounting evidence shows that populations can undergo rapid evolution during range expansions for dispersal behaviour, life-history strategy, and adaptation to the local environment. However, little is known about the genetic nature of such adaptation. We here studied genetic adaptation during experimental range expansions of the protist *Tetrahymena thermophila* in landscapes with a uniform environment or a pH-gradient. We controlled the reproductive mode (asexual/sexual) and the presence of gene flow during range expansion. We investigated which genes were under selection due to the range expansion (general adaptation) and due to the pH-gradient (gradient-specific adaptation).

Furthermore, we investigated how the presence of a pH-gradient, gene flow and sexual reproduction affected genetic changes on standing variation and *de novo* mutation. We show that general adaptation acts on genes involved in cell divisions and DNA repair, whereas gradient-specific adaptation acts primarily on genes involved in ion transport and binding, and oxidoreductase reactions. We argue that these genetic adaptations are associated with selection on growth rate, and adaptation to the local pH. Additionally, we found that sexual reproduction affected genetic change through *de novo* mutation and standing variation, whereas, gene flow and the presence of a pH-gradient only affected genetic change from standing variation.

Introduction

Range expansions and invasions of new habitats are increasingly common in many species. They often result from anthropogenic disturbances in the environment or from human-driven species introductions (Parmesan et al., 1999; Kowarik, 2003; Chen et al., 2011). Because they can have dramatic consequences on species distributions and ecosystems (see for example Grosholz, 2002; Phillips et al., 2009), it is ecologically and economically important to understand their ecological and evolutionary consequences.

Expanding populations are under strong selection for both dispersal and population growth (Burton et al., 2010; Phillips et al., 2010; Shine et al., 2011). Furthermore, when populations expand into novel abiotic environments, they may be subject to additional selection pressures that affect how they adapt to the expanding range. In recent years, both experimental studies and field studies have demonstrated that expanding populations indeed rapidly evolve their dispersal behaviour (Brown et al., 2007; Williams et al., 2016; Ochocki and Miller, 2017) and life-history strategy (Phillips, 2009; Fronhofer and

Altermatt, 2015). They also evolve specific adaptations to local abiotic conditions, such as temperature and novel food sources (Van Petegem et al., 2016; Szűcs et al., 2017). Such local adaptations can in turn affect the range expansion rate (Weiss-Lehman et al., 2017; Ochocki and Miller, 2017; Williams et al., 2019).

Because selection pressures during range expansion are strong, populations at a range edge may need to adapt quickly. Such adaptation can be facilitated by reshuffling existing genetic variation through sexual reproduction (Smith, 1978; Bell, 1982; Otto and Lenormand, 2002). This benefit of sexual reproduction has been demonstrated repeatedly, (Colegrave, 2002; McDonald et al., 2016; Luijckx et al., 2017; Petkovic and Colegrave, 2019), and is especially pronounced in the presence of high genetic diversity (Lachapelle and Bell, 2012). Increased genetic variation or an influx of locally adapted genes can also increase the success of invasions and range expansions (Schmeller et al., 2005; Lavergne and Molofsky, 2007; Currat et al., 2008).

New genetic variation created by sexual reproduction is not always beneficial. It can also be detrimental, for example in the process of "gene swamping". Gene swamping occurs when populations expand their range against an environmental gradient, and when genes ill-adapted to the range edge flow from a high density core population to a low density population at the range edge. According to the gene swamping hypothesis, such gene flow can decelerate adaptation a population at the range edge (Haldane and Ford, 1956; García-Ramos and Kirkpatrick, 1997; Kirkpatrick and Barton, 1997; Polechová and Barton, 2015; Polechová, 2018). Gene swamping may reduce the range expansion rate or even halt expansion and lead to the formation of a stable range border (Lenormand, 2002; Gaston, 2009; Sexton et al., 2009). Such detrimental gene swamping has recently been demonstrated both in an experimental study (Moerman et al., 2020b) and a field study (Bachmann et al., 2020).

With few exceptions (Bosshard et al., 2020), experimental and field studies on the evolutionary genetics of range expansions have focused on population genetic structure and diversity (see for example Swaegers et al., 2013; Bors et al., 2019). This population genetic work has demonstrated that, first, populations at the edge of a range typically harbour much less genetic variation than the core populations (Excoffier et al., 2009). Second, populations at the range edge are also strongly influenced by genetic drift, which can lead to "allele surfing", the increase in frequency and potential fixation of neutral or maladaptive mutations at a range edge (Klopfstein et al., 2006; Excoffier et al., 2009). Despite such work, the genetic basis of phenotypic evolution during range expansions remains poorly understood, as does the genetic basis of gene swamping. For example, we know little about the kinds of genes that are involved in phenotypic evolution during range expansion. We know even less about genes involved in gene swamping.

Because phenotypic change could be caused by genetic change, by phenotypic plasticity, or by maternal effects (Bonduriansky and Day, 2018) it is important to disentangle genetic and non-genetic causes of phenotypic change. The traits that affect range expansion — life-history strategy, dispersal ability, and adaptation to the local environment — can have both a complex genetic basis and show phenotypic plasticity. For example, dispersal behaviour can have a strong genetic component (Saastamoinen et al., 2018), but it can also be a plastic response to population density or habitat quality (see chapter 1 in Clobert et al., 2012). In addition, it can be modified by maternal effects (Donohue, 1999).

We here studied the population genomics of range expansions in the protist *Tetrahymena thermophila*. We were especially interested in population changes caused by sexual reproduction and gene swamping, when a population expands either into a uni-

form environment or into an abiotic (pH) gradient.

To this end, we performed whole genome sequencing of pooled *T. thermophila* populations from a previously published range expansion experiment, in which we allowed populations to expand their range during ten weeks (250 generations; Moerman et al., 2020b). Briefly, in this experiment we had used connected two-patch landscapes to emulate the range edge of an expanding population. We used a full factorial design in which populations reproduced either sexually or asexually, and in which gene flow from the range core to the range edge was either allowed or prohibited. After ten weeks of experimental evolution, we identified the populations with the strongest phenotypic changes, pooled individuals from these populations, and sequenced the genomic DNA of the resulting pools.

Evolutionary adaptation during such an experiment can occur in two different ways. The first is through changes in standing genetic variation, i.e., through statistically significant changes in the frequency of alleles that were already present in the starting (ancestral) population. The second is through *de novo* mutations. We studied both kinds of genetic change.

Populations in such an experiment can also experience two different kinds of adaptations. The first comprises “general” adaptations shared by all populations, i.e., adaptations to the general laboratory environment and to the expanding range. The second comprises adaptations to the pH-gradient that we imposed on some populations. We refer to such adaptations as “gradient-specific” adaptation. We aimed to distinguish these two kinds of adaptations with our population genomic data.

We investigated how reproductive mode (asexual or sexual), gene flow, and a pH-gradient affected both *de novo* mutations and standing genetic variation. In addition, we assessed whether reproduction and gene flow result in gene swamping on both the phe-

notypic and genotypic level. Furthermore, we identified genes involved in adaptation to the general conditions and to the range expansion itself, as well as genes involved in gradient-specific adaptation. We found that sexual reproduction increased the number of *de novo* mutations whose frequency rose to detectable values under all conditions we examined. In contrast, sexual reproduction only affected allele frequency changes in standing genetic variation in the absence of gene flow. Genes involved in general adaptation were preferentially associated with DNA repair, mitosis, and gene expression. In contrast, genes involved in gradient-specific adaptation were associated with ion transport and oxidoreductase reactions.

Material and methods

Study organism and experimental populations

Tetrahymena thermophila is a freshwater ciliate commonly used in ecological and evolutionary microcosm experiments (Collins, 2012; Altermatt et al., 2015; Cairns et al., 2020; Moerman et al., 2020a). We used ancestral and evolved populations from a range expansion experiment by Moerman et al. (2020b) to investigate the genomic basis of adaptation during range expansions. We explain the most pertinent details of this experiment here and refer the reader for other details to Moerman et al. (2020b).

Briefly, in this experiment, we mixed four phenotypically divergent (Moerman et al., 2020a) clonal strains of *T. thermophila* to create a genetically diverse ancestral population. These four ancestral clones, which we obtained from the Tetrahymena Stock Center were strain B2086.2 (Research Resource Identifier TSC_SD00709), strain CU427.4 (TSC_SD00715), strain CU428.2 (TSC_SD00178) and strain SB3539 (TSC_SD00660).

We created this ancestral population by first growing the four clones separately to equilibrium density and measuring cell counts. Subsequently, we mixed equal volumes of the resulting four cultures. Because each clone may grow to a different equilibrium density, the clones may not be represented by equal cell numbers in the ancestral population. The starting proportions of the four clones in the ancestral population (i.e. the proportion of cells of the ancestral population originating from each of the four clones) are shown in Table 4.1. Subsequently, we allowed multiple replicates of this ancestral population to expand their range for ten weeks (approximately 250 generations). We kept all stock cultures and populations during experimental evolution in a climate room at 20 °C.

Clone	Starting proportion
Clone B2086.2	0.3402
Clone CU427.4	0.1287
Clone CU428.2	0.2595
Clone SB3539	0.2716

Table 4.1: Starting proportions of cells in our ancestral population that originated from each of the indicated ancestral clones.

During this experimental range expansion, we used an established system of two-patch landscapes (Fronhofer and Altermatt, 2015) to emulate an expanding range front. These two-patch landscapes consist of two 25 mL Sarstedt tubes, each filled with 15 mL of modified Neff medium (Cassidy-Hanley, 2012). The Sarstedt tubes are connected by an 8 cm long silicone tube (inner diameter 4 mm), that can be opened or closed using a plastic clamp. We initiated the experiment by inoculating one patch of the two-patch landscape (“home patch”) with 200 μ L of the ancestral population. During experimental

range expansion, we controlled 1) the abiotic conditions ("uniform": pH always equals 6.5 over the course of range expansion, "pH-gradient": pH gradually decreases from 6.5 to 4.0 during range expansion to emulate an environmental pH-gradient), 2) reproduction ("asexual": pure asexual reproduction, "sexual": sexual reproduction induced at regular intervals) and 3) gene flow ("absent": no gene flow; "present": regular gene flow). Details of each treatment are explained in the next section. Altogether, our experiment used eight treatments. For each treatment, we evolved five replicate populations, resulting in a total of 40 populations (Moerman et al., 2020a).

Experimental evolution

We then subjected the populations to ten weeks of experimental evolution, during which we repeated the same cyclical procedure every 14 days. Specifically, we subjected each population to three dispersal events, which took place on days 1, 3 and 5 of the 14-day cycle. After the last dispersal event, we subjected populations of the appropriate treatment groups to a gene flow and/or sexual reproduction event on day 8. Lastly, we subjected the populations to an additional two dispersal events on days 10 and 12 of the 14-day cycle.

A dispersal event consisted of opening the plastic clamps of the two-patch landscapes for one hour, which allowed cells to swim from the home patch to the target patch. After dispersal, we measured cell densities in the home and target patches using an established video analysis method (Pennekamp et al., 2015) and a Leica M165FC stereomicroscope with top-mounted Hamamatsu Orca Flash 4.0 camera (see Supplementary Material section S.4.1 for video analysis script and parameters). We then prepared 40 new two-patch landscapes. For all populations that had successfully dispersed

into the target patch, we transferred the content of the target patch to the home patch of the new two-patch landscape. For all other populations, we transferred the content of the home patch to the new two-patch landscape. For populations designated for range expansion in a pH-gradient, we gradually lowered the pH of the Neff medium in the new two-patch landscapes. Specifically, we lowered the pH from 6.5 in steps of 0.5 after every 2-3 successful dispersal events, until a minimal value of pH 4.0 had been reached. From that time onward, we kept the populations at pH 4.0 for the remainder of the range expansion experiment. Although genetic drift may play an important role during range expansions (Hallatschek et al., 2007; Excoffier et al., 2009), is not likely to play a major role in our experiments. Firstly, population densities in our experiments were high ($10^4 - 10^6$ individuals). Secondly, between 1 % and 20 % of our populations typically dispersed, such that dispersal never led to extreme population bottlenecks. Therefore, genetic drift is thus negligible on the timescale of this experiment (Hartl and Clark, 2006).

To implement long-distance gene flow from the range core to the range edge, we replaced 1.5 mL of culture in the appropriate populations with 1.5 mL of a replicate of the ancestral population. We created this replicate by mixing the four ancestral clones in the same proportions as we had used to create the ancestral population from which we had started the experiment.

Following a gene flow event, we induced sex in populations designated for sexual reproduction. *T. thermophila* only mates when starved (Lynn and Doerder, 2012). Therefore, we transferred all populations after a gene flow event to a starvation medium, and incubated them on a shaker rotating at 120 rpm for 36 hours. Subsequently, we removed populations designated for sexual reproduction from the shaker, but kept populations designated for asexual reproduction on the shaker, because the shaking prevents cells

from mating. We then allowed cells to mate overnight, before transferring all populations back from starvation medium to modified Neff medium. At the end of the range expansion experiment, we quantified changes in the growth rate of the surviving (34 out of 40) evolved populations, as detailed in the next section. A schematic representation of the evolution experiment can be found in the Supplementary Material section S.4.2.

Common garden and growth assessment

After experimental evolution, we transferred 200 μ L of culture from all surviving populations to a new Sarstedt tube containing 15 mL of Neff medium. We subjected these populations to common garden conditions for 72 hours to reduce epigenetic and maternal effects.

We then assessed the change in intrinsic growth rate of the evolved populations compared to the ancestral population. To do so, we prepared Sarstedt tubes containing modified Neff medium with the pH adjusted to eight values (pH 6.5, 6.0, 5.5, 5.0, 4.5, 4.0, 3.5 and 3.0) for the ancestral population and for each evolved populations. We then inoculated the Sarstedt tubes either with 100 μ L of culture from the ancestral population or from one of the evolved populations. We grew these populations for 12 days, during which we sampled populations twice on day one and two as well as once on every subsequent day. We then used an existing video analysis methods (Pennekamp et al., 2015), using a Leica M165FC stereomicroscope with top-mounted Hamamatsu Orca Flash 4.0 camera to assess population densities (see section S.4.1 for video analysis script and parameters).

After video analysis, we analyzed population growth using a continuous-time version of the Beverton-Holt population growth model (Beverton and Holt, 1993). This

model is well suited for microcosm data and has biologically interpretable parameters (Thieme, 2003; Fronhofer et al., 2018). The Beverton-Holt model is given by the equation

$$\frac{dN}{dt} = \left(\frac{r_0 + d}{1 + \alpha N} - d \right) N, \quad (7)$$

where the intraspecific competitive ability (α) is given by

$$\alpha = \frac{r_0}{\widehat{N}d}. \quad (8)$$

In these equations, r_0 is the intrinsic population growth rate, N is the population size, α is the intraspecific competitive ability, \widehat{N} is the equilibrium population density and d is the death rate of the population. We used a Bayesian approach adapted from Rosenbaum et al. (2019) for parameter estimation. Model code is available at <https://zenodo.org/record/2658131>.

We then calculated the change in fitness that occurred in each evolved population as the change in the population's intrinsic growth rate r_0 relative to the ancestral population, and did so for the pH value that a population experienced during range expansion (i.e. pH 4.0 for populations expanding into a pH-gradient, pH 6.5 for populations expanding into a uniform environment). More specifically, we calculated the log-ratio response as

$$\ln\left(\frac{r_{0,e}}{r_{0,a}}\right), \quad (9)$$

where $r_{0,e}$ is the intrinsic growth rate of the evolved populations and $r_{0,a}$ is the intrinsic growth rate of the ancestral population.

Sequencing and identification of variants

To identify candidate loci for genetic adaptation during range expansion, we performed population level sequencing ("PoolSeq"; Schlötterer et al., 2014) for samples from our evolved populations as well as for the ancestral clones. Specifically, we sequenced the four ancestral clones, as well as 16 evolved populations that had undergone the aforementioned ten weeks of experimental evolution.

Tetrahymena thermophila cells have a diploid non-expressed micronucleus and a highly polyploid (n=45) expressed macronucleus (Lynn and Doerder, 2012). We only wished to sequence the macronuclear DNA, because only the expressed macronuclear DNA affects the phenotype. We thus first separated macronuclei from micronuclei, as described in the next section. Following nuclear separation, we extracted DNA from each population sample. Subsequently, we selected populations for genomic sequencing based on their intrinsic growth rate r_0 . Specifically, we sequenced DNA from the two populations with the highest intrinsic growth rate r_0 in each of the eight treatment groups (uniform/gradient, asexual/sexual, gene flow/no gene flow; see Table S4.7 for a list of all r_0 -values used to select populations of interest). Next, we mapped the obtained reads to the *T. thermophila* reference genome, and performed variant calling to identify genetic variants. In analyzing the resulting data, we studied standing genetic variation and its allele frequency change, as well as mutations that had occurred *de novo* during our experiment. In the next sections, we describe each of these steps in detail.

Nuclear separation and DNA extraction

We separated macronuclei and micronuclei of the four ancestral clones and of all 34 surviving evolved populations using a protocol adapted from Sweet and Allis (2006). Prior

to nuclear separation, we prepared the required media (medium A and nuclei wash buffer, see Supplementary Material section S.4.3 for a list of reagents). Briefly, to prepare medium A, we mixed 34.23 g of sucrose, 0.407 g of $\text{MgCl}_2(\times\text{H}_2\text{O}_6)$, 40 g gum arabic, and 0.185 g iodoacetamide in a 1 liter Schott bottle containing 800 mL of ultrapure water (i.e. water filtered using a Barnstead Waterpure filtration system to remove organic and inorganic compounds; see <https://assets.thermofisher.com/TFS-Assets/LED/manuals/D01316~.pdf> for the manufacturer protocol). We then added 0.918 μL butyric acid and 1.211 g of Tris at pH 7.5. We prepared this pH-adjusted Tris by first creating a stock solution from Tris-Base, and adjusted the pH to 7.5 using 1M HCl. After thoroughly mixing all ingredients of medium A, we then filled the Schott bottle with ultrapure water, until the total volume was 1 L. After mixing again, we then transferred 40 mL of medium A to 50 mL Falcon tubes, and stored the Falcon tubes in a -20°C freezer until needed. One Falcon tube suffices for the nuclear separation of one population.

We prepared the nuclei wash buffer by mixing 85.574 g of sucrose, 0.441 g CaCl_2 , 0.2033 g MgCl_2 and 0.185 g iodoacetamide in a 1 L Schott bottle containing 800 mL of ultrapure water. We then added 0.918 μL butyric acid and 1.211 g of Tris at pH 7.5. We then filled the bottle with ultrapure water until the total volume was 1 L, and mixed thoroughly. After mixing, we transferred 15 mL of nuclei wash buffer to 15 mL Falcon tubes, and stored them in a -20°C freezer until needed.

Before starting the nuclear separation protocol, we moved the required number of Falcon tubes to a 4°C refrigerator to thaw overnight. We then prepared medium B by adding 50 μL of octanol to the Falcon tubes containing medium A. After adding the octanol, we thoroughly mixed the Falcon tubes by vortexing, and stored them on ice.

Next, we determined the population density of all populations from which we

wanted to extract the DNA. To do so, we used an existing video analysis method (Pennekamp et al., 2015) to measure the number of cells in a small volume of culture for each population, using a Leica M165FC stereomicroscope with top-mounted Hamamatsu Orca Flash 4.0 camera (see S.4.1 for video analysis script and parameters). One Falcon tube of medium B suffices for nuclear separation of approximately 4×10^7 cells of *T. thermophila*. Therefore, we collected for every population the volume of culture containing at total of 4×10^7 cells, and transferred this volume to 50 mL Falcon tubes. We then centrifuged these Falcon tubes at 2000 g and 4 °C for 5 minutes, using a Sigma 3-16PK centrifuge. After centrifugation, we decanted the supernatant, and resuspended the cells in 5 mL of medium B. We then transferred the suspended cells to a glass homogenizer dounce (Kimble 15 mL tissue grinder; product ID: 885300-0015). Subsequently, we ruptured cells and separated their nuclei using 40 pushes of the glass dounce. After cell disruption, we verified that cells had been disrupted and that nuclei were separated in at least 90 % of the cells (i.e. smaller micronuclei were dislodged from the "cup" next to the larger macronuclei). To do so, we stained a small droplet of the ruptured cells using SyBr-green dye to colour the DNA. We then visually inspected the droplet under a Leica M165FC stereomicroscope with a green fluorescence filter to verify that macronuclei and micronuclei were separated.

After cell disruption, we transferred the cell material to the remaining 35 mL of medium B in the Falcon tube, and thoroughly mixed the content of the Falcon tubes. We then centrifuged the Falcon tubes (2000 g at 4 °C for 5 minutes) using a Sigma 3-16PK centrifuge to pellet the macronuclei. We decanted the supernatant (containing micronuclei, unpelleted macronuclei, and other cell material) in a new 50 mL Falcon tube, and resuspended the pellet in 1 mL of nuclei wash buffer (pellet P1). We then transferred the resuspended pellet to a 1.5 mL Eppendorf tube, and immediately stored the Eppendorf

tube on ice. Next, we mixed the supernatant by vortexing, and centrifuged it again at a higher speed (2300 g at 4 °C for 5 minutes; Sigma 3-16PK centrifuge) to pellet remaining macronuclei. We then again decanted the supernatant in a new 50 mL Falcon tube, and resuspended the second pellet (pellet P2) in 1 mL of nuclei wash buffer. We transferred the resuspended P2 pellet to a 1 mL Eppendorf tube which we then stored on ice. Subsequently, we again mixed the remaining supernatant by vortexing, and centrifuged it at an increased speed (2500 g at 4 °C for 5 minutes; Sigma 3-16PK centrifuge). We then decanted the supernatant in a waste disposal collection bottle, and resuspended the pellet in 1 mL of nuclei wash buffer (pellet P3). Subsequently, we transferred the resuspended P3 pellet to a 1 mL Eppendorf tube which we stored on ice. After nuclear separation, we immediately started the DNA extraction from the resuspended pellets containing the macronuclei.

For every population, we extracted the DNA from each of the three macronuclear pellets using a Qiagen[®] DNeasy Blood and Tissue kit (Cat No./ID: 69506), following the manufacturer's protocol (see <https://www.qiagen.com/us/resources/resourcedetail?id=63e22fd7-6eed-4bcb-8097-7ec77bcd4de6&lang=en>). After DNA extraction, we determined the quality and quantity of the DNA using a Nanodrop spectrophotometer (model ND-1000), to verify that the 260 nm/280 nm and 260 nm/230 nm ratios were within acceptable values, and ranked the pellets by DNA quality and quantity. Specifically, we chose for sequencing the DNA extracted from the pellet with a 260 nm/280 nm ratio closest to 1.8, a 260 nm/230 nm ratio larger than 2, and the highest concentration of DNA among all three pellets. If these criteria were similar between the macronuclear pellets, we always chose the DNA extracted from the first pellet (P1). We stored DNA samples in a -80 °C freezer until sequencing. Library preparation and sequencing was performed by the Functional Genomics Center

Zürich, which prepared 2X150 bp paired-end libraries and sequenced them using the Illumina Novaseq 6000 platform. We aimed to obtain population level DNA-sequences at approximately 100X genome coverage. A table containing coverage statistics for each of the ancestral clones and evolved populations can be found in the Supplementary Material, section S.4.5.

Quality control and mapping

We trimmed the reads of all fastq files using Trimmomatic version 0.39 (Bolger et al., 2014). We used trimming to remove any Illumina adapter sequences (ILLUMINA-CLIP option) and low quality segments (SLIDINGWINDOW:4:15). Additionally, we removed any reads falling below a length of 36 base pairs (MINLEN:36). On average over all samples, trimming preserved 95 % of paired-end reads.

After trimming, we mapped the reads for each of the 20 sequenced populations to the *Tetrahymena thermophila* macronuclear reference genome (Eisen et al., 2006) using the Burrows-Wheeler aligner (Li and Durbin, 2009) version 0.7.17-r1188. On average, 97.7 % of the reads aligned to the reference genome across all populations. A full list of the percentage of mapped reads for each of the ancestral clones and evolved population can be found in the Supplementary Material section S.4.4.

Variant calling

For all analyses, we called genetic variants using the multiallelic caller in BCFtools (Danecek et al., 2016). We first called multiallelic variants to identify sites where the four ancestral and 16 evolved populations differed from the reference genome, and stored the resulting allele counts for every position along the genome.

Mapping variants to genes

We mapped all variants to genes using bedtools (v2.27.1; Quinlan and Hall, 2010). To this end, we first obtained the genome annotation file from the *T. thermophila* reference genome (Eisen et al., 2006), and filtered this file to only keep entries corresponding to protein-coding genes. We then used the intersect function of the bedtools package to map the variants in the vcf file to the gene entries in the genome annotation file.

Quantifying allele frequencies

To detect changes in allele frequencies, we first calculated the initial frequency of alleles, i.e., the frequency of each allele present in the ancestral four-clone population. Because we had sequenced the clones in this population individually, we started by identifying all positions along the genome where at least one of the ancestral clones differed from the reference genome. As mentioned above, cells of *T. thermophila* have a highly polyploid macronucleus ($n=45$), and during asexual divisions the macronuclear chromosomes divide randomly (Lynn and Doerder, 2012; Ruehle et al., 2016). This means that a locus for which a clone is heterozygous in the micronucleus can be present in zero to 45 chromosome copies of the macronuclear DNA of a single cell. We therefore first needed to calculate, for each of the four ancestral clones, the allele frequency at all genome positions in which we observed a difference from the reference genome. Subsequently, we calculated a weighted mean of these four allele frequencies, using the starting proportion of the four ancestral clones in the ancestral population (Table 4.1). These weighted allele frequencies thus represent the expected allele frequencies of all variants that were initially present in the ancestral population.

Next, we filtered these positions to avoid sequencing errors for all 20 populations,

using the following criteria. Firstly, we removed any positions where at least one of the 20 populations had an extremely low (<30) number of high quality reads, thus excluding genomic regions with very low sequence coverage. Secondly, we removed positions with an extremely high (>300) number of high quality reads, which could be caused by sequencing artefacts, such as duplicated segments in the sequenced populations which are not present in the reference genome and may falsely map to the same genomic region. Thirdly, to reduce the incidence of false positives variant alleles, we removed any positions where only a single read differed from the reference genome in all 20 populations. Lastly, we considered only genomic positions for which we had high quality data (QUAL score ≤ 30) for all four ancestral clones, as well as for the 16 evolved populations. We then calculated the allele frequencies for the 16 evolved populations at all positions along the genome that had not been eliminated by filtering. For each of the evolved populations, this resulted in a list of positions where genetic variation had initially been present in the ancestral population, and where allele frequency changes in this standing variation were therefore possible.

Identifying *de novo* mutations

To detect *de novo* mutations, we kept only those variants that differed from the reference genome in an evolved population, and that were not present in any of the four ancestral clones. From the collection of these variants, we removed variants with an extremely low (<30) number of high quality reads, as well as variants with a low quality score (QUAL <30). We then filtered the remaining variants by removing variants where only a single read differed from the ancestral clones, in order to exclude false positive *de novo* mutations caused by sequencing errors.

Statistical analyses

We performed all statistical analyses, unless otherwise specified, using the R statistical language version 4.0.2 (R Core Team, 2020), and created all figures using the ggplot2 package (version 3.3.0 Wickham 2016).

Analyzing fitness changes

We applied the fitness assay described in Moerman et al. (2020b) to the populations included in the genomic analysis. Briefly, we determined the change in the intrinsic growth rate r_0 of each evolved population relative to the ancestral population in the pH conditions experienced during range expansion (that is, pH 6.5 for populations expanding into a uniform environment, and pH 4.0 for populations expanding into a pH-gradient). We then calculated a log-ratio response as described above in the section "Common garden and growth assessment". Subsequently, we fit a linear model (lm function R Core Team 2020) to assess the effect of the mode of reproduction, gene flow, and presence of the pH-gradient (explanatory variables) on the log-ratio response (response variable). We then used the dredge function in the MuMIn package (version 1.43.17; Bartoń, 2009) to find the best fitting model based on the AICc value (Akaike information criterion, corrected for small sample size; Hurvich and Tsai 1989). This method allows a ranking of linear models based on the maximum likelihood of each model, where a lower AICc score indicates a better model fit. We report model weights and statistical output (type-III Anova table and model summary) for the best fitting model according to this AICc comparison. Additionally, we plotted the population's mean fitness change against the number of alleles that changed significantly in frequency. We calculated the correlation between the two metrics, and did so for different

cut-off values of the magnitude of allele frequency change.

Quantifying frequency changes in standing genetic variation.

We first determined for all sites polymorphic in the ancestral population if the alleles at the site had experienced a significant change in frequency for any of the 16 evolved populations. To do so, we performed a binomial test comparing the number of reference and non-reference reads in evolved populations with the expected allele frequency of the ancestral population. We used a p-value of 0.001 in this test, to which we applied a Bonferroni correction (rounded down to the nearest power of ten) to avoid falsely detecting allele frequency changes due to multiple testing. As a result of this false detection rate correction, we considered only variants with a p-value smaller than 10^{-10} as significantly different from the expected allele frequency.

In a preliminary analysis of standing genetic variation, we observed that clone SB3539 of our four ancestral clones showed a number of anomalies that made it desirable to exclude it from further analysis. First, this clone contained approximately 30 times more non-reference alleles than the other ancestral clones and than each of the evolved populations (Table S4.6). Additionally, clone SB3539 deviated strongly in its transition/transversion ratio (clone SB3539: 0.9344; other populations 0.6544—0.7611; Table S4.6). Furthermore, we observed that selection acted very strongly against this clone as a whole, as evidenced by post-evolution allele frequencies that were dramatically different from those in all other populations (Fig. S4.2). Relatedly, all evolved populations showed an extremely high number of variants (approx. 1.1×10^4) that changed in their frequency by approximately 0.25, a value that corresponds closely to the initial frequency of clone SB3539 in the ancestral population (27 % of the ancestral population; Table 4.1). Although we do not know the reason for the strong selection

against this clone, we needed to account in all our analyses for allele frequency changes that were only caused by changes in the frequency of this clone during our experiment. To this end, we limited our analyses to those alleles whose frequency changed by an amount that is larger than could possibly be caused by selection against this clone. Specifically, we only analyzed alleles whose frequency changed by a value of 0.3 or higher (rounded up from 0.27, the starting frequency of clone SB3539), to exclude the effects of this clonal selection.

Next, we assessed if the number of alleles whose frequency changed significantly was affected by mode of reproduction, gene flow, or the presence of a pH-gradient. To do so, we counted for every evolved population the number of variants that significantly changed in allele frequency ($p < 10^{-10}$). In this analysis, we applied various cut-offs for the magnitude of the allele frequency change, i.e., the minimum absolute difference between the ancestral allele frequency and the observed allele frequency of the evolved population. We used in total six cut-off values of increasing stringency (0.3, 0.4, 0.5, 0.6, 0.7 and 0.8) in the minimum magnitude of allele frequency change required for variants to be included. We fit a generalized linear mixed model with a Poisson distribution to the resulting data, using the `lme` function of the `nlme` R-package (version 3.1-147; Pinheiro et al., 2020). We first created a model in which reproduction, gene flow, abiotic conditions and the cut-off value are all allowed to interact as fixed effects (full interaction model), and using the replicate population (i.e. the identity of each replicate evolved population) as a random effect. We then used the `dredge` function in the `MuMIn` package (version 1.43.17; Bartoń, 2009) to compare all possible models based on the Bayesian Information Criterion (BIC; Gelman et al., 2014). This method is similar to the AICc method, in that it allows a ranking of models based on their maximum likelihood (lower BIC score indicates better model fit), but is more commonly used

for mixed effect models. We report model weights following the BIC comparison, as well as summary statistics (type-III Anova table and model summary) of the best fitting model.

Quantifying presence of *De novo* mutations

To assess how the mode of reproduction, gene flow, and the presence/absence of a pH-gradient affect the evolutionary dynamics of *de novo* mutations in our populations, we counted in each of the 16 evolved populations the number of novel variants and their allele frequencies. To do so, we used eight cut-off values of increasing allele frequencies, ranging from 0.1 to 0.8. For each of these values we counted the number of *de novo* alleles that had reached an allele frequency larger than the cut-off in the post-evolution populations. To find out whether this number of variants was affected by reproduction, gene flow, and the pH-gradient, we fit a linear mixed model using the `lme` function of the `nlme` R-package (version 3.1-147; Pinheiro et al., 2020) using reproduction, gene flow, presence of a pH-gradient, and cut-off as fixed effects, and replicate population as a random effect. Next, we used the `dredge` function of the `MuMIn` package (version 1.43.17; Bartoń, 2009), to rank all possible models based on the Bayesian information criterion (BIC; Gelman et al., 2014). We report model weights as well as summary statistics (type-III anova table and model summary) of the best model from this BIC comparison.

General adaptations during range expansion

To identify allele frequency changes likely to be associated with general adaptations — they were subject to selection regardless of reproductive mode, gene flow, or the presence of a pH-gradient — we focused on alleles whose frequency increased or de-

creased consistently across all or most populations. Specifically, we started from allelic variants that had been present in the ancestral population, that changed significantly in frequency (p-value $<10^{-10}$), and that could not be attributed to selection against clone SB3539 (allele frequency change >0.3). Among these alleles, we then considered only those whose frequency changed significantly and in the same direction for 75 % (12/16) of all evolved populations. We call the resulting dataset the "general adaptation dataset". Within this data set, we focused on alleles within protein-coding genes and examined the functions of these genes.

Gradient-specific adaptations: Cochran-Mantel-Haenszel test

To identify allelic changes specifically associated with the presence or absence of the pH-gradient, we performed a Cochran-Mantel-Haenszel test using the PoPoolation2 package (Kofler et al., 2011). This test compares pairs of populations and it can identify genomic loci with standing genetic variation that show consistently different allele frequencies. To account for the effect of reproduction and gene flow, we always compared pairs of populations with the same reproduction or gene flow treatment, and that only differed in the presence of the gradient. In other words, we compared an asexual population without gene flow expanding into a pH-gradient with another asexual population without gene flow but expanding into a uniform environment (see Supplementary Material section S.4.14.1). With this approach, we aimed at detecting loci that display consistent differences between populations expanding into a pH-gradient and populations expanding into a uniform environment, independent of gene flow and reproductive mode. To account for multiple testing, we used a Bonferroni correction (Bland and Altman, 1995). Because our genomes harboured approximately 10^5 genetically variable positions, and we wished to use a conservative p-value of 0.001, we only classified po-

sitions with a p-value smaller than 10^{-8} significant. We refer to this data set, which contains all loci experiencing differential selection between populations expanding into a pH-gradient and populations expanding into a uniform environment as the "gradient-specific adaptation" dataset. We then identified the alleles in this data set that lie inside protein-coding genes, and compared the function of these genes between populations expanding into a pH-gradient and populations expanding into a uniform environment.

Gene ontology enrichment

To assess whether allele frequency changes occur in genes associated with specific functions, we performed a gene ontology (GO) term enrichment analysis using GOWINDA (version 1.12; Kofler and Schlötterer, 2012). Specifically, we aimed at identifying gene functions for alleles involved in general and gradient-specific adaptations. To this end, we first queried the Uniprot Knowledgebase to obtain all entries associated with the *T. thermophila* reference genome (TaxID: 312017). This resulted in a list of genes encoded in the Tetrahymena genome together with GO-term associated with each gene. We then performed a GOWINDA analysis using this dataset as a reference database. We performed this analysis for two sets of genes, the genes associated with general adaptations and the genes associated with gradient-specific adaptations

GOWINDA analysis corrects for multiple testing with the Benjamini-Hochberg procedure (Benjamini and Hochberg, 1995). For both GO-term analyses, we thus filtered the resulting GO-terms based on this procedure and kept only those GO-terms with an FDR-value < 0.05. Next, we grouped the enriched GO-terms into 13 different categories of cellular mechanisms (see Supplementary Material Section S.4.9. We then compared the proportion of all GO-terms associated with the 13 categories between the general adaptation genes and the gradient-specific genes, using a χ^2 -test. Finally, we performed

a post-hoc test to assess which categories are differently enriched in the gradient-specific genes and the general adaptation genes using a Benjamini-Hochberg correction to avoid false positive results (Benjamini and Hochberg, 1995; Ebbert, 2019).

Results

Gene swamping alters fitness changes

We first asked whether gene swamping affects genotypic and phenotypic evolution, i.e., the evolution of population fitness (intrinsic population growth rate) during range expansions. To this end, we focused on those 16 among 34 surviving populations previously evolved and studied phenotypically by Moerman et al. (2020b) that had evolved the highest population growth rate (r_0) increase in one of eight experimental conditions (asexual/sexual reproduction, presence/absence of gene flow, presence/absence of a pH-gradient during range expansion, two populations per condition, see also section "Experimental evolution" in the Material and Methods). We analyzed the phenotypic evolution in these population, subjected samples from each population to genome sequencing (see also section "Sequencing and identification of variants" in the Material and Methods), and then juxtaposed patterns of genotypic change with those of phenotypic change.

To study phenotypic evolution, we first assessed how the mode of reproduction, gene flow and the pH-gradient affected the evolution of the intrinsic population growth rate r_0 . Specifically, this meant we created all models of change in r_0 (response variable) as a function of the mode of reproduction, gene flow and presence/absence of a pH-gradient (response variable), ranging from an intercept model to a full interaction model, where all these response variables are allowed to interact. We then compared these models (i.e.

using the AICc (Akaike Information criterion adjusted for small sample size; Hurvich and Tsai 1989) to find the best fitting model. This analysis showed that gene swamping (i.e. an interaction between mode of reproduction and gene flow) and the presence of a pH-gradient affected the fitness change during range expansions.

Specifically, as show in Figure 4.1, fitness increased in all evolved populations (data from each evolved population is shown as a circle in Figure 4.1; lines and shaded areas represent model predictions and confidence intervals). Fitness increased more strongly for populations expanding into a pH-gradient (panels B and D in Figure 4.1) compared to populations expanding into a uniform environment (panels A and C in Figure 4.1; $F_{1,29}=299.16$, $p<0.001$). This is not surprising, because the low pH experienced during range expansion into a pH-gradient represents a novel environment to which populations had to adapt during range expansion, whereas the uniform environment more closely matched the abiotic conditions to which the ancestral clones were already adapted.

In addition, fitness increased on average more strongly in sexually reproducing populations (blue points in Figure 4.1) than in asexually reproducing populations (yellow points in Figure 4.1; $F_{1,11}=6.44$, $p=0.027$). This suggests that recombination can facilitate adaptation during range expansion. Additionally, fitness increased more strongly for populations that expanded their range in the presence of gene flow (panel C and D in Figure 4.1) than in the absence of gene flow (panels A and B in Figure 4.1; $F_{1,11}=8.09$, $p=0.016$). This in turn suggests that the influx of genetic material through gene flow can facilitate adaptation. However, we also observed a significant interaction between reproduction and gene flow ($F_{1,11}=14.36$, $p=0.003$). Specifically, in the absence of gene flow (Figure 4.1, panels A and B in Figure 4.1), sexually reproducing populations increased more strongly in fitness than asexually reproducing populations. In contrast, in the presence of gene flow (Figure 4.1, panels C and D in Figure 4.1), sexually repro-

ducing populations increased their fitness less than asexually reproducing populations. This observation suggests that recombination is only beneficial when a population is not being swamped with maladapted genes. We observed this gene swamping effect both in populations expanding into a uniform environment (Figure 4.1, panels A and C) and in populations expanding into a pH-gradient (Figure 4.1, panels B and D), although the gene swamping hypothesis only predicts this pattern in presence of an environmental gradient (Kirkpatrick and Barton, 1997; García-Ramos and Kirkpatrick, 1997). The observations made here are consistent with our previous observations based on a larger number of populations (Moerman et al., 2020b).

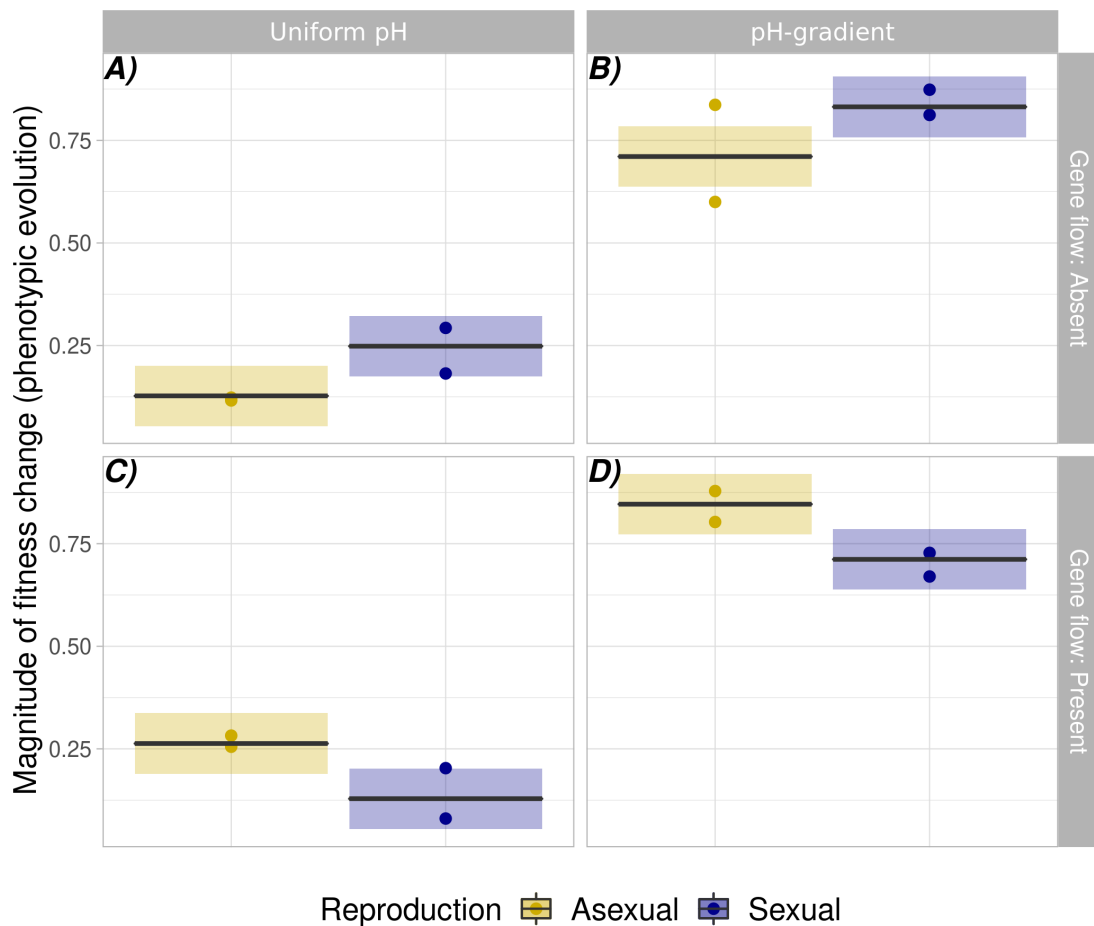


Figure 4.1: Gene swamping affects fitness changes during range expansion. Fitness change expressed as the log-ratio change in intrinsic population growth rate, calculated as the ratio of the logarithm (base 2) of the intrinsic growth rate (r_0) of an evolved population and the intrinsic growth rate (r_0) of the ancestral population. Circles represent data for individual populations. Black lines and shaded areas represent mean predictions and 95 % confidence intervals of the best model. Colours represent mode of reproduction (yellow=asexual, blue=sexual). Left subplots (panels A and C) show data and model predictions for populations expanding into a uniform environment, right subplots (panels B and D) for populations expanding into a pH-gradient. Upper subplots (panels A and B) show data and model predictions for populations where gene flow is absent, and lower subplots (panel C and D) for populations where gene flow is present. Adapted from Moerman et al. (2020b).

Reproduction and gene flow alter allele frequency change.

In a next analysis, we assessed whether the above phenotypic changes in intrinsic population growth rate are mirrored in genotypic changes. To this end, we first sequenced the 16 evolved populations and four ancestor clones ("PoolSeq", Schlötterer et al., 2014) using the Illumina Novaseq 6000 platform. The average genome coverage was 112X among all sequenced populations and was 66X for the population with the lowest coverage.

After we had eliminated likely false positive allele frequency changes due to multiple testing and clonal selection on one of our ancestral clones (see section "Statistical analyses" in the Material and Methods), we observed significant allele frequency changes in 13,278 alleles. Only 29.39 % of these alleles occurred in protein-coding regions of the genome. The percentage of macronuclear DNA predicted to occur in protein-coding genes of *T. thermophila* equals 47.78 % (Eisen et al., 2006). This means that we observed significantly fewer allele frequency changes in protein-coding genes than expected by chance alone (exact binomial test: $p < 0.001$). More than half (57.1 %) of the alleles were indels as opposed to single nucleotide polymorphisms (42.9 %). More indels and SNPs than expected by chance occurred in non-coding regions (exact binomial test; $p < 0.001$ for both). However, there were significantly more SNPs (34.61 %) than indels (25.46 %; Pearson Chi-squared test: $\chi^2_1 = 130.89$; $p < 0.001$) in protein-coding regions of the genome, consistent with the expectation that indels are likely to be more deleterious than SNPs.

Next, we investigated how the mode of reproduction, gene flow and the abiotic conditions affected the number of alleles which changed in allele frequency. To do so, we created all models of the number of allele frequency changes (response variable) as a

function of the mode of reproduction, gene flow, presence/absence of a pH-gradient and the cut-off in magnitude for allele frequency change (response variable), while accounting for population identity (random effect). These models ranged from an intercept model to a full interaction model, where all these response variables are allowed to interact. We then compared all possible models (ranging from an intercept model to a full interaction model) to find the best fitting model, according to the Bayesian Information Criterion (BIC; Gelman et al., 2014). After comparison of all possible models, we found only support for the full interaction model (weight=1, δ BIC of second model = 136.09), showing that all explanatory variables (mode of reproduction, gene flow, abiotic conditions and the cut-off), as well as their interaction had an important effect on the number of alleles that changed in frequency.

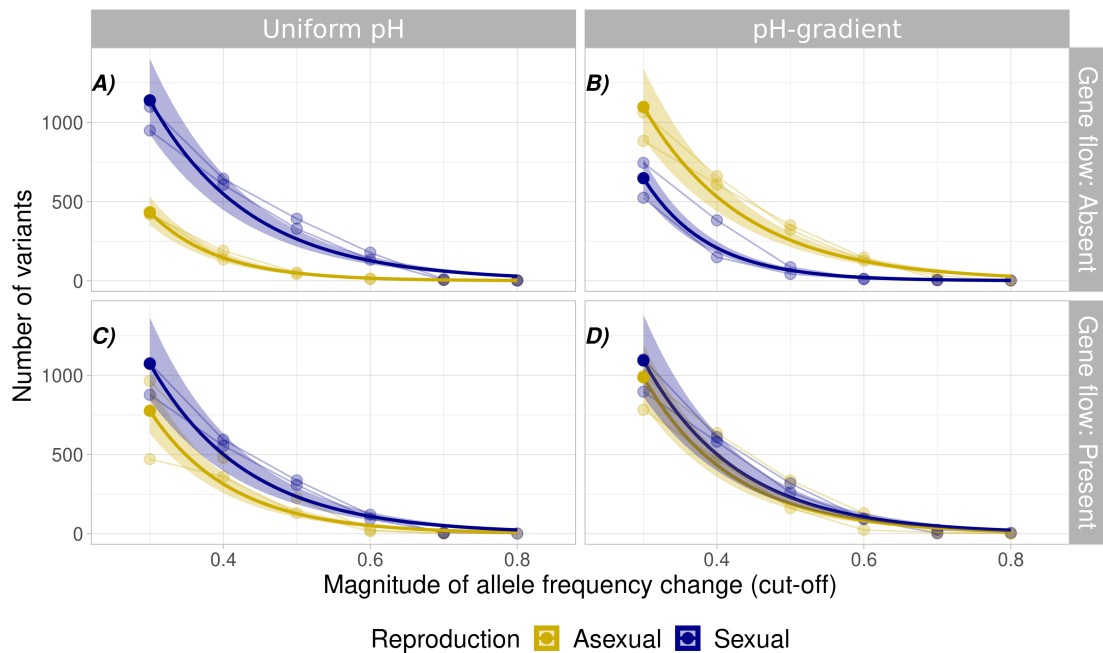


Figure 4.2: **Reproduction and gene flow alter genetic changes in standing genetic variation.** Number of alleles that changed significantly in frequency during range expansion into a uniform environment (panel A and C) or into a pH-gradient (panel B and D). The x-axis shows the cut-off value in the magnitude of allele frequency. The y-axis shows the number of variants analyzed at each cut-off value. Thin faint lines and circles represent allele frequency data, with lines connecting data from the same replicate population. Thick opaque lines show the model predictions for the best model. Shaded areas show 95 %-confidence intervals from the best model. Colours represent mode of reproduction (yellow: asexual, blue:sexual).

More specifically, the total number of alleles that changed significantly in frequency was on average similar for populations expanding into a uniform environment (Figure 4.2, panels A and C) and into a pH-gradient (Figure 4.2, panels B and D). However, the effect of reproduction and gene flow differed between these populations. When populations expanded into a uniform environment in the absence of gene flow (Figure 4.2, panel A), sexual reproduction strongly increased the number of variants which changed in allele frequency. In contrast, when such populations expanded into a pH-gradient

(Figure 4.2, panel B), sexual reproduction decreased the number of alleles whose frequency changed (Reproduction \times Abiotic conditions; $\chi^2_{1,92}=8.3981$; $p=0.0038$). When populations experience gene flow during range expansion (Figure 4.2, panels C and D), this difference between populations with a sexual and asexual mode of reproduction disappeared. Specifically, both when expanding into uniform environments (Figure 4.2, panel C) and when expanding into a pH-gradient (Figure 4.2, panel D), sexually reproducing populations displayed only marginally more variants that changed in allele frequency than asexual populations. Together, these results suggest that the effects of reproductive mode on standing variation depend on the presence of a pH-gradient, but only in the absence of gene flow. Complete model statistics can be found in the Supplementary Material section S.4.10.1.

Next, to investigate whether the number of genetic changes during range expansion can help predict the extent of fitness change, we compared the number of variants whose allele frequency changed significantly with the change in the intrinsic growth rate (r_0) of the evolved populations. To do so, we calculated the correlation coefficient between these two metrics. We calculated this correlation for each cut-off value for the magnitude of allele frequency change. We did so separately for populations expanding into uniform conditions and populations expanding into a pH-gradient, as well as for sexual and asexual populations.

Figure 4.3 displays the relationship between the number of alleles changing their frequency and the extent of fitness change. This relationship depends on the mode of reproduction and the abiotic condition. For asexual populations (yellow circles and triangles), the allele frequency change and fitness are not correlated. A possible reason is that the lack of sexual recombination in asexual populations limits the separation of maladaptive and beneficial alleles, and may therefore have limited selection of beneficial

alleles.

In contrast, for sexual populations (blue circles and triangles), the number of alleles changing their frequency and the extent of fitness change are correlated, depending on the abiotic conditions. Specifically, for populations expanding into a uniform environment, populations in which more variants change their frequency also increase their fitness to a greater extent, and significantly so for three out of five cut-off values (4.3, left panels). In contrast for populations expanding into a pH-gradient, the number of variants changing in allele frequency and fitness change are not significantly correlated at all cut-off values (4.3, right panels). One possible explanation is that in a new and stressful environments such as our pH-gradient, *de novo* mutations may be more important than standing variation for adaptive variation. However, this is not the case (see Fig. S4.3 in the Supplementary Material).

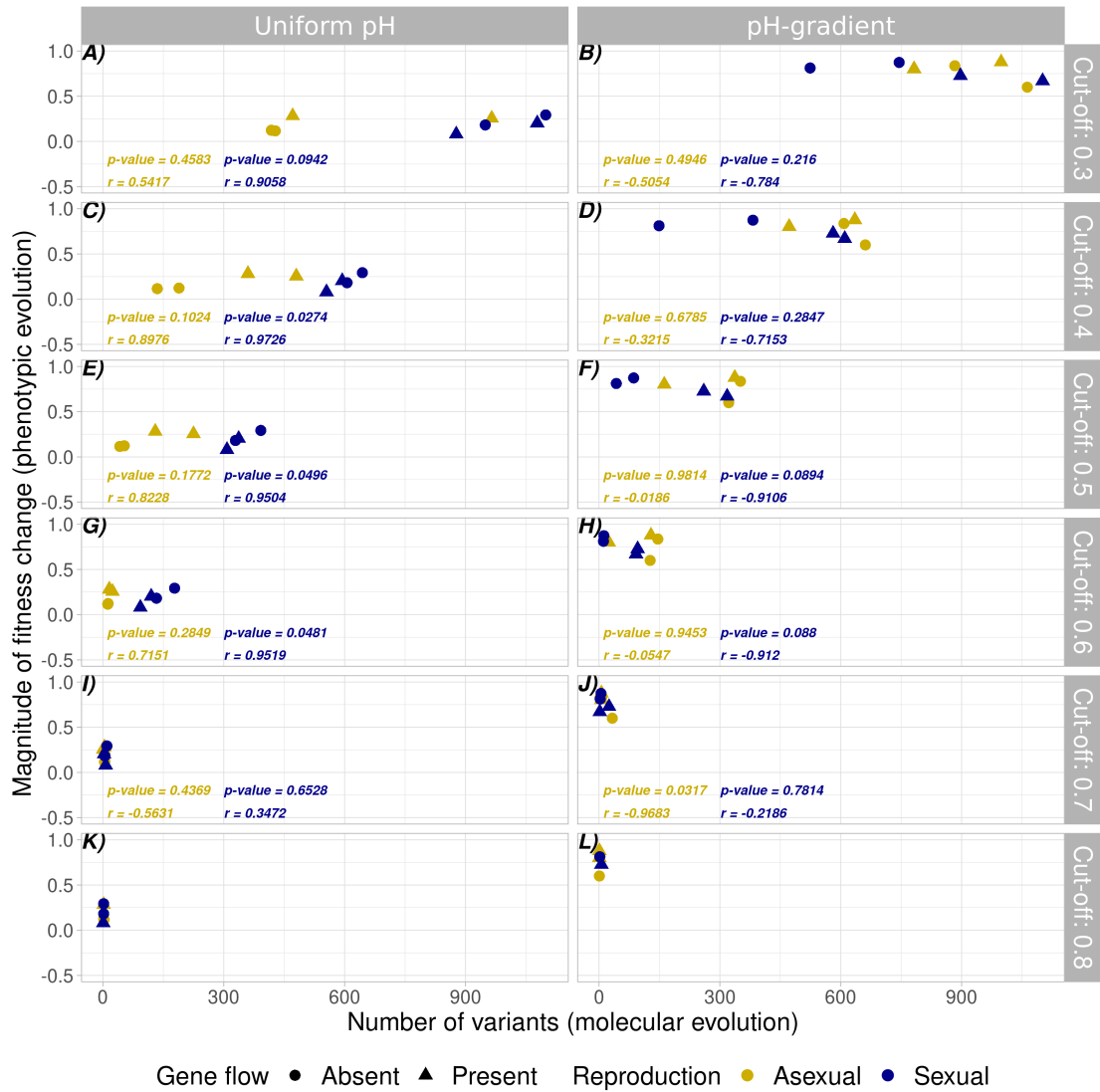


Figure 4.3: **A positive relationship between fitness change and genetic change when sexual populations expand into a uniform environment.** Statistical association between change in fitness and the number of allele frequency changes in standing genetic variation, for populations expanding into a uniform environment (panels A, C, E, G, I, and K) and populations expanding into a pH-gradient (panels B, D, F, H, J, and L). The x-axis shows the number of standing genetic variants that changed significantly in allele frequency. The y-axis shows the change in growth rate (fitness) of evolved populations compared to the ancestral population ($\log_2(r_0 \text{ of evolved population} / r_0 \text{ of ancestral population})$). Horizontal subplots show the data for different cut-off values used for the minimum change in allele frequency at the end of evolution for inclusion in the analysis. Each geometric symbol within a subplot represents a single population, with colour representing reproductive mode (yellow=asexual, blue=sexual) and shape representing gene flow (circle=gene flow absent, triangle=gene flow present). Text insets shows the correlation coefficient r and significance p , based on a correlation test for sexual populations (blue text) and asexual populations (yellow text). For the most stringent cut-off value (allele frequency change >0.8), we did not calculate the correlation, because several populations did not harbour any variants that changed so dramatically in allele frequency.

Frequencies of *de novo* mutations change most strongly in sexually reproducing populations.

Adaptive evolution is not exclusively caused by changes in the standing variation we analyzed in the preceding section. It can also be caused by mutations that occurred *de novo* during experimental evolution, and that rise to varying frequencies by the end of the experiment. We thus studied such variants and their allele frequencies. We note again that our populations are large $10^4 - 10^6$ such that most *de novo* mutations would rise to detectable frequencies by natural selection rather than genetic drift.

We found a total of 27,694 *de novo* mutations across all 16 evolved populations. They reached frequencies between 1.9 % and 100 % in the evolved populations. Only 0.02 % of these *de novo* variants went to fixation. 31.73 % percent of them occurred in protein-coding genes. Given that 47.87 percent of the *Tetrahymena* genome is protein-

coding (Eisen et al., 2006), *de novo* variants are less likely to occur in protein coding regions than expected by chance (exact binomial test, $p < 0.001$). Most (82.30 %) *de novo* variants were indels. Significantly fewer indels (29.14 %) than SNPs (46.36 %) occurred in protein-coding regions (Pearson Chi-squared test: $\chi^2_1=130.89$; $p < 0.001$). Unlike for standing genetic variation (discussed in the previous section), only *de novo* indels but not SNPs were less likely to occur in protein-coding regions than expected by chance (indels: 29.14 %; $p < 0.001$; SNPs; 46.36 %, $p=0.066$, exact binomial test).

Next, we investigated the role of reproductive mode, gene flow and the pH gradient on the number of *de novo* mutation. To do so, we created all possible models fitting the number of mutations (response variable) as a function of the mode of reproduction, gene flow, presence/absence of a pH-gradient and the cut-off in the allele frequency that mutations reached (response variable), while accounting for population identity (random effect). These models ranged from an intercept model to a full interaction model, where all explanatory variables were allowed to interact. We then compared these models based on the Bayesian Information Criterion (BIC; Gelman et al., 2014). We found clear support for only one model, which had the cut-off for allele frequency that mutations reached, mode of reproduction and the interaction between these two variables as fixed effects (weight=0.753, δBIC of second model = 3.66).

Specifically, we found that the number *de novo* mutations that reached measurable frequencies was similar between populations expanding into a uniform environment (Figure 4.4, panel A) and into a pH-gradient (Figure 4.4, panel B). We observed more *de novo* mutations in sexually reproducing populations (Figure 4.4, blue lines and circles) than in asexual populations (Figure 4.4, yellow lines and circles; $\chi^2_{1,14}=13.567$). At increasingly higher allele frequency cut-offs, the number of novel variants become more similar for populations with asexual and sexual reproduction (Reproduction \times Cut-off;

$\chi^2_{1,126}=18.696$).

The increased number of *de novo* mutations that rise to detectable frequency in sexually reproducing populations is consistent with the notion that recombination facilitates adaptative evolution by separating maladaptive mutations from beneficial mutations, (Peck, 1994; Otto and Barton, 1997; Gerrish and Lenski, 1998; Burt, 2000; Johnson and Barton, 2002; Gray and Goddard, 2012).

The higher number of mutations in sexual populations was independent from the presence of a pH-gradient or from gene flow, because neither of these conditions occurred in the model that best explained the data. (See Supplementary Material section S.4.10.2 for statistical details on the best model.)

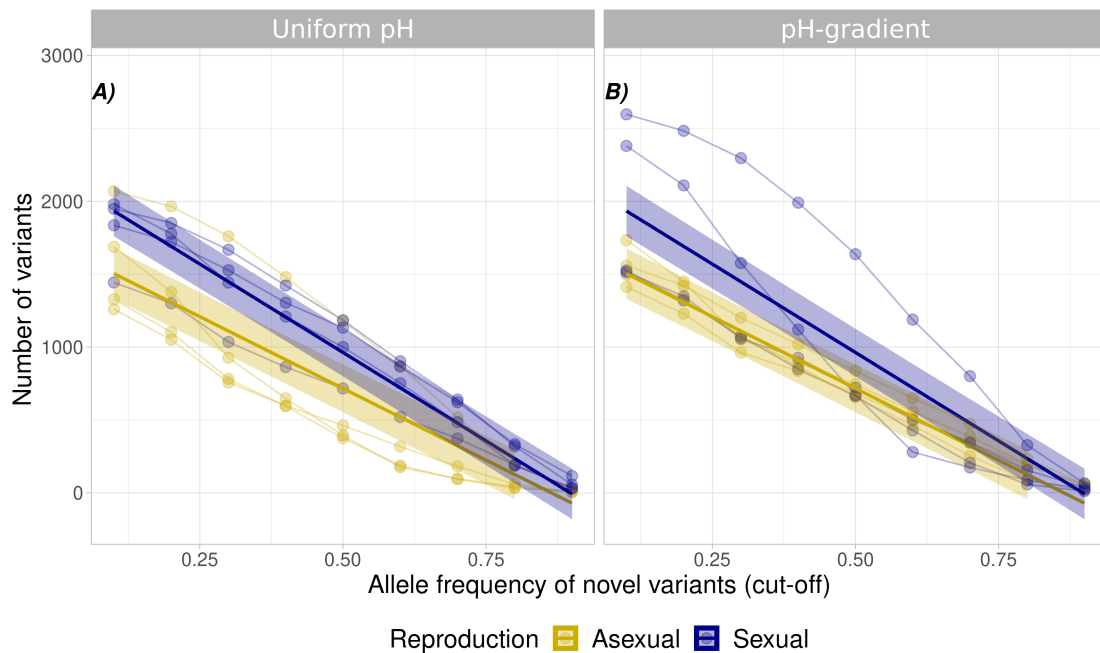


Figure 4.4: ***De novo* variants increase to higher frequency in sexual populations.** The figure shows the number of novel variants for the evolved populations expanding into a uniform environment (panel A) or into a pH-gradient (panel B). The x-axis shows the cut-off value in minimum allele frequency of the variants. The y-axis shows the number of *de novo* variants (mutations) whose frequency is above a given cut-off. Thin faint lines and circles represent the data, with every line representing a single replicate population. The thicker opaque lines and shaded areas show the predicted means and 95 % confidence intervals for the best model. Colours represent the mode of reproduction (yellow=asexually reproducing populations, blue=sexually reproducing populations).

Genes involved in adaptive evolution through allele frequency changes.

In our next analysis, we wanted to identify specific classes of genes that may be involved in adaptive evolution during range expansion. In such an analysis, it is useful to distinguish between genes involved in general adaptation to conditions experienced by all populations, such as the growth medium and the expanding range, and genes that are specifically involved in adaptation to our pH gradient. For both classes of genes, we here focus on alleles that changed significantly in frequency during evolution, and

report an analogous analysis of *de novo* mutations in Supplementary Material section S.4.13.

To identify general adaptations, we first identified polymorphic genes that had experienced significant changes in allele frequency in at least 75 % of our populations, and for which allele frequency either always increased or always decreased. To identify gradient-specific adaptations, we performed a Cochran-Mantel-Haenszel test to identify genes whose alleles consistently differed in frequency between populations expanding into a uniform environment and populations expanding into a pH-gradient.

Changes in standing variation associated with general adaptation involve transmembrane proteins and kinase domains.

Of all polymorphic genomic loci at which significant allele frequency changes occurred, 242 loci fit our general adaptation criterion. Of these 242 loci, 53 occurred in gene coding regions, which fell into 43 different genes (Table S4.15). Of these 43 genes, 12 encode transmembrane proteins, four encode proteins with a kinase domain, three encode proteins with a cyclic nucleotide-binding domain, three encode zinc finger proteins, and two encode cation channel proteins. All other genes either encode uncharacterized proteins (10 out of 43 genes) or encoded various other proteins (nine out of 43 genes) that were not encoded by multiple genes in this dataset (i.e. nine genes, all coding for different proteins; see also Table S4.15).

Gradient-specific changes in allele frequency are associated with ion balance.

We found 97,690 genomic positions for which we could quantify differences in allele frequencies through the Cochran-Mantel-Haenszel test. After Bonferroni correction, we retained 4,388 positions with significantly different allele frequencies between populations expanding into a pH-gradient and populations expanding into a uniform environment. 1,758 of these positions occurred in protein-coding regions, and fell into 636 different genes (Table S4.16 in the Supplementary Material). The largest subset of these genes with a functional annotation (136 genes) encode transmembrane proteins. Other highly represented groups include genes that encode kinase domain proteins (99 genes), cyclic nucleotide binding domain proteins (39 genes), cation channel proteins (18 genes) and zinc-fingers (14 genes). The remaining genes either encode uncharacterized proteins (132 genes) or genes encoding for various different proteins (188 genes) that were not encoded by many genes (i.e. only few genes coded for proteins with the same or a similar cellular function). Notably, two genes, a gene encoding a cation channel family protein and a gene encoding an oxalate/formate antiporter were involved in both gradient-specific changes in allele frequency and gradient-specific mutations (Table S4.16 and Table S4.18 in the Supplementary Material). Because both cation channels and oxalate/formate antiporters can play a role in ion transport (Wada et al., 1987; Ruan et al., 1992; Cyert and Philpott, 2013), we speculate that these genes help maintain the ion balance in the cell caused by the pH-stress.

General adaptation preferentially affects genes involved in DNA repair and gene expression.

To find out whether general adaptation and gradient-specific adaptation involved genes with different functions, we studied the differential enrichment of gene ontology terms in these sets of genes.

Among 701 GO-terms associated with the 43 general adaptation genes, 72 terms in 13 major categories were significantly enriched at a false discovery rate (FDR) of <0.05 after multiple testing correction (Benjamini and Hochberg, 1995; Kofler et al., 2011). Likewise, among 1928 GO-terms associated with 626 gradient-specific genes, 693 terms in 13 major categories were significantly enriched.

In Figure 4.5, the percentage of the 13 major categories is shown for the GO-terms associated with general adaptation (Figure 4.5 panel A) and gradient-specific adaptation (Figure 4.5 panel B). We found only two significantly differentially enriched GO-term categories. The first comprise transcription and translation functions, which were more likely to be associated with genes involved in general adaptation (8.97 % of all GO-terms) than with genes involved in gradient-specific adaptation (1.3 % of all GO-terms; $FDR < 0.001$). The second comprises mitosis, DNA repair and chromosome division, which were also more likely to be associated with genes involved in general adaptation (16.67 % of all GO-terms) than in genes associated with gradient-specific adaptation (3.75 % of all GO-terms; $FDR < 0.001$). We speculate that these cellular functions may be important when selection for faster population growth results in faster cell division and therefore potentially more DNA damage.

Genes involved in gradient-specific adaptation were associated more often with ion binding and transport, as well as with mitochondrial functioning and oxidoreductase

reactions. However, these differences were no longer significant after correcting for multiple testing. Nonetheless, both functions may play a role in the maintenance of ionic balance and the oxidative stress response associated with low pH (Lambert and Brand, 2004; Lemarie et al., 2011; Cyert and Philpott, 2013; Lindberg and Collins, 2020).

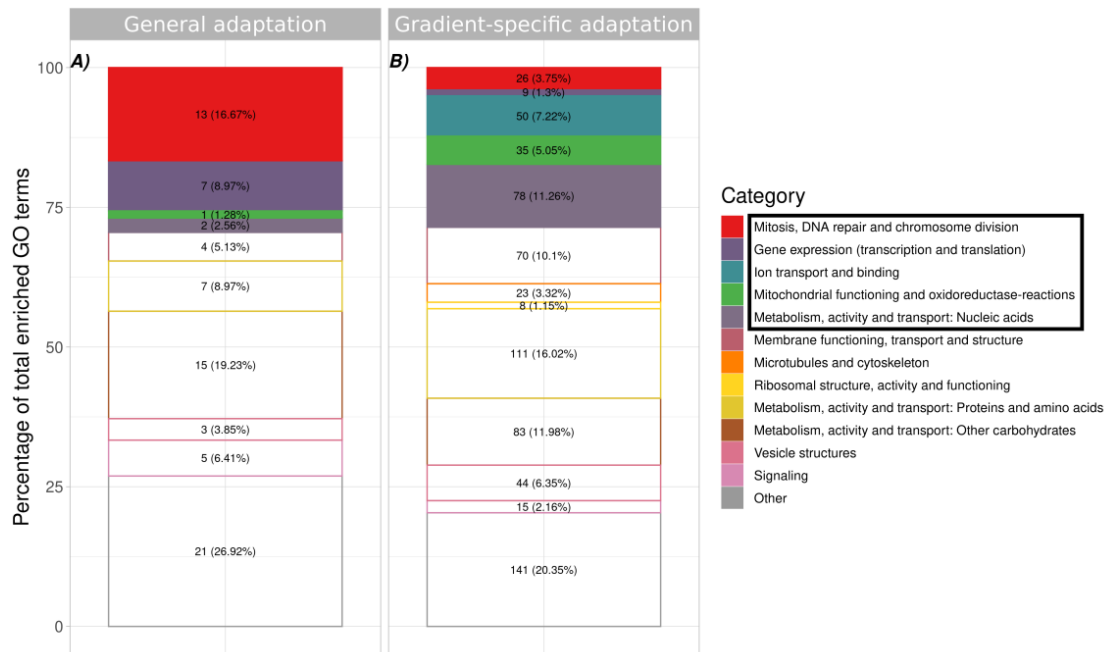


Figure 4.5: **General and gradient-specific adaptations during range expansion.** Partitioning of all enriched gene ontology terms among 13 major functional categories for genes involved in (panel A) general adaptations and (panel B) gradient specific adaptations. Colours correspond to the 13 major GO categories we used. Numbers in each rectangle represent the number and percentage of genes whose annotation fell in each category. Differentially enriched categories are displayed as filled rectangles, the remaining categories are displayed as open rectangles with a coloured border.

Discussion

We investigated the genetic basis of adaptations that occur when populations of *T. thermophila* expand their range. Specifically, we investigated how a pH-gradient, sexual reproduction, and gene flow affect the number of allele frequency changes in standing genetic variation and the number of *de novo* mutations that rise to detectable frequency during adaptive evolution. Additionally, we investigated which kinds of genes may have been involved in general adaptations to the growth environment and the expanding range, as opposed to adaptations specific to the pH gradient.

We found that sexual reproduction increased the incidence of *de novo* mutations that rise to detectable frequencies. The effect of sexual reproduction on standing genetic variation was more complex. In the absence of gene flow, sexual reproduction increased the number of allele frequency changes for populations expanding into uniform environments. In contrast, it decreased the number of such changes for populations expanding into a pH-gradient. In the presence of gene flow, this difference between sexual and asexual populations disappeared. We found that general adaptation mostly involved genes associated with mitosis, DNA-repair and gene expression. Gradient-specific adaptation mostly involved genes associated with ion transport and oxidoreductase reactions.

The role of sexual recombination on genetic changes during range expansions

By reshuffling genetic variation, sexual reproduction can have important consequences on adaptive evolution (Smith, 1978; Bell, 1982; Otto, 2009). Indeed, we here observed that sexual reproduction increased the number of *de novo* mutations which rose to de-

tectable frequencies.

Most mutations that arise have a negative or neutral effect of fitness (Loewe and Hill, 2010). In asexual lineages, the accumulation of mutations therefore often leads to a gradual decrease in fitness, but sexual reproduction can help increase fitness by purging such deleterious mutations (Muller, 1932; Smith, 1978; Fisher, 2000; Johnson and Barton, 2002; McDonald et al., 2016). However, sex may also play a positive role by separating the rare beneficial mutations from maladaptive mutations. In asexual lineages, the negative effects of maladaptive mutations may counteract selection for beneficial mutations (Smith, 1978; Peck, 1994).

Notably, we observed in this experiment that more mutations rose to detectable allele frequency in populations with a sexual mode of reproduction. Because chromosome division in the polyploid ($n=45$) macronucleus of asexual lineages of *T. thermophila* happens randomly, offspring of the same individual may vary in the copy numbers of specific mutations (Ruehle et al., 2016). Therefore, in asexual *T. thermophila* populations, selection likely acts against individuals carrying deleterious mutations at a high copy number. In contrast, sexual recombination may reduce this mutational load by separating maladaptive mutations from neutral or beneficial mutations (Smith, 1978), which could alleviate the selection against *de novo* mutations in our experiment.

The effect of sexual reproduction on allele frequency changes in standing genetic variation is more difficult to explain. In the absence of gene flow, sexual reproduction resulted in more such changes for populations expanding into a uniform environment, and fewer such changes for populations expanding into a pH-gradient than asexual reproduction. One possible explanation is that *de novo* mutations were more important for populations expanding into a pH-gradient, whereas selection on standing genetic variation was more important for populations expanding into a uniform environment. Be-

cause the conditions a population experiences when expanding into a uniform environment are similar to those experienced by the ancestral population, selection on standing genetic variation may suffice for adaptation in this case. This possibility is supported by the positive correlation between the number of genetic changes and the fitness increase for populations expanding into a uniform environment (Figure 4.3). Sexual recombination could be adaptive for such populations by bringing together adaptive alleles from the different ancestor clones (Smith, 1978).

In asexual populations, however, the lack of sexual recombination implies that any mutations that arise can not be separated from their genetic background. This means that if a beneficial mutation is under strong positive selection, other alleles that co-occur on the same genome may hitch-hike to high allele frequencies, without these other alleles necessarily having a strong effect on fitness themselves. This idea would also be supported by the observation that in asexual populations, the number of allelic changes does not correlate with fitness (see also Figure 4.3), suggesting that most allelic changes don't affect fitness strongly. Whether mutations play a more important role in stressful or new environments can be highly dependent on the model organism and the specific stressor (Agrawal and Whitlock, 2010; Arbuthnott and Whitlock, 2018). For example, a previous experiment showed that clonal populations of *T. thermophila* were under stronger selection when under pH-stress (low pH; Moerman et al., 2020a), suggesting that mutations may indeed play a more important role in stressful conditions for *T. thermophila*. However, to validate this hypothesis, fitness measurements of individual mutations would be needed, which we did not perform, because the large number of mutations and difficulty in transforming the genome of *T. thermophila* made it unfeasible to investigate the fitness effect of all mutations.

We here focussed mainly on the role of sexual reproduction, and less on the role

of gene flow. This is because gene flow affected genetic adaptation less strongly than sexual reproduction in this experiment. The main effect we found associated with gene flow was that it reduced the differences in genetic changes from standing variation between populations with an asexual and sexual mode of reproduction. Likely, this result stems from the counteracting effect gene flow can have on adaptation (Lenormand, 2002). It is important to consider here that in this experiment, gene flow and sexual reproduction were distinct events that were linked to each other in time. This means that in presence of gene flow, sexual reproduction may not have provided much benefits and even may have undone much of the selection that happened, because sexual reproduction would result in the incorporation of maladapted genes from the range core. This means that in presence of gene flow, both asexual and sexual populations may have undergone adaptation primarily via selection on asexual clones.

Genes under selection during range expansions

Genes related to mitosis, DNA repair and chromosome division are involved in general adaptations that occur during range expansions in our experiments. This observation is consistent with range expansion theory, which predicts strong selection on population growth rate (Burton et al., 2010; Phillips et al., 2010; Shine et al., 2011). Faster growth and cell division leads to a decreased nucleotide generation time (i.e., the average time it takes before a nucleotide is copied for replication or repair), which can be associated with greater mutation rate (Martin and Palumbi, 1993). In addition, because many mutations are associated with DNA replication (Friedberg et al., 2002; Kunkel, 2004; Friedberg et al., 2005), shorter generation times may lead to a higher mutation rate per unit time. General selection in this experiment also acted on genes related to

DNA repair, which may be an adaptation to reduce the accumulation of mutations due to faster cell division. Because maladaptive mutations accumulate at the edge of a population's range (Excoffier et al., 2009; Peischl and Excoffier, 2015; Peischl et al., 2015) an increase in mutation rate may be especially harmful at this edge.

Range expansion theory also predicts strong selection for increased dispersal in an experiment like ours (Burton et al., 2010; Shine et al., 2011). In addition, several empirical and experimental studies demonstrated rapid evolution of dispersal during range expansions (Brown et al., 2007; Williams et al., 2016; Ochocki and Miller, 2017; Weiss-Lehman et al., 2017). Although dispersal behaviour often has a genetic basis (Saastamoinen et al., 2018), we did not observe selection on genes obviously associated with dispersal, such as genes involved in motility. This observation could have at least two explanations. Firstly, dispersal is often energetically costly (Bonte et al., 2012), and may require investment of resources. Selection on dispersal could therefore be exerted through genes not obviously related to motility, such as genes involved in metabolism or feeding behaviour. Secondly, changes in dispersal may be caused by phenotypic plasticity rather than by genetic change (Clobert et al., 2012, see also Petegem et al. 2018). Because *Tetrahymena* shows strong plasticity in dispersal behaviour (Jacob et al., 2016; Fronhofer et al., 2017b), and because we observed no stable phenotypic changes in dispersal (Moerman et al., 2020b), the latter explanation may be more likely.

We found that gradient-specific adaptations were mostly associated with ion transport and binding, as well as with oxidoreductase reactions. Selection on genes related to ion transport and binding are likely a response to osmotic stress under low pH conditions (Bremer and Krämer, 2019). Oxidoreductase plays an important role in the production of reactive oxygen species (ROS), which are harmful to cells (Esterházy et al., 2008). Low pH can also contribute to elevated production of ROS (Lambert and Brand, 2004;

Lemarie et al., 2011). A previous study found that selection for the capacity to metabolize ROS is an important aspect of evolution under pH-stress due to ocean acidification in phytoplankton (Lindberg and Collins, 2020). Consequently, genes associated with mitochondrial functioning and oxidoreductase reactions may help cope with the harmful consequences of ROS.

Limitations and concluding remarks

Although our results show that selection can lead to rapid genetic evolution during range expansions in *Tetrahymena thermophila*, there are three important limitations to our work. Firstly, the strong clonal selection we observed (see the section "Quantifying frequency changes in standing genetic variation" in the Material and Methods) may have masked some signatures of general adaptation. This possibility is consistent with the larger number of genes associated with gradient-specific adaptation than with general adaptation. Secondly, to fully distinguish the importance of standing variation from that of *de novo* mutations, it would be necessary to assess the fitness effect of individual genetic changes in genes. However, due to the large number of genetic changes and the difficulty and work involved in transforming cells of *T. thermophila*, this was not feasible to do in this experiment. Thirdly, because of the large genome size it was only possible to sequence pooled samples from a limited number of populations. This means we have only limited replication, and lose any information concerning linkage, which could be informative to investigate the role of sexual reproduction.

We show in this experiment that selection during range expansions can rapidly lead to genetic adaptation on traits associated with growth rate and with adaptation to the local environment, it is currently not well understood how generally applicable these

results are. In fact, for many other model systems, evolution of dispersal-related traits may be more important (e.g. Brown et al., 2007; Williams et al., 2016; Ochocki and Miller, 2017; Weiss-Lehman et al., 2017). Additionally, we show here that sexual reproduction and gene flow can alter genetic adaptation during range expansion, but it is currently poorly researched how important the role of gene flow and sexual reproduction is in natural populations. Future research efforts may alleviate both questions by further investigating genetic adaptations during range expansions in experimental and empirical studies. Empirical studies could provide further insights in the genetic nature of adaptations during range expansions by investigating how genetic traits changes along species range (via genome wide association studies; Bush and Moore, 2012), and by quantifying how gene flow and sexual reproduction alter adaptation (e.g. Bachmann et al., 2020). Experimental studies may provide new insight, by applying an integrative approach to the study of genetic adaptation during range expansions, and investigating jointly how genetic changes as well as changes in gene expression and plasticity may alter traits of expanding populations.

Acknowledgments

We thank Samuel Hürlemann, Silvana Käser and Sarah Bratschi for help with laboratory work, Vanessa Weber De Melo for aid on the nuclear separation protocol, and Carla Bello and H el ene Boulain for help with the bioinformatics. Funding is from the University of Zurich URPP Evolution in Action and the Swiss National Science Foundation, Grant No PP00P3_179089. This is publication ISEM-YYYY-XXX of the Institut des Sciences de l'Evolution – Montpellier. We would also like to acknowledge support by Swiss National Science Foundation grant 31003A_172887 and European Research

Council Advanced Grant No. 739874.

Data availability statement

Phenotypic data and output files from variant calling, Cochran-Mantel-Haenszel test and GO-enrichment analyses will be uploaded to Dryad upon acceptance. Raw sequence files will be uploaded to the European Sequence Archive upon acceptance. All analysis scripts will be deposited to Github on acceptance.

Author contributions

FM, EAF, AW and FA designed the experiment. FM performed experimental work and statistical analyses. FM, FA, AW and EAF interpreted the results. FM and AW wrote the first version of the manuscript and all authors commented on and approved of the final version.

Discussion and conclusions

Summary of the main results

In this thesis, I investigated how adaptation to new environments (biotic and abiotic) as well as gene swamping (i.e. the interaction between sexual reproduction and gene flow) alter evolution during range expansions.

In **Chapter 1**, I demonstrated that the population densities affect adaptation to the abiotic environment, resulting in a maximization of population growth rate under the population density conditions experienced during evolution. This selection for a maximization of population growth rate led to a convergence of life-history strategy between the four clones. Next, in **Chapter 2**, I showed that evolution of prey species led to a decrease in the population growth rate of the predator, but evolution of the predator resulted in behavioural and morphological changes that can aid in prey capture and ingestion. In **Chapter 3**, I demonstrated that sexual reproduction aided adaptation during range expansions when there was no gene flow from the range core to the range edge. However, when gene flow from the range core to the range edge resulted in a large influx of maladapted individuals, sexual reproduction actually hindered adaptation by swamping the gene pool at the range edge with genes from maladapted individuals. Although theoretical work expects to see a gene swamping effect only in the presence of an abiotic

gradient in the environment (Haldane and Ford, 1956; García-Ramos and Kirkpatrick, 1997; Kirkpatrick and Barton, 1997), I observed the effects of gene swamping both in the presence and the absence of the pH-gradient. Lastly, in **Chapter 4**, I showed that sexual reproduction increased the number of *de novo* mutations that rose to a detectable allele frequency. In contrast, the number of genetic variants that changed in allele frequency depended on reproduction, gene flow and the presence of an abiotic gradient. I found that selection during range expansion led to genetic changes in genes regulating DNA repair, mitosis, and gene expression, whereas the presence of a pH-gradient was associated with selection on genes involved in ion transport and oxidoreductase reactions.

Together, these results provide a number of insights into the eco-evolutionary dynamics during range expansions. They also highlight gaps in the current state of knowledge that may warrant further investigation. Specifically, I highlight four discussion points which arise from the work in this thesis: 1) the importance of integrating-life-history and demography in eco-evolutionary research, 2) the need to explicitly consider biotic interactions during range expansions, 3) how pushed versus pulled waves may alter range expansion dynamics and 4) the need for integrative genetic research on expanding populations. In the next sections, I discuss each of these four points individually, and provide some suggestions for future research.

Integrating demographic conditions and life-history strategy to understand evolutionary trajectories

Several decades of research have demonstrated that life-history strategy can affect the ecology and evolution of species (Stearns, 1977, 1992, 2000). The importance of life-history traits (and the evolution thereof) has also been recognized in the context of range expansions. During range expansions, populations in a range core continuously experience high population densities, which result in high competition, whereas populations at the range edge are released from this competition (Burton et al., 2010; Phillips et al., 2010). Consequently, populations in a range core are under selection for traits associated with competitive ability, whereas populations at the range edge typically show increased growth rates (Phillips, 2009; Fronhofer and Altermatt, 2015; Ochocki et al., 2020).

Although the evolution of these life-history traits has been studied extensively in the past, it is only more recently that biologists have considered how the ecology and evolution of life-history traits may interact with the evolution of other traits. In recent years, there has been growing attention to study such interactions or feedbacks in ecology and evolution (Pelletier et al., 2009; Hendry, 2016; Govaert et al., 2019). This work on eco-evolutionary feedback loops has demonstrated how ecology and evolution can act and feed back on each other within short time scales. Although recent models have started integrating life-history into eco-evolutionary theory (Govaert et al., 2019), this is still rarely done in experimental studies (for an important exception, see Nørgaard et al. 2019). In the experiments described in this thesis, I did see two specific examples of how consideration of life-history may aid in understanding the evolutionary trajectories during range expansions.

Firstly, in **Chapter 1**, we observed a convergence in life-history strategy when I subjected four strains of *T. thermophila* to high population densities and low pH. One would expect that high density population would evolve more competitive behaviour at the expense of a decreased population growth rate (Mueller and Ayala, 1981; Reznick et al., 2002; Fronhofer et al., 2018). However, because pH stress strongly decreased population growth, we observed a shift in life-history evolution resulting in an increase of density-dependent growth rate under the specific density conditions experienced during evolution. These observations suggest that knowledge of experimental conditions (in my experiment, population densities) is essential to understand evolutionary trajectories. Using simpler assumptions or metrics (for example measuring adaptation to a new stressor like pH-stress simply as an increase in the intrinsic growth rate), may not be sufficient to understand evolutionary changes.

Secondly, in **Chapter 3**, I observed that gene swamping altered adaptation during range expansions in the presence and the absence of an abiotic gradient. In contrast, theory predicts gene swamping only in the presence of an abiotic gradient (Haldane and Ford, 1956; García-Ramos and Kirkpatrick, 1997; Kirkpatrick and Barton, 1997). The argument behind this prediction is that an abiotic gradient will also result in a gradient in population density due to harsh conditions it imposes. However, even in the absence of an abiotic gradient, individuals along a species range show a gradient in life-history strategy, and consequently also in population density. In a typical species range, we expect to see a gradient with high population densities in the range core and low population densities at the range edge (Burton et al., 2010; Phillips et al., 2010; Chuang and Peterson, 2016, but see Fronhofer and Altermatt 2015 and Dallas et al. 2017 for a differing result). However, genetic swamping due to life-history strategy is unlikely to result in a complete halt of range expansion.

Both in the case of gene swamping (**Chapter 3**) as well as in the case of adaptation to pH-stress (**Chapter 1**), I found that it was vital to consider life-history conditions to understand the evolutionary trajectories of the populations. These examples indicate how the explicit integration of life-history is necessary to understanding eco-evolutionary dynamics during. Although I focus on range expansions, this likely is also the case more generally.

Biotic interactions may strongly affect success of invaders

During range expansions and invasions, populations often experience new biotic interactions (Elton, 1958) that may affect the ecology and evolution of invading and expanding populations. This may be especially the case for invading species, which are transported to new locations, because the invading species and the local species do not share a common history. For example the invasive cane toad has had a strong impact on the ecology and evolution of local species in its area of invasion, leading to negative effects on competitors and prey species (Greenlees et al., 2006; Crossland et al., 2008) as well the evolution of prey choice of native predators (Phillips and Shine, 2006).

The consequences of ecological and evolutionary interactions between invaders and native species hinges on two specific aspects of their relationship. Firstly, the type of interaction (e.g. cooperation, competition, predator-prey relation) can strongly affect how biotic interactions may alter ecological and evolutionary dynamics during range expansions and invasions (Brooker et al., 2007; Van der Putten et al., 2010; Kubisch et al., 2014). Secondly, relative generation times may have a major effect on the co-evolutionary interactions between invading species and the local interacting species.

Specifically for predator-prey relationships or host-parasite relationships, the gener-

ation time may differ strongly between the interacting species (Dawkins et al., 1979). Consequently, if the invading species is the interacting species with the shorter lifespan (for example a prey species or pathogen), it may have an evolutionary advantage because it can undergo more rapid evolution. Indeed, as discussed in **Chapter 2**, I did observe in this experiment that evolution of the prey species determines changes in the interaction between predator and prey. Similarly, another recent study found that rapid adaptation of pathogens can alter their invasion success in experimental populations (Nørgaard et al., 2019). Although these results generally indicate an advantage for the interacting species with the shorter life-cycle, this does not imply that evolution of the species with the slower life-cycle is unimportant. For example, we did observe in **Chapter 2** that predators evolved changes in behaviour and morphology, which may aid prey capture and ingestion. Similarly, other studies found that host species can evolve increased resistance (Zilio et al., 2020), or that predators can evolve changes in prey preference (Phillips and Shine, 2006).

Evolutionary interactions between interacting species may fundamentally alter the invasion or range expansion process. For example, in a study by Zilio et al. (2020), the evolution of increased resistance of pathogens came at the expense of decreased dispersal. Consequently, evolution due to biotic interactions may lead to feedbacks on the ecological dynamics (eco-evolutionary dynamics, Pelletier et al., 2009; Hendry, 2016; Govaert et al., 2019). Currently, the evolution of biotic interactions during range expansions remains poorly investigated. This may in part be due to the high complexity of the evolutionary changes, because such studies require the consideration of two evolving species and their interaction. Yet, as demonstrated in studies like those by Zilio et al. (2020) and Nørgaard et al. (2019), the evolution due to biotic interactions may have important consequences for invasions and range expansions. Therefore, a further sys-

tematic investigation of evolving biotic interactions in natural populations and through experimental studies is needed, if we want to gain a thorough understanding of the role of biotic interactions and their evolution on the range expansion process.

Gene swamping: natural occurrences and the influence of pushed versus pulled waves

I show in **Chapter 3** of this thesis that gene swamping can limit adaptation, and may affect species ranges. However, my results also highlight gaps in our current state of knowledge pertaining to gene swamping. Firstly, it is currently poorly investigated how frequently gene swamping actually limits adaptation in natural populations (Lenormand, 2002; Bridle and Vines, 2007; Gaston, 2009; Sexton et al., 2009, but for an important recent exception, see Bachmann et al. 2020). Secondly, the results of **Chapter 3** suggest that the effects of gene swamping may strongly differ in pushed versus pulled waves, but this hypothesis has not yet been investigated explicitly.

Gene swamping has the potential to limit adaptation of populations at a range edge, when the population at the range edge is swamped by genes from the range core (Haldane and Ford, 1956; García-Ramos and Kirkpatrick, 1997; Kirkpatrick and Barton, 1997; Polechová and Barton, 2015; Polechová, 2018). Although one recent study demonstrated that gene swamping limits adaptation in populations of the frog species *Rana temporaria* along an elevation gradient (Bachmann et al., 2020), it is currently unknown how commonly gene swamping affects natural populations. Although steep environmental gradients like elevation gradients (e.g. Bachmann et al., 2020) may be common in nature, there are other requirements that need to be satisfied for gene

swamping to occur. An important requirement is that mating is random and there is no preference for mates from the local habitat. However, many species show some form of mate preference or choosiness (Jennions and Petrie, 1997; Ah-King and Gowaty, 2016). Indeed, unless a very strong mate-finding Allee effect (see for example Gascoigne et al., 2009) forces individuals to mate indiscriminately, assortative mating with well-adapted individuals would be under strong selection. Further empirical studies that quantify environmental gradients, gene flow and population genetic structure will therefore be key to improve our understanding of gene swamping, and how commonly it shapes species ranges in nature.

Additionally, another often implicitly made assumption of the gene swamping hypothesis is that a population spreads as a pulled wave, where early dispersers drive the expansion rate of the population (van Saarloos, 2003; Panja, 2004). However, as evidenced both by the results in **Chapter 3** and other studies (see for example Pachepsky and Levine, 2011; Gandhi et al., 2016; Birzu et al., 2018; Erm and Phillips, 2019), the presence of an abiotic gradient or Allee effects may shift the range expansion dynamics from a pulled to a pushed wave. In a pushed wave, the population density gradient along the species range is likely to be less steep. Consequently, populations at a range edge in pushed waves may be more robust against the effects of gene swamping, because the relative proportion of individuals moving from the range core and the local population at the range edge is less skewed. Investigating the role of pushed and pulled waves during range expansions may require careful manipulation of the test conditions and may be difficult in field studies. Likely, a better approach would be to include an Allee effect in existing models of gene swamping (for example Polechová and Barton, 2015; Polechová, 2018), or to use experimental studies with carefully controlled conditions to investigate how the presence of an Allee effect would alter predictions from the gene

swamping hypothesis.

Through these combined empirical, experimental and theoretical approaches, we can further the understanding of the gene swamping process itself, and how it affects species ranges in natural populations.

Towards an integrative view of molecular adaptation in expanding populations

Populations at a range edge are subject to rapid evolution, primarily through two mechanisms. Firstly, populations at the range edge experience strong selection for increased dispersal and population growth rate (Burton et al., 2010; Phillips et al., 2010). Secondly, the low population densities at the range edge can result in strong stochasticity, potentially leading to the fixation of genetic variants through drift alone (Klopfstein et al., 2006; Excoffier et al., 2009). To gain a thorough understanding of the genetic consequences of range expansions, it is therefore important to thoroughly investigate both the effects of evolution through selection and evolution through drift.

The latter of these two mechanisms, evolution through drift, has been researched extensively in past work (Excoffier et al., 2009; Chuang and Peterson, 2016). Experimental work has demonstrated that drift at the range edge can lead to the fixation of neutral and maladaptive mutations (Klopfstein et al., 2006; Hallatschek et al., 2007; Hallatschek and Nelson, 2010; Gralka et al., 2016). These mutations can subsequently "surf" on the expansion front, as long as range expansion continues. Such gene surfing can affect population fitness. For example, it has been linked to a high prevalence of maladaptive mutations in human populations following recent range expansions (Pei-

schl et al., 2018).

Selection driven evolution at a range edge has been studied less extensively on a genetic level. For example, some studies have quantified adaptations in the metabolome (Petegem et al., 2016) or used transcriptomics to determine changes in gene expression during range expansions (Sun et al., 2012). Additionally, several studies have investigated the genetic consequences of range expansions. However, to try and identify selective sweeps during range expansions, most studies focussed on population genetic structure or use a limited number of genetic markers (see for example Swaegers et al., 2013, 2015), whereas direct identification of variants under selection is rarely done. One important example investigating genetic changes through selection is the study by Bosshard et al. (2020). Here, the authors demonstrated that selection on new mutations was predominantly associated with membrane structures and with DNA repair. In our genetic analysis described in **Chapter 4**, we found that genetic variants under selection during range expansion were associated with similar cellular functions as in Bosshard et al. (2020). Because growth rate is predicted to be under strong selection during range expansions (Burton et al., 2010; Phillips et al., 2010), this result is not entirely surprising. A more surprising result was the lack of clear indication of selection on genetic variants associated with dispersal in our experiment. *T. thermophila* has a distinct dispersal behaviour, and range expansion theory would suggest that dispersal would be under strong selection (Burton et al., 2010; Phillips et al., 2010). However, dispersal can have a complex genetic basis (Saastamoinen et al., 2018), but is often also a highly plastic behaviour (Clobert et al., 2012). Therefore, it may be highly species dependent whether dispersal changes are due to genetic changes or plastic responses to the environment. Indeed, whereas several studies found evolutionary changes in dispersal behaviour during range expansion (Brown et al., 2007; Fronhofer and Altermatt,

2015; Williams et al., 2016; Weiss-Lehman et al., 2017), dispersal changes during range expansions can also be driven by plasticity alone (Petegem et al., 2018).

Consequently, it may well be the case that in our experiment, there were no genetic changes in dispersal. To further elucidate the complex relation between phenotypic changes and genetic changes, further research may be necessary. This additional research could be undertaken following two approaches: Firstly, empirical investigation of species undergoing recent range expansions can be used to identify genes under selection (genome wide association studies; Bush and Moore, 2012). Due to the strong drift at range edges (Excoffier et al., 2009), results of such field studies may either have to be interpreted with the appropriate care, unless parallel range expansions of the same species can be investigated, in order to distinguish genetic changes due to drift from genetic changes due to selection. Secondly, to elucidate how frequently phenotypic changes are driven by selection on genetic variants or changes in gene expression, experimental studies combining both genetic and transcriptomic analyses may be needed across multiple different species. Although such studies may be limited by model systems with a properly annotated reference genome and the sequencing costs, they may be necessary to fully disentangle the genetic basis of adaptations during range expansion.

Concluding remarks

In this thesis, I investigated how changing biotic and abiotic environments, as well as gene swamping affect the evolution of populations during range expansions. When considering all results, I can draw two main conclusions. Firstly, we need a more extensive eco-evolutionary perspective that integrates evolution of life-history, abiotic conditions and biotic interactions, to gain a holistic view on range expansion dynamics. Secondly,

gene swamping can potentially limit adaptation, yet the current state of research is incomplete, and needs to consider of aspects like life-history evolution and pushed versus pulled wave dynamics, as well as further empirical and experimental validation. Although I managed to answer several questions related to range expansions in this thesis, several knowledge gaps still remain. I am eager to see how the field develops in the near future, and how it may influence policy in a changing world.

Acknowledgements

This thesis would not have been possible without the support and guidance of many people that I hereby wish to express my thanks to.

I would like to thank my supervisors, Prof. Dr. Florian Altermatt, Prof. Dr. Andreas Wagner, and Dr. Emanuel A. Fronhofer. What initially drew me so strongly to this particular PhD was the integrative nature of the project, focussing on the interaction between ecology and evolution, and combining diverse methods including experiments, theory, and genomics. I very much appreciate how this diverse nature was also reflected in the supervision, where all three supervisors aided me with their own specific insights and background in a very synergistic way. I benefited strongly from this diverse supervision, both in the development and execution of the work described in this thesis, but also generally as a scientist and as a person.

Likewise, I would like to thank the members of my PhD committee, Prof. Dr. Hanna Kokko and Prof. Dr. Rolf Kümmerli, as well as Dr. Heidi Tschanz-Lischer and Dr. Carla Bello. Their feedback contributed strongly to the conceptual ideas I investigated in this thesis, and in the translation of those ideas to achievable experiments and analyses.

I would also like to thank the people and institutions which made my stay in Zürich such a nice experience. Firstly, I would like to the department of Aquatic Ecology at Eawag and the Department of Evolutionary Biology and Environmental Science at the

University Zürich for providing a great research environment. I truly appreciate the open culture in both places, where it was possible to freely discuss science with colleagues, in a very open and collegial atmosphere. Such scientific exchanges are the cornerstone of Academia, and I greatly appreciate the enthusiasm that colleagues at both places express for their own as well as other people's research ideas. In particular, I would like to thank all my colleagues from the Altermatt lab and from the Wagner lab, who were always there for a good scientific discussion, or a coffee break to discuss life in general. I would also like to thank l'Institut des Sciences de l'Evolution de Montpellier (ISEM), for remotely hosting me as a PhD student, and in particular the Experimental Evolution of Communities group. Due to covid-19, many of our scientific and social interactions became more difficult to maintain during the last year. Ironically, as a remote member of the group, the current situation increased my interactions with the group at ISEM, and I greatly value these exchanges in the last few months. Lastly, I would like to thank the URPP Evolution in Action, who not only funded my PhD project, but also provided an excellent environment for learning and scientific exchange. I greatly appreciate the organization of our yearly retreat, where we could exchange our ideas and progress. Additionally, I truly appreciate the investment from the URPP — and in particular Dr. Heidi Tschanz-Lischer, Dr. Stefan Wyder, Dr. Carla Bello and Dr Gregor Rot — in organizing the tutorial sessions, where we could learn new analysis skills, highly tailored to our needs as PhD students. A particular thanks also goes to the current and former members of the coordination office of the URPP: Dr. Annegret Lesslauer, Mira Portmann, Dr. Jasmin Winkler, Dr. Yvonne Steinbach and Angela Leu. Without them, the great support from the URPP to us PhD students would not have been possible.

Starting a PhD can be daunting, and therefore I would like to thank my fellow PhD

students in the URPP Evolution in Action. Having a group of people who go through the same process, with whom one can share struggles and achievements, that one can ask for advice and opinions, or simply have a beer with at the end of the day was truly a great support. I strongly value these interactions, as well as the friendships that formed along the way.

Many people have in some way contributed to the work in this thesis and all of them are acknowledged in the individual studies. However, I would here like to mention a few people that contributed especially to this thesis. Firstly, I would like to thank Samuel Hürlemann and Silvana Käser, who taught me the skills to work in a protist lab, and aided me greatly with my experiments. Secondly, I would like to thank Prof. Dr. Teppo Hiltunen and Dr. Johannes Cairns, for the collaboration on the project described in Chapter 2. I very much appreciated the opportunity to work together. Thirdly, I would like to thank Dr. Lynn Govaert, Dr. Claire Jacquet, Elena Gimmi, Eva Cereghetti, Dr. Roman Alther, Dr. Heidi Käch, Dr. Natalia Zajac, Nadine Tardent, Linda Haltiner and Teo Cereghetti, who commented on various chapters of this thesis.

Lastly, I would like to acknowledge my family who supported me during my PhD. In particular, I would like to thank my mother who fostered my interest in science and the natural world from a young age, and my life partner Rebecca, who supported me during these last few months, when I was stuck behind my desk, trying to finish writing this thesis.

Bibliography

Abrams, P. A. 2000: The evolution of predator-prey interactions: Theory and evidence. *Annu. Rev. Ecol. Evol. Syst.* 31(1):79–105.

Agrawal, A. F. and Whitlock, M. C. 2010: Environmental duress and epistasis: How does stress affect the strength of selection on new mutations? *Trends Ecol. Evol.* 25(8):450–458.

Ah-King, M. and Gowaty, P. A. 2016: A conceptual review of mate choice: stochastic demography, within-sex phenotypic plasticity, and individual flexibility. *Ecol. Evol.* 6(14):4607–4642.

Altermatt, F.; Alther, R.; Fišer, C.; Jokela, J.; Konec, M.; Küry, D.; Mächler, E.; Stucki, P.; and Westram, A. M. 2014: Diversity and distribution of freshwater amphipod species in Switzerland (Crustacea: Amphipoda). *PLoS One* 9(10):e110328.

Altermatt, F.; Alther, R.; and Mächler, E. 2016: Spatial patterns of genetic diversity, community composition and occurrence of native and non-native amphipods in naturally replicated tributary streams. *BMC Ecol.* 16(1):1–11.

Altermatt, F.; Bieger, A.; Carrara, F.; Rinaldo, A.; and Holyoak, M. 2011: Effects of

connectivity and recurrent local disturbances on community structure and population density in experimental metacommunities. *PLoS One* 6(4):e19525.

Altermatt, F.; Fronhofer, E. A.; Garnier, A.; Giometto, A.; Hammes, F.; Klecka, J.; Legrand, D.; Mächler, E.; Massie, T. M.; Pennekamp, F.; Plebani, M.; Pontarp, M.; Schtickzelle, N.; Thuillier, V.; and Petchey, O. L. 2015: Big answers from small worlds: a user's guide for protist microcosms as a model system in ecology and evolution. *Methods Ecol. Evol.* 6(2):218–231.

Altermatt, F. and Holyoak, M. 2012: Spatial clustering of habitat structure effects patterns of community composition and diversity. *Ecology* 93(5):1125–1133.

Andrews, J. H. and Rouse, D. I. 1982: Plant pathogens and the theory of *r*- and *K*-selection. *Am. Nat.* 120(3):283–296.

Angilletta, M. J. 2009: Thermal adaptation: A theoretical and empirical synthesis. OUP Oxford.

Arbuthnott, D. and Whitlock, M. C. 2018: Environmental stress does not increase the mean strength of selection. *J. Evol. Biol.* 31(10):1599–1606.

Arnold, M. L. and Kunte, K. 2017: Adaptive genetic exchange: A tangled history of admixture and evolutionary innovation. *Trends Ecol. Evol.* 32(8):601–611.

Bachmann, J. C.; Jansen van Rensburg, A.; Cortazar-Chinarro, M.; Laurila, A.; and Van Buskirk, J. 2020: Gene flow limits adaptation along steep environmental gradients. *Am. Nat.* 195(3):E67–E86.

Bailey, M. J.; Lilley, A. K.; Thompson, I. P.; Rainey, P. B.; and Ellis, R. J. 1995: Site directed chromosomal marking of a fluorescent pseudomonad isolated from the phyto-

- sphere of sugar beet; stability and potential for marker gene transfer. *Mol. Ecol.* 4(6):755–764.
- Bartoń, K. 2009: MuMIn: Multi-model inference.
- Becks, L. and Agrawal, A. F. 2010: Higher rates of sex evolve in spatially heterogeneous environments. *Nature* 468(7320):89–92.
- . 2012: The evolution of sex Is favoured during adaptation to new environments. *PLoS Biol.* 10(5):e1001317.
- Becks, L.; Hilker, F. M.; Malchow, H.; Jürgens, K.; and Arndt, H. 2005: Experimental demonstration of chaos in a microbial food web. *Nature* 435(7046):1226–1229.
- Bell, G. 1982: *The masterpiece of nature: The evolution and genetics of sexuality.* Univ of California Pr, Berkeley.
- Bell, G. and Gonzalez, A. 2011: Adaptation and evolutionary rescue in metapopulations experiencing environmental deterioration. *Science* 332(6035):1327–1330.
- Benjamini, Y. and Hochberg, Y. 1995: Controlling the false discovery rate: A practical and powerful approach to multiple testing. *J. Royal Stat. Soc. B* 57(1):289–300.
- Beverton, R. and Holt, S. 1993: *On the dynamics of exploited fish populations.* Springer.
- Beyers, R. J. and Odum, H. T. 2012: *Ecological microcosms.* Springer Science & Business Media.
- Bidner, L. R.; Matsumoto-Oda, A.; and Isbell, L. A. 2018: The role of sleeping sites in the predator-prey dynamics of leopards and olive baboons. *Am. J. Primat.* 80(12):e22932.

- Bijlsma, R. and Loeschcke, V. 2005: Environmental stress, adaptation and evolution: an overview. *J. Evol. Biol.* 18(4):744–749.
- Birzu, G.; Hallatschek, O.; and Korolev, K. S. 2018: Fluctuations uncover a distinct class of traveling waves. *Proc. Natl. Acad. Sci. U.S.A.* 115(16):E3645–E3654.
- Bland, J. M. and Altman, D. G. 1995: Multiple significance tests: the Bonferroni method. *BMJ* 310(6973):170.
- Blount, Z. D.; Lenski, R. E.; and Losos, J. B. 2018: Contingency and determinism in evolution: Replaying life’s tape. *Science* 362(6415):eaam5979.
- Bolger, A. M.; Lohse, M.; and Usadel, B. 2014: Trimmomatic: a flexible trimmer for Illumina sequence data. *Bioinformatics* 30(15):2114–2120.
- Bolnick, D. I.; Barrett, R. D. H.; Oke, K. B.; Rennison, D. J.; and Stuart, Y. E. 2018: (Non)parallel evolution. *Annual Review of Ecology, Evolution, and Systematics*, Vol 49, (edited by D. J. Futuyma), volume 49, pages 303–330. Annual Reviews, Palo Alto.
- Bonduriansky, R. and Day, T. 2018: *Extended heredity: A new understanding of inheritance and evolution*. Princeton.
- Bono, L. M.; Smith, L. B.; Pfennig, D. W.; and Burch, C. L. 2017: The emergence of performance trade-offs during local adaptation: insights from experimental evolution. *BMC Mol. Biol.* 26(7):1720–1733.
- Bonte, D.; Van Dyck, H.; Bullock, J. M.; Coulon, A.; Delgado, M.; Gibbs, M.; Lehouck, V.; Matthysen, E.; Mustin, K.; Saastamoinen, M.; Schtickzelle, N.; Stevens, V. M.; Vandewoestijne, S.; Baguette, M.; Barton, K.; Benton, T. G.; Chaput-Bardy,

- A.; Clobert, J.; Dytham, C.; Hovestadt, T.; Meier, C. M.; Palmer, S. C. F.; Turlure, C.; and Travis, J. M. J. 2012: Costs of dispersal. *Biol. Rev.* 87(2):290–312.
- Bors, E. K.; Herrera, S.; Morris, J. A.; and Shank, T. M. 2019: Population genomics of rapidly invading lionfish in the Caribbean reveals signals of range expansion in the absence of spatial population structure. *Ecol. Evol.* 9(6):3306–3320.
- Bosshard, L.; Peischl, S.; Ackermann, M.; and Excoffier, L. 2020: Dissection of the mutation accumulation process during bacterial range expansions. *BMC Genomics* 21(1):253.
- Bremer, E. and Krämer, R. 2019: Responses of microorganisms to osmotic stress. *Ann. Rev. Microb.* 73(1):313–334.
- Bridle, J. R. and Vines, T. H. 2007: Limits to evolution at range margins: when and why does adaptation fail? *Trends Ecol. Evol.* 22(3):140–147.
- Brito, P. H.; Guilherme, E.; Soares, H.; and Gordo, I. 2010: Mutation accumulation in *Tetrahymena*. *BMC Evol. Biol.* 10:354.
- Brodie, E. D. and Brodie, E. D. 1999: Predator-prey arms races: Asymmetrical selection on predators and prey may be reduced when prey are dangerous. *BioScience* 49(7):557–568.
- Brook, B. W. and Bradshaw, C. J. A. 2006: Strength of evidence for density dependence in abundance time series of 1198 species. *Ecology* 87(6):1445–1451.
- Brooker, R. W.; Travis, J. M. J.; Clark, E. J.; and Dytham, C. 2007: Modelling species' range shifts in a changing climate: The impacts of biotic interactions, dispersal distance and the rate of climate change. *J. Theor. Biol.* 245(1):59–65.

- Brown, G. P.; Shilton, C.; Phillips, B. L.; and Shine, R. 2007: Invasion, stress, and spinal arthritis in cane toads. *Proc. Natl. Acad. Sci. U.S.A.* 104(45):17698–17700.
- Brown, J. H. and Lomolino, M. V. 2000: Concluding remarks: historical perspective and the future of island biogeography theory. *Glob. Ecol. Biogeogr.* 9(1):87–92.
- Bullock, J. M.; Bonte, D.; Pufal, G.; Carvalho, C. d. S.; Chapman, D. S.; García, C.; García, D.; Matthysen, E.; and Delgado, M. M. 2018: Human-mediated dispersal and the rewiring of spatial networks. *Trends Ecol. Evol.* 33(12):958–970.
- Burns, D. A.; Aherne, J.; Gay, D. A.; and Lehmann, C. M. B. 2016: Acid rain and its environmental effects: Recent scientific advances. *Atmos. Environ.* 146:1–4.
- Burt, A. 2000: Perspective: Sex, recombination, and the efficacy of selection—Was Weismann right? *Evolution* 54(2):337–351.
- Burton, O. J.; Phillips, B. L.; and Travis, J. M. J. 2010: Trade-offs and the evolution of life-histories during range expansion. *Ecol. Lett.* 13(10):1210–1220.
- Bush, W. S. and Moore, J. H. 2012: Chapter 11: Genome-wide association studies. *PLOS Comput. Biol.* 8(12):e1002822.
- Buskey, E. J. and Stoecker, D. K. 1988: Locomotory patterns of the planktonic ciliate *Favella* sp.: Adaptations for remaining within food patches. *Bull. Mar. Sci.* 43(3):783–796.
- Cadotte, M. W. 2006: Metacommunity influences on community richness at multiple spatial scales: A microcosm experiment. *Ecology* 87(4):1008–1016.

- Cadotte, M. W.; Drake, J. A.; and Fukami, T. 2005: Constructing nature: laboratory models as necessary tools for investigating complex ecological communities. *Advances in Ecological Research*, volume 37 of *Population Dynamics and Laboratory Ecology*, pages 333–353. Academic Press.
- Cairns, J.; Jalasvuori, M.; Ojala, V.; Brockhurst, M.; and Hiltunen, T. 2016: Conjugation is necessary for a bacterial plasmid to survive under protozoan predation. *Biol. Lett.* 12(2):20150953.
- Cairns, J.; Moerman, F.; Fronhofer, E. A.; Altermatt, F.; and Hiltunen, T. 2019: Co-evolution alters predator life history traits, behavior and morphology in experimental microbial communities. bioRxiv page 748582.
- . 2020: Evolution in interacting species alters predator life-history traits, behaviour and morphology in experimental microbial communities. *Proc. R. Soc. B-Biol. Sci.* 287(1928):20200652.
- Cairns, J.; Ruokolainen, L.; Hultman, J.; Tamminen, M.; Virta, M.; and Hiltunen, T. 2018: Ecology determines how low antibiotic concentration impacts community composition and horizontal transfer of resistance genes. *Comm. Biol.* 1(1):1–8.
- Caldeira, K. and Wickett, M. E. 2003: Anthropogenic carbon and ocean pH. *Nature* 425(6956):365.
- Cantrell, R. S. and Cosner, C. 2004: *Spatial ecology via reaction-diffusion equations.* John Wiley & Sons.
- Cassidy-Hanley, D. M. 2012: *Tetrahymena* in the laboratory: Strain resources, methods

- for culture, maintenance, and storage. *Methods in Cell Biology*, volume 109, pages 237–276. Elsevier.
- Chaine, A. S.; Schtickzelle, N.; Polard, T.; Huet, M.; and Clobert, J. 2010: Kin-based recognition and social aggregation in a ciliate. *Evolution* 64(5):1290–1300.
- Charles, H. and Dukes, J. S. 2007: Impacts of invasive species on ecosystem services. *Biological Invasions*, (edited by W. Nentwig), *Ecological Studies*, pages 217–237. Springer, Berlin, Heidelberg.
- Chen, I.-C.; Hill, J. K.; Ohlemüller, R.; Roy, D. B.; and Thomas, C. D. 2011: Rapid range shifts of species associated with high levels of climate warming. *Science* 333(6045):1024–1026.
- Chuang, A. and Peterson, C. R. 2016: Expanding population edges: theories, traits, and trade-offs. *Glob. Change. Biol.* 22(2):494–512.
- Clarke, G. S.; Shine, R.; and Phillips, B. L. 2019: May the (selective) force be with you: Spatial sorting and natural selection exert opposing forces on limb length in an invasive amphibian. *J. Evol. Biol.* 32(9):994–1001.
- Clobert, J.; Baguette, M.; Benton, T. G.; and Bullock, J. M. 2012: *Dispersal ecology and evolution*. Oxford University Press, USA, Oxford, first edition.
- Clobert, J.; Danchin, E.; Dhondt, A. A.; and Nichols, J. D. 2001: *Dispersal*. Oxford University Press, Oxford; New York.
- Closs, G. P.; Balcombe, S. R.; and Shirley, M. J. 1999: Generalist predators, interaction strength and food-web stability. *Advances in Ecological Research*, (edited by A. H. Fitter and D. Raffaelli), volume 28, pages 93–126. Academic Press.

- Cobben, M. M. P.; Mitesser, O.; and Kubisch, A. 2017: Evolving mutation rate advances the invasion speed of a sexual species. *BMC Evol Biol* 17(1):150.
- Colegrave, N. 2002: Sex releases the speed limit on evolution. *Nature* 420(6916):664–666.
- Collins, K. 2012: *Tetrahymena thermophila*. Academic Press.
- Collins, S. and Bell, G. 2004: Phenotypic consequences of 1,000 generations of selection at elevated CO₂ in a green alga. *Nature* 431(7008):566.
- Coyne, R. S.; Stovert, N. A.; and Miao, W. 2012: Whole genome studies of *Tetrahymena*. *Tetrahymena Thermophila*, (edited by K. Collins), volume 109, pages 53–81. Elsevier Academic Press Inc, San Diego.
- Crawford, D. W. 1992: Metabolic cost of motility in planktonic protists: Theoretical considerations on size scaling and swimming speed. *Microb. Ecol.* 24(1):1–10.
- Crossland, M. R.; Brown, G. P.; Anstis, M.; Shilton, C. M.; and Shine, R. 2008: Mass mortality of native anuran tadpoles in tropical Australia due to the invasive cane toad (*Bufo marinus*). *Biol. Conserv.* 141(9):2387–2394.
- Curat, M.; Ruedi, M.; Petit, R. J.; and Excoffier, L. 2008: The hidden side of invasions: massive introgression by local genes. *Evolution* 62(8):1908–1920.
- Cyert, M. S. and Philpott, C. C. 2013: Regulation of cation balance in *Saccharomyces cerevisiae*. *Genetics* 193(3):677–713.
- Dallas, T.; Decker, R. R.; and Hastings, A. 2017: Species are not most abundant in the centre of their geographic range or climatic niche. *Ecol. Lett.* 20(12):1526–1533.

- Danecek, P.; Schiffels, S.; and Durbin, R. 2016: Multiallelic calling model in bcftools (-m).
- Darwin, C. 1869: On the origin of species by means of natural selection: Or the preservation of favoured races in the struggle for life. D. Appleton.
- David, P.; Thébault, E.; Anneville, O.; Duyck, P. F.; Chapuis, E.; and Loeuille, N. 2017: Chapter one - Impacts of invasive species on food webs: A review of empirical data. *Advances in Ecological Research*, (edited by D. A. Bohan; A. J. Dumbrell; and F. Massol), volume 56 of *Networks of Invasion: A Synthesis of Concepts*, pages 1–60. Academic Press.
- Dawkins, R.; Krebs, J. R.; Maynard Smith, J.; and Holliday, R. 1979: Arms races between and within species. *Proc. R. Soc. B-Biol. Sci.* 205(1161):489–511.
- DeLorenzo, M. E.; Scott, G. I.; and Ross, P. E. 2001: Toxicity of pesticides to aquatic microorganisms: A review. *Environ. Toxicol. Chem.* 20(1):84–98.
- Derry, A. M. and Arnott, S. E. 2007: Adaptive reversals in acid tolerance in copepods from lakes recovering from historical stress. *Ecol. Appl.* 17(4):1116–1126.
- Donohue, K. 1999: Seed dispersal as a maternally influenced character: Mechanistic basis of maternal effects and selection on maternal characters in an annual plant. *Am. Nat.* 154(6):674–689.
- Dukes, J. S. and Mooney, H. A. 2004: Disruption of ecosystem processes in western North America by invasive species. *Rev. Chil. Hist. Nat.* 77(3):411–437.
- Dunson, W. and Travis, J. 1991: The Role of abiotic factors in community organization. *Am. Nat.* 138(5):1067–1091.

- Ebbert, D. 2019: `chisq.posthoc.test`: Perform post hoc analysis based on residuals of Pearson's... in `chisq.posthoc.test`: A Post Hoc Analysis for Pearson's Chi-Squared Test for Count Data.
- Eisen, J. A.; Coyne, R. S.; Wu, M.; Wu, D.; Thiagarajan, M.; Wortman, J. R.; Badger, J. H.; Ren, Q.; Amedeo, P.; Jones, K. M.; Tallon, L. J.; Delcher, A. L.; Salzberg, S. L.; Silva, J. C.; Haas, B. J.; Majoros, W. H.; Farzad, M.; Carlton, J. M.; Smith, R. K.; Garg, J.; Pearlman, R. E.; Karrer, K. M.; Sun, L.; Manning, G.; Elde, N. C.; Turkewitz, A. P.; Asai, D. J.; Wilkes, D. E.; Wang, Y.; Cai, H.; Collins, K.; Stewart, B. A.; Lee, S. R.; Wilamowska, K.; Weinberg, Z.; Ruzzo, W. L.; Wloga, D.; Gaertig, J.; Frankel, J.; Tsao, C.-C.; Gorovsky, M. A.; Keeling, P. J.; Waller, R. F.; Patron, N. J.; Cherry, J. M.; Stover, N. A.; Krieger, C. J.; del Toro, C.; Ryder, H. F.; Williamson, S. C.; Barbeau, R. A.; Hamilton, E. P.; and Orias, E. 2006: Macronuclear genome sequence of the viliate *Tetrahymena thermophila*, a model eukaryote. *PLoS Biol.* 4(9):e286.
- Elton, C. S. 1958: *The ecology of invasions by animals and plants*. Springer, Boston MA.
- Erm, P. and Phillips, B. L. 2019: Evolution transforms pushed waves into pulled waves. *Am. Nat.* 195(3):E87–E99.
- Esterházy, D.; King, M. S.; Yakovlev, G.; and Hirst, J. 2008: Production of reactive oxygen species by Complex I (NADH:Ubiquinone Oxidoreductase) from *Escherichia coli* and comparison to the enzyme from mitochondria. *Biochemistry* 47(12):3964–3971.

- Excoffier, L.; Foll, M.; and Petit, R. J. 2009: Genetic consequences of range expansions. *Annu. Rev. Ecol. Evol. Syst.* 40(1):481–501.
- Fisher, R. A. 2000: The genetical theory of natural selection. Oxford University Press, Oxford, annotated edition.
- Fjerdingstad, E. J.; Schtickzelle, N.; Manhes, P.; Gutierrez, A.; and Clobert, J. 2007: Evolution of dispersal and life history strategies – *Tetrahymena* ciliates. *BMC Evol. Biol.* 7(1):133.
- Fletcher, E.; Feizi, A.; Bisschops, M. M. M.; Hallström, B. M.; Khoomrung, S.; Siewers, V.; and Nielsen, J. 2017: Evolutionary engineering reveals divergent paths when yeast is adapted to different acidic environments. *Metab. Eng.* 39:19–28.
- Flowers, T. J.; Galal, H. K.; and Bromham, L. 2010: Evolution of halophytes: multiple origins of salt tolerance in land plants. *Funct. Plant. Biol.* 37(7):604–612.
- for the Management of Noxious and Exotic Weeds, F. I. C. and Westbrooks, R. 1998: Invasive plants: changing the landscape of America. All U.S. Government Documents (Utah Regional Depository) .
- Franks, S. J. and Hoffmann, A. A. 2012: Genetics of climate change adaptation. *Annual Review of Genetics*, Vol 46, (edited by B. L. Bassler), volume 46, pages 185–208. Annual Reviews, Palo Alto.
- Fraser, D. J.; Weir, L. K.; Bernatchez, L.; Hansen, M. M.; and Taylor, E. B. 2011: Extent and scale of local adaptation in salmonid fishes: review and meta-analysis. *Heredity* 106(3):404–420.

- Frenot, Y.; Chown, S. L.; Whinam, J.; Selkirk, P. M.; Convey, P.; Skotnicki, M.; and Bergstrom, D. M. 2005: Biological invasions in the Antarctic: extent, impacts and implications. *Biol. Rev.* 80(1):45–72.
- Friedberg, E. C.; Wagner, R.; and Radman, M. 2002: Specialized DNA polymerases, cellular survival, and the genesis of mutations. *Science* 296(5573):1627–1630.
- Friedberg, E. C.; Walker, G. C.; Siede, W.; Wood, R. D.; Schultz, R. A.; and Ellenberger, T. 2005: DNA repair and mutagenesis. ASM Press, Washington, D.C, 2nd edition edition.
- Friman, V.-P.; Jousset, A.; and Buckling, A. 2014: Rapid prey evolution can alter the structure of predator–prey communities. *J. Evol. Biol.* 27(2):374–380.
- Fronhofer, E. A. and Altermatt, F. 2015: Eco-evolutionary feedbacks during experimental range expansions. *Nat. Commun.* 6:6844.
- Fronhofer, E. A.; Govaert, L.; O’Connor, M. I.; Schreiber, S. J.; and Altermatt, F. 2018: The shape of density dependence and the relationship between population growth, intraspecific competition and equilibrium population density. *bioRxiv* page 485946.
- Fronhofer, E. A.; Gut, S.; and Altermatt, F. 2017a: Evolution of density-dependent movement during experimental range expansions. *J. Evol. Biol.* 30(12):2165–2176.
- Fronhofer, E. A.; Kropf, T.; and Altermatt, F. 2015: Density-dependent movement and the consequences of the Allee effect in the model organism *Tetrahymena*. *J. Animal Ecol.* 84(3):712–722.
- Fronhofer, E. A.; Nitsche, N.; and Altermatt, F. 2017b: Information use shapes the

- dynamics of range expansions into environmental gradients. *Glob. Ecol. Biogeogr.* 26(4):400–411.
- Gallet, R.; Latour, Y.; Hughes, B. S.; and Lenormand, T. 2014: The dynamics of niche evolution upon abrupt environmental change. *Evolution* 68(5):1257–1269.
- Gallet, R.; Tully, T.; and Evans, M. E. K. 2009: Ecological conditions affect evolutionary trajectory in a predator–prey system. *Evolution* 63(3):641–651.
- Gandhi, S. R.; Yurtsev, E. A.; Korolev, K. S.; and Gore, J. 2016: Range expansions transition from pulled to pushed waves as growth becomes more cooperative in an experimental microbial population. *Proc. Natl. Acad. Sci. U.S.A.* 113(25):6922–6927.
- García-Ramos, G. and Kirkpatrick, M. 1997: Genetic models of adaptation and gene flow in peripheral populations. *Evolution* 51(1):21–28.
- Gascoigne, J.; Berec, L.; Gregory, S.; and Courchamp, F. 2009: Dangerously few liaisons: a review of mate-finding Allee effects. *Popul. Ecol.* 51(3):355–372.
- Gaston, K. J. 2009: Geographic range limits: achieving synthesis. *Proc. R. Soc. B-Biol. Sci.* 276(1661):1395–1406.
- Gattuso, J.-P. and Hansson, L. 2011: *Ocean acidification*. OUP Oxford.
- Gelman, A.; Hwang, J.; and Vehtari, A. 2014: Understanding predictive information criteria for Bayesian models. *Stat. Comput.* 24(6):997–1016.
- Gerrish, P. J. and Lenski, R. E. 1998: The fate of competing beneficial mutations in an asexual population. *Genetica* 102(0):127.

- Gill, D. E. and Hairston, N. G. 1972: The dynamics of a natural population of *Paramecium* and the role of interspecific competition in community structure. *J. Animal Ecol.* 41(1):137–151.
- Giometto, A.; Altermatt, F.; Maritan, A.; Stocker, R.; and Rinaldo, A. 2015: Generalized receptor law governs phototaxis in the phytoplankton *Euglena gracilis*. *Proc. Natl. Acad. Sci. U.S.A.* 112(22):7045–7050.
- Giometto, A.; Altermatt, F.; and Rinaldo, A. 2017: Demographic stochasticity and resource autocorrelation control biological invasions in heterogeneous landscapes. *Oikos* 126(11):1554–1563.
- Giometto, A.; Nelson, D. R.; and Murray, A. W. 2018: Physical interactions reduce the power of natural selection in growing yeast colonies. *Proc. Natl. Acad. Sci. U.S.A.* 115(45):11448–11453.
- Giometto, A.; Rinaldo, A.; Carrara, F.; and Altermatt, F. 2014: Emerging predictable features of replicated biological invasion fronts. *Proc. Natl. Acad. Sci. U.S.A.* 111(1):297–301.
- Govaert, L.; Fronhofer, E. A.; Lion, S.; Eizaguirre, C.; Bonte, D.; Egas, M.; Hendry, A. P.; Martins, A. D. B.; Melián, C. J.; Raeymaekers, J. A. M.; Ratikainen, I. I.; Saether, B.-E.; Schweitzer, J. A.; and Matthews, B. 2019: Eco-evolutionary feedbacks—Theoretical models and perspectives. *Funct. Ecol.* 33(1):13–30.
- Gozlan, R. E.; Britton, J. R.; Cowx, I.; and Copp, G. H. 2010: Current knowledge on non-native freshwater fish introductions. *J. Fish Biol.* 76(4):751–786.
- Gralka, M.; Stiewe, F.; Farrell, F.; Möbius, W.; Waclaw, B.; and Hallatschek, O. 2016:

- Allele surfing promotes microbial adaptation from standing variation. *Ecol. Lett.* 19(8):889–898.
- Gray, J. C. and Goddard, M. R. 2012: Sex enhances adaptation by unlinking beneficial from detrimental mutations in experimental yeast populations. *BMC Evol. Biol.* 12(1):43.
- Greenlees, M. J.; Brown, G. P.; Webb, J. K.; Phillips, B. L.; and Shine, R. 2006: Effects of an invasive anuran [the cane toad (*Bufo marinus*)] on the invertebrate fauna of a tropical Australian floodplain. *Animal. Conserv.* 9(4):431–438.
- Grosholz, E. 2002: Ecological and evolutionary consequences of coastal invasions. *Trends Ecol. Evol.* 17(1):22–27.
- Gross, L. 2018: Confronting climate change in the age of denial. *PLoS Biol.* 16(10):e3000033.
- Gunde-Cimerman, N.; Oren, A.; and Plemenitaš, A. 2006: Adaptation to life at high salt concentrations in Archaea, Bacteria, and Eukarya. Springer Science & Business Media.
- Haafke, J.; Chakra, M. A.; and Becks, L. 2016: Eco-evolutionary feedback promotes Red Queen dynamics and selects for sex in predator populations. *Evolution* 70(3):641–652.
- Haldane, J. B. S. and Ford, E. B. 1956: The relation between density regulation and natural selection. *Proc. R. Soc. B-Biol. Sci.* 145(920):306–308.
- Hall, A. R.; Meyer, J. R.; and Kassen, R. 2008: Selection for predator resistance varies with resource supply in a model adaptive radiation. *Evol. Ecol. Res.* 10(5):735–746.

- Hallatschek, O.; Hersen, P.; Ramanathan, S.; and Nelson, D. R. 2007: Genetic drift at expanding frontiers promotes gene segregation. *Proc. Natl. Acad. Sci. U.S.A.* 104(50):19926–19930.
- Hallatschek, O. and Nelson, D. R. 2010: Life at the Front of an expanding population. *Evolution* 64(1):193–206.
- Hammes, F.; Berney, M.; Wang, Y.; Vital, M.; Köster, O.; and Egli, T. 2008: Flow-cytometric total bacterial cell counts as a descriptive microbiological parameter for drinking water treatment processes. *Water Res.* 42(1):269–277.
- Hammes, F. A. and Egli, T. 2005: New method for assimilable organic carbon determination using flow-cytometric enumeration and a natural microbial consortium as inoculum. *Environ. Sci. Technol.* 39(9):3289–3294.
- Hangartner, S.; Laurila, A.; and Räsänen, K. 2011: Adaptive divergence of the moor frog (*Rana arvalis*) along an acidification gradient. *BMC Evol. Biol.* 11:366.
- Harden, M. M.; He, A.; Creamer, K.; Clark, M. W.; Hamdallah, I.; Martinez, K. A.; Kresslein, R. L.; Bush, S. P.; and Slonczewski, J. L. 2015: Acid-adapted strains of *Escherichia coli* K-12 obtained by experimental evolution. *Appl. Environ. Microbiol.* 81(6):1932–1941.
- Harmand, N.; Gallet, R.; Martin, G.; and Lenormand, T. 2018: Evolution of bacteria specialization along an antibiotic dose gradient. *Evol. Lett.* 2(3):221–232.
- Harrison, P. A.; Berry, P. M.; Simpson, G.; Haslett, J. R.; Blicharska, M.; Bucur, M.; Dunford, R.; Egoh, B.; Garcia-Llorente, M.; Geamănă, N.; Geertsema, W.;

- Lommelen, E.; Meiresonne, L.; and Turkelboom, F. 2014: Linkages between biodiversity attributes and ecosystem services: A systematic review. *Ecosyst. Serv.* 9:191–203.
- Hartl, D. L. and Clark, A. G. 2006: Principles of population genetics. Sinauer Associates is an imprint of Oxford University Press, Sunderland, Mass, 4th edition edition.
- Harvey, E.; Gounand, I.; Fronhofer, E. A.; and Altermatt, F. 2020: Metaecosystem dynamics drive community composition in experimental, multi-layered spatial networks. *Oikos* 129(3):402–412.
- Hendry, A. P. 2016: Eco-evolutionary dynamics. Princeton University Press.
- Hill, J. K.; Thomas, C. D.; and Huntley, B. 1999: Climate and habitat availability determine 20th century changes in a butterfly's range margin. *Proc. R. Soc. B-Biol. Sci.* 266(1425):1197–1206.
- HilleRisLambers, J.; Adler, P. B.; Harpole, W. S.; Levine, J. M.; and Mayfield, M. M. 2012: Rethinking community assembly through the lens of coexistence theory. *Annual Review of Ecology, Evolution, and Systematics*, Vol 43, (edited by D. J. Futuyma), volume 43, pages 227–248. Annual Reviews, Palo Alto.
- Hiltunen, T. and Becks, L. 2014: Consumer co-evolution as an important component of the eco-evolutionary feedback. *Nat. Commun.* 5(1):5226.
- Hiltunen, T.; Cairns, J.; Frickel, J.; Jalasvuori, M.; Laakso, J.; Kaitala, V.; Künzel, S.; Karakoc, E.; and Becks, L. 2018: Dual-stressor selection alters eco-evolutionary dynamics in experimental communities. *Nat. Ecol. Evol.* 2(12):1974–1981.

- Hiltunen, T.; Kaitala, V.; Laakso, J.; and Becks, L. 2017: Evolutionary contribution to coexistence of competitors in microbial food webs. *Proc. R. Soc. B-Biol. Sci.* 284(1864):20170415.
- Hiltunen, T. and Laakso, J. 2013: The relative importance of competition and predation in environment characterized by resource pulses – an experimental test with a microbial community. *BMC Ecol.* 13(1):29.
- Hoffmann, A. A. and Sgro, C. M. 2011: Climate change and evolutionary adaptation. *Nature* 470(7335):479–485.
- Holding, M. L.; Biardi, J. E.; and Gibbs, H. L. 2016: Coevolution of venom function and venom resistance in a rattlesnake predator and its squirrel prey. *Proc. R. Soc. B-Biol. Sci.* 283(1829):20152841.
- Huang, W.; Traulsen, A.; Werner, B.; Hiltunen, T.; and Becks, L. 2017: Dynamical trade-offs arise from antagonistic coevolution and decrease intraspecific diversity. *Nat. Commun.* 8(1):2059.
- Hughes, A. R.; Inouye, B. D.; Johnson, M. T. J.; Underwood, N.; and Vellend, M. 2008: Ecological consequences of genetic diversity. *Ecol. Lett.* 11(6):609–623.
- Hughes, B. S.; Cullum, A. J.; and Bennett, A. F. 2007: Evolutionary adaptation to environmental pH in experimental lineages of *Escheria coli*. *Evolution* 61(7):1725–1734.
- Hurvich, C. M. and Tsai, C.-L. 1989: Regression and time series model selection in small samples. *Biometrika* 76(2):297–307.

- Intergovernmental Science-Policy Platform on Biodiversity and Ecosystem Services, I. 2019: Summary for policymakers of the global assessment report on biodiversity and ecosystem services. Technical report, Zenodo.
- Jacob, S.; Bestion, E.; Legrand, D.; Clobert, J.; and Cote, J. 2015: Habitat matching and spatial heterogeneity of phenotypes: implications for metapopulation and meta-community functioning. *Evol. Ecol.* 29(6):851–871.
- Jacob, S.; Wehi, P.; Clobert, J.; Legrand, D.; Schtickzelle, N.; Huet, M.; and Chainé, A. 2016: Cooperation-mediated plasticity in dispersal and colonization. *Evolution* 70(10):2336–2345.
- Jacquet, C. and Altermatt, F. 2020: The ghost of disturbance past: long-term effects of pulse disturbances on community biomass and composition. *Proc. R. Soc. B-Biol. Sci.* 287(1930):20200678.
- Jennions, M. D. and Petrie, M. 1997: Variation in mate choice and mating preferences: A review of causes and consequences. *Biol. Rev.* 72(2):283–327.
- Johnson, T. and Barton, N. H. 2002: The effect of deleterious alleles on adaptation in asexual populations. *Genetics* 162(1):395–411.
- Johnston, I. A.; Clarke, A.; Laws, R. M.; and Franks, F. 1990: Cold adaptation in marine organisms. *Philos. Trans. Royal Soc. B* 326(1237):655–667.
- Joshi, A.; Prasad, N. G.; and Shakarad, M. 2001: *K*-selection, *alpha*-selection, effectiveness, and tolerance in competition: density-dependent selection revisited. *J. Genet.* 80(2):63–75.

- Kaitala, V.; Hiltunen, T.; Becks, L.; and Scheuerl, T. 2020: Co-evolution as an important component explaining microbial predator-prey interaction. *J. Theor. Biol.* 486:110095.
- Kawecki, T. J. and Ebert, D. 2004: Conceptual issues in local adaptation. *Ecol. Lett.* 7(12):1225–1241.
- Keller, S. R. and Taylor, D. R. 2010: Genomic admixture increases fitness during a biological invasion. *J. Evol. Biol.* 23(8):1720–1731.
- Kelly, M. W. and Hofmann, G. E. 2013: Adaptation and the physiology of ocean acidification. *Funct. Ecol.* 27(4):980–990.
- Ketola, T.; Laakso, J.; Kaitala, V.; and Airaksinen, S. 2004: Evolution of Hsp90 expression in *Tetrahymena thermophila* (protozoa, Ciliata) populations exposed to thermally variable environments. *Evolution* 58(4):741–748.
- Kirkpatrick, M. and Barton, N. H. 1997: Evolution of a species' range. *Am. Nat.* 150(1):1–23.
- Klerks, P. L. and Weis, J. S. 1987: Genetic adaptation to heavy metals in aquatic organisms: A review. *Environ. Pollut.* 45(3):173–205.
- Kley, A. and Maier, G. 2006: Reproductive characteristics of invasive gammarids in the Rhine-Main-Danube catchment, South Germany. *Limnologica* 36(2):79–90.
- Klopfstein, S.; Currat, M.; and Excoffier, L. 2006: The fate of mutations surfing on the wave of a range expansion. *Mol. Biol. Evol.* 23(3):482–490.

- Kofler, R.; Pandey, R. V.; and Schlötterer, C. 2011: PoPoolation2: identifying differentiation between populations using sequencing of pooled DNA samples (Pool-Seq). *Bioinformatics* 27(24):3435–3436.
- Kofler, R. and Schlötterer, C. 2012: Gowinda: unbiased analysis of gene set enrichment for genome-wide association studies. *Bioinformatics* 28(15):2084–2085.
- Kondrashov, A. S. 1993: Classification of hypotheses on the advantage of amphimixis. *J. Hered.* 84(5):372–387.
- Kooyers, N. J. 2015: The evolution of drought escape and avoidance in natural herbaceous populations. *Plant Sci.* 234:155–162.
- Korolev, K. S.; Müller, M. J. I.; Karahan, N.; Murray, A. W.; Hallatschek, O.; and Nelson, D. R. 2012: Selective sweeps in growing microbial colonies. *Phys. Biol.* 9(2):026008.
- Kot, M.; Lewis, M. A.; and Driessche, P. v. d. 1996: Dispersal data and the spread of invading organisms. *Ecology* 77(7):2027–2042.
- Kowarik, I. 2003: Human agency in biological invasions: Secondary releases foster naturalisation and population expansion of alien plant species. *Biol. Invasions* 5(4):293–312.
- Krijthe, J. H. 2015: Rtsne: T-distributed stochastic neighbor embedding using Barnes-Hut implementation.
- Kubisch, A.; Holt, R. D.; Poethke, H.-J.; and Fronhofer, E. A. 2014: Where am I and why? Synthesizing range biology and the eco-evolutionary dynamics of dispersal. *Oikos* 123(1):5–22.

- Kunkel, T. A. 2004: DNA replication fidelity. *J. Biol. Chem.* 279(17):16895–16898.
- Lachapelle, J. and Bell, G. 2012: Evolutionary rescue of sexual and asexual populations in a deteriorating environment. *Evolution* 66(11):3508–3518.
- Lachapelle, J. and Colegrave, N. 2017: The effect of sex on the repeatability of evolution in different environments. *Evolution* 71(4):1075–1087.
- Lambert, A. J. and Brand, M. D. 2004: Superoxide production by NADH:ubiquinone oxidoreductase (complex I) depends on the pH gradient across the mitochondrial inner membrane. *Biochem. J.* 382(2):511–517.
- Lavergne, S. and Molofsky, J. 2007: Increased genetic variation and evolutionary potential drive the success of an invasive grass. *Proc. Natl. Acad. Sci. U.S.A.* 104(10):3883–3888.
- Leimu, R. and Fischer, M. 2008: A meta-analysis of local adaptation in plants. *PLoS One* 3(12):e4010.
- Lemarie, A.; Huc, L.; Pazarentzos, E.; Mahul-Mellier, A.-L.; and Grimm, S. 2011: Specific disintegration of complex II succinate:ubiquinone oxidoreductase links pH changes to oxidative stress for apoptosis induction. *Cell Death Differ.* 18(2):338–349.
- Lenormand, T. 2002: Gene flow and the limits to natural selection. *Trends Ecol. Evol.* 17(4):183–189.
- Lenski, R. E.; Rose, M. R.; Simpson, S. C.; and Tadler, S. C. 1991: Long-term experimental evolution in *Escherichia coli*. I. Adaptation and divergence during 2,000 generations. *Am. Nat.* 138(6):1315–1341.

- Lenski, R. E. and Travisano, M. 1994: Dynamics of adaptation and diversification: a 10,000-generation experiment with bacterial populations. *Proc. Natl. Acad. Sci. U.S.A.* 91(15):6808–6814.
- Leuven, R. S. E. W.; van der Velde, G.; Baijens, I.; Snijders, J.; van der Zwart, C.; Lenders, H. J. R.; and bij de Vaate, A. 2009: The river Rhine: a global highway for dispersal of aquatic invasive species. *Biol. Invasions* 11(9):1989.
- Li, H. and Durbin, R. 2009: Fast and accurate short read alignment with Burrows-Wheeler transform. *Bioinformatics* 25(14):1754–1760.
- Likens, G. E. and Bormann, F. H. 1974: Acid rain: A serious regional environmental problem. *Science* 184(4142):1176–1179.
- Likens, G. E.; Driscoll, C. T.; and Buso, D. C. 1996: Long-term effects of acid rain: Response and recovery of a forest ecosystem. *Science* 272(5259):244–246.
- Lindberg, R. T. and Collins, S. 2020: Quality–quantity trade-offs drive functional trait evolution in a model microalgal ‘climate change winner’. *Ecol. Lett.* 23(5):780–790.
- Little, C. J. and Altermatt, F. 2018: Species turnover and invasion of dominant freshwater invertebrates alter biodiversity–ecosystem-function relationship. *Ecol. Monogr.* 88(3):461–480.
- Loewe, L. and Hill, W. G. 2010: The population genetics of mutations: good, bad and indifferent. *Philos. Trans. Royal Soc. B* 365(1544):1153–1167.
- Lohbeck, K. T.; Riebesell, U.; and Reusch, T. B. H. 2012: Adaptive evolution of a key phytoplankton species to ocean acidification. *Nat. Geosci.* 5(5):346–351.

- Losos, J. B. and Ricklefs, R. E. 2009: The theory of island biogeography revisited. Princeton University Press.
- Lotka, A. 1925: Elements of physical biology. *Nature* 116(2917):461–461.
- Luckinbill, L. S. 1978: *r* and *K* selection in experimental populations of *Escherichia coli*. *Science* 202(4373):1201–1203.
- Luijckx, P.; Ho, E. K. H.; Gasim, M.; Chen, S.; Stanic, A.; Yanchus, C.; Kim, Y. S.; and Agrawal, A. F. 2017: Higher rates of sex evolve during adaptation to more complex environments. *Proc. Natl. Acad. Sci. U.S.A.* 114(3):534–539.
- Lurling, M. and Beekman, W. 2006: Palmelloids formation in *Chlamydomonas reinhardtii* : defence against rotifer predators? *Ann. Limnol. - Int. J. Lim.* 42(2):65–72.
- Lynn, D. H. and Doerder, F. P. 2012: The life and times of *Tetrahymena*. *Methods Cell Biol.* 109:9–27.
- Lytle, D. A. and Poff, N. L. 2004: Adaptation to natural flow regimes. *Trends Ecol. Evol.* 19(2):94–100.
- MacArthur, R. H. and Wilson, E. O. 1967: The theory of island biogeography. Princeton University Press.
- Martin, A. P. and Palumbi, S. R. 1993: Body size, metabolic rate, generation time, and the molecular clock. *Proc. Natl. Acad. Sci. U.S.A.* 90(9):4087–4091.
- Matz, C. and Jürgens, K. 2005: High motility reduces grazing mortality of planktonic bacteria. *Appl. Environ. Microbiol.* 71(2):921–929.

- Matz, C. and Kjelleberg, S. 2005: Off the hook – how bacteria survive protozoan grazing. *Trends Microb.* 13(7):302–307.
- McDonald, M. J.; Rice, D. P.; and Desai, M. M. 2016: Sex speeds adaptation by altering the dynamics of molecular evolution. *Nature* 531(7593):233–236.
- McElreath, R. 2015: *Statistical rethinking: A Bayesian course with examples in R and Stan*. Chapman and Hall/CRC, Boca Raton, 1st edition.
- Meyer, J. R.; Ellner, S. P.; Hairston, N. G.; Jones, L. E.; and Yoshida, T. 2006: Prey evolution on the time scale of predator–prey dynamics revealed by allele-specific quantitative PCR. *Proc. Natl. Acad. Sci. U.S.A.* 103(28):10690–10695.
- Meyer, J. R. and Kassen, R. 2007: The effects of competition and predation on diversification in a model adaptive radiation. *Nature* 446(7134):432–435.
- Michel, J.; Ebert, D.; and Hall, M. D. 2016: The trans-generational impact of population density signals on host-parasite interactions. *BMC Evol. Biol.* 16.
- Moerman, F. 2019: Analysis scripts: Gene swamping alters evolution during range expansions in the protist *Tetrahymena thermophila*.
- Moerman, F.; Arquint, A.; Merkli, S.; Wagner, A.; Altermatt, F.; and Fronhofer, E. A. 2020a: Evolution under pH stress and high population densities leads to increased density-dependent fitness in the protist *Tetrahymena thermophila*. *Evolution* 74(3):573–586.
- Moerman, F.; Fronhofer, E. A.; Wagner, A.; and Altermatt, F. 2019: Gene swamping alters evolution during range expansions in the protist *Tetrahymena thermophila*. Dryad Digital Repository.

- . 2020b: Gene swamping alters evolution during range expansions in the protist *Tetrahymena thermophila*. *Biol. Lett.* 16(6):20200244.
- Motychak, J. E.; Brodie, E. D.; and Iii, E. D. B. 1999: Evolutionary response of predators to dangerous prey: Preadaptation and the evolution of tetrodotoxin resistance in garter snakes. *Evolution* 53(5):1528–1535.
- Mueller, L. D. and Ayala, F. J. 1981: Trade-off between *r*-selection and *K*-selection in *Drosophila* populations. *Proc. Natl. Acad. Sci. U.S.A.* 78(2):1303–1305.
- Mueller, L. D.; Guo, P. Z.; and Ayala, F. J. 1991: Density-dependent natural selection and trade-offs in life history traits. *Science* 253(5018):433–435.
- Muller, H. J. 1932: Some genetic aspects of sex. *Am. Nat.* 66(703):118–138.
- Nørgaard, L. S.; Phillips, B. L.; and Hall, M. D. 2019: Infection in patchy populations: Contrasting pathogen invasion success and dispersal at varying times since host colonization. *Evol. Lett.* 3(5):555–566.
- Ochocki, B. M. and Miller, T. E. X. 2017: Rapid evolution of dispersal ability makes biological invasions faster and more variable. *Nat. Commun.* 8:14315.
- Ochocki, B. M.; Saltz, J. B.; and Miller, T. E. X. 2020: Demography-dispersal trait correlations modify the eco-evolutionary dynamics of range expansion. *Am. Nat.* 195(2):231–246.
- Otto, S. 2009: The evolutionary enigma of sex. *Am. Nat.* 174(S1):S1–S14.
- Otto, S. P. and Barton, N. H. 1997: The evolution of recombination: removing the limits to natural selection. *Genetics* 147(2):879–906.

- Otto, S. P. and Lenormand, T. 2002: Resolving the paradox of sex and recombination. *Nat. Rev. Genet.* 3(4):252–261.
- Pachepsky, E. and Levine, J. 2011: Density dependence slows invader spread in fragmented landscapes. *Am. Nat.* 177(1):18–28.
- Padfield, D.; Yvon-Durocher, G.; Buckling, A.; Jennings, S.; and Yvon-Durocher, G. 2016: Rapid evolution of metabolic traits explains thermal adaptation in phytoplankton. *Ecol. Lett.* 19(2):133–142.
- Panja, D. 2004: Effects of fluctuations on propagating fronts. *Phys. Rep.* 393(2):87–174.
- Parmesan, C. 2006: Ecological and evolutionary responses to recent climate change. *Annu. Rev. Ecol. Evol. Syst.* 37(1):637–669.
- Parmesan, C.; Ryrholm, N.; Stefanescu, C.; Hill, J. K.; Thomas, C. D.; Descimon, H.; Huntley, B.; Kaila, L.; Kullberg, J.; Tammaru, T.; Tennent, W. J.; Thomas, J. A.; and Warren, M. 1999: Poleward shifts in geographical ranges of butterfly species associated with regional warming. *Nature* 399(6736):579–583.
- Peck, J. R. 1994: A ruby in the rubbish: beneficial mutations, deleterious mutations and the evolution of sex. *Genetics* 137(2):597–606.
- Peischl, S.; Dupanloup, I.; Foucal, A.; Jomphe, M.; Bruat, V.; Grenier, J.-C.; Gouy, A.; Gilbert, K. J.; Gbeha, E.; Bosshard, L.; Hip-Ki, E.; Agbessi, M.; Hodgkinson, A.; Vézina, H.; Awadalla, P.; and Excoffier, L. 2018: Relaxed selection during a recent human expansion. *Genetics* 208(2):763–777.

- Peischl, S. and Excoffier, L. 2015: Expansion load: recessive mutations and the role of standing genetic variation. *Mol. Ecol.* 24(9):2084–2094.
- Peischl, S.; Kirkpatrick, M.; and Excoffier, L. 2015: Expansion load and the evolutionary dynamics of a species range. *Am. Nat.* 185(4):E81–E93.
- Pejchar, L. and Mooney, H. A. 2009: Invasive species, ecosystem services and human well-being. *Trends Ecol. Evol.* 24(9):497–504.
- Pelletier, F.; Garant, D.; and Hendry, A. P. 2009: Eco-evolutionary dynamics. *Proc. R. Soc. B-Biol. Sci.* 364(1523):1483–1489.
- Pennekamp, F.; Mitchell, K. A.; Chaine, A.; and Schtickzelle, N. 2014: Dispersal propensity in *Tetrahymena thermophila* ciliates - A reaction norm perspective. *Evolution* 68(8):2319–2330.
- Pennekamp, F. and Schtickzelle, N. 2013: Implementing image analysis in laboratory-based experimental systems for ecology and evolution: a hands-on guide. *Methods Ecol. Evol.* 4(5):483–492.
- Pennekamp, F.; Schtickzelle, N.; and Petchey, O. L. 2015: BEMOVI, software for extracting behavior and morphology from videos, illustrated with analyses of microbes. *Ecol. Evol.* 5(13):2584–2595.
- Perkins, A.; Phillips, B. L.; Baskett, M. L.; and Hastings, A. 2013: Evolution of dispersal and life history interact to drive accelerating spread of an invasive species. *Ecol. Lett.* 16(8):1079–1087.
- Petegem, K. H. P. V.; Renault, D.; Stoks, R.; and Bonte, D. 2016: Metabolic adaptations in a range-expanding arthropod. *Ecol. Evol.* 6(18):6556–6564.

- Petegem, K. V.; Moerman, F.; Dahirel, M.; Fronhofer, E. A.; Vandegehuchte, M. L.; Leeuwen, T. V.; Wybouw, N.; Stoks, R.; and Bonte, D. 2018: Kin competition accelerates experimental range expansion in an arthropod herbivore. *Ecol. Lett.* 21(2):225–234.
- Petkovic, N. and Colegrave, N. 2019: Sex increases the probability of evolutionary rescue in the presence of a competitor. *J. Evol. Biol.* 32(11):1252–1261.
- Phillips, B. 2009: The evolution of growth rates on an expanding range edge. *Biol. Lett.* 5(6):802–804.
- Phillips, B. L.; Brown, G. P.; Greenlees, M.; Webb, J. K.; and Shine, R. 2007: Rapid expansion of the cane toad (*Bufo marinus*) invasion front in tropical Australia. *Austral Ecol.* 32(2):169–176.
- Phillips, B. L.; Brown, G. P.; and Shine, R. 2010: Life-history evolution in range-shifting populations. *Ecology* 91(6):1617–1627.
- Phillips, B. L. and Shine, R. 2006: An invasive species induces rapid adaptive change in a native predator: cane toads and black snakes in Australia. *Proc. R. Soc. B-Biol. Sci.* 273(1593):1545–1550.
- Phillips, I. D.; Vinebrooke, R. D.; and Turner, M. A. 2009: Ecosystem consequences of potential range expansions of *Orconectes virilis* and *Orconectes rusticus* crayfish in Canada — a review. *Environ. Rev.* 17:235–248.
- Pinheiro, J.; Bates, D.; DebRoy, S.; Sarkar, D.; and R Core Team. 2020: nlme: Linear and nonlinear mixed effects models.

- Polechová, J. 2018: Is the sky the limit? On the expansion threshold of a species' range. *PLoS Biol.* 16(6):e2005372.
- Polechová, J. and Barton, N. H. 2015: Limits to adaptation along environmental gradients. *Proc. Natl. Acad. Sci. U.S.A.* 112(20):6401–6406.
- Quinlan, A. R. and Hall, I. M. 2010: BEDTools: a flexible suite of utilities for comparing genomic features. *Bioinformatics* 26(6):841–842.
- R Core Team. 2017: R: A language and environment for statistical computing. R Foundation for Statistical Computing, Vienna, Austria.
- . 2020: R: A language and environment for statistical computing. R Foundation for Statistical Computing, Vienna, Austria.
- Raven, J.; Caldeira, K.; Elderfield, H.; Hoegh-Guldberg, O.; Liss, P. S.; Riebesell, U.; Sheperd, J.; Turley, C.; and Watson, A. 2005: Ocean acidification due to increasing atmospheric carbon dioxide. Royal Society Policy Document.
- Reusch, T. B. H. and Boyd, P. W. 2013: Experimental evolution meets marine phytoplankton. *Evolution* 67(7):1849–1859.
- Reznick, D.; Bryant, M. J.; and Bashey, F. 2002: *r*- and *K*-selection revisited: the role of population regulation in life-history evolution. *Ecology* 83(6):1509–1520.
- Ricciardi, A. and MacIsaac, H. J. 2008: The book that began invasion ecology. *Nature* 452(7183):34–34.
- Richardson, D. M. 2011: Fifty years of invasion ecology: The legacy of Charles Elton. John Wiley & Sons.

- Rosenbaum, B.; Raatz, M.; Weithoff, G.; Fussmann, G. F.; and Gaedke, U. 2019: Estimating parameters from multiple time series of population dynamics using Bayesian inference. *Front. Ecol. Evol.* 6:234.
- Rosenzweig, M. L. and MacArthur, R. H. 1963: Graphical representation and stability conditions of predator-prey interactions. *Am. Nat.* 97(895):209–223.
- Ruan, Z. S.; Anantharam, V.; Crawford, I. T.; Ambudkar, S. V.; Rhee, S. Y.; Allison, M. J.; and Maloney, P. C. 1992: Identification, purification, and reconstitution of OxIT, the oxalate: formate antiport protein of *Oxalobacter formigenes*. *J. Biol. Chem.* 267(15):10537–10543.
- Ruehle, M. D.; Orias, E.; and Pearson, C. G. 2016: *Tetrahymena* as a unicellular model Eukaryote: Genetic and genomic tools. *Genetics* 203(2):649–665.
- Saastamoinen, M.; Bocedi, G.; Cote, J.; Legrand, D.; Guillaume, F.; Wheat, C. W.; Fronhofer, E. A.; Garcia, C.; Henry, R.; Husby, A.; Baguette, M.; Bonte, D.; Coulon, A.; Kokko, H.; Matthysen, E.; Niitepõld, K.; Nonaka, E.; Stevens, V. M.; Travis, J. M. J.; Donohue, K.; Bullock, J. M.; and Delgado, M. d. M. 2018: Genetics of dispersal. *Biol. Rev.* 93(1):574–599.
- Sakai, A. K.; Allendorf, F. W.; Holt, J. S.; Lodge, D. M.; Molofsky, J.; With, K. A.; Baughman, S.; Cabin, R. J.; Cohen, J. E.; Ellstrand, N. C.; McCauley, D. E.; O’Neil, P.; Parker, I. M.; Thompson, J. N.; and Weller, S. G. 2001: The population biology of invasive species. *Annu. Rev. Ecol. Syst.* 32(1):305–332.
- Sanders, N. J.; Gotelli, N. J.; Heller, N. E.; and Gordon, D. M. 2003: Community disassembly by an invasive species. *Proc. Natl. Acad. Sci. U.S.A.* 100(5):2474–2477.

- Sanford, E. and Kelly, M. W. 2011: Local adaptation in marine invertebrates. *Annu. Rev. Mar. Sci.* 3(1):509–535.
- Scheuerl Thomas; Cairns Johannes; Becks Lutz; and Hiltunen Teppo. 2019: Predator coevolution and prey trait variability determine species coexistence. *Proc. R. Soc. B-Biol. Sci.* 286(1902):20190245.
- Schlötterer, C.; Tobler, R.; Kofler, R.; and Nolte, V. 2014: Sequencing pools of individuals — mining genome-wide polymorphism data without big funding. *Nat. Rev. Genet.* 15(11):749–763.
- Schlüter, L.; Lohbeck, K. T.; Gutowska, M. A.; Gröger, J. P.; Riebesell, U.; and Reusch, T. B. H. 2014: Adaptation of a globally important coccolithophore to ocean warming and acidification. *Nat. Clim. Chang.* 4(11):1024–1030.
- Schmeller, D. S.; Seitz, A.; Crivelli, A.; and Veith, M. 2005: Crossing species' range borders: interspecies gene exchange mediated by hybridogenesis. *Proc. R. Soc. B-Biol. Sci.* 272(1572):1625–1631.
- Schtickzelle, N.; Fjerdingstad, E. J.; Chaine, A.; and Clobert, J. 2009: Cooperative social clusters are not destroyed by dispersal in a ciliate. *BMC Evol. Biol.* 9:251.
- Sexton, J. P.; McIntyre, P. J.; Angert, A. L.; and Rice, K. J. 2009: Evolution and ecology of species range limits. *Annu. Rev. Ecol. Evol. Syst.* 40:415–436.
- Shaw, A. 1994: Adaptation to metals in widespread and endemic plants. *Environ. Health Perspect.* 102:105–108.
- Shine, R.; Brown, G. P.; and Phillips, B. L. 2011: An evolutionary process that as-

- sembles phenotypes through space rather than through time. *Proc. Natl. Acad. Sci. U.S.A.* 108(14):5708–5711.
- Simmons, A. D. and Thomas, C. D. 2004: Changes in dispersal during species' range expansions. *Am. Nat.* 164(3):378–395.
- Singh, J. S. 2002: The biodiversity crisis: A multifaceted review. *Curr. Sci.* 82(6):638–647.
- Skellam, J. G. 1951: Random dispersal in theoretical populations. *Biometrika* 38(1/2):196–218.
- Smith, J. 1978: *The evolution of sex*. Cambridge University Press, Cambridge Eng. ; New York, reissue edition edition.
- Srivastava, D. S. and Vellend, M. 2005: Biodiversity-ecosystem function research: Is it relevant to conservation? *Annu. Rev. Ecol. Evol. Syst.* 36(1):267–294.
- Stan Development Team. 2018: RStan: the R interface to Stan.
- Stearns, S. C. 1977: The evolution of life history traits: A critique of the theory and a review of the data. *Annu. Rev. Ecol. Syst.* 8(1):145–171.
- . 1992: *The evolution of life histories*. Oxford University Press, Oxford, New York.
- . 2000: Life history evolution: successes, limitations, and prospects. *Naturwissenschaften* 87(11):476–486.
- Stillman, J. H. and Paganini, A. W. 2015: Biochemical adaptation to ocean acidification. *J. Exp. Biol.* 218(12):1946–1955.

- Sun, J.; Wang, M.; Wang, H.; Zhang, H.; Zhang, X.; Thiagarajan, V.; Qian, P. Y.; and Qiu, J. W. 2012: De novo assembly of the transcriptome of an invasive snail and its multiple ecological applications. *Mol. Ecol. Resour.* 12(6):1133–1144.
- Sunday, J. M.; Calosi, P.; Dupont, S.; Munday, P. L.; Stillman, J. H.; and Reusch, T. B. H. 2014: Evolution in an acidifying ocean. *Trends Ecol. Evol.* 29(2):117–125.
- Swaegers, J.; Mergeay, J.; Geystelen, A. V.; Therry, L.; Larmuseau, M. H. D.; and Stoks, R. 2015: Neutral and adaptive genomic signatures of rapid poleward range expansion. *Mol. Ecol.* 24(24):6163–6176.
- Swaegers, J.; Mergeay, J.; Therry, L.; Larmuseau, M. H. D.; Bonte, D.; and Stoks, R. 2013: Rapid range expansion increases genetic differentiation while causing limited reduction in genetic diversity in a damselfly. *Heredity* 111(5):422–429.
- Sweet, M. T. and Allis, C. D. 2006: Isolation and purification of *Tetrahymena* nuclei. *Cold Spring Harb Protoc* 2006(4):pdb.prot4500.
- Szűcs, M.; Vahsen, M. L.; Melbourne, B. A.; Hoover, C.; Weiss-Lehman, C.; and Hufbauer, R. A. 2017: Rapid adaptive evolution in novel environments acts as an architect of population range expansion. *Proc. Natl. Acad. Sci. U.S.A.* 114(51):13501–13506.
- Sánchez-Bayo, F. and Wyckhuys, K. A. G. 2019: Worldwide decline of the entomofauna: A review of its drivers. *Biol. Conserv.* 232:8–27.
- Therry, L.; Nilsson-Örtman, V.; Bonte, D.; and Stoks, R. 2014: Rapid evolution of larval life history, adult immune function and flight muscles in a poleward-moving damselfly. *J. Evol. Biol.* 27(1):141–152.
- Thieme, H. R. 2003: *Mathematics in population biology*. Princeton University Press.

- Tingley, R.; Ward-Fear, G.; Schwarzkopf, L.; Greenlees, M. J.; Phillips, B. L.; Brown, G.; Clulow, S.; Webb, J.; Capon, R.; Sheppard, A.; Strive, T.; Tizard, M.; and Shine, R. 2017: New weapons in the toad toolkit: A review of methods to control and mitigate the biodiversity impacts of invasive cane toads (*Rhinella Marina*). *Quart. Rev. Biol.* 92(2):123–149.
- Van Den Brink, F. W. B.; Van Der Velde, G.; and Bij De Vaate, A. 1991: Amphipod invasion on the Rhine. *Nature* 352(6336):576–576.
- Van der Putten, W. H.; Macel, M.; and Visser, M. E. 2010: Predicting species distribution and abundance responses to climate change: why it is essential to include biotic interactions across trophic levels. *Philos. Trans. Royal Soc. B* 365(1549):2025–2034.
- Van Petegem, K. H. P.; Boeye, J.; Stoks, R.; and Bonte, D. 2016: Spatial selection and local adaptation jointly shape life-history evolution during range expansion. *Am. Nat.* 188(5):485–498.
- van Saarloos, W. 2003: Front propagation into unstable states. *Phys. Rep.* 386(2):29–222.
- van Velzen, E. and Gaedke, U. 2017: Disentangling eco-evolutionary dynamics of predator-prey coevolution: the case of antiphase cycles. *Sci. Rep.* 7(1):17125.
- Vermeij, G. J. 1994: The evolutionary interaction among species: Selection, escalation, and coevolution. *Annu. Rev. Ecol. Evol. Syst.* 25(1):219–236.
- Visser, A. W. 2007: Motility of zooplankton: fitness, foraging and predation. *J. Plankton. Res.* 29(5):447–461.

- Visser, M. E.; te Marvelde, L.; and Lof, M. E. 2012: Adaptive phenological mismatches of birds and their food in a warming world. *J. Ornithol.* 153(1):75–84.
- Volterra, V. 1928: Variations and fluctuations of the number of individuals in animal species living together. *ICES. J. Mar. Sci.* 3(1):3–51.
- Wada, Y.; Ohsumi, Y.; Tanifuji, M.; Kasai, M.; and Anraku, Y. 1987: Vacuolar ion channel of the yeast, *Saccharomyces cerevisiae*. *J. Biol. Chem.* 262(36):17260–17263.
- Wallace, A. R. 1876: The geographical distribution of animals. Harper and brothers.
- Warren, P. H.; Law, R.; and Weatherby, A. J. 2003: Mapping the assembly of protist communities in microcosms. *Ecology* 84(4):1001–1011.
- Weiss-Lehman, C.; Hufbauer, R. A.; and Melbourne, B. A. 2017: Rapid trait evolution drives increased speed and variance in experimental range expansions. *Nat. Commun.* 8:14303.
- Westerberhard, M. 1989: Phenotypic plasticity and the origins of diversity. *Annu. Rev. Ecol. Syst.* 20:249–278.
- Whittaker, R. J.; Triantis, K. A.; and Ladle, R. J. 2008: A general dynamic theory of oceanic island biogeography. *J. Biogeogr.* 35(6):977–994.
- Wickham, H. 2016: *ggplot2: Elegant graphics for data analysis*. Springer-Verlag New York.
- Wildschutte, H.; Wolfe, D. M.; Tamewitz, A.; and Lawrence, J. G. 2004: Protozoan predation, diversifying selection, and the evolution of antigenic diversity in *Salmonella*. *Proc. Natl. Acad. Sci. U.S.A.* 101(29):10644–10649.

- Williams, J. L.; Hufbauer, R. A.; and Miller, T. E. X. 2019: How evolution modifies the variability of range expansion. *Trends Ecol. Evol.* 34(10):903–913.
- Williams, J. L.; Kendall, B. E.; and Levine, J. M. 2016: Rapid evolution accelerates plant population spread in fragmented experimental landscapes. *Science* 353(6298):482–485.
- Williamson, M. and Griffiths, B. 1996: *Biological invasions*. Springer Science & Business Media.
- Wood, T. E.; Burke, J. M.; and Rieseberg, L. H. 2005: Parallel genotypic adaptation: when evolution repeats itself. *Genetica* 123(1-2):157–170.
- Yoshida, T.; Jones, L. E.; Ellner, S. P.; Fussmann, G. F.; and Hairston, N. G. 2003: Rapid evolution drives ecological dynamics in a predator–prey system. *Nature* 424(6946):303–306.
- Zeebe, R. E.; Zachos, J. C.; Caldeira, K.; and Tyrrell, T. 2008: Carbon Emissions and Acidification. *Science* 321(5885):51–52.
- Zhang, J.; Wu, C.; Du, G.; and Chen, J. 2012: Enhanced acid tolerance in *Lactobacillus casei* by adaptive evolution and compared stress response during acid stress. *Biotechnol. Bioprocess Eng.* 17(2):283–289.
- Zilio, G.; Nørgaard, L. S.; Gougat-Barbera, C.; Hall, M. D.; Fronhofer, E. A.; and Kaltz, O. 2020: Travelling with a parasite: the evolution of resistance and dispersal syndrome during experimental range expansion. *bioRxiv* page 2020.01.29.924498.
- Zollner, P. A. and Lima, S. L. 1999: Search strategies for landscape-level interpatch movements. *Ecology* 80(3):1019–1030.

FELIX MOERMAN

Claridenstrasse 22, CH-8600, Dübendorf · 078 694 01 06

Felix.moerman@hotmail.com · www.felixmoerman.com · [twitter: @femoerman](https://twitter.com/femoerman)

PERSONAL INFO

Nationality: Belgian
Date/place of birth: 29/04/1993, Ghent, Belgium
Work address: Office G09
Eawag, Dept. of Aquatic Ecology
Überlandstrasse 133
CH-8600 Dübendorf
Switzerland
Phone no.: (+41) 078 694 01 06
Email: Felix.moerman@hotmail.com
Homepage: www.felixmoerman.com
Orcid ID: 0000-0002-5164-0978
Google scholar ID: [PGsthCIAAAAJ](https://scholar.google.com/citations?user=PGsthCIAAAAJ)



EDUCATION

JANUARY 2017 – NOW

PHD IN EVOLUTIONARY BIOLOGY, UNIVERSITY OF ZÜRICH, EAWAG AND SIB, SWITZERLAND; ISEM FRANCE

Topic: Understanding Invasions: from the Genetic Basis to the Ecological Dynamics of Spreading Populations

Supervision: Prof. Dr. Florian Altermatt, Prof. Dr. Andreas Wagner and Dr. Emanuel A. Fronhofer.

Scheduled defence date: 14/01/2021

SEPTEMBER 2014 – JULY 2016

MSC. IN BIOLOGY, UNIVERSITY OF GHENT, BELGIUM

Graduated summa cum laude; Major in global change ecology; Minor in research. Master thesis supervised by Prof. Dr. Dries Bonte.

SEPTEMBER 2011-JUNE 2014

BSC. IN BIOLOGY, UNIVERSITY OF GHENT, BELGIUM

Graduated cum laude.

EMPLOYMENT HISTORY

JANUARY 2017 – NOW

PHD IN EVOLUTIONARY BIOLOGY, UNIVERSITY OF ZÜRICH, EAWAG AND SIB, SWITZERLAND; ISEM FRANCE

Topic: Understanding Invasions: from the Genetic Basis to the Ecological Dynamics of Spreading Populations

Supervision: Prof. Dr. Florian Altermatt, Prof. Dr. Andreas Wagner and Dr. Emanuel A. Fronhofer.

SCHEDULED DEFENCE DATE: 14/01/2021

JULY-AUGUST 2016

LAB ASSISTENT, UNIVERSITY OF GHENT, BELGIUM

Assistance with laboratory work at the terrestrial ecology (TEREC) department at the university of Ghent.

2012-2015

VOLUNTEER WORK, ROCK WERCHTER (TUMBADOR VZW)

Non-profit work at the Rock Werchter music festival, sponsoring the NGO “Tumbador vzw”.

2008-2011

ADMINISTRATIVE SUMMER JOB, ANTWERP MARITIME ACADEMY

Summer job aiding in general administrative and technical tasks.

ACTIVE MEMBERSHIP IN SOCIETIES

- European Society for Evolutionary Biology (ESEB)
- Society for the Study of Evolution (SSE)
- British Ecological Society (BES)

SUPERVISION OF STUDENTS/JUNIOR RESEARCHERS

- **2020:** Supervision of group technician, Samuel Hürlemann for the Diplomarbeit in his further education “Advanced Federal Diploma of Higher Education, systems engineering, pharmaceutical and chemical engineering.” At Aprentas (Muttenz, Switzerland)

TEACHING ACTIVITIES

- **BIO 309: Limnoecology course** (ETH Zürich and University of Zürich; 150 hours): Supervision of student projects on protist experiments assessing protist evolution to pH stress (2017) and plastic effects of pH on performance and dispersal ability of protists (2018).
- **Bio 144: Data analysis in Biology** (2018 – University of Zürich; 40 hours) - Supervision of biology students in statistics practicals and helping students to learn to perform and interpret statistical analyses on biological data using the R statistical language
- **Bio 134: Programming in Biology** (2017 - University of Zürich; 110 hours): Supervision of biology students in programming practicals and aiding students in learning to solve biological problems using computational tools in Python

SCIENTIFIC REVIEWING ACTIVITIES

Total: 11 peer reviews

- Ecology Letters: 4 reviews
- Journal of Animal Ecology: 3 reviews
- Scientific Reports: 2 reviews
- Oikos: 2 reviews

ORGANISATION OF CONFERENCES

2018

INDO-SWISS PRIMER, UNIVERSITY OF ZÜRICH, SWITZERLAND

Co-organization of the “Indo-Swiss primer in Evolution and Ecology”, in collaboration with Dr. Shraddha Karve and Dr. Xiang-Yi Li. Organization of a scientific exchange project between researchers working on evolution and ecology in India and Switzerland, to foster future research collaborations.

PRIZES, AWARDS AND FELLOWSHIPS (TOTAL: 10'950 CHF)

- University Zürich: Graduate Campus Travel grant (May 2018)
 - **Aim:** Travel grant, financing a research stay in ISEM, Montpellier, France
 - **Applicants: Moerman Felix**
 - **Amount: 950 CHF**
- University Zürich: Graduate Campus Project grant (May 2018)
 - **Aim:** Project grant, financing „Indo-Swiss collaboration primer in Evolution and Ecology”, a scientific exchange project promoting scientific collaboration between evolutionary biologists and ecologists working in Switzerland and India.
 - **Applicants: Karve Shraddha, Li Xiang-Yi, Moerman Felix**
 - **Amount: 10'000 CHF**

PERSONAL SKILLS

- **Languages:** Native Dutch speaker; English (fluent); French (advanced comprehension; medium expression) and German (advanced comprehension; basic expression).
- **Lab skills:** Wet lab work with spider mites and protists; clean culturing of axenic cultures; DNA extractions; gel electrophoresis.
- **Operating systems:** Extensive experience with Windows and Linux operating systems
- **Programming languages/statistics:** Extensive knowledge of Python, C++ and R statistical language; Basic knowledge of Julia; Experience with frequentist and Bayesian statistics.
- **Additional skills:** B driver's license; Basic mountaineering degree (Climbing and mountaineering federation Belgium); PADI open water diver license.

PUBLICATION LIST

Felix Moerman

1) PUBLICATIONS IN PEER-REVIEWED SCIENTIFIC JOURNALS

- **Moerman F.**, Fronhofer E. A., Wagner A & Altermatt F. [Gene swamping alters evolution during range expansions in the protist *Tetrahymena thermophila*](#). *Biology Letters* 16, 20200244. (doi:10.1098/rsbl.2020.0244)
- Cairns J., **Moerman F.**, Fronhofer E. A., Altermatt F. & Hiltunen T., [Evolution in interacting species alters predator life history traits, behavior and morphology in experimental microbial communities](#). *Proceedings of the Royal Society B: Biological Sciences* 287, 20200652. (doi:10.1098/rspb.2020.0652)
- **Moerman F.**, Arquint A., Merkli S., Wagner A., Altermatt F. & Fronhofer E. A. [Evolution under pH stress and high population densities leads to increased density-dependent fitness in the protist *Tetrahymena thermophila*](#). *Evolution*. 2020;74(3):573–86. (doi.org/10.1111/evo.13921)
- Van Petegem K. H. P., **Moerman F.**, Dahirel M., Fronhofer E. A., Vandegheuchte M., Van Leeuwen T., Wybouw N., Stocks R. & Bonte D. (2018) [Kin competition accelerates experimental range expansion in an arthropod herbivore](#). *Ecology Letters* 21: 225-234. (doi.org/10.1111/ele.12887)

2) CONTRIBUTIONS TO INTERNATIONAL CONFERENCES.

6.1) ORAL PRESENTATIONS

- **Moerman F.**, Wagner A., Fronhofer E. A. and Altermatt F., (2019) Adaptation and demographic rescue during range expansions., *Biology* 19, Zürich, Switzerland
- **Moerman F.**, Wagner A., Fronhofer E. A. and Altermatt F., (2018) Adaptation during range expansions in selective landscapes., *Second Joint Congress on Evolutionary Biology*, Montpellier, France.
- **Moerman F.**, Wagner A., Fronhofer E. A. and Altermatt F., (2017) *Modelling reproductive strategies during range expansions.*, *Movement and Dispersal symposium*, Ghent, Belgium.
- **Moerman F.**, Van Petegem K.H.P., Bonte D., Stoks R., (2016) *Eco-evolutionary responses along an experimental dispersal front, using *Tetranychus urticae* as a model species*, *Ecology and Behaviour* 2016, Lyon, France.

6.2) POSTER PRESENTATIONS

- **Moerman F.**, Wagner A., Fronhofer E. A. and Altermatt F., (2019) *Sex and gene flow modulate adaptation during range expansions.*, *ESEB 2019*, Turku, Finland.
- **Moerman F.**, Wagner A., Fronhofer E. A. and Altermatt F., (2017) *Adaptive strategies during range expansions.*, *Ecology Across Borders: Joint Annual Meeting 2017*, Ghent, Belgium.

3) OUTREACH ACTIVITIES.

- **SCIENTIFICA 2019, ZÜRICH, SWITZERLAND**

Participation to the exhibit “Täuschung im Reich der Pflanzen”, organized by the URPP evolution in action (University Zürich).

4) GENERAL CONTRIBUTIONS TO SCIENCE.

- **INDO-SWISS PRIMER 2018, UNIVERSITY OF ZÜRICH, SWITZERLAND**

Co-organization of the “Indo-Swiss primer in Evolution and Ecology”, in collaboration with Dr. Shraddha Karve and Dr. Xiang-Yi Li. Organization of a scientific exchange project between researchers working on evolution and ecology in India and Switzerland, to foster future research collaborations.

5) UNPUBLISHED WORK.

- **Moerman F., Fronhofer E. A., Altermatt F. & Wagner A.,** Selection on growth rate and local adaptation drive genetic adaptation during range expansions in the protist *Tetrahymena thermophila*. (In preparation)

Chapter S.1

Supplementary Material of Chapter 1

S.1.1 Relationship between HCl and pH

Amount HCl added (μL)	Total amount HCl (μL)	pH
0	0	6.61
40	40	6.56
160	200	6.31
200	400	5.97
200	600	5.60
200	800	5.27
200	1000	5.0
200	1200	4.82
200	1400	4.64
200	1600	4.50
200	1800	4.37
200	2000	4.24
50	2050	4.21
50	2100	4.19
50	2150	4.15
50	2200	4.12
50	2250	4.11
50	2300	4.08
50	2350	4.06
50	2400	4.03
50	2450	4.00
100	2550	3.95
100	2650	3.89

Table S1.1: Table showing the amount of 1M HCl added to 100mL of the SSP medium, and the corresponding measured pH.

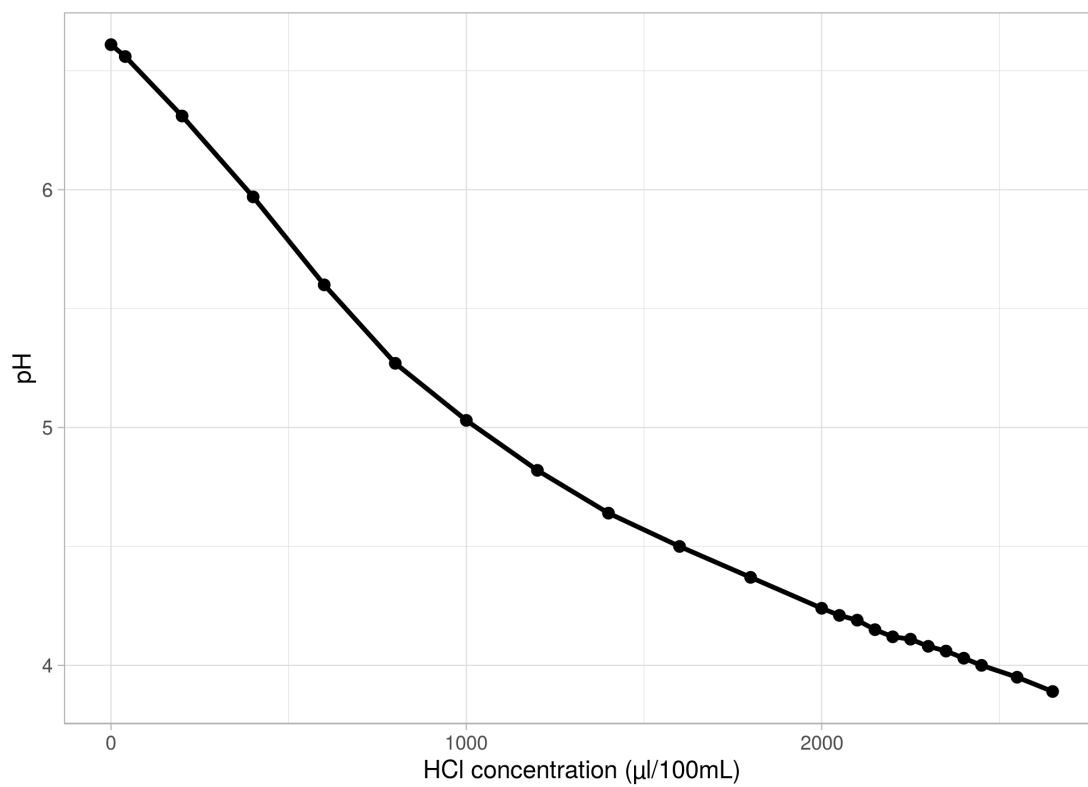


Figure S1.1: Measured pH (y-axis) as a function of HCl concentration (x-axis).

S.1.2 PCA plot showing genotype differences

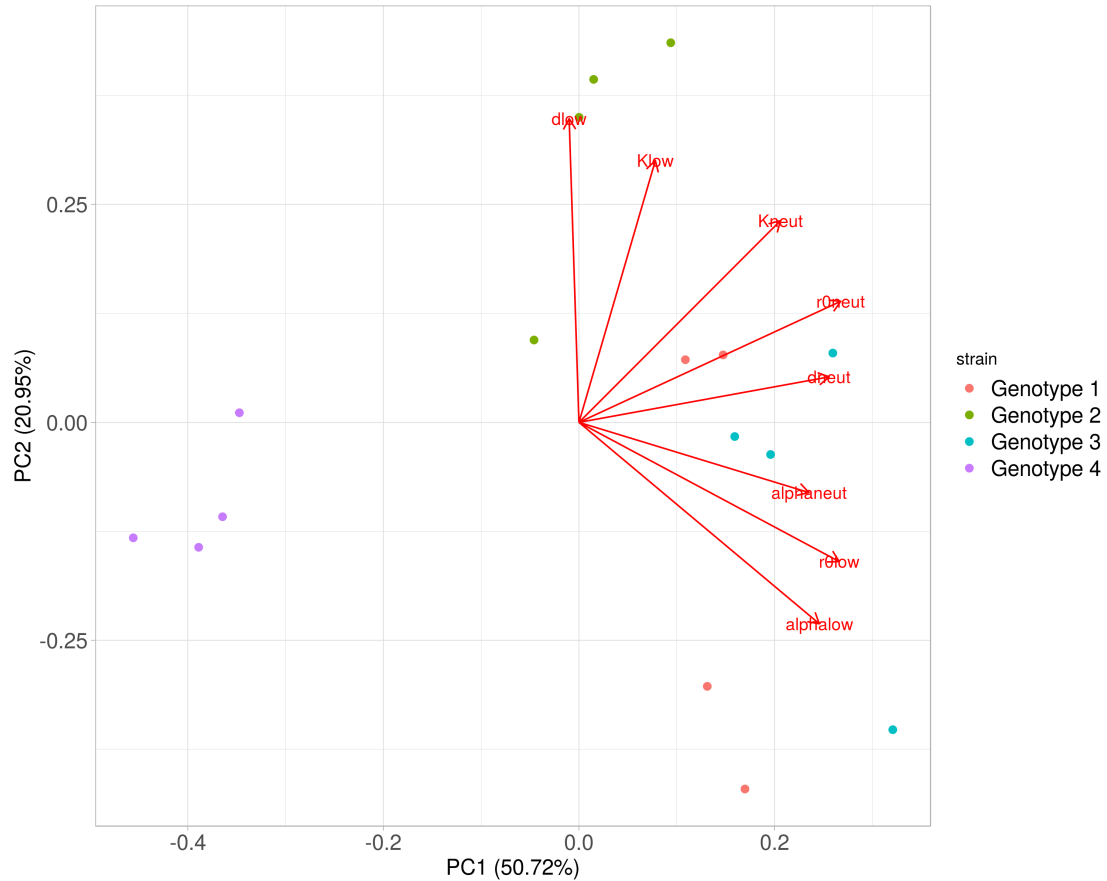


Figure S1.2: PCA of the ancestral genotypes, using the population growth parameters (intrinsic rate of increase (r_0), competitive ability (α), mortality (d) and equilibrium population density (K)) measured both at low (4.5) and neutral (6.5) pH. Genotypes are coloured in red (genotype 1 – B2086.2), green (genotype 2 – CU427.4), blue (genotype 3 – CU428.2) and purple (genotype 4 – SB3539).

S.1.3 Video analysis script

```
#####  
# R script for analysing video files with BEMOVI (www.bemovi.info)  
rm(list=ls())  
# load package  
library(devtools)  
install_github("efronhofer/bemovi", ref="experimental")  
library(bemovi)  
  
#####  
# VIDEO PARAMETERS  
  
# video frame rate (in frames per second)  
fps <- 25  
# length of video (in frames)  
total_frames <- 500  
  
# measured volume (in microliter)  
measured_volume <- 34.4 # for Leica M205 C with 1.6 fold magnification,  
Sample height 0.5 mm and Hamamatsu Orca Flash 4  
  
# size of a pixel (in micrometer)  
pixel_to_scale <- 4.05 # for Leica M205 C with 1.6 fold magnification,  
Sample height 0.5 mm and Hamamatsu Orca Flash 4  
  
# specify video file format (one of "avi","cxd","mov","tiff")  
# bemovi only works with avi and cxd. other formats are reformatted  
# to avi below  
video.format <- "cxd"  
  
# setup  
difference.lag <- 10  
thresholds <- c(10,255) # don't change the second value  
#thresholds <- c(50,255)  
  
#####  
# FILTERING PARAMETERS  
# min and max size: area in pixels  
particle_min_size <- 5  
particle_max_size <- 1000
```

```

# number of adjacent frames to be considered for linking particles
trajectory_link_range <- 3
# maximum distance a particle can move between two frames
trajectory_displacement <- 16

# these values are in the units defined by the parameters above:
# fps (seconds),
#measured_volume (microliters) and pixel_to_scale (micrometers)
filter_min_net_disp <- 25
filter_min_duration <- 1
filter_detection_freq <- 0.1
filter_median_step_length <- 3

#####
# MORE PARAMETERS (USUALLY NOT CHANGED)

# set paths to ImageJ and particle linker standalone
IJ.path <- "/home/felix/bin/ImageJ"
to.particlelinker <- "/home/felix/bin/ParticleLinker"

# directories and file names
to.data <- paste(getwd(),"/",sep="")
video.description.folder <- "0_video_description/"
video.description.file <- "video_description.txt"
raw.video.folder <- "1_raw/"
particle.data.folder <- "2_particle_data/"
trajectory.data.folder <- "3_trajectory_data/"
temp.overlay.folder <- "4a_temp_overlays/"
overlay.folder <- "4_overlays/"
merged.data.folder <- "5_merged_data/"
ijmacs.folder <- "ijmacs/"

# RAM allocation
memory.alloc <- c(60000)

# RAM per particle linker instance
memory.alloc.perLinker <- c(10000)

#####

```

```

# VIDEO ANALYSIS

# identify particles
locate_and_measure_particles(to.data, raw.video.folder,
particle.data.folder,
difference.lag, thresholds, min_size = particle_min_size,
max_size = particle_max_size, IJ.path, memory.alloc)

# link the particles
link_particles(to.data, particle.data.folder, trajectory.data.folder,
linkrange = trajectory_link_range, disp = trajectory_displacement,
start_vid = 1, memory = memory.alloc,
memory_per_linkerProcess = memory.alloc.perLinker)

# merge info from description file and data
merge_data(to.data, particle.data.folder, trajectory.data.folder,
video.description.folder, video.description.file, merged.data.folder)

# load the merged data
load(paste0(to.data, merged.data.folder, "Master.RData"))

# filter data: minimum net displacement, their duration, the detection
#frequency and the median step length
trajectory.data.filtered <- filter_data(trajectory.data,
filter_min_net_disp, filter_min_duration, filter_detection_freq,
filter_median_step_length)

# summarize trajectory data to individual-based data
morph_mvt <- summarize_trajectories(trajectory.data.filtered,
calculate.median=F, write = T, to.data, merged.data.folder)

# get Sample level info
summarize_populations(trajectory.data.filtered, morph_mvt,
write=T, to.data, merged.data.folder, video.description.folder,
video.description.file, total_frames)

# create overlays for validation
create_overlays(trajectory.data.filtered, to.data,
merged.data.folder, raw.video.folder, temp.overlay.folder,
overlay.folder, 2048, 2048, difference.lag, type = "label",

```

```
predict_spec = F, IJ.path, contrast.enhancement = 1,  
memory = memory.alloc)
```

S.1.4 Model priors for fitting Bayesian evolution models

Models were always fit with intercept estimates that corresponded to the genotype mean, but with a broad enough standard deviation so the model was not constrained too much. We ran all models with a long chain length (warmup = 40,000 iterations, chain = 160,000 iterations).

S.1.4.1 Models for r_0

Models were fit with the following priors:

- Intercepts were fit following a normal distribution with a genotype specific mean and standard deviation 0.5: $\text{int} \sim \text{normal}(\mu_{\text{genotype}}, 0.5)$
- All other fixed effects were modelled using a normal distribution with mean 0 and standard deviation 1: $\text{effect} \sim \text{normal}(0, 1)$
- Model standard deviation was fit using a cauchy distribution: $\text{sigma} \sim \text{cauchy}(0, 1)$

S.1.4.2 Models for K

Models were fit with the following priors:

- Intercepts were fit following a normal distribution with a genotype specific mean and standard deviation 0.5: $\text{int} \sim \text{normal}(\mu_{\text{genotype}}, 0.5)$
- All other fixed effects were modelled using a normal distribution with mean 0 and standard deviation 1: $\text{effect} \sim \text{normal}(0, 1)$
- Model standard deviation was fit using a cauchy distribution: $\text{sigma} \sim \text{cauchy}(0, 1)$

S.1.4.3 Models for α

Models were fit with the following priors:

- Intercepts were fit following a normal distribution with a genotype specific mean and standard deviation 0.5: $\text{int} \sim \text{normal}(\mu_{\text{genotype}}, 0.5)$
- All other fixed effects were modelled using a normal distribution with mean 0 and standard deviation 1: $\text{effect} \sim \text{normal}(0, 1)$
- Model standard deviation was fit using a cauchy distribution: $\text{sigma} \sim \text{cauchy}(0, 1)$

S.1.5 Correlation r_0 - α

S.1.5.1 Model code

```
#Stan code
{
model <- "
  // Pearson Correlation
  data {
    int<lower=1> n;
    vector[2] x_obs[n];
    vector[2] x_sd[n];
  }
  parameters {
    vector[2] mu;
    vector<lower=0>[2] lambda;
    real<lower=-1,upper=1> r;
    vector[2] x_est[n];

  }
  transformed parameters {
    vector<lower=0>[2] sigma;
    cov_matrix[2] T;

    // Reparameterization
    sigma[1] = sqrt(lambda[1]);
    sigma[2] = sqrt(lambda[2]);
    T[1,1] = square(sigma[1]);
    T[1,2] = r * sigma[1] * sigma[2];
    T[2,1] = r * sigma[1] * sigma[2];
    T[2,2] = square(sigma[2]);
  }
  model {
    // Priors
    mu ~ normal(0, 10);
    lambda ~ normal(0,1);
    r ~ normal(0,1);

    // Data
    x_est ~ multi_normal(mu, T);
```

```

for (i in 1:n){
x_obs[i][1] ~ normal(x_est[i][1], x_sd[i][1]);
x_obs[i][2] ~ normal(x_est[i][2], x_sd[i][2]);
}

}"
}

```

S.1.5.2 Correlation test for individual groups

Origin	R^2 (low pH of assay medium)	R^2 (neutral pH of assay medium)
ANC	0.97	0.33
LpH	0.49	0.42
NpH	0.97	0.45

Table S1.2: Correlation (median R^2) between intrinsic rate of increase r_0 and competitive ability α for the ANC, LpH and NpH populations, measured either at low pH of the assay medium or neutral pH of the assay medium. Numbers rounded to 2 decimal digits.

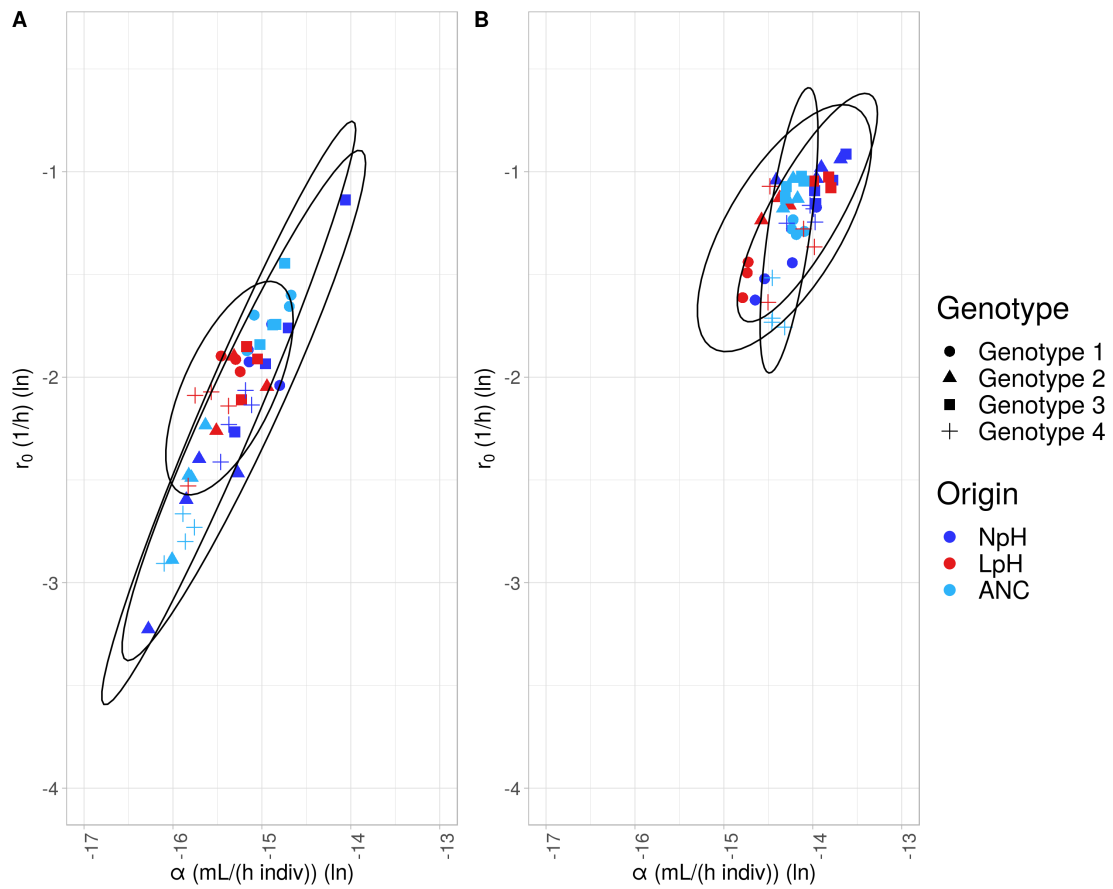


Figure S1.3: Correlation between the intrinsic rate of increase (r_0) and competitive ability (α) at low pH (A), and at neutral pH (B) of the assay medium, separate for the ANC, LpH and NpH populations. Symbols represent the different genotypes (see legend); Light blue = ANC (ancestor populations), dark blue = NpH (populations evolved under neutral pH conditions), red = LpH (populations evolved under low pH conditions). Ellipses represents 95% probability intervals.

S.1.6 Density regulation functions

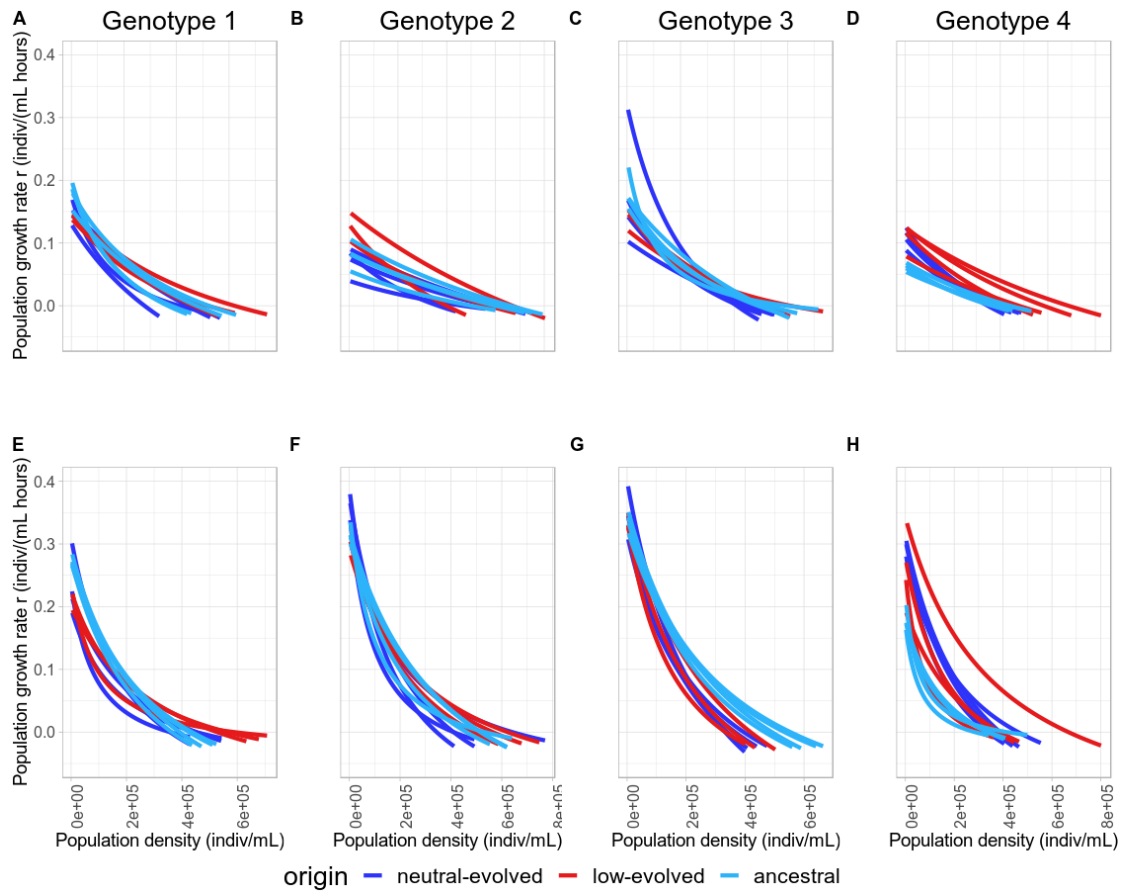


Figure S1.4: Density-regulation functions of the four genotypes. The y-axis depicts the population growth rate (r), x-axis shows the density of the population. Red lines = LpH populations, dark blue lines = NpH populations (populations evolved under low pH conditions), light blue = ANC populations (ancestral populations). Top row is the density-regulation for low pH of the assay medium Bottom row for neutral pH of the assay medium

S.1.7 Model construction tables

	pHmedium	Evolved	LpH	NpH	Evolved*pHmedium	LpH*pHmedium	NpH*pHmedium
Model 1							
Model 2	X						
Model 3		X					
Model 4			X				
Model 5				X			
Model 6			X	X			
Model 7	X	X					
Model 8	X	X				X	
Model 9	X		X				
Model 10	X		X			X	
Model 11	X			X			
Model 12	X			X			X
Model 13	X		X	X			
Model 14	X		X	X		X	
Model 15	X		X	X			X
Model 16	X		X	X		X	X

Table S1.3: The different statistical models included for the model averaging of r_0 , K and α . Rows are the different models and columns the different factors. pHmedium = plastic effect of assay medium pH, evolved = general evolutionary shifts. LpH = evolution effect in population evolving at low pH, NpH = evolution effect in populations evolving at neutral pH. interaction effects show pH specific evolution effects for the evolution factors.

	Evolved	LpH	NpH	Strain effects
Model 1				
Model 2	X			
Model 3		X		
Model 4			X	
Model 5		X	X	
Model 6				X
Model 7	X			X
Model 8		X		X
Model 9			X	X
Model 10		X	X	X

Table S1.4: Parameters included in the different models for analyzing group differences in variation in life-history traits. Evolved = general difference between ANC and evolved populations. LpH = specific differences for populations evolved at low pH. NpH = specific differences for populations evolved at neutral pH. Genotypes effects = inclusion of random genotype intercepts.

	Centered r_0	Origin	Origin* Centered r_0
Model 1			
Model 2	X		
Model 3		X	
Model 4	X	X	
Model 5	X	X	X

Table S1.5: Parameters included in the different models for analyzing density-dependent fitness estimates. Included explanatory variables are a) Centered r_0 : numerical variable associated with effect of the centered intrinsic rate of increase r_0), b) Origin: Categorical variable, with factors LpH (1) or Ancestral (0), c) Origin*Centered r_0 : Numerical variable, interaction term between Centered r_0 and Origin

S.1.8 Relative importance tables

		Genotype 1		Genotype 2		Genotype 3		Genotype 4	
		RI	Effect	RI	Effect	RI	Effect	RI	Effect
r_0	pHmedium	1	+	1	+	1	+	1	+
	evolved	0.51	-	0.02	+	0.34	-	0.56	+
	LpH	0.37	-	0.92	+	0.38	-	0.43	+
	NpH	0.42	-	0.4	-	0.35	-	0.43	+
	evolved*								
	pHmedium	0.06	+	0.01	-	0.16	+	0.22	-
	NpH*								
	pHmedium	0.14	+	0.16	+	0.15	+	0.13	+/-
	LpH*								
	pHmedium	0.1	-	0.74	-	0.14	+	0.19	-
K	pHmedium	0.9	-	0.56	-	0.94	-	0.96	-
	evolved	0.01	+	0.12	-	0.45	-	0.11	+
	LpH	0.89	+	0.35	+	0.4	-	0.75	+
	NpH	0.49	-	0.42	-	0.55	-	0.38	+/-
	evolved*								
	pHmedium	0	/	0.02	+	0.21	-	0.03	+
	NpH*								
	pHmedium	0.17	+	0.07	-	0.53	-	0.15	+
	LpH*								
	pHmedium	0.12	+	0.06	+	0.21	-	0.26	-
α	pHmedium	1	+	1	+	1	+	1	+
	evolved	0.03	-	0.16	+	0.28	-	0.16	+
	LpH	0.93	-	0.52	+	0.35	-	0.34	+/-
	NpH	0.34	+/-	0.39	+/-	0.31	+	0.69	+
	evolved*								
	pHmedium	0.01	-	0.05	+	0.23	+	0.05	-
	NpH*								
	pHmedium	0.11	-	0.17	+	0.13	+	0.26	-
	LpH*								
	pHmedium	0.27	-	0.36	-	0.18	+	0.1	+

Table S1.6: Relative importance (RI) of explanatory variables for r_0 , K and α for the 4 different genotypes. pHmedium = plastic effect of assay medium pH, evolved = general evolutionary shifts (difference between ANC and evolved populations). LpH = evolution effect in population evolving at low pH, NpH = evolution effect in populations evolving at neutral pH. Interaction effects show pH specific evolution effects for the evolutionary origin (LpH or NpH). RI gives the relative importance of the factors, effect shows the direction of the effect (+ = positive, - = negative, +/- = different depending on model).

		r_0		K		α	
		RI	Effect	RI	Effect	RI	Effect
Low assay medium pH	Evolved	0.05	-	0.26	0	0.18	-
	LpH	0.92	-	0.29	0	0.77	-
	NpH	0.25	-	0.25	0	0.18	-
Neutral assay medium pH	Evolved	0.71	0	0.04	0	0.15	+
	LpH	0.29	0	0.7	+	0.86	+
	NpH	0.29	0	0.46	-	0.85	+

Table S1.7: Relative importance (RI) of evolutionary origin on trait convergence. RI gives relative importance associated with evolutionary history (evolved = general evolutionary response, LpH = evolution effect in populations evolving at low pH, NpH = evolution effect in populations evolving at neutral pH). The “Effect” column shows the direction (sign) of change.

	RI	Effect
Centered r_0	1	+
Origin	1	+
Origin*Centered r_0	0.6	+

Table S1.8: Relative importance (RI) for density-dependent fitness models. RI gives relative importance associated with a) Centered r_0 : numerical variable associated with effect of the centered intrinsic rate of increase r_0 , b) Origin: Categorical variable, with factors LpH (1) or Ancestral (0), c) Origin*Centered r_0 : Numerical variable, interaction term between Centered r_0 and Origin. The “Effect” column shows the direction (sign) of change.

S.1.9 Density-dependent fitness of the NpH populations

We repeated the analysis for density-dependent fitness for the NpH populations. We calculated the population growth rate (r) for the NpH and for ANC populations over all observed population densities during the evolution experiment and integrated over these values to calculate a weighted density-dependent fitness estimate. We then used Bayesian models to fit these density-dependent fitness values as a function of a) population origin (ANC = 0 or NpH = 1), b) centered intrinsic rate of increase (r_0), and c) an interaction term between r_0 and population origin. Centered r_0 represents the intrinsic rate of increase, rescaled to have its mean at zero, and was calculated by subtracting the mean r_0 from all r_0 values. In this analysis, we also included a random intercept for the different genotypes. We fit all five models, starting from the intercept model to the full

interaction model. Subsequently, we ranked these models using the WAIC criterion.

Only the full interaction model was considered. Below, in Tab. S1.9 are listed the summary statistics of the model (mean estimates, standard deviation and 95 %-confidence intervals). Note how the density-dependent fitness of NpH populations does on average not differ (0 is included in the 95 %-confidence interval; Tab. S1.9) and even has the tendency to be slightly lower than the ANC populations. Note also how the relation between density-dependent fitness and centered r_0 changes from positive in ANC to negative in NpH (Fig. S1.5).

Variable	Mean estimate	Standard deviation	95 %-confidence interval
Intercept	2.43	0.92	(0.56, 4.18)
Genotype 1 (random intercept)	-1.34	0.97	(-3.25, 0.56)
Genotype 2 (random intercept)	-0.08	0.97	(-1.98, 1.84)
Genotype 3 (random intercept)	-1.10	0.97	(-3.02, 0.79)
Genotype 4 (random intercept)	2.63	0.99	(0.70, 4.55)
Centered r_0	19.90	4.98	(10.08, 29.50)
Origin	-0.72	0.40	(-1.50, 0.07)
centered r_0 * origin	-31.80	5.45	(-42.22, -20.86)

Table S1.9: Mean estimate, standard deviation and 95 %-confidence intervals for the fixed and random factors included in the best (and single considered model) from WAIC comparison. All numbers are rounded to 2 decimal digits.

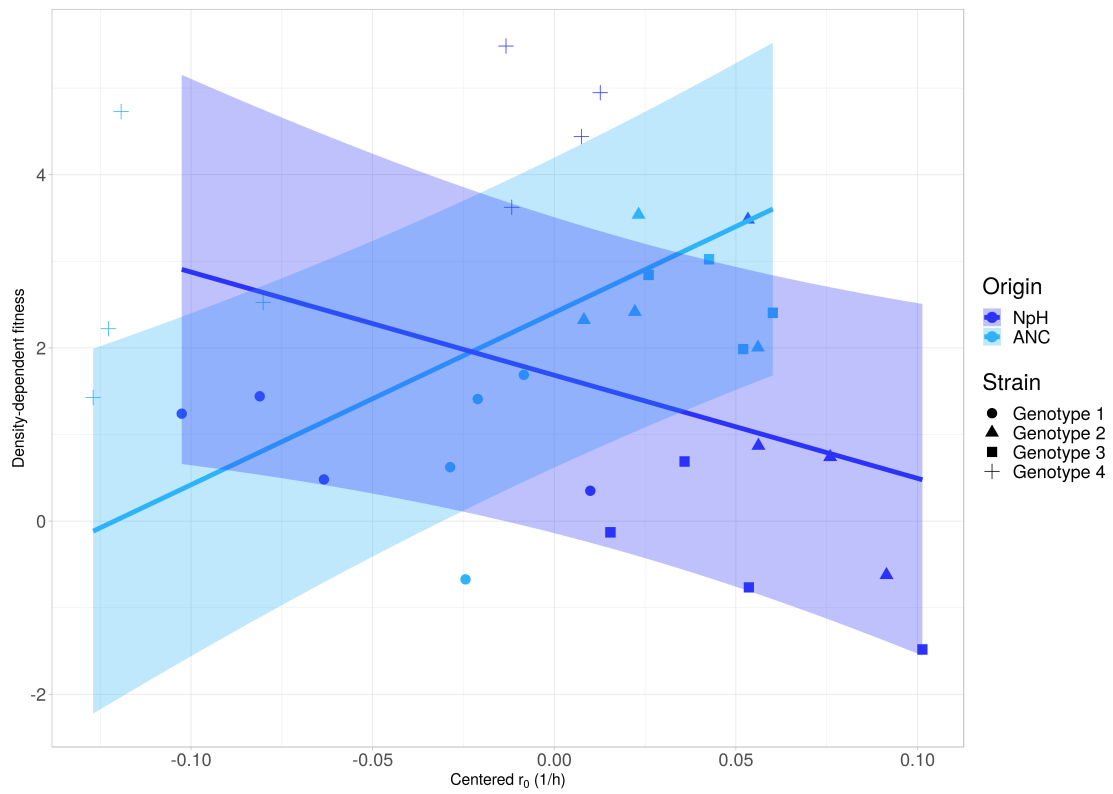


Figure S1.5: Density-dependent fitness depending on the (centered) intrinsic rate of increase (r_0). Symbols correspond to data from NpH (dark blue) or ANC (light blue) populations (shape represents genotype, see legend). Lines and shaded areas represent the weighted posterior predictions and the 95% probability intervals for the four genotypes.

S.1.10 Population growth assessment: raw data and posterior predictions

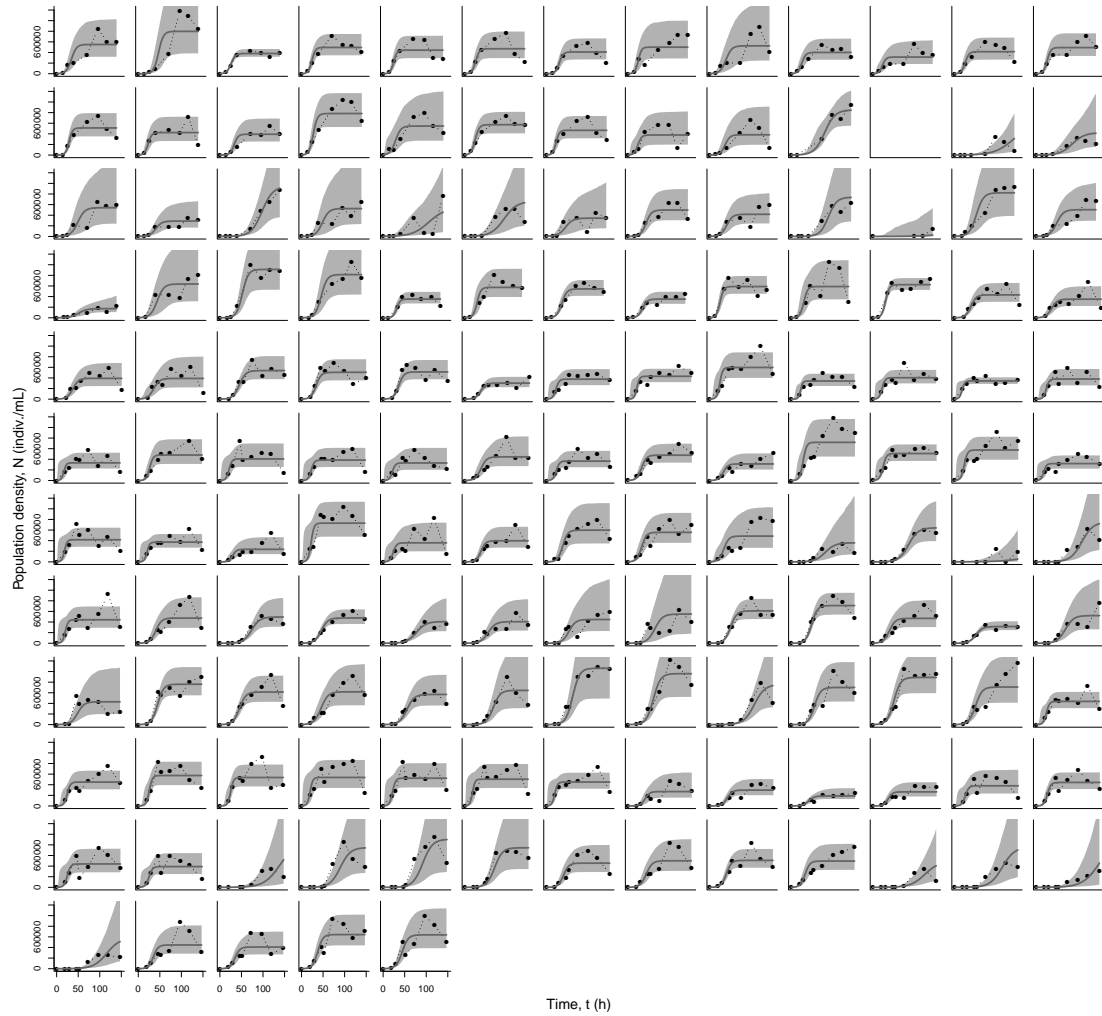


Figure S1.6: Individual subplots show the population density measurements and model predictions for a single population during the population growth assessments. Points are measured population densities. Lines show the mean model predictions, and shaded areas the 95 % confidence intervals of the posterior predictions.

Replicate	$\log(r_0)$		$\log(K)$		$\log(d)$		$\log(\alpha)$	
	mean	sd	mean	sd	mean	sd	mean	sd
Sample 0001	-1.033	0.276	12.925	0.123	-2.480	0.765	-13.958	0.291

Sample 0002	-0.979	0.318	12.925	0.195	-1.623	1.110	-13.904	0.393
Sample 0003	-1.041	0.239	13.372	0.144	-2.321	0.876	-14.413	0.270
Sample 0004	-0.939	0.267	12.748	0.215	-1.660	1.107	-13.687	0.363
Sample 0005	-1.092	0.291	12.888	0.157	-1.617	1.069	-13.980	0.336
Sample 0006	-0.914	0.301	12.714	0.120	-1.164	0.979	-13.628	0.338
Sample 0007	-1.155	0.277	12.811	0.214	-1.537	1.097	-13.966	0.367
Sample 0008	-1.041	0.346	12.735	0.200	-1.424	1.069	-13.776	0.423
Sample 0009	-1.251	0.235	13.043	0.196	-1.911	1.037	-14.293	0.313
Sample 0010	-1.164	0.340	12.867	0.243	-1.479	1.120	-14.031	0.445
Sample 0011	-1.181	0.336	12.810	0.245	-1.565	1.129	-13.991	0.441
Sample 0012	-1.245	0.393	12.729	0.276	-1.799	1.159	-13.974	0.523
Sample 0013	-1.624	0.254	13.024	0.225	-2.576	1.083	-14.648	0.333
Sample 0014	-1.173	0.329	12.787	0.217	-1.766	1.104	-13.959	0.421
Sample 0015	-1.521	0.267	13.021	0.193	-2.096	1.103	-14.542	0.330
Sample 0016	-1.443	0.279	12.787	0.226	-2.878	1.052	-14.230	0.327
Sample 0017	-1.234	0.301	13.342	0.239	-1.999	1.152	-14.577	0.397
Sample 0018	-1.163	0.289	13.100	0.152	-1.797	1.008	-14.263	0.332
Sample 0019	-1.127	0.298	13.244	0.169	-1.898	1.092	-14.371	0.337
Sample 0020	-1.078	0.363	12.718	0.201	-1.812	1.118	-13.797	0.436
Sample 0021	-1.046	0.310	12.945	0.174	-1.286	1.043	-13.991	0.379
Sample 0022	-1.025	0.317	12.797	0.192	-1.486	1.074	-13.822	0.394
Sample 0023	-1.366	0.291	12.617	0.286	-2.782	1.176	-13.983	0.397
Sample 0024	-1.071	0.298	13.411	0.192	-1.678	1.005	-14.482	0.376
Sample 0025	-1.278	0.354	12.825	0.258	-1.967	1.182	-14.104	0.457
Sample 0026	-1.636	0.196	12.868	0.237	-1.904	1.183	-14.504	0.321
Sample 0027	-1.613	0.250	13.176	0.241	-1.968	1.173	-14.789	0.363
Sample 0028	-1.492	0.249	13.245	0.183	-2.404	1.037	-14.737	0.295
Sample 0029	-1.440	0.304	13.287	0.272	-3.282	1.009	-14.727	0.377
Sample 0030	-2.466	0.210	12.806	0.383	-2.138	1.392	-15.272	0.473
Sample 0031	-2.397	0.090	13.309	0.224	-1.304	1.170	-15.706	0.257
Sample 0032	-3.225	0.453	13.051	0.502	-2.579	1.665	-16.277	0.742
Sample 0033	-2.595	0.168	13.255	0.381	-1.835	1.259	-15.850	0.432
Sample 0034	-1.138	0.360	12.923	0.258	-1.574	1.137	-14.061	0.471
Sample 0035	-1.760	0.251	12.945	0.267	-2.018	1.202	-14.705	0.388
Sample 0036	-2.267	0.101	13.037	0.228	-1.251	1.164	-15.304	0.260
Sample 0037	-1.935	0.116	13.025	0.149	-1.790	1.005	-14.960	0.194
Sample 0038	-2.413	0.120	13.051	0.266	-1.734	1.264	-15.464	0.307
Sample 0039	-2.135	0.145	12.980	0.248	-1.622	1.244	-15.116	0.304
Sample 0040	-2.064	0.182	13.120	0.298	-2.019	1.260	-15.184	0.369
Sample 0041	-2.230	0.259	13.141	0.385	-2.006	1.333	-15.372	0.489

Sample 0042	-1.926	0.110	13.219	0.167	-1.195	1.053	-15.144	0.211
Sample 0043	-1.866	0.137	13.287	0.214	-1.153	1.111	-15.153	0.270
Sample 0044	-1.742	0.194	13.148	0.188	-2.686	0.956	-14.890	0.255
Sample 0045	-2.040	0.082	12.760	0.138	-1.254	1.118	-14.800	0.164
Sample 0046	-2.260	0.145	13.251	0.284	-1.831	1.237	-15.512	0.331
Sample 0047	-2.046	0.229	12.897	0.327	-1.579	1.285	-14.943	0.414
Sample 0048	-1.899	0.128	13.414	0.188	-1.032	1.108	-15.313	0.239
Sample 0049	-1.911	0.182	13.138	0.228	-1.445	1.140	-15.049	0.312
Sample 0050	-1.851	0.198	13.322	0.210	-2.562	1.037	-15.173	0.292
Sample 0051	-2.110	0.143	13.121	0.236	-1.309	1.172	-15.231	0.292
Sample 0052	-2.140	0.151	13.235	0.293	-1.503	1.189	-15.375	0.336
Sample 0053	-2.089	0.153	13.663	0.296	-1.401	1.157	-15.751	0.344
Sample 0054	-2.072	0.154	13.498	0.270	-1.428	1.156	-15.570	0.325
Sample 0055	-2.529	0.117	13.300	0.319	-1.484	1.200	-15.829	0.350
Sample 0056	-1.973	0.142	13.271	0.252	-1.426	1.151	-15.244	0.302
Sample 0057	-1.897	0.144	13.561	0.181	-1.877	1.034	-15.458	0.246
Sample 0058	-1.913	0.174	13.381	0.231	-2.170	1.137	-15.295	0.300
Sample 0059	-1.131	0.213	13.041	0.132	-1.799	0.976	-14.172	0.249
Sample 0060	-1.034	0.275	13.187	0.161	-2.696	0.948	-14.221	0.277
Sample 0061	-1.178	0.255	13.156	0.194	-1.470	1.057	-14.335	0.339
Sample 0062	-1.134	0.214	13.155	0.175	-1.438	1.084	-14.289	0.283
Sample 0063	-1.072	0.300	13.224	0.184	-1.608	1.076	-14.297	0.366
Sample 0064	-1.122	0.282	13.188	0.163	-1.569	1.019	-14.310	0.339
Sample 0065	-1.022	0.341	13.105	0.191	-1.433	1.039	-14.127	0.415
Sample 0066	-1.045	0.283	13.054	0.133	-1.531	1.027	-14.099	0.319
Sample 0067	-1.713	0.217	12.741	0.325	-2.555	1.282	-14.454	0.404
Sample 0068	-1.733	0.149	12.728	0.212	-2.289	1.143	-14.460	0.258
Sample 0069	-1.757	0.156	12.560	0.274	-3.296	0.947	-14.316	0.279
Sample 0070	-1.517	0.158	12.939	0.256	-3.497	0.861	-14.456	0.263
Sample 0071	-1.290	0.309	12.804	0.244	-1.599	1.134	-14.095	0.424
Sample 0072	-1.278	0.235	12.962	0.180	-1.654	1.090	-14.240	0.305
Sample 0073	-1.234	0.293	12.988	0.216	-1.755	1.166	-14.221	0.377
Sample 0074	-1.306	0.269	12.880	0.199	-1.436	1.121	-14.185	0.352
Sample 0075	-2.888	0.234	13.123	0.460	-2.134	1.394	-16.010	0.543
Sample 0076	-2.489	0.173	13.303	0.363	-1.628	1.241	-15.792	0.412
Sample 0077	-2.477	0.186	13.346	0.378	-1.665	1.251	-15.822	0.430
Sample 0078	-2.234	0.148	13.401	0.300	-1.463	1.202	-15.635	0.346
Sample 0079	-1.743	0.161	13.100	0.199	-1.944	1.076	-14.843	0.270
Sample 0080	-1.841	0.171	13.180	0.208	-2.161	1.063	-15.022	0.276
Sample 0081	-1.746	0.111	13.133	0.147	-1.339	1.042	-14.879	0.193

Sample 0082	-1.445	0.186	13.298	0.174	-3.207	0.713	-14.743	0.223
Sample 0083	-2.800	0.172	13.061	0.414	-2.102	1.343	-15.861	0.480
Sample 0084	-2.665	0.187	13.223	0.414	-1.935	1.346	-15.888	0.471
Sample 0085	-2.906	0.248	13.193	0.470	-2.134	1.396	-16.099	0.556
Sample 0086	-2.731	0.196	13.029	0.426	-2.121	1.401	-15.759	0.498
Sample 0087	-1.601	0.200	13.072	0.214	-2.286	1.097	-14.672	0.285
Sample 0088	-1.656	0.168	13.036	0.188	-2.107	1.066	-14.691	0.253
Sample 0089	-1.698	0.139	13.389	0.165	-1.930	1.002	-15.087	0.222
Sample 0090	-1.871	0.163	13.297	0.218	-1.584	1.148	-15.168	0.288

Table S1.10: Summarized posteriors from the Beverton-Holt model fitting, showing means and standard deviations for the log-transformed parameters r_0 , K , d and α . Note the large standard deviations for the death rate (d) estimates.

Chapter S.2

Supplementary Material of Chapter 2

Supporting Information for
Evolution in interacting species alters predator life history traits, behavior and
morphology in experimental microbial communities

Johannes Cairns, Felix Moerman, Emanuel A. Fronhofer, Florian Altermatt, Teppo Hiltunen

Correspondence to: florian.altermatt@eawag.ch / teppo.hiltunen@helsinki.fi

This PDF file includes:

Supplementary methods:

R-code used in video analysis step for protist density measurements

Tables S1 to S14

Figures S1 to S14

Supplementary methods

R-code (including used parameter values) used in video analysis step for protist density measurements

```
#####  
# R script for analysing video files with BEMOVI (www.bemovi.info)  
#  
# Emanuel A. Fronhofer  
#  
# October 2016  
#####  
rm(list=ls())  
  
# load package  
#library(devtools)  
#install_github("efronhofer/bemovi", ref="experimental")  
library(bemovi)  
  
#####  
# VIDEO PARAMETERS  
  
# video frame rate (in frames per second)  
fps <- 25  
# length of video (in frames)  
total_frames <- 500  
  
# measured volume (in microliter)  
measured_volume <- 34.4 # for Leica M205 C with 1.6 fold magnification, sample height 0.5 mm and Hamamatsu  
Orca Flash 4  
  
# size of a pixel (in micrometer)  
pixel_to_scale <- 4.05 # for Leica M205 C with 1.6 fold magnification, sample height 0.5 mm and Hamamatsu  
Orca Flash 4
```

```

# setup
difference.lag <- 10
thresholds <- c(10,255) # don't change the second value

#####
# FILTERING PARAMETERS
#(optimized for Leica M205 C with 1.6 fold magnification, sample height 0.5 mm and Hamamatsu Orca Flash 4)
# tested species: Tet, Col, Pau, Eug, Chi, Ble, Ceph, Lox, Spi

# min and max size: area in pixels
particle_min_size <- 5
particle_max_size <- 1000

# number of adjacent frames to be considered for linking particles
trajectory_link_range <- 3
# maximum distance a particle can move between two frames
trajectory_displacement <- 16

# these values are in the units defined by the parameters above: fps (seconds), measured_volume (microliters) and
pixel_to_scale (micrometers)
filter_min_net_disp <- 25
filter_min_duration <- 1
filter_detection_freq <- 0.1
filter_median_step_length <- 3
#####
# MORE PARAMETERS (USUALLY NOT CHANGED)

# UNIX
# set paths to ImageJ and particle linker standalone
IJ.path <- "/home/felix/bin/ImageJ"
to.particlelinker <- "/home/felix/bin/ParticleLinker"

# directories and file names
to.data <- paste(getwd(),"/",sep="")

```

```

video.description.folder <- "0_video_description/"
video.description.file <- "video_description.txt"
raw.video.folder <- "1_raw/"
particle.data.folder <- "2_particle_data/"
trajectory.data.folder <- "3_trajectory_data/"
temp.overlay.folder <- "4a_temp_overlays/"
overlay.folder <- "4_overlays/"
merged.data.folder <- "5_merged_data/"
ijmacs.folder <- "ijmacs/"

# RAM allocation
memory.alloc <- c(60000) # hp machine

# RAM per particle linker instance
memory.alloc.perLinker <- c(10000)
#####

#####

# VIDEO ANALYSIS

# identify particles
locate_and_measure_particles(to.data, raw.video.folder, particle.data.folder, difference.lag, thresholds, min_size
= particle_min_size, max_size = particle_max_size, IJ.path, memory.alloc)

# link the particles
link_particles(to.data, particle.data.folder, trajectory.data.folder, linkrange = trajectory_link_range, disp =
trajectory_displacement, start_vid = 1, memory = memory.alloc, memory_per_linkerProcess =
memory.alloc.perLinker)

# merge info from description file and data
merge_data(to.data, particle.data.folder, trajectory.data.folder, video.description.folder, video.description.file,
merged.data.folder)

# load the merged data

```

```

load(paste0(to.data, merged.data.folder, "Master.RData"))

# filter data: minimum net displacement, their duration, the detection frequency and the median step length
trajectory.data.filtered <- filter_data(trajectory.data, filter_min_net_disp, filter_min_duration,
filter_detection_freq, filter_median_step_length)

# summarize trajectory data to individual-based data
morph_mvt <- summarize_trajectories(trajectory.data.filtered, calculate.median=F, write = T, to.data,
merged.data.folder)

# get sample level info
summarize_populations(trajectory.data.filtered, morph_mvt, write=T, to.data, merged.data.folder,
video.description.folder, video.description.file, total_frames)

# create overlays for validation
create_overlays(trajectory.data.filtered, to.data, merged.data.folder, raw.video.folder, temp.overlay.folder,
overlay.folder, 2048, 2048, difference.lag, type = "label", predict_spec = F, IJ.path, contrast.enhancement = 1,
memory = memory.alloc)

```

Table S1. ANOVA table (Type III test) for linear model on log-transformed intrinsic growth rate (r_0) of ciliate.

Model terms	<i>d.f.</i>	<i>SS</i>	<i>F</i>	<i>p</i>
Prey evolution	1	0.93	15.32	< 0.001
Predator evolution	1	0.14	2.30	0.134
Prey species	6	6.41	17.51	< 0.001
Prey evolution × predator evolution	1	0.19	3.10	0.082
Prey evolution × prey species	6	3.31	9.03	< 0.001
Residuals	78	4.7589		

Table S2. ANOVA table (Type III test) for linear model on log-transformed competitive ability (α) of ciliate.

Model terms	<i>d.f.</i>	<i>SS</i>	<i>F</i>	<i>p</i>
Prey evolution	1	0.5	4.7927	0.031
Prey species	6	9.3	14.4450	< 0.001
Prey evolution × prey species	6	3.5	5.3986	< 0.001
Residuals	80	8.6		

Table S3. ANOVA table (Type III test) for linear model on log-transformed equilibrium density (K) of ciliate.

Model terms	<i>d.f.</i>	<i>SS</i>	<i>F</i>	<i>p</i>
Prey evolution	1	0.1	2.43	0.123
Prey species	6	1.6	11.2	< 0.001
Prey evolution × prey species	6	1.9	13.7	< 0.001
Residuals	80	1.9		

Table S4. ANOVA table (Type III test) for linear model on cell size of ciliate.

Model terms	<i>d.f.</i>	<i>SS</i>	<i>F</i>	<i>p</i>
Prey evolution	1	483	4.58	0.033
Predator evolution	1	830	7.87	0.005
Log prey population size	1	24	0.23	0.633
Log predator population size	1	722	6.85	0.009
Log prey population size × predator evolution	1	725	6.87	0.009
Log predator population size × predator evolution	1	266	2.52	0.113
Log predator population size × log prey population size	1	725	5.24	0.022
Residuals	767	80886		

Table S5. ANOVA table (Type III test) for linear model on gross speed of ciliate.

Model terms	<i>df.</i>	<i>SS</i>	<i>F</i>	<i>p</i>
Prey evolution	1	14526	2.17	0.141
Predator evolution	1	9314	1.90	0.239
Prey species	6	366264	9.11	< 0.001
Log predator population size	1	778688	116.20	< 0.001
Log predator population size × prey evolution	1	36601	5.46	0.020
Log predator population size × predator evolution	1	29248	4.36	0.037
Residuals	763	5113281		

Table S6. ANOVA table (Type III test) for linear model on cell turning angle distribution of ciliate.

Model terms	<i>df.</i>	<i>SS</i>	<i>F</i>	<i>p</i>
Predator evolution	1	0.27	10.15	0.001
Prey evolution	1	0.08	3.10	0.079
Prey species	6	1.98	12.40	< 0.001
Log prey population size	1	0.27	10.26	0.001
Log predator population size	1	0.90	33.90	< 0.001
Log predator population size × predator evolution	1	0.14	5.44	0.02
Log predator population size × prey species	1	1.08	6.76	< 0.001
Log prey population size × prey evolution	1	0.07	2.76	0.097
Residuals	756	20.09		

Table S7. Summary table for linear model on log-transformed intrinsic growth rate (r_0) of ciliate.

<i>Model terms</i>	<i>Estimate</i>	<i>SE</i>	<i>t-value</i>	<i>Pr(> t)</i>	<i>Significance</i>
Intercept (<i>B. diminuta</i>)	-2.111	0.107	-19.707	<0.001	***
Prey evolution (evolved)	-0.026	0.151	-0.172	0.864	
Predator evolution (evolved)	-0.013	0.072	-0.174	0.862	
Prey species (<i>C. testosteroni</i>)	-0.210	0.124	-1.697	0.094	.
Prey species (<i>E. coli</i>)	-0.314	0.143	-2.201	0.031	*
Prey species (<i>J. lividum</i>)	-0.421	0.143	-2.949	0.004	**
Prey species (<i>P. fluorescens</i>)	-0.092	0.143	-0.642	0.523	
Prey species (<i>S. capsulata</i>)	0.023	0.143	0.160	0.873	
Prey species (<i>S. marcescens</i>)	-0.980	0.150	-6.542	<0.001	***
Prey evolution (evolved) * Predator evolution (evolved)	0.180	0.102	1.762	0.082	.
Prey evolution (evolved) * Prey species (<i>C. testosteroni</i>)	-0.718	0.175	-4.112	<0.001	***
Prey evolution (evolved) * Prey species (<i>E. coli</i>)	-0.212	0.202	-1.052	0.296	
Prey evolution (evolved) * Prey species (<i>J. lividum</i>)	-0.066	0.207	-0.321	0.749	
Prey evolution (evolved) * Prey species (<i>P. fluorescens</i>)	-0.075	0.202	-0.370	0.713	
Prey evolution (evolved) * Prey species (<i>S. capsulata</i>)	-0.938	0.202	-4.649	<0.001	***
Prey evolution (evolved) * Prey species (<i>S. marcescens</i>)	0.116	0.207	0.562	0.576	

Table S8. Summary table for linear model on log-transformed competitive ability (α) of ciliate.

<i>Model terms</i>	<i>Estimate</i>	<i>SE</i>	<i>t-value</i>	<i>Pr(> t)</i>	<i>Significance</i>
Intercept (<i>B. diminuta</i>)	-10.980	0.141	-78.121	<0.001	***
Prey evolution (evolved)	-0.204	0.199	-1.028	0.307	
Predator evolution (evolved)	-0.018	0.095	-0.195	0.846	
Prey species (<i>C. testosteroni</i>)	-0.416	0.162	-2.565	0.012	*
Prey species (<i>E. coli</i>)	-0.861	0.187	-4.602	<0.001	***
Prey species (<i>J. lividum</i>)	-0.655	0.187	-3.501	<0.001	***
Prey species (<i>P. fluorescens</i>)	-0.584	0.187	-3.123	0.003	**
Prey species (<i>S. capsulata</i>)	-0.412	0.187	-2.203	0.031	*
Prey species (<i>S. marcescens</i>)	-1.188	0.197	-6.044	0.000	***
Prey evolution (evolved) * Predator evolution (evolved)	0.201	0.134	1.502	0.137	
Prey evolution (evolved) * Prey species (<i>C. testosteroni</i>)	-0.779	0.229	-3.399	0.001	**
Prey evolution (evolved) * Prey species (<i>E. coli</i>)	0.078	0.265	0.293	0.770	
Prey evolution (evolved) * Prey species (<i>J. lividum</i>)	0.040	0.271	0.149	0.882	
Prey evolution (evolved) * Prey species (<i>P. fluorescens</i>)	0.274	0.265	1.034	0.304	
Prey evolution (evolved) * Prey species (<i>S. capsulata</i>)	-0.110	0.265	-0.416	0.678	
Prey evolution (evolved) * Prey species (<i>S. marcescens</i>)	0.132	0.271	0.485	0.629	

Table S9. Summary table for linear model on log-transformed equilibrium density (*K*) of ciliate.

<i>Model terms</i>	<i>Estimate</i>	<i>SE</i>	<i>t-value</i>	<i>Pr(> t)</i>	<i>Significance</i>
Intercept (<i>B. diminuta</i>)	8.873	0.062	142.519	<0.001	***
Prey evolution (evolved)	0.168	0.088	1.904	0.060	.
Prey species (<i>C. testosteroni</i>)	0.206	0.076	2.703	0.008	**
Prey species (<i>E. coli</i>)	0.547	0.088	6.218	<0.001	***
Prey species (<i>J. lividum</i>)	0.235	0.088	2.664	0.009	**
Prey species (<i>P. fluorescens</i>)	0.493	0.088	5.599	<0.001	***
Prey species (<i>S. capsulata</i>)	0.435	0.088	4.943	<0.001	***
Prey species (<i>S. marcescens</i>)	0.209	0.092	2.259	0.027	*
Prey evolution (evolved) * Prey species (<i>C. testosteroni</i>)	0.061	0.108	0.564	0.574	
Prey evolution (evolved) * Prey species (<i>E. coli</i>)	-0.290	0.125	-2.328	0.022	*
Prey evolution (evolved) * Prey species (<i>J. lividum</i>)	-0.108	0.128	-0.848	0.399	
Prey evolution (evolved) * Prey species (<i>P. fluorescens</i>)	-0.348	0.125	-2.797	0.006	**
Prey evolution (evolved) * Prey species (<i>S. capsulata</i>)	-0.828	0.125	-6.646	<0.001	***
Prey evolution (evolved) * Prey species (<i>S. marcescens</i>)	-0.016	0.128	-0.125	0.901	

Table S10. Summary table for linear model on cell size of ciliate.

<i>Model terms</i>	<i>Estimate</i>	<i>SE</i>	<i>t-value</i>	<i>Pr(> t)</i>	<i>Significance</i>
Intercept	11.142	20.710	0.538	0.591	
Log (Predator density)	-5.956	2.431	-2.450	0.015	*
Log (Prey density)	1.323	1.044	1.267	0.206	
Predator evolution (evolved)	39.120	13.945	2.805	0.005	**
Prey evolution (evolved)	-1.629	0.761	-2.140	0.033	*
Log (Prey density) * Log (Predator density)	0.287	0.125	2.289	0.022	*
Log (Prey density) * Predator evolution (evolved)	-1.800	0.687	-2.622	0.009	**
Log (Predator density) * Predator evolution (evolved)	-0.509	0.321	-1.588	0.113	

Table S11. Summary table for linear model on gross speed of ciliate.

<i>Model terms</i>	<i>Estimate</i>	<i>SE</i>	<i>t-value</i>	<i>Pr(> t)</i>	<i>Significance</i>
Intercept (<i>B. diminuta</i>)	341.529	15.332	22.276	<0.001	***
Log (Predator density)	-12.184	1.922	-6.340	<0.001	***
Prey species (<i>C. testosteroni</i>)	-13.444	9.735	-1.381	0.168	
Prey species (<i>E. coli</i>)	-14.996	11.327	-1.324	0.186	
Prey species (<i>J. lividum</i>)	-72.371	12.319	-5.875	<0.001	***
Prey species (<i>P. fluorescens</i>)	-29.134	11.603	-2.511	0.012	*
Prey species (<i>S. capsulata</i>)	-19.143	11.293	-1.695	0.091	.
Prey species (<i>S. marcescens</i>)	-61.507	12.695	-4.845	<0.001	***
Predator evolution (evolved)	-17.989	15.259	-1.179	0.239	
Prey evolution (evolved)	22.698	15.417	1.472	0.141	
Log (Predator density) * Predator evolution (evolved)	4.703	2.251	2.089	0.037	*
Log (Predator density) * Prey evolution (evolved)	-5.316	2.275	-2.337	0.020	*

Table S12. Summary table for linear model on cell turning angle distribution of ciliate.

<i>Model terms</i>	<i>Estimate</i>	<i>SE</i>	<i>t-value</i>	<i>Pr(> t)</i>	<i>Significance</i>
Intercept (<i>B. diminuta</i>)	-0.208	0.139	-1.499	0.134	
Prey species (<i>C. testosteroni</i>)	0.068	0.064	1.057	0.291	
Prey species (<i>E. coli</i>)	0.044	0.070	0.637	0.525	
Prey species (<i>J. lividum</i>)	0.379	0.068	5.599	<0.001	***
Prey species (<i>P. fluorescens</i>)	0.304	0.066	4.597	<0.001	***
Prey species (<i>S. capsulata</i>)	0.075	0.073	1.028	0.304	
Prey species (<i>S. marcescens</i>)	0.128	0.069	1.849	0.065	.
Log (Predator density)	-0.002	0.008	-0.236	0.813	
Log (Prey density)	-0.008	0.006	-1.188	0.235	
Predator evolution (evolved)	-0.100	0.031	-3.187	0.002	**
Prey evolution (evolved)	0.305	0.174	1.759	0.079	.
Log (Predator density) * Prey species (<i>C. testosteroni</i>)	-0.014	0.009	-1.611	0.108	
Log (Predator density) * Prey species (<i>E. coli</i>)	-0.005	0.010	-0.490	0.624	
Log (Predator density) * Prey species (<i>J. lividum</i>)	-0.041	0.010	-4.281	<0.001	***
Log (Predator density) * Prey species (<i>P. fluorescens</i>)	-0.036	0.009	-3.928	<0.001	***
Log (Predator density) * Prey species (<i>S. capsulata</i>)	-0.006	0.011	-0.601	0.548	
Log (Predator density) * Prey species (<i>S. marcescens</i>)	-0.023	0.011	-2.165	0.031	*
Log (Predator density) * Predator evolution (evolved)	0.011	0.005	2.333	0.020	*
Log (Prey density) * Prey evolution (evolved)	-0.015	0.009	-1.661	0.097	.

Table S13. Summary statistics for the Beverton-Holt model fitting. Rows represent growth curve fits for individual populations, showing mean and standard deviation for the posterior distribution of r_0 , α , K and d . For r_0 , α and d , quality statistics (effective sample size N_EFF and Rhat scores) are also shown. Note the absence of Rhat and N_eff values for α , since α is calculated from the other parameters. Large effective sample sizes and Rhat scores that are not too divergent from 1 are indicative for a healthy MCMC chain, and hence of good model convergence.

Name	$\log(r_0)$		$\log(r_0)$	$\log(r_0)$	$\log(K)$		$\log(K)$	$\log(K)$	$\log(K)$	$\log(\alpha)$		$\log(d)$		$\log(d)$	$\log(d)$
	mean	sd			mean	sd				mean	sd	mean	sd		
sample_00030	-2,566	0,205	7596	1,000	9,411	0,440	10086	1,000	-11,977	0,491	-2,100	0,936	9458	1,000	
sample_00031	-2,271	0,196	5751	1,000	9,444	0,403	8138	1,000	-11,716	0,456	-2,017	0,927	7158	1,000	
sample_00032	-2,476	0,188	4391	1,000	9,455	0,389	8546	1,000	-11,932	0,445	-2,023	0,938	8735	1,000	
sample_00033	-2,825	0,279	9101	1,001	9,073	0,481	12073	1,000	-11,898	0,577	-2,332	1,015	10082	1,000	
sample_00034	-2,483	0,217	4885	1,000	9,069	0,419	9973	1,000	-11,552	0,475	-2,167	0,974	9104	1,000	
sample_00035	-2,675	0,292	7540	1,000	9,100	0,468	11232	1,000	-11,775	0,578	-2,307	0,999	11251	1,000	
sample_00036	-1,509	0,196	3955	1,000	8,933	0,277	6211	1,000	-10,442	0,364	-1,836	0,878	6888	1,000	
sample_00037	-2,086	0,127	4082	1,001	9,158	0,220	5726	1,000	-11,245	0,266	-1,747	0,865	4913	1,000	
sample_00038	-2,080	0,149	4901	1,000	9,638	0,269	6809	1,000	-11,718	0,327	-1,766	0,839	5922	1,000	
sample_00039	-1,982	0,225	6460	1,000	8,840	0,356	8636	1,000	-10,822	0,450	-2,010	0,915	8449	1,000	
sample_00040	-2,092	0,244	5798	1,000	8,878	0,379	8892	1,000	-10,971	0,474	-2,026	0,912	7816	1,000	
sample_00041	-2,195	0,257	6000	1,000	8,828	0,388	7360	1,000	-11,023	0,489	-2,139	0,950	7739	1,000	
sample_00042	-1,673	0,239	3584	1,000	9,362	0,370	7318	1,000	-11,035	0,434	-1,910	0,871	6303	1,000	
sample_00043	-2,632	0,292	8438	1,000	9,274	0,466	10593	1,000	-11,907	0,569	-2,256	0,984	11079	1,000	
sample_00044	-2,399	0,203	7208	1,000	9,217	0,412	10505	1,000	-11,616	0,469	-2,083	0,940	10133	1,000	
sample_00045	-2,398	0,231	6805	1,000	9,297	0,368	9565	1,000	-11,695	0,460	-2,253	0,956	8551	1,000	
sample_00046	-2,296	0,198	5070	1,000	9,145	0,348	6422	1,000	-11,441	0,418	-2,062	0,929	6743	1,000	
sample_00047	-2,349	0,222	4770	1,001	9,204	0,355	7649	1,000	-11,553	0,442	-2,111	0,949	7689	1,000	
sample_00048	-2,264	0,222	5000	1,000	8,872	0,366	6340	1,000	-11,136	0,440	-2,028	0,961	7220	1,000	

sample_00049	-2,278	0,237	5734	1,000	8,891	0,358	7157	1,000	-11,169	0,447	-2,067	0,955	6838	1,000
sample_00050	-2,355	0,150	4181	1,000	9,380	0,280	6514	1,000	-11,735	0,337	-2,016	0,905	6814	1,000
sample_00051	NA	NA	NA	NA	NA	NA	NA	NA	NA	NA	NA	NA	NA	NA
sample_00052	-3,152	0,242	5611	1,000	9,313	0,483	9476	1,000	-12,465	0,564	-2,232	0,976	10639	1,000
sample_00053	-3,136	0,684	1885	1,000	9,003	0,529	4018	1,000	-12,139	0,970	-2,444	1,083	5256	1,000
sample_00054	-2,475	0,182	5627	1,000	9,420	0,382	8121	1,000	-11,896	0,431	-1,989	0,909	9882	1,000
sample_00055	-2,650	0,226	4337	1,000	9,345	0,393	8882	1,000	-11,995	0,481	-2,161	0,957	7340	1,000
sample_00056	-2,889	0,413	8531	1,000	9,200	0,495	12297	1,000	-12,089	0,651	-2,308	1,008	11962	1,000
sample_00057	-2,639	0,269	8348	1,000	9,220	0,455	12106	1,000	-11,859	0,543	-2,248	0,971	11052	1,000
sample_00058	NA	NA	NA	NA	NA	NA	NA	NA	NA	NA	NA	NA	NA	NA
sample_00059	-2,529	0,195	5614	1,001	9,470	0,450	5945	1,000	-11,999	0,494	-2,066	0,922	6375	1,000
sample_00060	-3,353	0,596	3432	1,000	8,891	0,575	6697	1,000	-12,244	0,973	-2,614	1,198	6851	1,000
sample_00061	-3,002	0,632	2524	1,001	8,612	0,609	3861	1,000	-11,614	1,063	-3,263	1,522	3075	1,001
sample_00062	-2,788	0,559	3602	1,000	8,446	0,600	3795	1,000	-11,234	0,969	-3,189	1,429	4934	1,000
sample_00063	-1,970	0,252	6403	1,000	9,040	0,367	8916	1,000	-11,010	0,465	-1,960	0,901	9479	1,000
sample_00064	-2,095	0,199	5027	1,000	9,111	0,272	7725	1,000	-11,205	0,358	-1,867	0,865	7731	1,000
sample_00065	-2,205	0,262	6197	1,000	8,888	0,363	7911	1,000	-11,093	0,468	-2,097	0,952	8552	1,000
sample_00066	-2,511	0,205	6804	1,000	9,135	0,431	9383	1,000	-11,646	0,485	-2,169	0,964	10682	1,000
sample_00067	-2,139	0,218	6529	1,000	9,127	0,378	9690	1,000	-11,266	0,447	-1,963	0,907	9782	1,000
sample_00068	-2,334	0,161	3430	1,001	9,027	0,381	8259	1,001	-11,361	0,429	-1,962	0,921	6484	1,000
sample_00069	-3,053	0,274	7379	1,000	9,298	0,481	11287	1,000	-12,351	0,568	-2,267	0,986	9991	1,000
sample_00070	-3,168	0,198	4374	1,000	9,308	0,459	8336	1,000	-12,476	0,522	-2,225	0,953	9085	1,000
sample_00071	-3,175	0,204	4892	1,000	9,407	0,456	8374	1,000	-12,581	0,524	-2,184	0,963	8918	1,000
sample_00072	-3,072	0,317	5796	1,000	9,246	0,498	9779	1,000	-12,319	0,631	-2,336	0,993	11166	1,000
sample_00073	-3,011	0,191	6272	1,000	9,337	0,437	10815	1,000	-12,348	0,495	-2,214	0,974	10006	1,000
sample_00074	-3,224	0,224	3461	1,000	9,355	0,438	6628	1,000	-12,579	0,538	-2,225	0,986	6706	1,000

sample_00075	-3,051	0,390	6521	1,000	9,176	0,506	10493	1,000	-12,227	0,659	-2,368	1,005	10026	1,000
sample_00076	-3,070	0,436	4765	1,000	9,196	0,504	9287	1,000	-12,266	0,680	-2,321	1,027	8960	1,000
sample_00077	-2,697	0,267	5555	1,000	9,315	0,431	7367	1,000	-12,012	0,540	-2,211	0,954	6439	1,000
sample_00078	-2,378	0,226	5482	1,000	9,441	0,402	10503	1,001	-11,819	0,476	-2,024	0,909	9211	1,000
sample_00079	-2,458	0,218	7480	1,000	9,394	0,419	10267	1,000	-11,852	0,481	-2,086	0,910	9988	1,000
sample_00080	-2,436	0,267	5465	1,001	9,374	0,402	7384	1,000	-11,810	0,507	-2,134	0,943	8092	1,000
sample_00081	-2,236	0,245	5390	1,000	9,079	0,418	7465	1,000	-11,315	0,489	-2,125	0,959	7673	1,000
sample_00082	-2,685	0,328	8940	1,000	9,116	0,468	10390	1,000	-11,800	0,584	-2,310	1,025	10137	1,000
sample_00083	-2,321	0,254	6832	1,001	9,206	0,425	12528	1,000	-11,528	0,504	-2,104	0,949	9795	1,000
sample_00084	-2,263	0,191	4572	1,001	9,381	0,309	8221	1,001	-11,644	0,383	-2,066	0,914	8560	1,000
sample_00085	-2,008	0,174	5096	1,000	9,311	0,290	7351	1,000	-11,320	0,358	-1,994	0,880	8367	1,000
sample_00086	-2,618	0,190	3826	1,000	9,426	0,318	5466	1,000	-12,044	0,414	-2,493	0,966	5718	1,000
sample_00087	-2,047	0,279	8179	1,000	8,832	0,385	8669	1,000	-10,880	0,501	-2,082	0,937	10311	1,000
sample_00088	-2,399	0,264	5221	1,001	8,966	0,389	10502	1,000	-11,364	0,494	-2,213	0,967	10118	1,000
sample_00089	-1,988	0,262	7163	1,000	8,891	0,373	9422	1,000	-10,879	0,474	-2,004	0,902	9342	1,000
sample_00090	-1,872	0,151	4758	1,000	9,647	0,332	5705	1,000	-11,520	0,364	-1,730	0,850	6867	1,000
sample_00091	-2,347	0,260	5342	1,000	9,368	0,417	10538	1,000	-11,715	0,525	-2,117	0,932	8601	1,000
sample_00092	-2,327	0,246	5151	1,000	9,325	0,376	10109	1,000	-11,652	0,473	-2,050	0,922	9267	1,000
sample_00093	-2,300	0,208	4756	1,000	8,995	0,334	7793	1,000	-11,295	0,414	-2,023	0,903	6347	1,000
sample_00094	-2,264	0,156	5092	1,000	8,992	0,252	5223	1,000	-11,256	0,315	-1,838	0,898	5265	1,000
sample_00095	-2,531	0,248	5116	1,000	9,094	0,398	9186	1,000	-11,625	0,489	-2,194	0,974	8949	1,000
sample_00096	-1,969	0,242	5559	1,000	8,945	0,329	6672	1,000	-10,914	0,428	-1,983	0,918	6885	1,000
sample_00097	-2,346	0,331	8855	1,000	9,184	0,459	12195	1,000	-11,530	0,580	-2,289	1,001	11671	1,000
sample_00098	-2,571	0,253	5226	1,000	8,945	0,391	7044	1,000	-11,515	0,491	-2,269	1,006	9423	1,000
sample_00099	-3,262	0,449	3889	1,000	8,945	0,525	7750	1,000	-12,207	0,779	-2,577	1,125	7451	1,000
sample_00100	-3,221	0,286	4523	1,000	9,272	0,480	8471	1,000	-12,493	0,603	-2,277	1,008	8037	1,000

sample_00101	-2,719	0,495	8428	1,000	8,873	0,522	8793	1,000	-11,591	0,804	-2,633	1,114	8919	1,000
sample_00102	-2,247	0,211	5219	1,000	9,562	0,378	8011	1,000	-11,809	0,445	-1,938	0,885	8359	1,000
sample_00103	-2,516	0,266	4494	1,001	9,249	0,374	7889	1,000	-11,765	0,494	-2,153	0,936	7723	1,000
sample_00104	-2,697	0,236	6083	1,000	9,011	0,410	8933	1,000	-11,709	0,509	-2,388	1,008	10108	1,000
sample_00105	-2,463	0,202	5443	1,000	9,059	0,399	7265	1,000	-11,522	0,452	-2,128	0,952	7061	1,000
sample_00106	-2,692	0,251	6166	1,000	9,103	0,461	7496	1,000	-11,795	0,543	-2,301	0,997	8325	1,000
sample_00107	-2,294	0,261	6784	1,000	8,980	0,423	10913	1,000	-11,274	0,505	-2,163	0,957	9361	1,000
sample_00108	-3,792	0,229	2290	1,000	9,068	0,526	5760	1,000	-12,860	0,631	-2,438	1,068	6508	1,000
sample_00109	-2,511	0,520	3720	1,000	8,378	0,439	4305	1,001	-10,889	0,735	-4,074	1,324	2748	1,000
sample_00110	-2,362	0,394	7416	1,000	8,493	0,529	7428	1,000	-10,855	0,736	-2,683	1,151	9270	1,000
sample_00111	-1,968	0,237	6345	1,000	9,064	0,352	9377	1,000	-11,032	0,438	-1,929	0,885	7894	1,000
sample_00112	-2,098	0,196	5695	1,000	9,191	0,294	7724	1,000	-11,289	0,373	-1,971	0,889	8753	1,000
sample_00113	-1,983	0,279	7702	1,000	8,948	0,383	10446	1,000	-10,931	0,495	-2,031	0,904	10991	1,000
sample_00114	-2,090	0,177	5739	1,000	9,228	0,352	9640	1,000	-11,318	0,406	-1,893	0,888	8851	1,000
sample_00115	-2,163	0,191	5003	1,000	9,324	0,386	7093	1,000	-11,487	0,440	-1,968	0,924	7116	1,001
sample_00116	-2,078	0,163	5714	1,000	9,268	0,355	8475	1,000	-11,346	0,399	-1,936	0,901	8589	1,000
sample_00117	-3,222	0,300	3613	1,002	9,283	0,468	7038	1,000	-12,505	0,619	-2,322	1,001	8618	1,000
sample_00118	-3,096	0,230	3977	1,000	9,359	0,427	7141	1,000	-12,455	0,540	-2,254	0,973	7220	1,000
sample_00119	-2,763	0,156	4991	1,000	9,475	0,359	5600	1,000	-12,238	0,415	-2,089	0,919	6594	1,000
sample_00120	-2,579	0,244	5104	1,000	9,035	0,406	8775	1,000	-11,615	0,494	-2,216	0,986	9368	1,001
sample_00121	-2,367	0,209	5185	1,000	9,367	0,340	8681	1,000	-11,734	0,425	-1,961	0,911	7323	1,000
sample_00122	-3,042	0,328	6956	1,000	9,217	0,493	10385	1,000	-12,259	0,625	-2,322	1,021	9399	1,000
sample_00123	-3,004	0,439	4124	1,001	9,213	0,501	7078	1,000	-12,217	0,739	-2,347	1,022	9253	1,000
sample_00124	-2,716	0,210	6081	1,000	9,292	0,400	9765	1,000	-12,008	0,488	-2,239	0,961	10454	1,000
sample_00125	-2,962	0,342	6050	1,000	9,205	0,494	10479	1,000	-12,167	0,636	-2,339	1,017	11857	1,000

Table S24. Ratios of the predicted trait values according to the linear models for cell size, gross speed and turning angles for evolved predators divided by ancestral predators. Prey and predator densities represent 2%, 50% and 95% quantiles of the observed prey and predator densities during the experiment. Note that for cell size, predictions are independent of prey species, and for movement speed, independent of prey densities.

<i>Prey species</i>	<i>Prey evolution</i>	<i>Log (Prey density)</i>	<i>Log (Predator density)</i>	<i>size_ratio</i>	<i>speed_ratio</i>	<i>turning_ratio</i>
<i>E. coli</i>	Ancestor	16,631	1,979	1,266	0,971	0,924
<i>E. coli</i>	Ancestor	16,631	6,066	1,235	1,042	0,965
<i>E. coli</i>	Ancestor	16,631	9,936	1,194	1,140	1,006
<i>E. coli</i>	Ancestor	19,021	1,979	1,110	0,971	0,924
<i>E. coli</i>	Ancestor	19,021	6,066	1,054	1,042	0,965
<i>E. coli</i>	Ancestor	19,021	9,936	0,994	1,140	1,006
<i>E. coli</i>	Ancestor	20,807	1,979	1,017	0,971	0,924
<i>E. coli</i>	Ancestor	20,807	6,066	0,963	1,042	0,965
<i>E. coli</i>	Ancestor	20,807	9,936	0,913	1,140	1,006
<i>E. coli</i>	Evolved	16,631	1,979	1,281	0,972	0,924
<i>E. coli</i>	Evolved	16,631	6,066	1,251	1,043	0,965
<i>E. coli</i>	Evolved	16,631	9,936	1,210	1,164	1,006
<i>E. coli</i>	Evolved	19,021	1,979	1,115	0,972	0,924
<i>E. coli</i>	Evolved	19,021	6,066	1,057	1,043	0,965
<i>E. coli</i>	Evolved	19,021	9,936	0,994	1,164	1,006
<i>E. coli</i>	Evolved	20,807	1,979	1,018	0,972	0,924
<i>E. coli</i>	Evolved	20,807	6,066	0,962	1,043	0,965
<i>E. coli</i>	Evolved	20,807	9,936	0,909	1,164	1,006
<i>J. lividum</i>	Ancestor	16,631	1,979	1,266	0,965	0,924
<i>J. lividum</i>	Ancestor	16,631	6,066	1,235	1,054	0,965
<i>J. lividum</i>	Ancestor	16,631	9,936	1,194	1,194	1,006
<i>J. lividum</i>	Ancestor	19,021	1,979	1,110	0,965	0,924
<i>J. lividum</i>	Ancestor	19,021	6,066	1,054	1,054	0,965
<i>J. lividum</i>	Ancestor	19,021	9,936	0,994	1,194	1,006
<i>J. lividum</i>	Ancestor	20,807	1,979	1,017	0,965	0,924
<i>J. lividum</i>	Ancestor	20,807	6,066	0,963	1,054	0,965
<i>J. lividum</i>	Ancestor	20,807	9,936	0,913	1,194	1,006
<i>J. lividum</i>	Evolved	16,631	1,979	1,281	0,966	0,924
<i>J. lividum</i>	Evolved	16,631	6,066	1,251	1,057	0,965
<i>J. lividum</i>	Evolved	16,631	9,936	1,210	1,244	1,006
<i>J. lividum</i>	Evolved	19,021	1,979	1,115	0,966	0,924
<i>J. lividum</i>	Evolved	19,021	6,066	1,057	1,057	0,965
<i>J. lividum</i>	Evolved	19,021	9,936	0,994	1,244	1,006

<i>J. lividum</i>	Evolved	20,807	1,979	1,018	0,966	0,924
<i>J. lividum</i>	Evolved	20,807	6,066	0,962	1,057	0,965
<i>J. lividum</i>	Evolved	20,807	9,936	0,909	1,244	1,006
<i>S. capsulata</i>	Ancestor	16,631	1,979	1,266	0,971	0,924
<i>S. capsulata</i>	Ancestor	16,631	6,066	1,235	1,042	0,965
<i>S. capsulata</i>	Ancestor	16,631	9,936	1,194	1,143	1,006
<i>S. capsulata</i>	Ancestor	19,021	1,979	1,110	0,971	0,924
<i>S. capsulata</i>	Ancestor	19,021	6,066	1,054	1,042	0,965
<i>S. capsulata</i>	Ancestor	19,021	9,936	0,994	1,143	1,006
<i>S. capsulata</i>	Ancestor	20,807	1,979	1,017	0,971	0,924
<i>S. capsulata</i>	Ancestor	20,807	6,066	0,963	1,042	0,965
<i>S. capsulata</i>	Ancestor	20,807	9,936	0,913	1,143	1,006
<i>S. capsulata</i>	Evolved	16,631	1,979	1,281	0,972	0,924
<i>S. capsulata</i>	Evolved	16,631	6,066	1,251	1,044	0,965
<i>S. capsulata</i>	Evolved	16,631	9,936	1,210	1,168	1,006
<i>S. capsulata</i>	Evolved	19,021	1,979	1,115	0,972	0,924
<i>S. capsulata</i>	Evolved	19,021	6,066	1,057	1,044	0,965
<i>S. capsulata</i>	Evolved	19,021	9,936	0,994	1,168	1,006
<i>S. capsulata</i>	Evolved	20,807	1,979	1,018	0,972	0,924
<i>S. capsulata</i>	Evolved	20,807	6,066	0,962	1,044	0,965
<i>S. capsulata</i>	Evolved	20,807	9,936	0,909	1,168	1,006
<i>B. diminuta</i>	Ancestor	16,631	1,979	1,266	0,973	0,924
<i>B. diminuta</i>	Ancestor	16,631	6,066	1,235	1,039	0,965
<i>B. diminuta</i>	Ancestor	16,631	9,936	1,194	1,130	1,006
<i>B. diminuta</i>	Ancestor	19,021	1,979	1,110	0,973	0,924
<i>B. diminuta</i>	Ancestor	19,021	6,066	1,054	1,039	0,965
<i>B. diminuta</i>	Ancestor	19,021	9,936	0,994	1,130	1,006
<i>B. diminuta</i>	Ancestor	20,807	1,979	1,017	0,973	0,924
<i>B. diminuta</i>	Ancestor	20,807	6,066	0,963	1,039	0,965
<i>B. diminuta</i>	Ancestor	20,807	9,936	0,913	1,130	1,006
<i>B. diminuta</i>	Evolved	16,631	1,979	1,281	0,974	0,924
<i>B. diminuta</i>	Evolved	16,631	6,066	1,251	1,041	0,965
<i>B. diminuta</i>	Evolved	16,631	9,936	1,210	1,151	1,006
<i>B. diminuta</i>	Evolved	19,021	1,979	1,115	0,974	0,924
<i>B. diminuta</i>	Evolved	19,021	6,066	1,057	1,041	0,965
<i>B. diminuta</i>	Evolved	19,021	9,936	0,994	1,151	1,006
<i>B. diminuta</i>	Evolved	20,807	1,979	1,018	0,974	0,924
<i>B. diminuta</i>	Evolved	20,807	6,066	0,962	1,041	0,965
<i>B. diminuta</i>	Evolved	20,807	9,936	0,909	1,151	1,006

<i>P. fluorescens</i>	Ancestor	16,631	1,979	1,266	0,970	0,924
<i>P. fluorescens</i>	Ancestor	16,631	6,066	1,235	1,044	0,965
<i>P. fluorescens</i>	Ancestor	16,631	9,936	1,194	1,150	1,006
<i>P. fluorescens</i>	Ancestor	19,021	1,979	1,110	0,970	0,924
<i>P. fluorescens</i>	Ancestor	19,021	6,066	1,054	1,044	0,965
<i>P. fluorescens</i>	Ancestor	19,021	9,936	0,994	1,150	1,006
<i>P. fluorescens</i>	Ancestor	20,807	1,979	1,017	0,970	0,924
<i>P. fluorescens</i>	Ancestor	20,807	6,066	0,963	1,044	0,965
<i>P. fluorescens</i>	Ancestor	20,807	9,936	0,913	1,150	1,006
<i>P. fluorescens</i>	Evolved	16,631	1,979	1,281	0,971	0,924
<i>P. fluorescens</i>	Evolved	16,631	6,066	1,251	1,046	0,965
<i>P. fluorescens</i>	Evolved	16,631	9,936	1,210	1,178	1,006
<i>P. fluorescens</i>	Evolved	19,021	1,979	1,115	0,971	0,924
<i>P. fluorescens</i>	Evolved	19,021	6,066	1,057	1,046	0,965
<i>P. fluorescens</i>	Evolved	19,021	9,936	0,994	1,178	1,006
<i>P. fluorescens</i>	Evolved	20,807	1,979	1,018	0,971	0,924
<i>P. fluorescens</i>	Evolved	20,807	6,066	0,962	1,046	0,965
<i>P. fluorescens</i>	Evolved	20,807	9,936	0,909	1,178	1,006
<i>C. testosteroni</i>	Ancestor	16,631	1,979	1,266	0,971	0,924
<i>C. testosteroni</i>	Ancestor	16,631	6,066	1,235	1,041	0,965
<i>C. testosteroni</i>	Ancestor	16,631	9,936	1,194	1,139	1,006
<i>C. testosteroni</i>	Ancestor	19,021	1,979	1,110	0,971	0,924
<i>C. testosteroni</i>	Ancestor	19,021	6,066	1,054	1,041	0,965
<i>C. testosteroni</i>	Ancestor	19,021	9,936	0,994	1,139	1,006
<i>C. testosteroni</i>	Ancestor	20,807	1,979	1,017	0,971	0,924
<i>C. testosteroni</i>	Ancestor	20,807	6,066	0,963	1,041	0,965
<i>C. testosteroni</i>	Ancestor	20,807	9,936	0,913	1,139	1,006
<i>C. testosteroni</i>	Evolved	16,631	1,979	1,281	0,973	0,924
<i>C. testosteroni</i>	Evolved	16,631	6,066	1,251	1,043	0,965
<i>C. testosteroni</i>	Evolved	16,631	9,936	1,210	1,162	1,006
<i>C. testosteroni</i>	Evolved	19,021	1,979	1,115	0,973	0,924
<i>C. testosteroni</i>	Evolved	19,021	6,066	1,057	1,043	0,965
<i>C. testosteroni</i>	Evolved	19,021	9,936	0,994	1,162	1,006
<i>C. testosteroni</i>	Evolved	20,807	1,979	1,018	0,973	0,924
<i>C. testosteroni</i>	Evolved	20,807	6,066	0,962	1,043	0,965
<i>C. testosteroni</i>	Evolved	20,807	9,936	0,909	1,162	1,006
<i>S. marcescens</i>	Ancestor	16,631	1,979	1,266	0,966	0,924
<i>S. marcescens</i>	Ancestor	16,631	6,066	1,235	1,051	0,965
<i>S. marcescens</i>	Ancestor	16,631	9,936	1,194	1,181	1,006

<i>S. marcescens</i>	Ancestor	19,021	1,979	1,110	0,966	0,924
<i>S. marcescens</i>	Ancestor	19,021	6,066	1,054	1,051	0,965
<i>S. marcescens</i>	Ancestor	19,021	9,936	0,994	1,181	1,006
<i>S. marcescens</i>	Ancestor	20,807	1,979	1,017	0,966	0,924
<i>S. marcescens</i>	Ancestor	20,807	6,066	0,963	1,051	0,965
<i>S. marcescens</i>	Ancestor	20,807	9,936	0,913	1,181	1,006
<i>S. marcescens</i>	Evolved	16,631	1,979	1,281	0,968	0,924
<i>S. marcescens</i>	Evolved	16,631	6,066	1,251	1,054	0,965
<i>S. marcescens</i>	Evolved	16,631	9,936	1,210	1,223	1,006
<i>S. marcescens</i>	Evolved	19,021	1,979	1,115	0,968	0,924
<i>S. marcescens</i>	Evolved	19,021	6,066	1,057	1,054	0,965
<i>S. marcescens</i>	Evolved	19,021	9,936	0,994	1,223	1,006
<i>S. marcescens</i>	Evolved	20,807	1,979	1,018	0,968	0,924
<i>S. marcescens</i>	Evolved	20,807	6,066	0,962	1,054	0,965
<i>S. marcescens</i>	Evolved	20,807	9,936	0,909	1,223	1,006

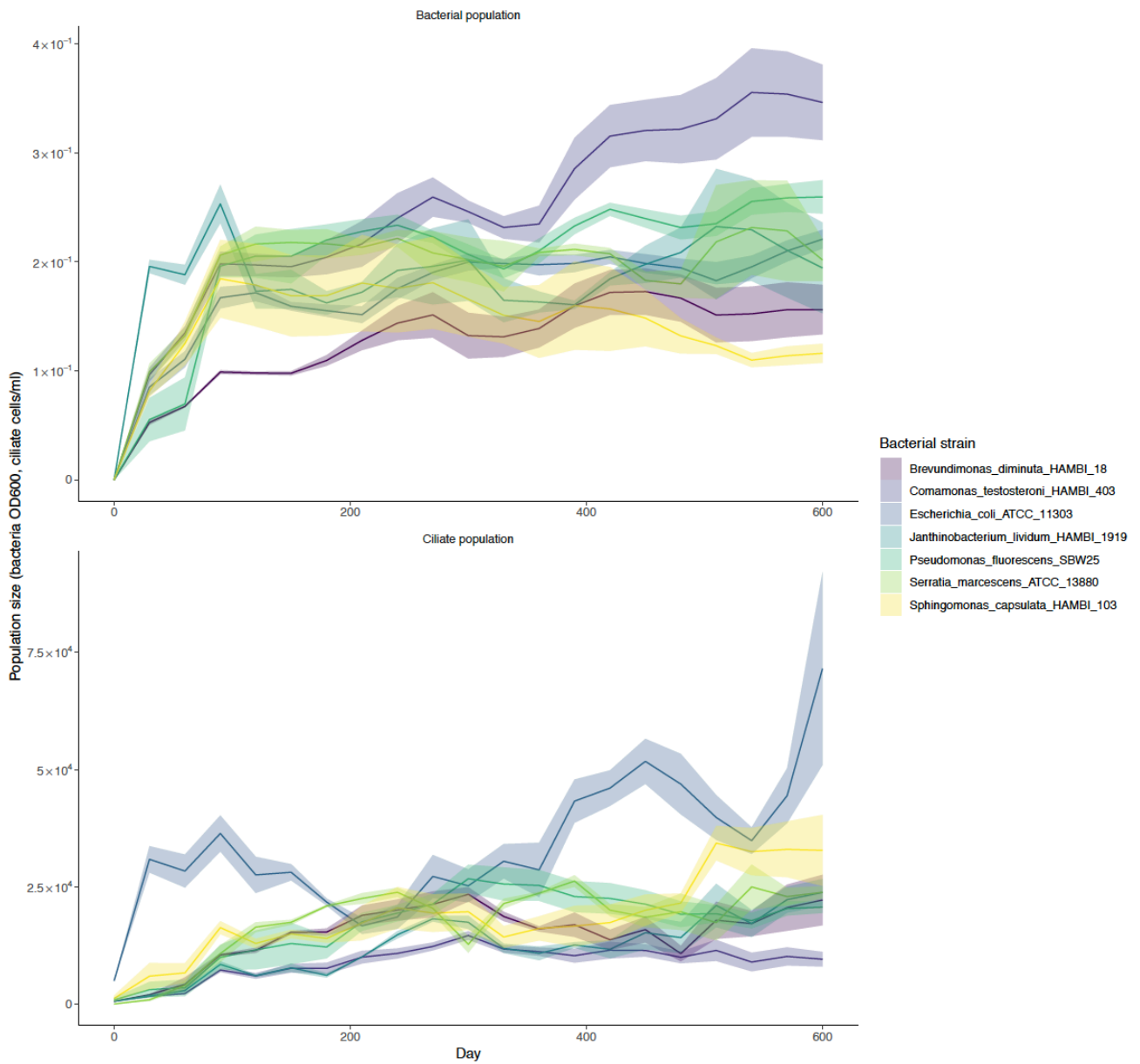


Figure S1. Bacterial and ciliate population size during first 20 months in long-term predator-prey coevolutionary experiment (mean \pm s.e.m. smoothed over 90 day sliding window). The figure shows different population sizes for different bacterial species and an increasing trend over time.

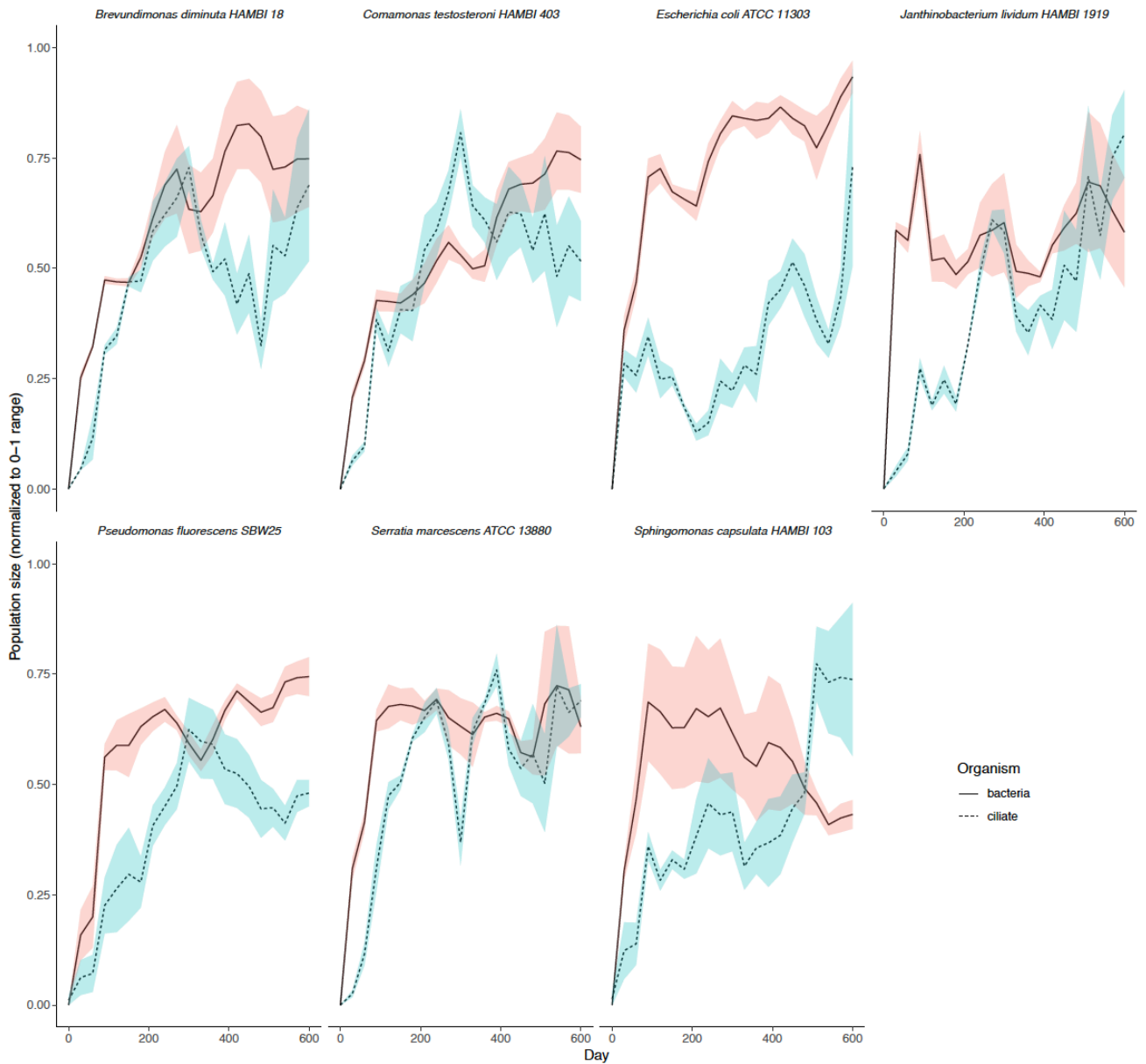


Figure S2. Bacteria-ciliate community dynamics during first 20 months in long-term predator-prey coevolutionary experiment (mean \pm s.e.m. standardized to 0-1 range and smoothed over 90 day sliding window). The figure shows a negative association between bacterial and ciliate population size as well as differences in community dynamics depending on the prey (bacterial) species.

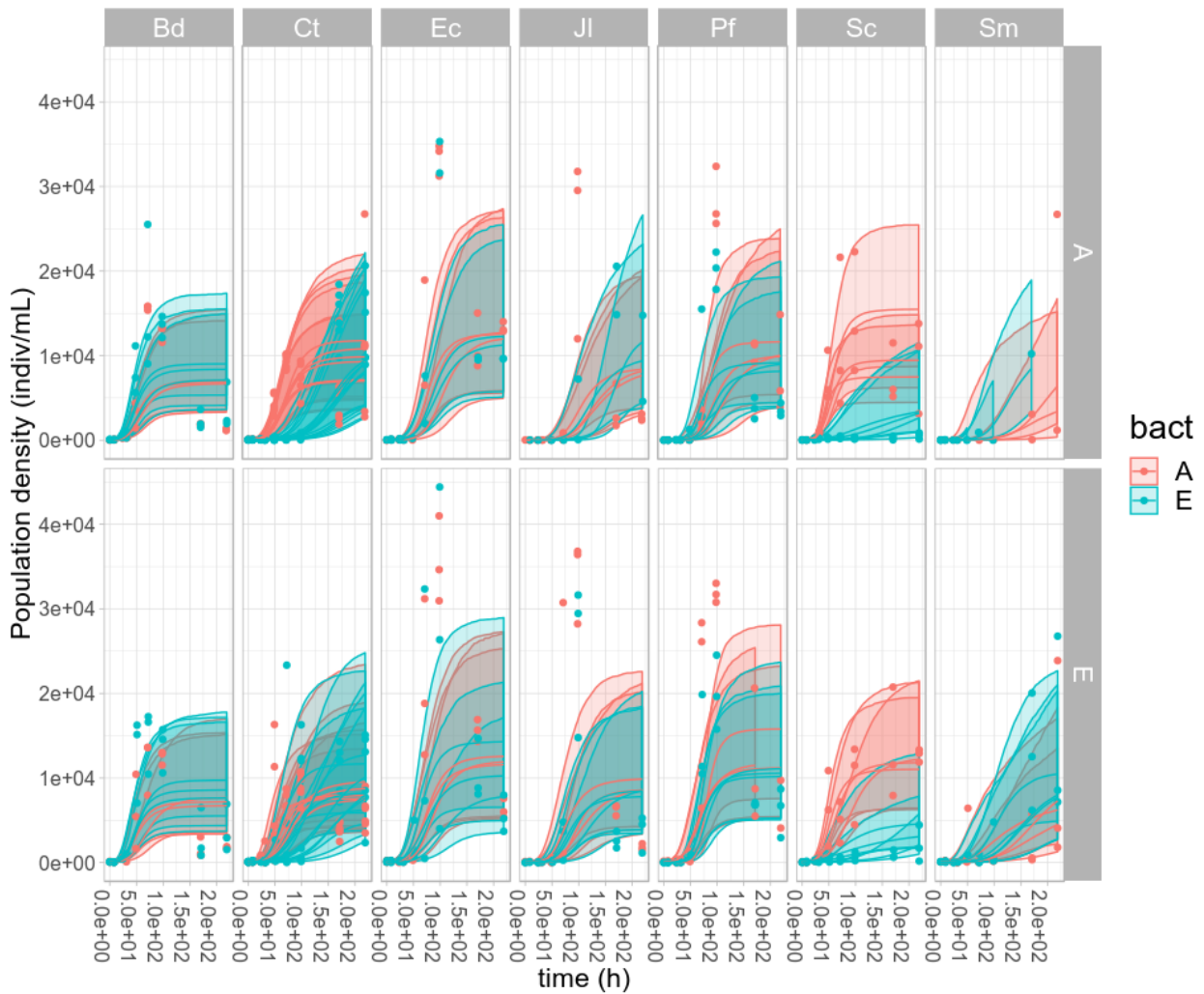


Figure S3. Beverton-Holt continuous-time growth models for ciliate population density (mean \pm 95 % confidence intervals). A = ancestral ciliate; E = evolved ciliate; Bd = *Brevundimonas diminuta* HAMBI 18; Ct = *Comamonas testosteroni* HAMBI 403; Ec = *Escherichia coli* ATCC 11303; Jl = *Janthinobacterium lividum* HAMBI 1919; Pf = *Pseudomonas fluorescens* SBW25; Sc = *Spingomonas capsulata* HAMBI 103; Sm = *Serratia marcescens* ATCC 13880.

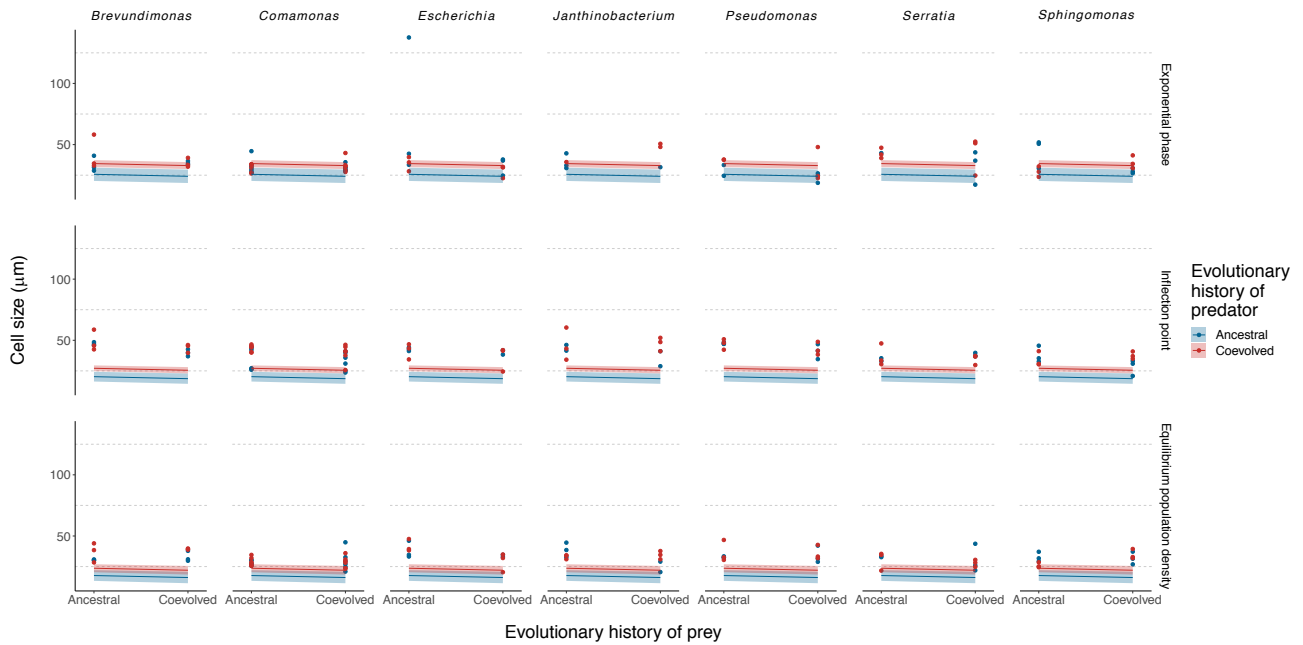


Figure S4. Reaction norms showing effect of predator-prey coevolution on cell size of predator at low (5 % quantile) prey density and three different predator densities (data points with linear model estimate \pm 95 % confidence intervals.; N = 3 except 6 for *Comamonas*). Predator densities have been taken from different growth phases estimated using Beverton-Holt population models. The reaction norms for predators (one strain of the ciliate *Tetrahymena thermophila*) feeding on ancestral or coevolved prey (seven bacterial strains indicated by genus name) are depicted separately for ancestral and coevolved predators (color coding). Predators coevolved with a particular prey taxon have always been coupled with ancestral or coevolved populations of the same taxon, while the ancestral predator is the same for all prey taxa.

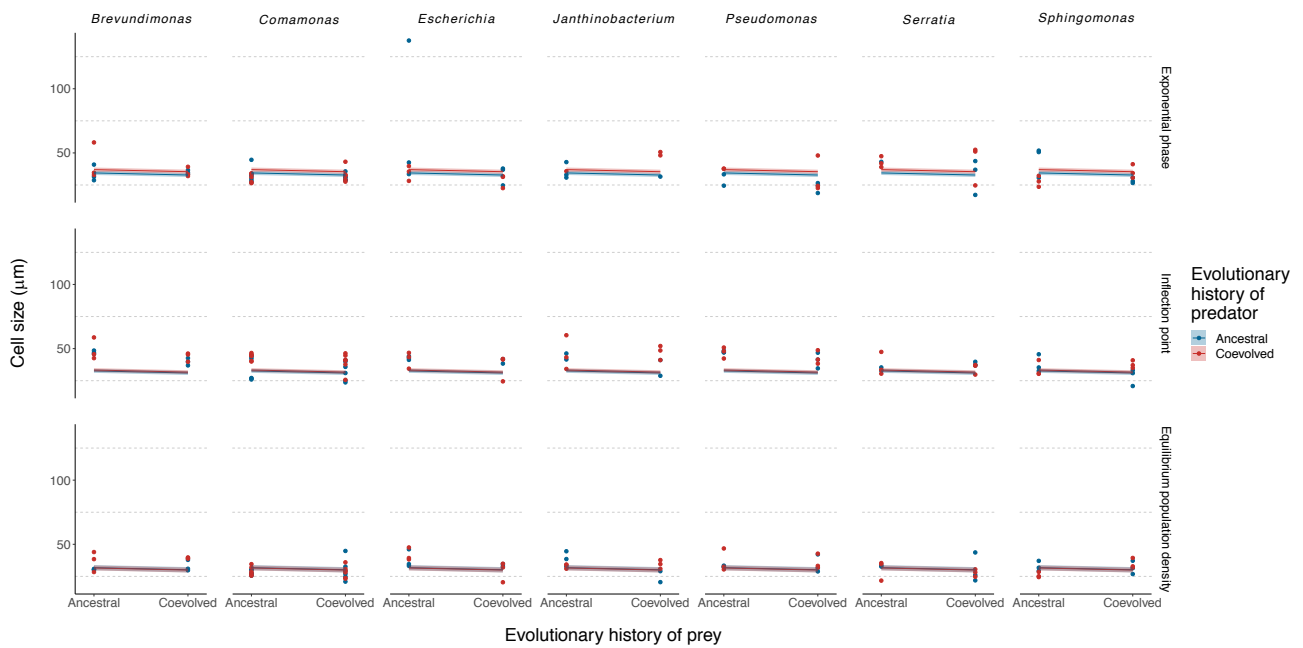


Figure S5. Reaction norms showing effect of predator-prey coevolution on cell size of predator at medium (50 % quantile) prey density and three different predator densities (data points with linear model estimate \pm 95 % confidence intervals.; $N = 3$ except 6 for *Comamonas*). Predator densities have been taken from different growth phases estimated using Beverton-Holt population models. The reaction norms for predators (one strain of the ciliate *Tetrahymena thermophila*) feeding on ancestral or coevolved prey (seven bacterial strains indicated by genus name) are depicted separately for ancestral and coevolved predators (color coding). Predators coevolved with a particular prey taxon have always been coupled with ancestral or coevolved populations of the same taxon, while the ancestral predator is the same for all prey taxa.

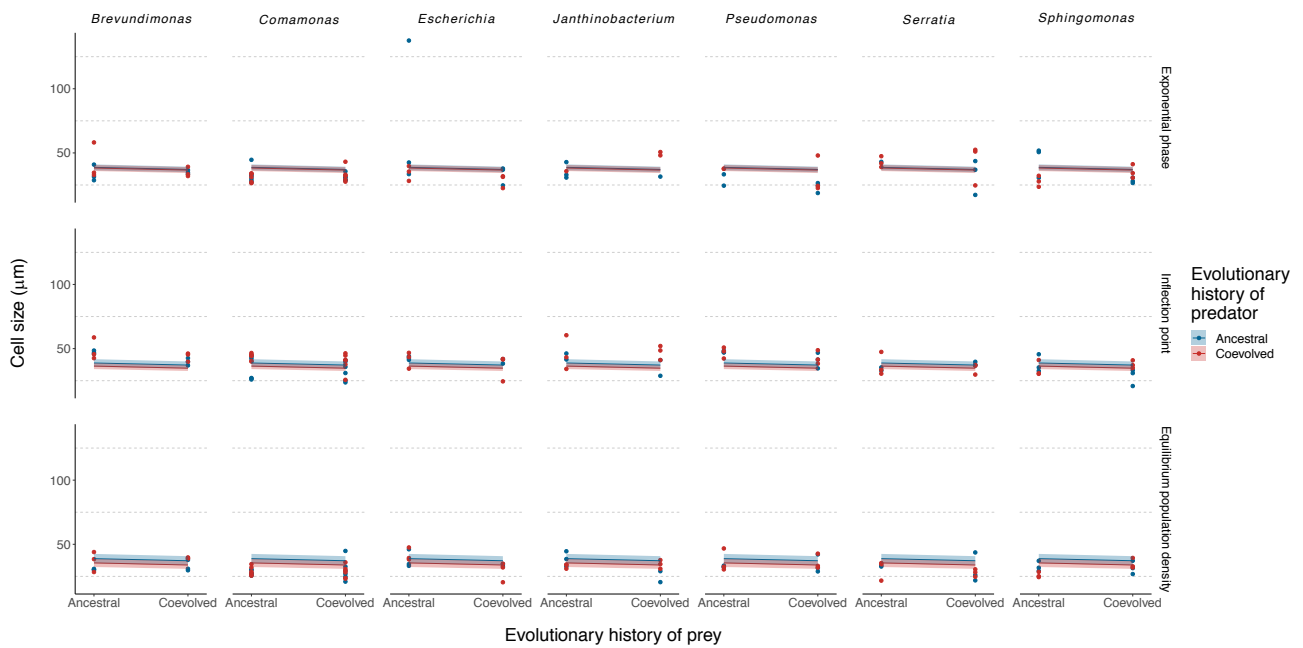


Figure S6. Reaction norms showing effect of predator-prey coevolution on cell size of predator at high (95 % quantile) prey density and three different predator densities (data points with linear model estimate \pm 95 % confidence intervals.; $N = 3$ except 6 for *Comamonas*). Predator densities have been taken from different growth phases estimated using Beverton-Holt population models. The reaction norms for predators (one strain of the ciliate *Tetrahymena thermophila*) feeding on ancestral or coevolved prey (seven bacterial strains indicated by genus name) are depicted separately for ancestral and coevolved predators (color coding). Predators coevolved with a particular prey taxon have always been coupled with ancestral or coevolved populations of the same taxon, while the ancestral predator is the same for all prey taxa.

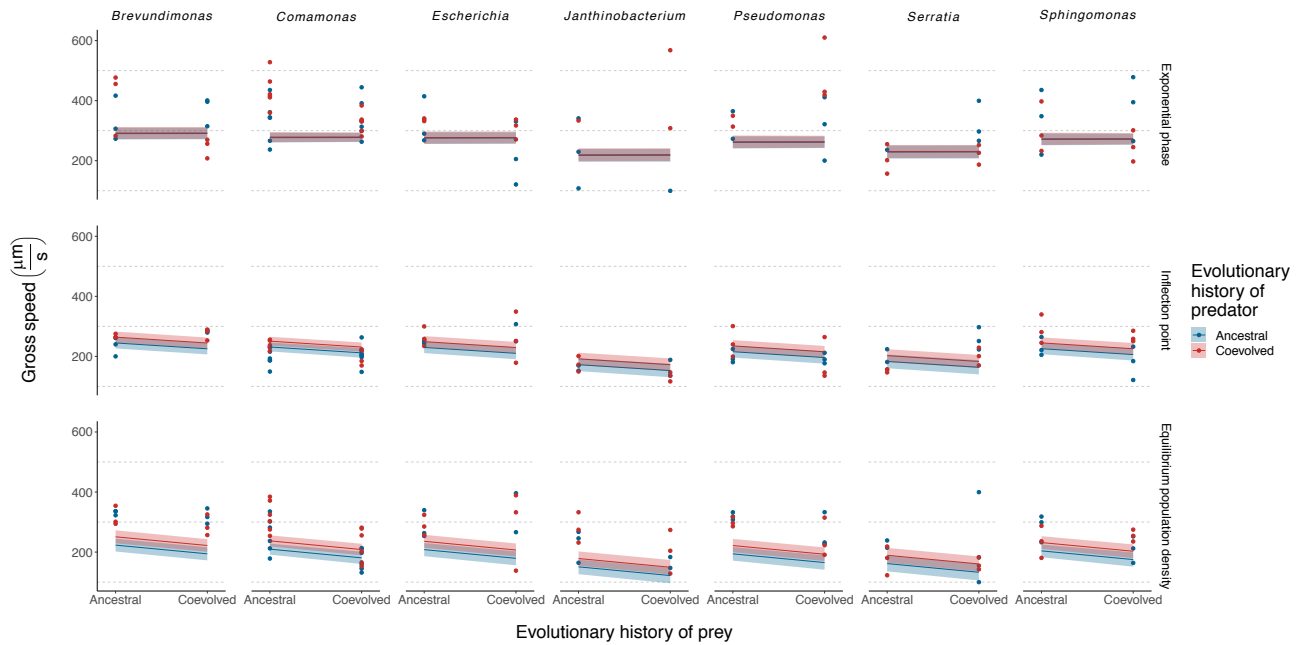


Figure S7. Reaction norms showing effect of predator-prey coevolution on gross speed of predator at medium (50 % quantile) prey density and three different predator densities (data points with linear model estimate \pm 95 % confidence intervals.; $N = 3$ except 6 for *Comamonas*). Since the statistical analysis did not show an effect of prey density on gross speed of the predator, only one prey density is plotted for speed unlike for cell size and turning angle distribution. Predator densities have been taken from different growth phases estimated using Beverton-Holt population models. The reaction norms for predators (one strain of the ciliate *Tetrahymena thermophila*) feeding on ancestral or coevolved prey (seven bacterial strains indicated by genus name) are depicted separately for ancestral and coevolved predators (color coding). Predators coevolved with a particular prey taxon have always been coupled with ancestral or coevolved populations of the same taxon, while the ancestral predator is the same for all prey taxa.

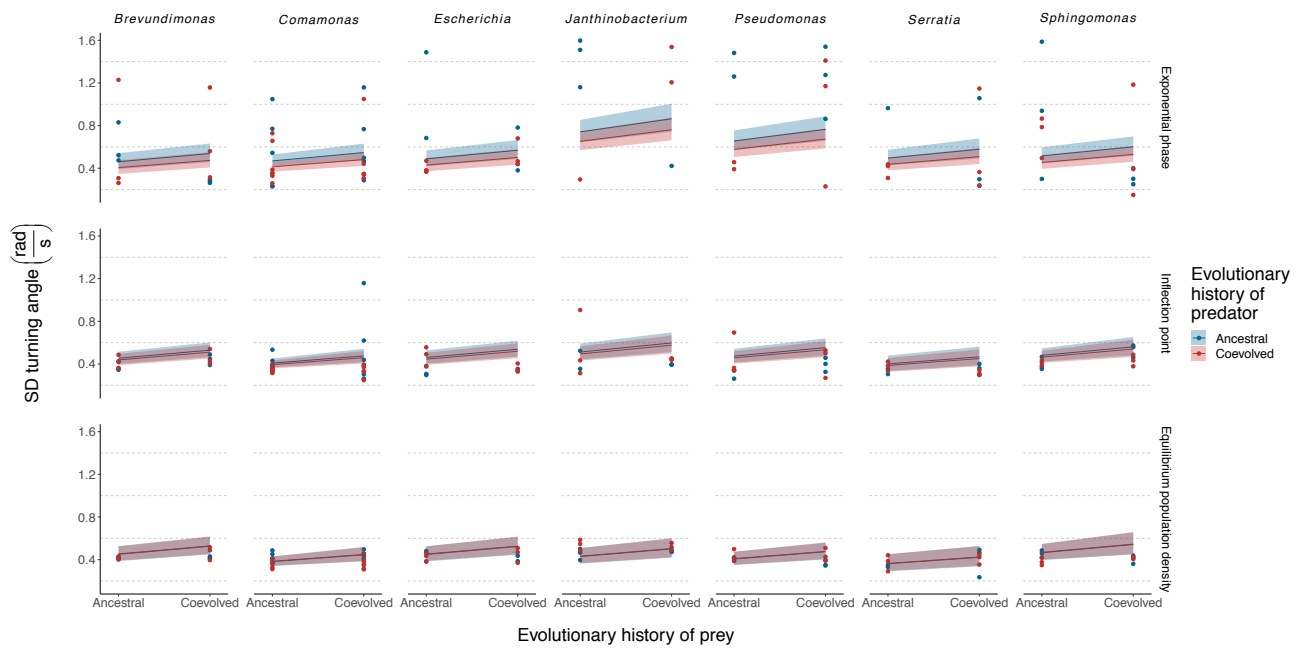


Figure S8. Reaction norms showing effect of predator-prey coevolution on turning angle distribution of predator at low (5 % quantile) prey density and three different predator densities (data points with linear model estimate \pm 95 % confidence intervals.; $N = 3$ except 6 for *Comamonas*). Cell turning angle distribution (standard deviation, SD) is used as a proxy for directionality of cell movement which is higher at lower values. Predator densities have been taken from different growth phases estimated using Beverton-Holt population models. The reaction norms for predators (one strain of the ciliate *Tetrahymena thermophila*) feeding on ancestral or coevolved prey (seven bacterial strains indicated by genus name) are depicted separately for ancestral and coevolved predators (color coding). Predators coevolved with a particular prey taxon have always been coupled with ancestral or coevolved populations of the same taxon, while the ancestral predator is the same for all prey taxa.

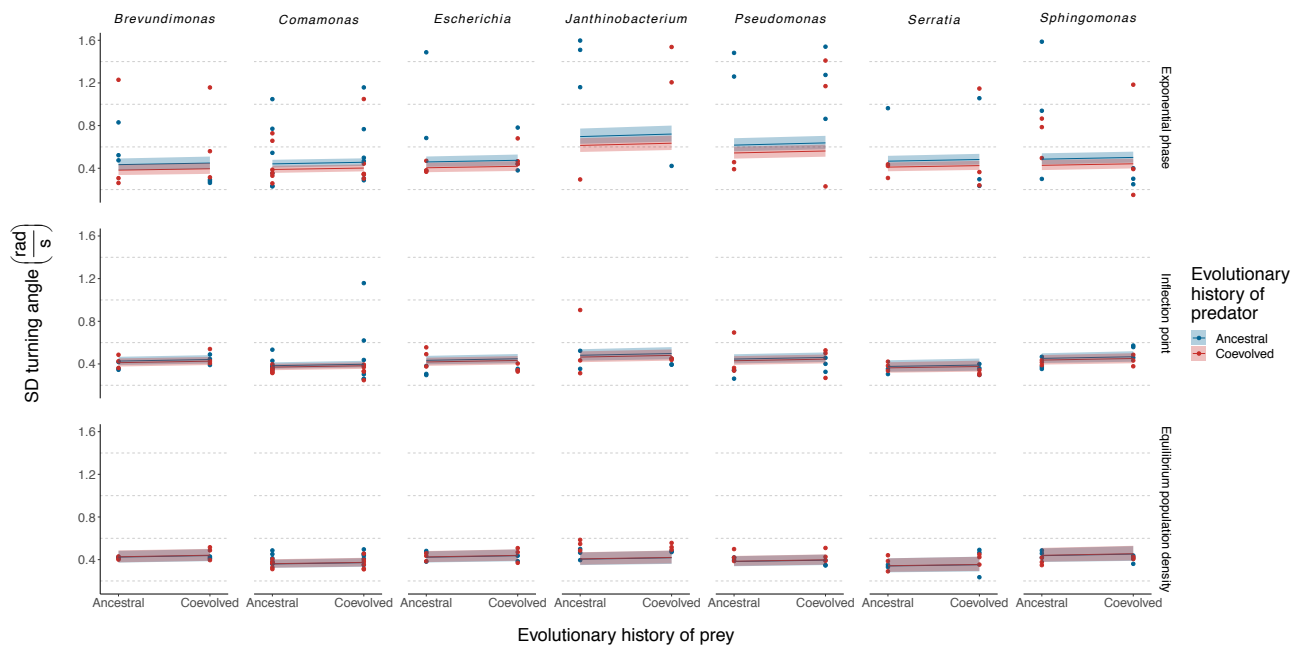


Figure S9. Reaction norms showing effect of predator-prey coevolution on turning angle distribution of predator at medium (50 % quantile) prey density and three different predator densities (data points with linear model estimate \pm 95 % confidence intervals.; $N = 3$ except 6 for *Comamonas*). Cell turning angle distribution (standard deviation, SD) is used as a proxy for directionality of cell movement which is higher at lower values. Predator densities have been taken from different growth phases estimated using Beverton-Holt population models. The reaction norms for predators (one strain of the ciliate *Tetrahymena thermophila*) feeding on ancestral or coevolved prey (seven bacterial strains indicated by genus name) are depicted separately for ancestral and coevolved predators (color coding). Predators coevolved with a particular prey taxon have always been coupled with ancestral or coevolved populations of the same taxon, while the ancestral predator is the same for all prey taxa.

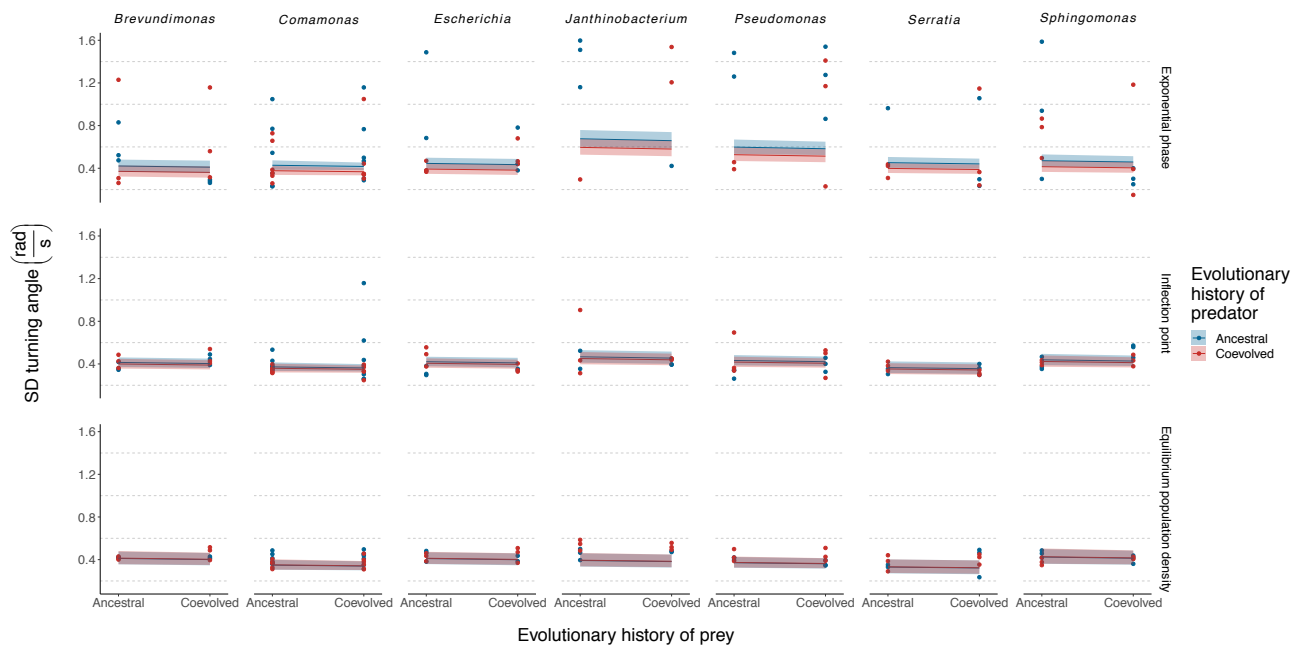


Figure S10. Reaction norms showing effect of predator-prey coevolution on turning angle distribution of predator at high (95 % quantile) prey density and three different predator densities (data points with linear model estimate \pm 95 % confidence intervals.; $N = 3$ except 6 for *Comamonas*). Cell turning angle distribution (standard deviation, SD) is used as a proxy for directionality of cell movement which is higher at lower values. Predator densities have been taken from different growth phases estimated using Beverton-Holt population models. The reaction norms for predators (one strain of the ciliate *Tetrahymena thermophila*) feeding on ancestral or coevolved prey (seven bacterial strains indicated by genus name) are depicted separately for ancestral and coevolved predators (color coding). Predators coevolved with a particular prey taxon have always been coupled with ancestral or coevolved populations of the same taxon, while the ancestral predator is the same for all prey taxa.

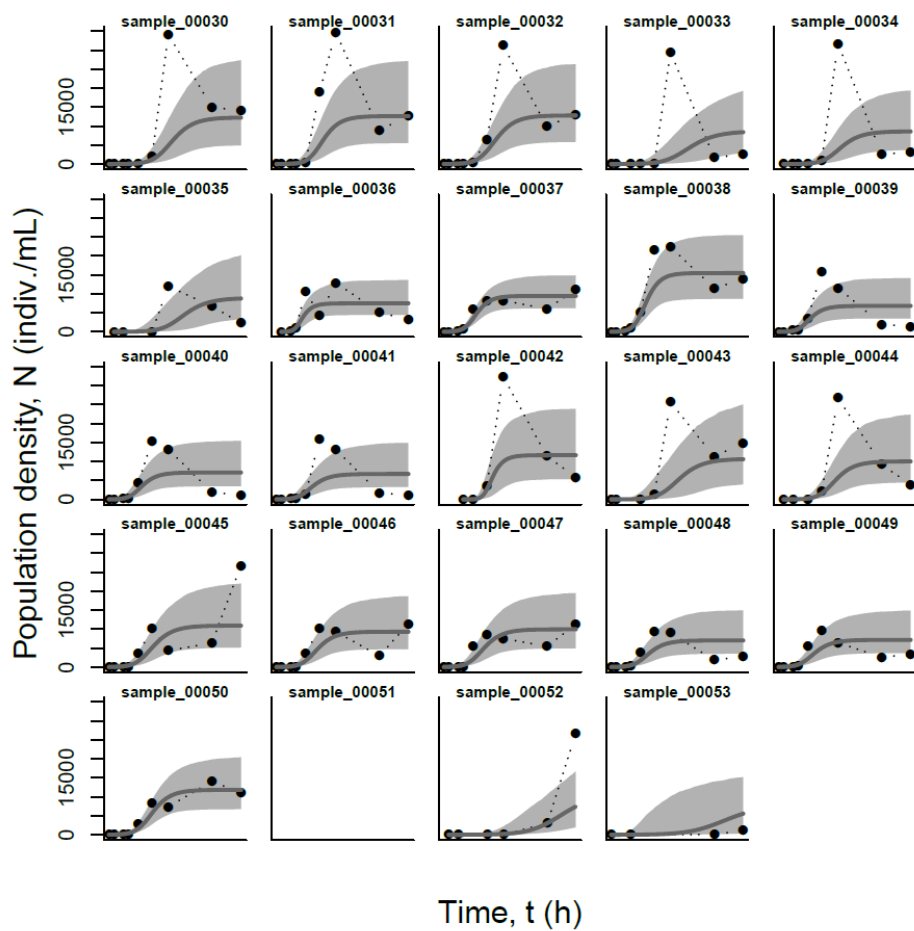


Figure S11. Beverton-Holt predictions for the individual populations (populations 1-24 (samples 30-53)). Dots represent population density measured using video analysis. The smooth grey line shows the mean model prediction, and shaded are the 95% probability interval of the model prediction.

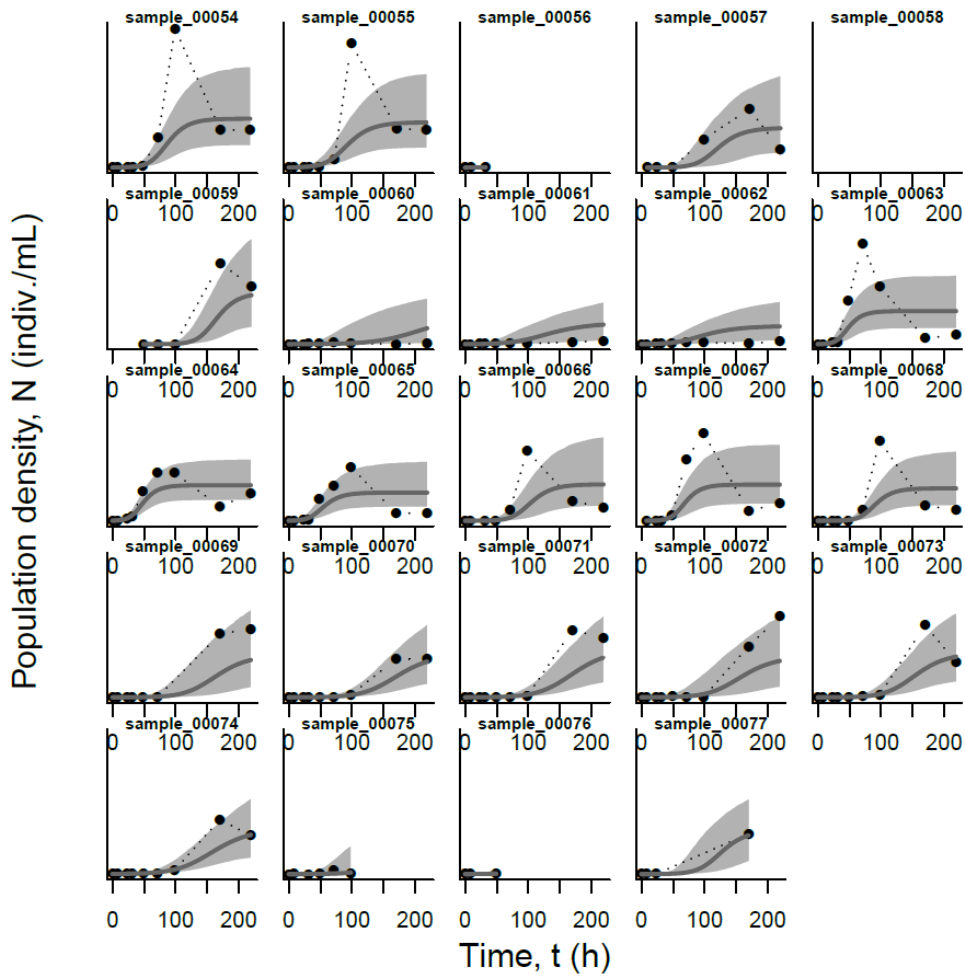


Figure S12. Beverton-Holt predictions for the individual populations (populations 25-48 (samples 54-77)). Dots represent population density measured using video analysis. The smooth grey line shows the mean model prediction, and shaded are the 95% probability interval of the model prediction.

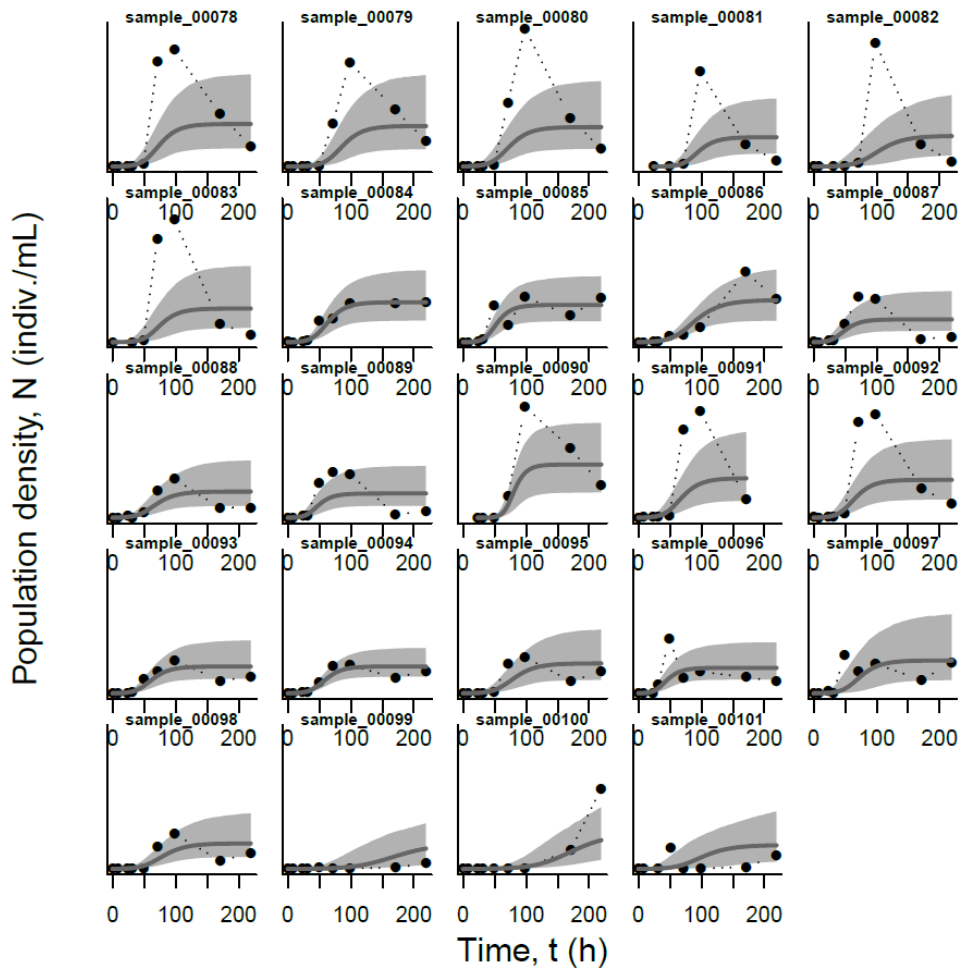


Figure S13. Beverton-Holt predictions for the individual populations (populations 49-72 (samples 78-101)). Dots represent population density measured using video analysis. The smooth grey line shows the mean model prediction, and shaded are the 95% probability interval of the model prediction.

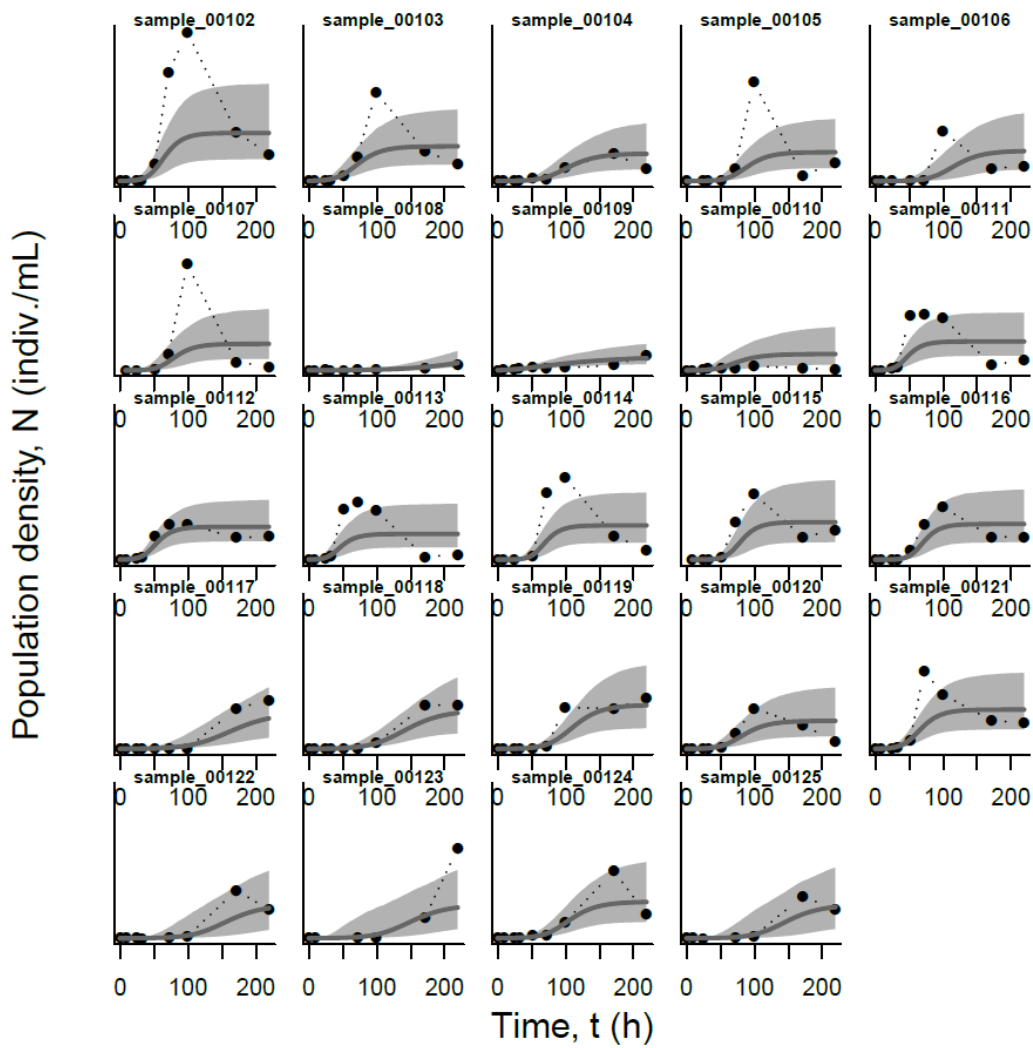


Figure S14. Beverton-Holt predictions for the individual populations (populations 49-72 (samples 78-101)). Dots represent population density measured using video analysis. The smooth grey line shows the mean model prediction, and shaded are the 95% probability interval of the model prediction.

Chapter S.3

Supplementary Material of Chapter 3

S.3.1 Experimental design

S.3.1.1 Treatment groups

Table S3.1: Overview showing the treatments, their treatment levels (column values) and the replication number included in the experimental design.

	Abiotic conditions	Reproduction	Gene flow	Replicates
Treatment combination 1	“Uniform”	“Asexual”	“Absent”	5
Treatment combination 2	“Uniform”	“Asexual”	“Present”	5
Treatment combination 3	“Uniform”	“Sexual”	“Absent”	5
Treatment combination 4	“Uniform”	“Sexual”	“Present”	5
Treatment combination 5	“Gradient”	“Asexual”	“Absent”	5
Treatment combination 6	“Gradient”	“Asexual”	“Present”	5
Treatment combination 7	“Gradient”	“Sexual”	“Absent”	5
Treatment combination 8	“Gradient”	“Sexual”	“Present”	5

S.3.1.2 Extended methodology experimental evolution

Figure S3.1 shows a graphic representation of the design used for the experimental range expansion. Panel A shows the time course of experimental evolution on the vertical axis. The horizontal axis indicates the distance along which populations expanded during the experiment. The leftmost section between the vertical axis and the solid vertical line shows the four ancestral populations (depicted as 4 separate tubes/microcosms). We kept these four ancestral populations at a neutral pH (6.5) conditions as slowly dividing cultures over the entire course of the experiment. Because these conditions were identical to the conditions in which the ancestral populations had been kept before the start of the experiment, we do not expect directed evolutionary change in these ancestral populations. Note, however, that although we maintain these four ancestral clones separately, we initiated the actual range expansion experiment with a mixture of the four ancestors. Keeping the four ancestral populations separately allowed us to mix the four ancestors at the exact same proportions as used at the start of the experiment to emulate gene flow during the experiment. On the right side of the vertical solid line, the figure shows the expanding range front. Because we only tracked the very front of the range expansion using our two-patch landscape, we indicate the front through a pair of brightly coloured and connected culture vessels, which represent two-patch landscapes. During the range expansion experiment, whenever populations successfully dispersed, the range front moves to the right, depicted here by the rightward shift of a brightly coloured culture vessel pair. By only tracking the very front of the range expansions, earlier intermediate patches were no longer maintained. We depict these no longer maintained locations as faintly coloured culture vessels. These faint culture vessels thus represent positions where the range expansion front was located in previous timepoints of the experiment. They are merely shown to help visualize the spatial aspect of the range expansion.

The timeline is divided into 7 distinct horizontal sections (demarcated by the numbers 1-7 in square brackets). The first section (labeled “Start experiment”) shows how we initiated the experiment, namely by inoculating the first tube of a two-patch landscape with 50 μ L culture volume from each of the four ancestral populations. The second section (Cycle 1) shows the steps involved in each of the five 14-day cycles. The steps in each cycle consisted of three dispersal events, followed by gene flow and sexual reproduction (in the relevant treatment groups), and two further dispersal events. Whereas a typical 14-day cycle is shown in Cycle 1, we made two exceptions to these steps, which are marked in figure S3.1 by an asterisk. In Cycle 1, we skipped the dispersal 1 step, as this dispersal step would have taken place on the same day as the initiation of the experiment. Population densities at this time were too low for measurable dispersal to take place. Consequently, we allowed the populations to grow for two days after the initiation, before initiating the first dispersal event (dispersal 2). The second exception regards to Cycle 5, in which we did not start another gene flow and

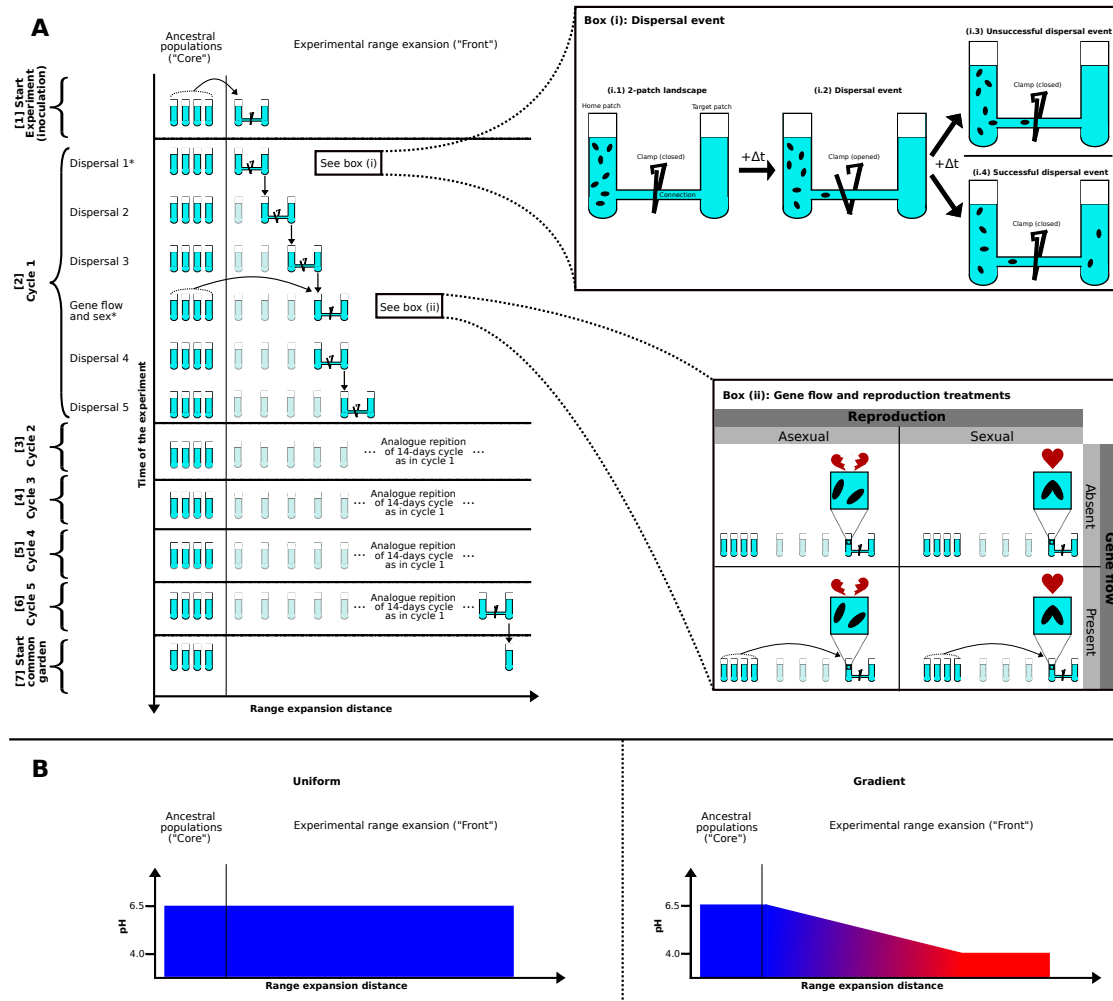


Figure S3.1: Schematic representation of the experimental range expansion. Panel A shows the timeline of the experiment, with the y-axis depicting time, and the x-axis the distance populations expanded during range expansion. Box (i) shows in more detail the experimental approach involved in a dispersal step, and box (ii) the treatments related to gene flow and reproduction. Panel B shows the abiotic conditions experienced during range expansion into a gradient or uniform environment.

sexual reproduction event, as this would have taken place too close to the end of the experiment. Sections 3-6 (Cycle 2-5) of the panel depict how we repeated the initial 14-day cycle an additional four times during the experiment.

The dispersal and gene flow/sexual reproduction events are shown in more detail in boxes (i) and (ii) of figure S3.1. Before a dispersal event (box i.1), all cells (depicted in the box as black ovals) are confined to the first tube (the home patch) of a two-patch landscapes, because plastic clamps keep the connection between the two patches closed. At the start of the dispersal event (box i.2), we opened this clamp and allowed cells to actively swim between the home patch and the target patch. We left the clamp open for one hour. After closure of the clamp, we measured population densities in the home patch and target patch, as described in the main text (Section “Sampling and video analysis”). If no measurable number of cells had dispersed to the target patch of the two-patch landscape (box i.3), we assumed that dispersal was unsuccessful, and we transferred the content of the home patch to a new two-patch landscape. When some cells had successfully dispersed (box i.4), we transferred the content of the target patch to a new two-patch landscape. At the end of the range expansions experiment, the total number of successful dispersal events was used to calculate the total range expansion distance as the sum of the number successful dispersal events.

Box (ii) of figure S3.1 shows the four treatments related to gene flow and sex. To permit gene flow (bottom panels in box (ii)), we removed 1.5 mL of culture from the population, and replaced it with 1.5 mL of the initial (ancestral) culture, containing the four ancestral strains. We prepared this replacement culture by mixing culture of the four ancestral clones so that population densities of each of the four ancestors was the same as the population densities used at the start of the experiment, so that the replacement mixture mimicked the starting conditions of the experiment. For populations in which we did not allow gene flow (top panels of box (ii)), we simply did not perform this replacement. We used this removal and replacement method, rather than simply transferring 1.5 mL of the ancestral culture to the range edge, in order to limit changes in population density, which in turn could alter dispersal rates and hence range expansion rates in the experiment.

After the gene flow step, we transferred all populations to starvation medium, because starvation triggers mating in *T. thermophila*. Specifically, we first transferred all populations to 15 mL Falcon tubes, and centrifuged them (5 min, 1100 G, 4 °C in order to pellet the cells, and discarded the supernatant. We subsequently resuspended cells in 10 mM Tris-HCl, with pH adjusted to 7.5. We then repeated the same centrifugation step, and again resuspended cells in 10 mM Tris-HCl with pH adjusted to 7.5. After the second centrifugation, we transferred the populations to autoclaved 100 mL Erlenmeyer bottles, and placed them for approximately 36 hours on a shaker rotating at 120 rpm to starve the cells. On the next day, we allowed sexual reproduction to occur in those populations designated for sexual reproduction (right panels in box (ii) of figure

S3.1), by simply stopping shaking, which allows cells to conjugate (blue squares in box (ii) of figure S3.1, where cells join). The populations designated for asexual reproduction (left panels in box (ii) of figure S3.1) remained on the shaker, whose movement prevented cells from successfully conjugating (blue squares in which cells remain separate). We had tested this protocol during pilot experiments). In shaken populations, no cell conjugation occurred, whereas in shaken populations, typically over 90 % of cells were engaged in conjugation, indicating that the vast majority of cells underwent sexual reproduction (visual inspection of mating propensity, data not shown).

After having left cells to mate overnight, we transferred all populations to new 15 mL Falcon tubes. We centrifuged the populations (5 min, 1100 G, 4 °C), removed the supernatant and resuspended cells in Neff medium with its pH adjusted to a specific value using 1 M HCl - either pH 6.5 for populations expanding into uniform abiotic conditions, or increasingly low pH for populations expanding into a gradient. We then transferred these cultures to fresh two-patch landscapes, and allowed them to rest for approximately one hour, before initiating the next dispersal event.

After the end of Cycle 5, we cultivated the populations that had not become extinct during the experiment (34 out of 40 initial population) in a common garden environment (“Start common garden” in panel A of figure S3.1). We classified a population as extinct if we did not find any living cells in either the home patch or the target patch of the 2-patch landscape. From every surviving population, we extracted culture from either the target patch of the two-patch landscape if the last dispersal event had been successful, or the home patch if dispersal was unsuccessful. We prepared common garden populations by adding 15 mL of Neff-medium to 25 mL Sarstedt tubes, and adding 100 μ L of culture from the appropriate population. Cultures remained in the common garden for approximately 72 hours, before starting the bioassays.

Panel B of figure S3.1 shows the abiotic conditions associated with the uniform and gradient treatment levels. For the uniform treatment level, a population experienced neutral pH of 6.5 (depicted as blue colour) everywhere along its expanding range. For the Gradient treatment level, the environment became increasingly harsher (lower pH; red colour) during range expansion, until a minimum of pH 4.0 was reached. After reaching this minimum, the pH remained constant for the remainder of the range expansion. We gradually lowered the pH in the Gradient treatment, by adjusting the pH of the target patch in steps of 0.5 every 2-3 successful dispersal events, so that if dispersal was always successful, the pH would decrease by 0.5 every week. We kept the ancestral populations as slow-dividing cultures under neutral pH conditions (pH 6.5) over the entire course of the experiment.

S.3.1.3 Experimental handling

Table S3.2: Overview of the experimental handling operations performed on the different days during the range expansion experiment.

Day of experiment	Handling
1	Start experiment
2	
3	Dispersal
4	
5	Dispersal
6	
7	
8	Gene Flow + Starvation
9	Sex
10	Dispersal
11	
12	Dispersal
13	
14	
15	Dispersal
16	
17	Dispersal
18	
19	Dispersal
20	
21	
22	Gene Flow + Starvation
23	Sex
24	Dispersal
25	
26	Dispersal
27	
28	
29	Dispersal
30	
31	Dispersal
32	
33	Dispersal
34	
35	
36	Gene Flow + Starvation
37	Sex

38	Dispersal
39	
40	Dispersal
41	
42	
43	Dispersal
44	
45	Dispersal
46	
47	Dispersal
48	
49	
50	Gene Flow + Starvation
51	Sex
52	Dispersal
53	
54	Dispersal
55	
56	
57	Dispersal
58	
59	Dispersal
60	
61	Dispersal
62	
63	
64	Dispersal
65	
66	Dispersal
67	
68	Transfer to common garden setting

S.3.2 Video analysis script

Below follows the script used for video analysis, including all the used parameters.

```
#####
# R script for analysing video files with BEMOVI (www.bemovi.info)
rm(list=ls())
# load package
library(devtools)
```

```

install_github("efronhofer/bemovi", ref="experimental")
library(bemovi)

#####
# VIDEO PARAMETERS

# video frame rate (in frames per second)
fps <- 25
# length of video (in frames)
total_frames <- 500

# measured volume (in microliter)
measured_volume <- 34.4 # for Leica M205 C with 1.6 fold magnification,
Sample height 0.5 mm and Hamamatsu Orca Flash 4

# size of a pixel (in micrometer)
pixel_to_scale <- 4.05 # for Leica M205 C with 1.6 fold magnification,
Sample height 0.5 mm and Hamamatsu Orca Flash 4

# specify video file format (one of "avi","cxd","mov","tiff")
# bemovi only works with avi and cxd. other formats are reformatted
# to avi below
video.format <- "cxd"

# setup
difference.lag <- 10
thresholds <- c(10,255) # don't change the second value
#thresholds <- c(50,255)

#####
# FILTERING PARAMETERS
# min and max size: area in pixels
particle_min_size <- 5
particle_max_size <- 1000

# number of adjacent frames to be considered for linking particles
trajectory_link_range <- 3
# maximum distance a particle can move between two frames
trajectory_displacement <- 16

```

```

# these values are in the units defined by the parameters above:
# fps (seconds),
#measured_volume (microliters) and pixel_to_scale (micrometers)
filter_min_net_disp <- 25
filter_min_duration <- 1
filter_detection_freq <- 0.1
filter_median_step_length <- 3

#####
# MORE PARAMETERS (USUALLY NOT CHANGED)

# set paths to ImageJ and particle linker standalone
IJ.path <- "/home/felix/bin/ImageJ"
to.particlelinker <- "/home/felix/bin/ParticleLinker"

# directories and file names
to.data <- paste(getwd(),"/",sep="")
video.description.folder <- "0_video_description/"
video.description.file <- "video_description.txt"
raw.video.folder <- "1_raw/"
particle.data.folder <- "2_particle_data/"
trajectory.data.folder <- "3_trajectory_data/"
temp.overlay.folder <- "4a_temp_overlays/"
overlay.folder <- "4_overlays/"
merged.data.folder <- "5_merged_data/"
ijmacs.folder <- "ijmacs/"

# RAM allocation
memory.alloc <- c(60000)

# RAM per particle linker instance
memory.alloc.perLinker <- c(10000)

#####
# VIDEO ANALYSIS

# identify particles
locate_and_measure_particles(to.data, raw.video.folder,
particle.data.folder,
difference.lag, thresholds, min_size = particle_min_size,

```

```

max_size = particle_max_size, IJ.path, memory.alloc)

# link the particles
link_particles(to.data, particle.data.folder, trajectory.data.folder,
linkrange = trajectory_link_range, disp = trajectory_displacement,
start_vid = 1, memory = memory.alloc,
memory_per_linkerProcess = memory.alloc.perLinker)

# merge info from description file and data
merge_data(to.data, particle.data.folder, trajectory.data.folder,
video.description.folder, video.description.file, merged.data.folder)

# load the merged data
load(paste0(to.data, merged.data.folder, "Master.RData"))

# filter data: minimum net displacement, their duration, the detection
#frequency and the median step length
trajectory.data.filtered <- filter_data(trajectory.data,
filter_min_net_disp, filter_min_duration, filter_detection_freq,
filter_median_step_length)

# summarize trajectory data to individual-based data
morph_mvt <- summarize_trajectories(trajectory.data.filtered,
calculate.median=F, write = T, to.data, merged.data.folder)

# get Sample level info
summarize_populations(trajectory.data.filtered, morph_mvt,
write=T, to.data, merged.data.folder, video.description.folder,
video.description.file, total_frames)

# create overlays for validation
create_overlays(trajectory.data.filtered, to.data,
merged.data.folder, raw.video.folder, temp.overlay.folder,
overlay.folder, 2048, 2048, difference.lag, type = "label",
predict_spec = F, IJ.path, contrast.enhancement = 1,
memory = memory.alloc)

```

S.3.3 Beverton-Holt model fitting

We ran population growth models with vaguely informative priors (i.e. mean estimates matched to observed data but with broad enough standard deviation to avoid constraining models). Model estimations were done using log-transformed parameters. Following parameters and priors were used for model fitting:

- $K.prior = \log(1e5)$
- $K.sd.prior = 0.5$
- $r0.prior = -2.3$
- $r0.sd.prior = 0.5$
- $d.prior = -2.3$
- $d.sd.prior = 1.5$
- $N0.prior = \log(1e3)$
- $N0.sd.prior = 0.5$
- $iter = 1e4$
- $warmup = 1e3$

S.3.4 Additional results

S.3.4.1 Model comparison and summary table local adaptation test

Table S3.3: Model comparison table (of the dredge function) for the model for evolution of intrinsic rate of increase r_0 using AICc comparison.

Intercept	Gene flow	Abiotic conditions	Reproduction	Gene flow × Abiotic conditions	Gene flow × Reproduction	Abiotic conditions × Reproduction	Gene flow × Abiotic conditions × Reproduction	df	logLik	AICc	delta	weight
0.0260	+	+	+		+			6	18.100	-21.088	0	0.32
-0.0009	+	+	+	+	+			7	19.383	-20.458	0.630	0.24
0.009	+	+	+		+	+		7	18.778	-19.249	1.839	0.13
-0.0223	+	+	+	+	+	+		8	20.334	-18.908	2.180	0.11
0.1085		+						3	12.5652	-18.330	2.757	0.08
0.1268		+	+					4	12.7706	-16.162	4.926	0.023
0.1064	+	+						4	12.5679	-15.756	5.331	0.021
-0.0104	+	+	+	+	+	+	+	9	20.545	-15.590	5.500	0.02
0.0932		+	+			+		5	13.797	-15.452	5.636	0.02
0.0742	+	+		+				5	13.542	-14.942	6.146	0.01
0.1258	+	+	+					5	12.771	-13.400	7.688	0.01
0.0955	+	+	+	+				6	13.835	-12.560	8.528	0.00
0.0951	+	+	+			+		6	13.800	-12.488	8.600	0.00
0.0588	+	+	+	+		+		7	15.162	-12.016	9.072	0.00
0.3616								2	-12.1237	28.635	49.722	0.00
0.3111	+							3	-11.8343	30.469	51.557	0.00
0.3799			+					3	-12.0759	30.952	52.040	0.00
0.1978	+		+		+			5	-10.016	32.1743	53.262	0.00
0.3278	+		+					4	-11.799	32.9766	54.064	0.00

Table S3.4: Relative importance (RI) of the different independent variables obtained with AICc comparison of all possible models testing local adaptation as the evolution of intrinsic rate of increase r_0 .

Independent factor	RI
Abiotic conditions	0.998
Gene flow	0.898
Reproduction	0.880
Reproduction×Gene flow	0.815
Abiotic conditions×Gene flow	0.387
Reproduction×Abiotic conditions	0.284
Abiotic conditions×Reproduction×Gene flow	0.021

Table S3.5: Summary table of the best model for evolution of intrinsic rate of increase r_0 according to AICc model comparison.

	Estimate	Std. Error	t value	Pr(> t)
(Intercept)	0.0260	0.0602	0.432	0.6688
Reproduction “Sexual”	0.1587	0.0798	1.9890	0.0562
Gene flow “Present”	0.1808	0.0767	2.356	0.0254
Abiotic conditions “Gradient”	0.6013	0.0543	11.072	<0.0001
Reproduction “Sexual”× Gene flow “Present”	-0.3488	0.1068	-3.267	0.0028

S.3.4.2 Expansion rate

In order to assess the effect of gradient, sex and gene flow on expansion rate (as in total number of patches expanded during the range expansion experiment), we fit a linear model (‘stats’-package) with total distance expanded as a function of pH gradient (gradient/no gradient), sex (sex/no sex) and gene flow (gene flow/no gene flow). We then used the dredge function (‘MuMin’-package, version 1.43.6) using AICc comparison to select the best model.

Table S3.6: Model comparison table (of the dredge function) for the model for expansion rate using AICc comparison.

Intercept	Gene flow	Abiotic conditions	Reproduction	Gene flow × Abiotic conditions	Gene flow × Reproduction	Abiotic conditions × Reproduction	Gene flow × Abiotic conditions × Reproduction	df	logLik	AICc	delta	weight
22.9500		+						3	-43.483	93.794	0.000	0.34
22.7374		+	+					4	-42.546	94.521	0.726	0.24
22.9000		+	+			+		5	-41.649	95.520	1.726	0.15
22.9822	+	+						4	-43.464	96.356	2.562	0.10
22.7659	+	+	+					5	-42.532	97.283	3.488	0.06
22.9230	+	+	+			+		6	-41.638	98.506	4.712	0.03
22.9000	+	+		+				5	-43.230	98.682	4.887	0.03
22.6905	+	+	+	+				6	-42.307	99.845	6.051	0.02
22.6933	+	+	+		+			6	-42.444	100.124	6.325	0.01
22.8182	+	+	+		+	+		7	-41.397	101.270	7.479	0.01
22.8500	+	+	+	+		+		7	-41.431	101.342	7.548	0.01
22.6143	+	+	+	+	+			7	-42.214	102.908	9.113	0.00
22.7422	+	+	+	+	+	+		8	-41.179	104.359	10.565	0.00
22.8000	+	+	+	+	+	+	+	9	-41.047	107.919	14.125	0.00
21.3939								2	-71.794	147.990	54.195	0.00
21.8571	+							3	-71.210	149.248	55.454	0.00
21.1177			+					3	-71.497	149.822	56.028	0.00
21.5824	+		+					4	-70.924	151.277	57.482	0.00
21.5714	+		+		+			5	-70.924	154.070	60.275	0.00

Table S3.7: Relative importance (RI) of the different independent variables obtained with AICc comparison of all possible models testing range expansion rate (total number of successful dispersal events).

Independent factor	RI
Gene flow	0.273
Abiotic conditions	1
Reproduction	0.531
Gene flow×Abiotic conditions	0.061
Gene flow×Reproduction	0.029
Abiotic conditions×Reproduction	0.196
Gene flow×Abiotic conditions×Reproduction	0

Table S3.8: Type III ANOVA table of the best model for expansion rate, based on the AICc criterion.

	Degrees of freedom	F-value	Pr (>F)
Abiotic conditions	1	141.4	<0.0001
Residuals	31		

Table S3.9: Summary table of the best model for expansion rate, based on the AICc criterion.

	Estimate	Std. Error	t value	Pr(> t)
(Intercept)	22.950	0.209	110.08	<0.0001
Abiotic conditions “Gradient”	-3.950	0.332	-11.89	<0.0001

S.3.4.3 Density dynamics during range expansion

We tested for changes in population density during the range expansion experiment by fitting a linear mixed model (‘nlme’-package, version 3.1-137) of population density as a function of 1) range expansion distance (number of successful dispersal events), 2) abiotic conditions, 3) reproduction and 4) gene flow, with replicate population as a random factor. We first fit a full interaction model using the maximum likelihood method, and then used the dredge function (‘MuMin’-package, version 1.43.6) to find the best model based on the BIC (Bayesian Information Criterion) score. We then refit the best model using the restricted maximum likelihood method and used this best model to create model predictions. Due to the large size of the table, full model comparison is not included in this document, but model code to recreate the table is shown below. Only abiotic conditions, range expansion distance and their interaction strongly influenced

population density (see table S3.10 for relative importances).

Model comparison code

```
full.model <- lme(data=data.all, dens.front~Gradient*Sex*
Gene.Flow*pos, random = ~1|ID, method = "ML")
comp <- dredge(full.model, rank = BIC)
best.model <- lme(data=data.all, dens.front~Gradient*pos,
random = ~1|ID, method = "REML")
```

Table S3.10: Relative importance (RI) of the different independent variables obtained with BIC comparison of all possible models testing population density during range expansion.

Independent factor	RI
Gene flow	0.266
Abiotic conditions	1
Distance expanded (position)	1
Reproduction	0.085
Gene flow×Abiotic conditions	0.011
Gene flow×Range expansion distance	0.012
Gene flow×Reproduction	0.001
Abiotic conditions×Range expansion distance	1
Abiotic conditions×Reproduction	0.003
Position×Reproduction	0.004
Gene flow×Abiotic conditions×Range expansion distance	0
Gene flow×Abiotic conditions×Reproduction	0
Gene flow×Range expansion distance×Reproduction	0
Abiotic conditions×Range expansion distance×Reproduction	0
Gene flow×Abiotic conditions×Range expansion distance×Reproduction	0

Table S3.11: Type III ANOVA table of the best model (fixed effects only) for population density dynamics, based on the BIC criterion.

	DF	χ^2	p-value
(Intercept)	1	660.541	<0.0001
Abiotic conditions	1	0.044	0.833
Range expansion distance	1	4.526	0.034
Abiotic conditions×Range expansion distance	1	108.258	<0.0001

Table S3.12: Summary table of the best model (fixed effects only) for population density dynamics, based on the BIC criterion.

	Value	Std.Error	DF	t-value	p-value
(Intercept)	165899.37	6454.979	746	25.701	<0.0001
Abiotic conditions “Gradient”	2016.96	9581.401	38	0.211	0.834
Range expansion distance	-924.67	434.642	746	-2.127	0.0337
Abiotic conditions “Gradient” × Range expansion distance	-7244.62	696.283	746	-10.405	<0.0001

S.3.4.4 Adaptation test raw evolution data

We tested differences using the raw intrinsic rate of increase r_0 (not standardized to the ancestor data by fitting a linear model (‘stats’-package) with abiotic conditions (“Uniform” or ”Gradient), reproduction (“Sexual”, “Asexual”) and gene flow (“Absent”, “Present”) as fixed factors. We fit the full interaction model, and then used the dredge function (‘MuMin’-package, version 1.43.6) to compare all models using the AICc criterion.

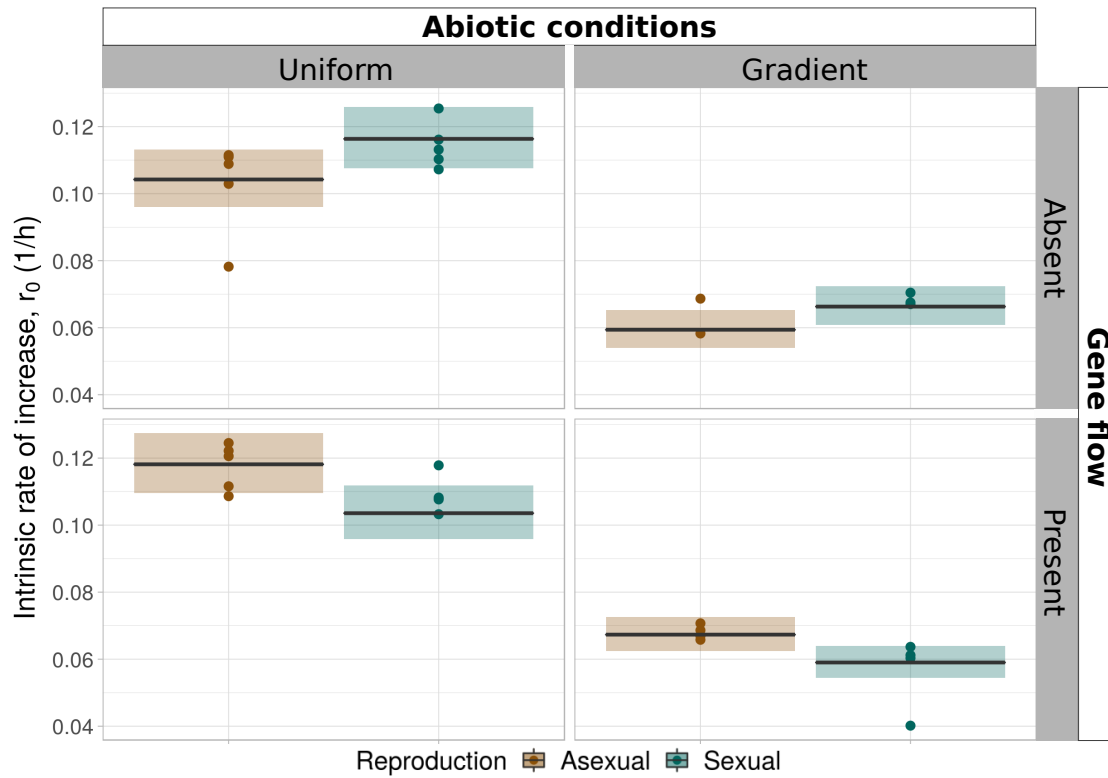


Figure S3.2: Evolution of intrinsic rate of increase r_0 based on the raw r_0 -values. Y-axis shows r_0 . Dots represent measurements, boxplots show the model predictions of the best model (mean and 95 % confidence intervals). Brown boxes and dots represent populations for treatment groups designated for asexual reproduction, green boxes and dots for treatment groups designated for sexual reproduction.

Table S3.13: Model comparison table (of the dredge function) for the model for evolution of intrinsic rate of increase r_0 based on the raw values, using AICc comparison.

Intercept	Gene flow	Abiotic conditions	Reproduction	Gene flow × Abiotic conditions	Gene flow × Reproduction	Abiotic conditions × Reproduction	Gene flow × Abiotic conditions × Reproduction	df	logLik	AICc	delta	weight
-2.2611	+	+	+		+			6	30.561	-46.011	0.000	0.32
-2.2798	+	+	+	+	+			7	31.844	-45.381	0.630	0.24
-2.2728	+	+	+		+	+		7	31.240	-44.172	1.839	0.13
-2.2946	+	+	+	+	+	+		8	32.795	-43.831	2.180	0.11
-2.2039		+						3	25.027	-43.253	2.757	0.08
-2.1912		+	+					4	25.232	-41.085	4.926	0.03
-2.2054	+	+						4	25.029	-40.679	5.331	0.02
-2.2864	+	+	+	+	+	+	+	9	33.007	-40.513	5.498	0.02
-2.2146		+	+			+		5	26.259	-40.375	5.636	0.02
-2.2277	+	+		+				5	26.004	-39.864	6.146	0.01
-2.1920	+	+	+					5	25.233	-38.323	7.688	0.01
-2.2129	+	+	+	+				6	26.297	-37.482	8.528	0.00
-2.2132	+	+	+			+		6	26.261	-37.411	8.600	0.00
-2.2384	+	+	+	+		+		7	27.623	-36.939	9.072	0.00
-2.4317								2	-6.835	18.058	64.069	0.00
-2.3899	+							3	-6.566	19.932	65.942	0.00
-2.4190			+					3	-6.804	20.408	66.419	0.00
-2.3740	+		+					4	-6.522	22.423	68.434	0.00
-2.4218	+		+		+			5	-6.207	24.556	70.567	0.00

Table S3.14: Type III ANOVA table of the best model for evolution of intrinsic rate of increase r_0 using raw r_0 -values, based on the AICc criterion.

	Degrees of freedom	F-value	Pr (>F)
--	--------------------	---------	---------

Reproduction	1	3.956	0.056
Gene flow	1	5.5525	0.025
Abiotic conditions	1	223.165	<0.0001
Reproduction × Gene flow	1	10.675	0.003
Residuals	29		

Table S3.15: Summary table of the best model for evolution of intrinsic rate of increase r_0 using raw r_0 -values, based on the AICc criterion.

	Estimate	Std. Error	t value	Pr(> t)
(Intercept)	-2.2611	0.0417	-54.2000	<.0001
Reproduction “Sexual”	0.1100	0.0553	1.9890	0.0562
Gene flow “Present”	0.1253	0.0532	2.356	0.0254
Abiotic conditions “Gradient”	-0.5624	0.0376	-14.9390	<.0001
Reproduction “Sexual” × Gene flow “Present”	-0.2418	0.0740	-3.267	0.0028

S.3.4.5 Evolution test over whole pH range

In order to test evolution of the entire pH-niche, we fit a linear mixed model (‘nlme’-package, version 3.1-137) of change in intrinsic rate of increase r_0 as a function of 1) abiotic conditions (“Uniform”. “Gradient”), 2) reproduction (“Asexual”. “Sexual”), 3) gene flow (“Absent”. “Present”) and 4) pH of the assay medium, using population ID as a random effect. To account for potential non-linear responses to pH, we fit pH of the assay medium as a factor (pHfact). Change in intrinsic rate of increase was calculated as before, by dividing the r_0 of an assay culture by the mean value of the ancestors, and subsequently calculating the logarithm (base 2) of this ratio. We first fit the full interaction model based on the maximum likelihood method, and then used the dredge function (‘MuMin’-package, version 1.43.6) with BIC criterion to determine the best model. We then refit this model using the restricted maximum likelihood method to obtain model estimates and model predictions. Due to the table size, a full model comparison is not included, but the code used to obtain this table is listed below. Model comparison resulted in one clearly preferred model (model weight = 0.713; all other models had $\delta\text{BIC} > 2$), with gradient and pHfact as the only included fixed effects. Note that only data with pH of 4.0 or higher is used, as ancestors typically only survived up to pH 4.0, and it was hence not possible for lower pH values to compare intrinsic rate of increase between ancestors and evolved populations.

Model comparison code:

```
full.model <- lme(data = dd.all, logratio ~ Gradient*Sex*Gene.Flow*pHfact, random = ~ 1|ID, method = "ML")
```

```
t.all <- dredge(full.model, rank = BIC)
```

```
best.model <- lme(data = dd.all, logratio ~ Gradient + pHfact, random = ~ 1|ID, method = "REML")
```

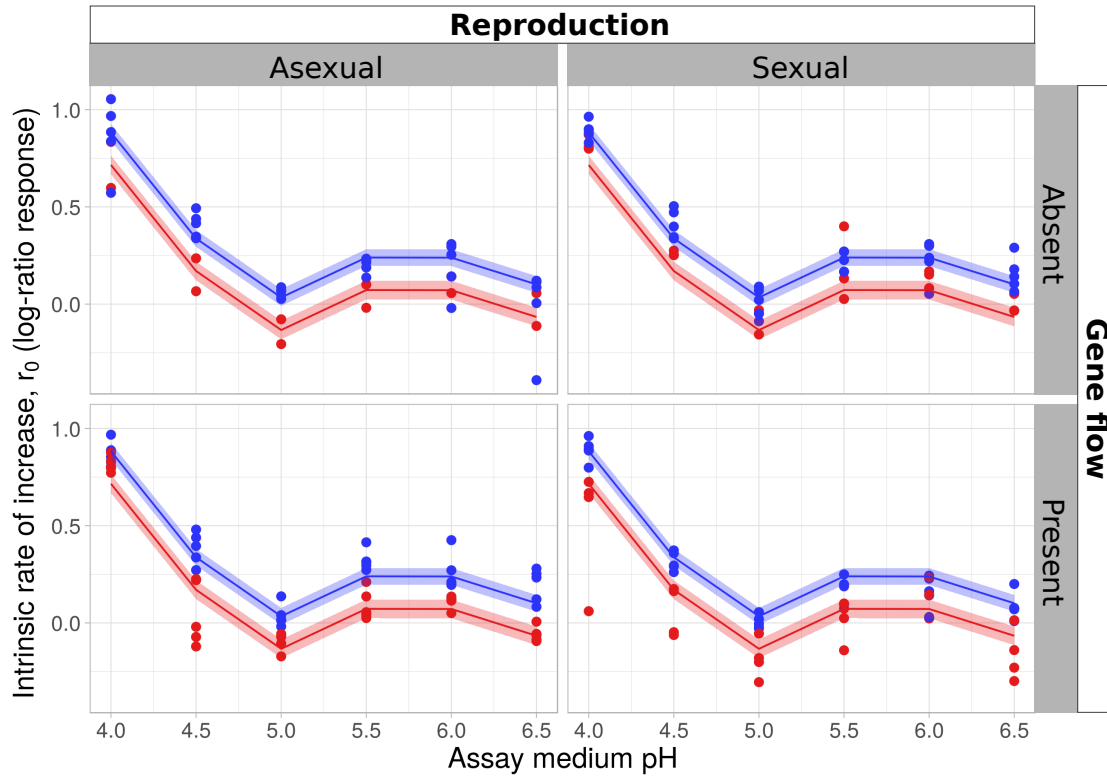


Figure S3.3: Evolution of intrinsic rate of increase r_0 over all pH values. The y-axis shows the change in r_0 compared to the ancestor, calculated as the logarithm (base 2) of the r_0 of the evolved population divided by the mean r_0 of the ancestors. Dots represent measurements, Lines and shaded areas show the model predictions of the best model (mean and 95 % confidence intervals). Blue lines, shaded areas and dots represent data and model predictions for the populations evolved without a pH gradient, red lines, shaded areas and dots for populations evolving with a pH gradient.

Table S3.16: Type III ANOVA table of the best model (fixed effects only) for evolution of intrinsic rate of increase r_0 over all measured pH values, based on the BIC criterion.

	DF	F-value	p-value
--	----	---------	---------

(Intercept)	1	356.2741	<.0001
Abiotic conditions	1	43.063	<.0001
pH of assay medium (factorial)	5	1796.068	<.0001

Table S3.17: Summary table (fixed effects only) of the best model for evolution of intrinsic rate of increase r_0 over all measured pH values, based on the BIC criterion.

	Value	Std.Error	DF	t-value	p-value
(Intercept)	0.8828	0.0219	165	40.2775	<.0001
Abiotic conditions “Gradient”	-0.1673	0.0255	32	-6.5622	<.0001
pH of assay medium (4.5)	-0.5452	0.02256	165	-24.1297	<.0001
pH of assay medium (5)	-0.8486	0.0226	165	-37.5602	<.0001
pH of assay medium (5.5)	-0.6431	0.0226	165	-28.4639	<.0001
pH of assay medium (6)	-0.6438	0.0226	165	-28.4958	<.0001
pH of assay medium (6.5)	-0.7816	0.0226	165	-34.5944	<.0001

S.3.4.6 Survival probability

We measured survival by assessing at the end of the experimental range expansion, how many populations survived until the common garden stage, as populations sometimes died out after colonizing a new patch in the two-patch landscape, especially when expanding into a gradient. In order to test how survival of populations was affected by 1) abiotic conditions (“Uniform”/“Gradient”), 2) reproduction (“Asexual”/“Sexual”) and 3) gene flow (“Absent”/“Present”), we used generalized linear models with survival as a binomial response variable. Due to limitations in the data, where many one (1/survived) values were present and only few zero (0/extinct), we used Bayesian generalized linear models, as frequentist models did not converge properly when estimating the parameters, resulting in inflated standard deviation estimates. We created all possible models using the ‘Rethinking’-package (version 1.59), starting from a full interaction model to the intercept models, and then weighted the models using the WAIC criterion. We used the weighted estimates to calculate relative importance (RI) of the independent factors and to create weighted predictions, as show in figure S3.4. We used vaguely informative priors, meaning we included estimates that approximately corresponded to expected values, but including broad enough standard deviations, so models were not constrained too strongly in convergence. Below follows a list of the prior information and model structure:

- Survival probability \sim binom(1, p)
- p = intercept + independent factors

- $\text{intercept} \sim \text{dnorm}(0, 1)$
- All other independent factors $\sim \text{dnorm}(0, 10)$

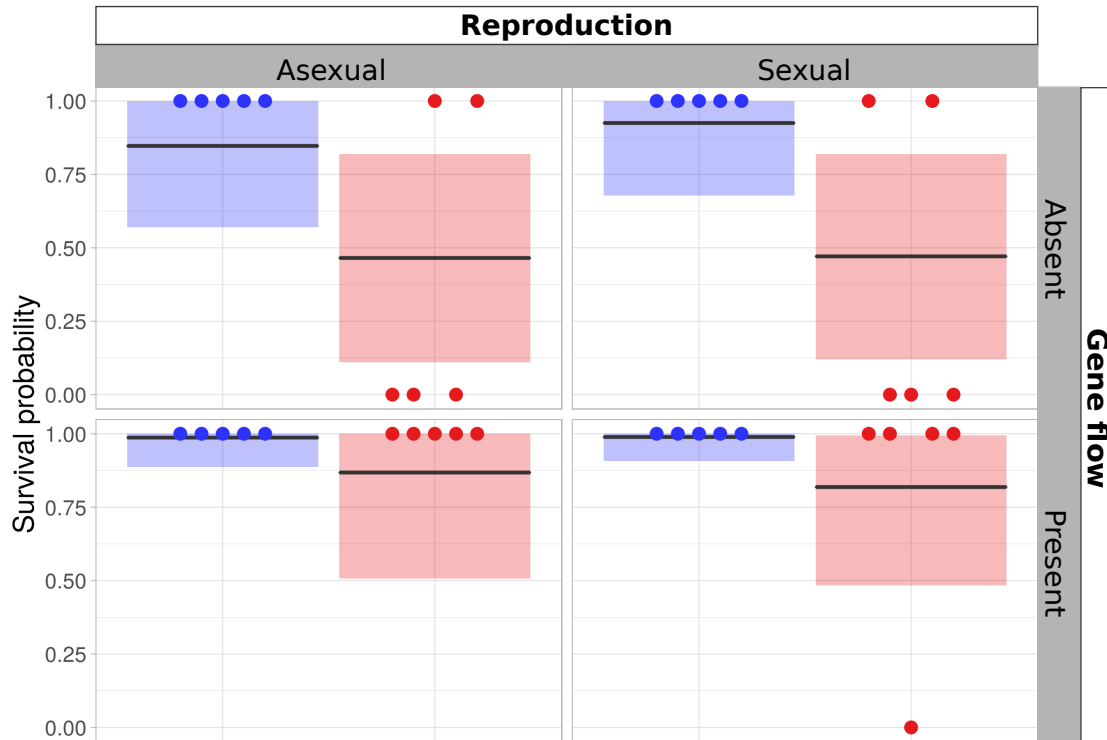


Figure S3.4: Survival of populations at the end of the range expansion experiment. Dots represent individual datapoints of populations that either survived (1) or went extinct (0). The boxes show the weighted predictions of survival based on the WAIC weighting on all Bayesian survival models, with the line representing the mean, and the range of the boxes the 95 % probability interval. Blue dots and boxes represent the populations expanding in a landscape without uniform abiotic conditions and red dots and boxes the populations expanding into a gradient.

Table S3.18: Relative importance (RI) of the effect of the independent factors on the survival probability of the populations during range expansion.

Independent factor	RI
Abiotic conditions	1
Gene flow	0.95
Reproduction	0.68

Reproduction×Gene flow	0.41
Abiotic conditions×Gene flow	0.34
Reproduction×Abiotic conditions	0.35
Abiotic conditions×Reproduction×Gene flow	0.09

S.3.4.7 Morphology: cell size

We assessed morphology (cell size and elongation) as well as cell movement (movement speed and turning angles) by fitting linear mixed models for these four response variables, using all the data of the bioassays (i.e. using measurements at every timepoint of the bioassays) as a function of 1) abiotic conditions, 2) reproduction, 3) gene flow, 4) pH of the assay medium and 5) population density (standardized as the proportion of population equilibrium density). We used this approach to test whether there was a difference between the eight treatment groups, while at the same time accounting for plastic effects associated with population density and pH. We used both replicate during experimental evolution and replicate population during bioassays as random effects. We compared models using the Dredge function in the MuMin package, however, as for the full model, the total number of levels of the explanatory variables exceeded the number the dredge function can handle (>30), we resorted to an extra step for model comparison.

We first created the full interaction model with all five explanatory variables, and calculated the BIC score. Next, we created all interaction models where one of the variables had been dropped from the full interaction model, and used the dredge function to compare all simplified models based on the BIC criterion. We then compared over all models which model had lowest BIC score.

Model comparison code:

```
#Do manual comparison
{
  full.model.size.evo <- lme(data = dd.evo,
    major_mean ~ percK*testpH*Gradient*Sex*Gene.Flow,
    random = list(ID=~1, curveID=~1), method = "ML")

  t1 <- dredge(lme(data = dd.evo,
    major_mean ~ testpH*Gradient*Sex*Gene.Flow,
    random = list(ID=~1, curveID=~1), method = "ML"), rank = BIC)

  t2 <- dredge(lme(data = dd.evo,
    major_mean ~ percK*Gradient*Sex*Gene.Flow,
    random = list(ID=~1, curveID=~1), method = "ML"), rank = BIC)
```

```

t3 <- dredge(lme(data = dd.evo,
  major_mean ~ percK*testpH*Sex*Gene.Flow,
  random = list(ID=~1, curveID=~1), method = "ML"), rank = BIC)

t4 <- dredge(lme(data = dd.evo,
  major_mean ~ percK*testpH*Gradient*Sex,
  random = list(ID=~1, curveID=~1), method = "ML"), rank = BIC)

t5 <- dredge(lme(data = dd.evo,
  major_mean ~ percK*testpH*Gradient*Gene.Flow,
  random = list(ID=~1, curveID=~1), method = "ML"), rank = BIC)

BIC(full.model.size.evo)
t1[1, "BIC"]
t2[1, "BIC"]
t3[1, "BIC"]
t4[1, "BIC"]
t5[1, "BIC"]
}

#best model
best.model.size.evo <- lme(data = dd.evo,
  major_mean ~ percK*testpH ,
  random = list(ID=~1, curveID=~1))

anova(best.model.size.evo)
summary(best.model.size.evo)
Anova(best.model.size.evo, contrasts=list(topic=contr.sum,
sys=contr.sum), type=3)

plot(best.model.size.evo)
}

```

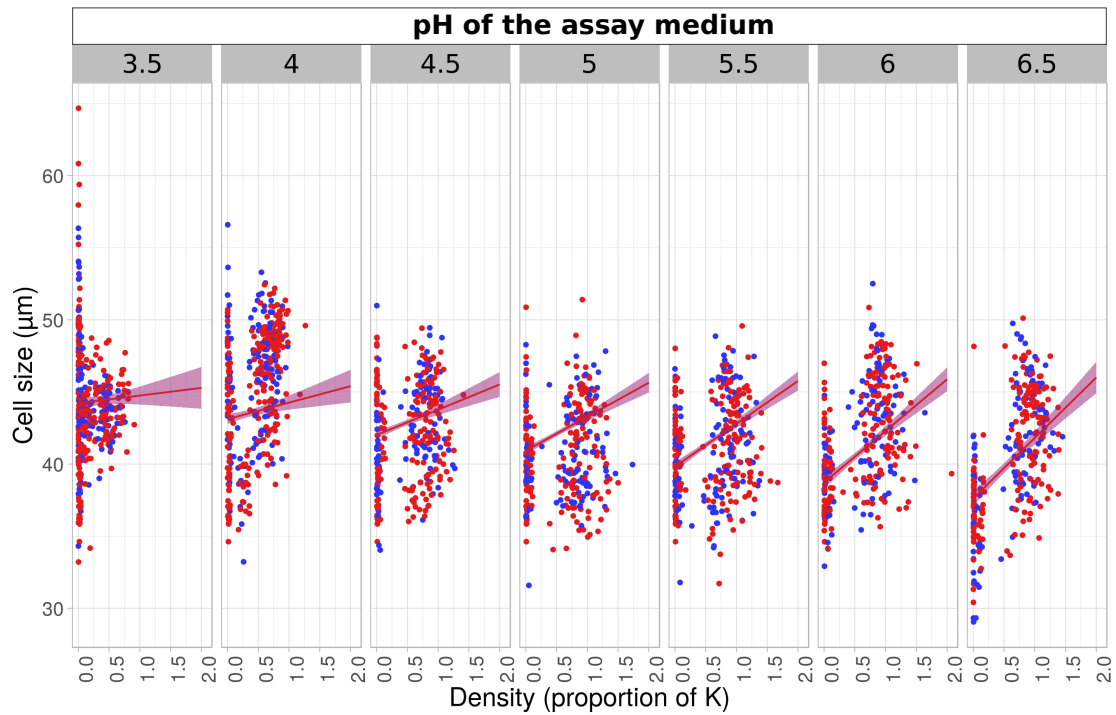


Figure S3.5: Cell size (longest axis through the cell) plotted to the standardized population density (percentage of the population equilibrium density K). Dots show datapoints, and full lines and shaded areas the model predictions (means and 95 % confidence intervals). Blue dots, lines and shaded areas represent data and predictions from populations that expanded into uniform abiotic conditions during the range expansion experiment. Red dots, lines and shaded areas show data and predictions for populations that expanded into a gradient during the range expansion experiment. The different panels represent the pH values of the assay medium in which the traits were measured.

Table S3.19: Type III ANOVA table of the best model for evolution of cell size, based on the BIC criterion.

	F-value	Degrees of freedom	Pr (>F)
(Intercept)	9.535	1	0.002
pH of assay medium	395.909	1	<0.0001
Density (prop. of K)	4.941	1	0.026
pH of assay medium \times Density (prop. of K)	24.277	1	<0.0001

Table S3.20: Summary table of the best model for evolution of cell size, based on the BIC criterion.

	Value	Std.Error	DF	t-value	p-value
(Intercept)	51.911	0.662	2024	78.380	<0.0001
pH of assay medium	-2.198	0.136	200	-16.220	<0.0001
Density (prop. of K)	-3.734	1.202	2024	-3.105	0.002
pH of assay medium × Density (prop. of K	1.219	0.228	2024	5.33	<0.0001

S.3.4.8 Morphology: cell elongation

We assessed morphology (cell size and elongation) as well as cell movement (movement speed and turning angles) by fitting linear mixed models for these four response variables, using all the data of the bioassays (i.e. using measurements at every timepoint of the bioassays) as a function of 1) abiotic conditions, 2) reproduction, 3) gene flow, 4) pH of the assay medium and 5) population density (standardized as the proportion of population equilibrium density). We used this approach to test whether there was a difference between the eight treatment groups, while at the same time accounting for plastic effects associated with population density and pH. We used both replicate during experimental evolution and replicate population during bioassays as random effects. We compared models using the Dredge function in the MuMin package, however, as for the full model, the total number of levels of the explanatory variables exceeded the number the dredge function can handle (>30), we resorted to an extra step for model comparison.

We first created the full interaction model with all five explanatory variables, and calculated the BIC score. Next, we created all interaction models where one of the variables had been dropped from the full interaction model, and used the dredge function to compare all simplified models based on the BIC criterion. We then compared over all models which model had lowest BIC score.

Model comparison code:

```
#Do manual comparison
{
  full.model.elong.evo <- lme(data = dd.evo,
    major_mean/minor_mean ~ perck*testpH*Gradient*Sex*Gene.Flow,
    random = list(ID=~1, curveID=~1), method = "ML")

  t1 <- dredge(lme(data = dd.evo,
    major_mean/minor_mean ~ testpH*Gradient*Sex*Gene.Flow,
    random = list(ID=~1, curveID=~1), method = "ML"), rank = BIC)
```

```

t2 <- dredge(lme(data = dd.evo,
  major_mean/minor_mean ~ percK*Gradient*Sex*Gene.Flow,
  random = list(ID=~1, curveID=~1), method = "ML"), rank = BIC)

t3 <- dredge(lme(data = dd.evo,
  major_mean/minor_mean ~ percK*testpH*Sex*Gene.Flow,
  random = list(ID=~1, curveID=~1), method = "ML"), rank = BIC)

t4 <- dredge(lme(data = dd.evo,
  major_mean/minor_mean ~ percK*testpH*Gradient*Sex,
  random = list(ID=~1, curveID=~1), method = "ML"), rank = BIC)

t5 <- dredge(lme(data = dd.evo,
  major_mean/minor_mean ~ percK*testpH*Gradient*Gene.Flow,
  random = list(ID=~1, curveID=~1), method = "ML"), rank = BIC)

BIC(full.model.elong.evo)
t1[1, "BIC"]
t2[1, "BIC"]
t3[1, "BIC"]
t4[1, "BIC"]
t5[1, "BIC"]
}

#best model
best.model.elong.evo <- lme(data = dd.evo,
  major_mean/minor_mean ~ Gradient*percK + percK*testpH ,
  random = list(ID=~1, curveID=~1))

anova(best.model.elong.evo)
summary(best.model.elong.evo)
Anova(best.model.elong.evo, contrasts=list(topic=contr.sum,
sys=contr.sum), type=3)

plot(best.model.elong.evo)
}

```

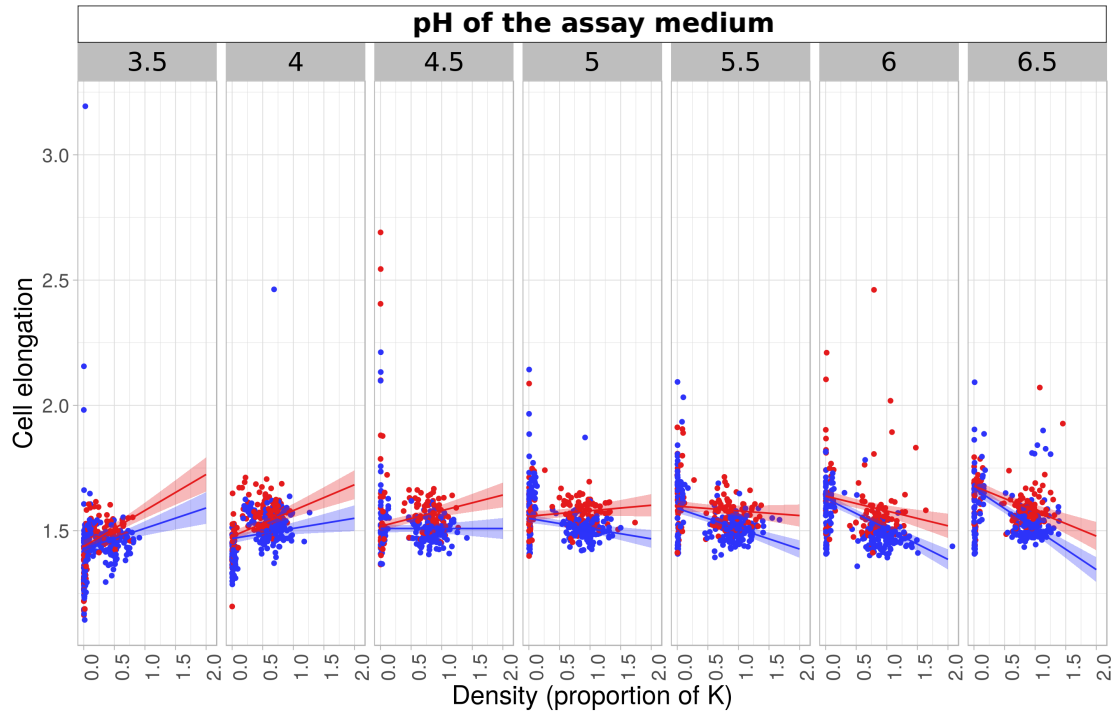


Figure S3.6: Cell elongation (ratio between longest and shortest axis through the cell) plotted to the standardized population density (percentage of the population equilibrium density K). Dots show datapoints, and full lines and shaded areas the model predictions (means and 95 % confidence intervals). Blue dots, lines and shaded areas represent data and predictions from populations that expanded into uniform abiotic conditions during the range expansion experiment. Red dots, lines and shaded areas show data and predictions for populations that expanded into a gradient during the range expansion experiment. The different panels represent the pH values of the assay medium in which the traits were measured.

Table S3.21: Type III ANOVA table of the best model for evolution of cell elongation, based on the BIC criterion.

	F-value	Degrees of freedom	Pr (>F)
(Intercept)	1692.8215	1	<0.0001
Abiotic conditions	0.3924	1	0.5311
Density (proportion of K)	54.4074	1	<0.0001
pH of assay medium	212.1209	1	<0.0001
Abiotic conditions "Gradient"×			
Density (prop. of K)	12.6971	1	0.0004
Density (proportion of K)×			

pH of assay medium | 76.2551 | 1 | <0.0001

Table S3.22: Summary table of the best model for evolution of cell elongation, based on the BIC criterion.

	Value	Std.Error	DF	t-value	p-value
(Intercept)	1.147	0.028	2023	41.143	<0.0001
Abiotic conditions “Gradient”	0.009	0.014	32	0.626	0.5355
Density (proportion of K)	0.365	0.049	2023	7.376	<0.0001
pH of assay medium	0.080	0.006	200	14.564	<0.0001
Abiotic conditions “Gradient”× Density (prop. of K)	0.063	0.018	2023	3.563	0.0004
Density (proportion of K)× pH of assay medium	-0.081	0.009	2023	-8.732	<0.0001

S.3.4.9 Movement: cell speed

We assessed morphology (cell size and elongation) as well as cell movement (movement speed and turning angles) by fitting linear mixed models for these four response variables, using all the data of the bioassays (i.e. using measurements at every timepoint of the bioassays) as a function of 1) abiotic conditions, 2) reproduction, 3) gene flow, 4) pH of the assay medium and 5) population density (standardized as the proportion of population equilibrium density). We used this approach to test whether there was a difference between the eight treatment groups, while at the same time accounting for plastic effects associated with population density and pH. We used both replicate during experimental evolution and replicate population during bioassays as random effects. We compared models using the Dredge function in the MuMin package, however, as for the full model, the total number of levels of the explanatory variables exceeded the number the dredge function can handle (>30), we resorted to an extra step for model comparison.

We first created the full interaction model with all five explanatory variables, and calculated the BIC score. Next, we created all interaction models where one of the variables had been dropped from the full interaction model, and used the dredge function to compare all simplified models based on the BIC criterion. We then compared over all models which model had lowest BIC score.

Model comparison code:

```
#Do manual comparison
{
  full.model.speed.evo <- lme(data = dd.evo,
```

```

gross_speed_mean ~ percK*testpH*Gradient*Sex*Gene.Flow,
random = list(ID=~1, curveID=~1), method = "ML")

t1 <- dredge(lme(data = dd.evo,
  gross_speed_mean ~ testpH*Gradient*Sex*Gene.Flow,
  random = list(ID=~1, curveID=~1), method = "ML"), rank = BIC)

t2 <- dredge(lme(data = dd.evo,
  gross_speed_mean ~ percK*Gradient*Sex*Gene.Flow,
  random = list(ID=~1, curveID=~1), method = "ML"), rank = BIC)

t3 <- dredge(lme(data = dd.evo,
  gross_speed_mean ~ percK*testpH*Sex*Gene.Flow,
  random = list(ID=~1, curveID=~1), method = "ML"), rank = BIC)

t4 <- dredge(lme(data = dd.evo,
  gross_speed_mean ~ percK*testpH*Gradient*Sex,
  random = list(ID=~1, curveID=~1), method = "ML"), rank = BIC)

t5 <- dredge(lme(data = dd.evo,
  gross_speed_mean ~ percK*testpH*Gradient*Gene.Flow,
  random = list(ID=~1, curveID=~1), method = "ML"), rank = BIC)

BIC(full.model.speed.evo)
t1[1, "BIC"]
t2[1, "BIC"]
t3[1, "BIC"]
t4[1, "BIC"]
t5[1, "BIC"]
}

#best model
best.model.speed.evo <- lme(data = dd.evo,
  gross_speed_mean ~ Gradient*percK + percK*testpH,
  random = list(ID=~1, curveID=~1))

anova(best.model.speed.evo)
summary(best.model.speed.evo)
Anova(best.model.speed.evo, contrasts=list(topic=contr.sum,
  sys=contr.sum), type=3)

```

```

plot(best.model.speed.evo)
}

```

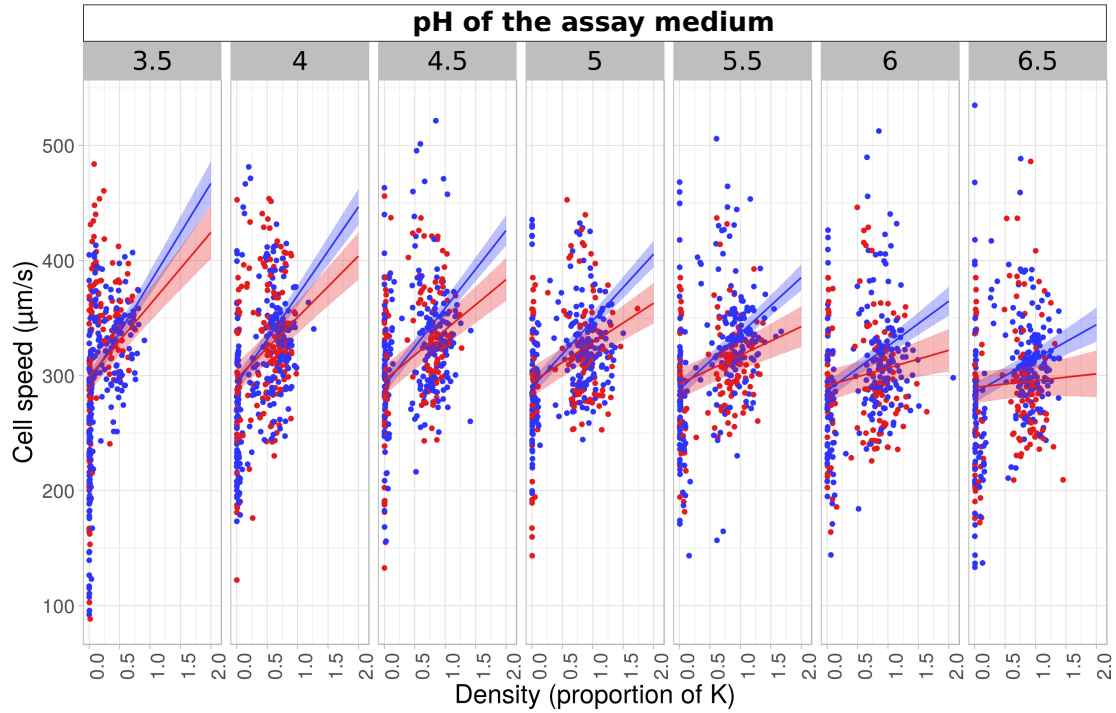


Figure S3.7: Cell swimming speed plotted to the standardized population density (percentage of the population equilibrium density K). Dots show datapoints, and full lines and shaded areas the model predictions (means and 95 % confidence intervals). Blue dots, lines and shaded areas represent data and predictions from populations that expanded into uniform abiotic conditions during the range expansion experiment. Red dots, lines and shaded areas show data and predictions for populations that expanded into a gradient during the range expansion experiment. The different panels represent the pH values of the assay medium in which the traits were measured.

Table S3.23: Type III ANOVA table of the best model for evolution of cell movement speed, based on the BIC criterion.

	F-value	Degrees of freedom	Pr (>F)
(Intercept)	1282.0050	1	<0.0001
Abiotic conditions	0.3693	1	0.543
Density (prop. of K)	117.2553	1	<0.0001

pH of assay medium	3.8034	1	0.051
Abiotic conditions × Density (prop. of K)	21.7046	1	<0.0001
Density (prop. of K) × pH of assay medium	51.4084	1	<0.0001

Table S3.24: Summary table of the best model for evolution of cell movement speed, based on the BIC criterion.

	Value	Std.Error	DF	t-value	p-value
(Intercept)	305.137	8.522	2326	35.8050	<0.0001
Abiotic conditions “Gradient”	4.680	7.701	73	0.607	0.54
Density (proportion of K)	152.605	14.093	2326	10.829	<0.0001
pH of assay medium	-3.083	1.581	200	-1.950	0.053
Abiotic conditions “Gradient” × Density (prop. of K)	-23.676	5.082	2326	-4.659	<0.0001
Density (proportion of K) × pH of assay medium	-18.932	2.640	2326	-7.170	<0.0001

S.3.4.10 Movement: cell turning

We assessed morphology (cell size and elongation) as well as cell movement (movement speed and turning angles) by fitting linear mixed models for these four response variables, using all the data of the bioassays (i.e. using measurements at every timepoint of the bioassays) as a function of 1) abiotic conditions, 2) reproduction, 3) gene flow, 4) pH of the assay medium and 5) population density (standardized as the proportion of population equilibrium density). We used this approach to test whether there was a difference between the eight treatment groups, while at the same time accounting for plastic effects associated with population density and pH. We used both replicate during experimental evolution and replicate population during bioassays as random effects. We compared models using the Dredge function in the MuMin package, however, as for the full model, the total number of levels of the explanatory variables exceeded the number the dredge function can handle (>30), we resorted to an extra step for model comparison.

We first created the full interaction model with all five explanatory variables, and calculated the BIC score. Next, we created all interaction models where one of the variables had been dropped from the full interaction model, and used the dredge function to compare all simplified models based on the BIC criterion. We then compared over all models which model had lowest BIC score.

Model comparison code:

```

#Do manual comparison
{
  full.model.turning.evo <- lme(data = dd.evo,
    sd_turning_mean ~ percK*testpH*Gradient*Sex*Gene.Flow,
    random = list(ID=~1, curveID=~1), method = "ML")

  t1 <- dredge(lme(data = dd.evo,
    sd_turning_mean ~ testpH*Gradient*Sex*Gene.Flow,
    random = list(ID=~1, curveID=~1), method = "ML"), rank = BIC)

  t2 <- dredge(lme(data = dd.evo,
    sd_turning_mean ~ percK*Gradient*Sex*Gene.Flow,
    random = list(ID=~1, curveID=~1), method = "ML"), rank = BIC)

  t3 <- dredge(lme(data = dd.evo,
    sd_turning_mean ~ percK*testpH*Sex*Gene.Flow,
    random = list(ID=~1, curveID=~1), method = "ML"), rank = BIC)

  t4 <- dredge(lme(data = dd.evo,
    sd_turning_mean ~ percK*testpH*Gradient*Sex,
    random = list(ID=~1, curveID=~1), method = "ML"), rank = BIC)

  t5 <- dredge(lme(data = dd.evo,
    sd_turning_mean ~ percK*testpH*Gradient*Gene.Flow,
    random = list(ID=~1, curveID=~1), method = "ML"), rank = BIC)

  BIC(full.model.turning.evo)
  t1[1, "BIC"]
  t2[1, "BIC"]
  t3[1, "BIC"]
  t4[1, "BIC"]
  t5[1, "BIC"]
}

#best model
best.model.turning.evo <- lme(data = dd.evo,
  sd_turning_mean ~ percK*testpH ,
  random = list(ID=~1, curveID=~1))

anova(best.model.turning.evo)

```

```

summary(best.model.turning.evo)
Anova(best.model.turning.evo, contrasts=list(topic=contr.sum,
sys=contr.sum), type=3)

plot(best.model.turning.evo)
}

```

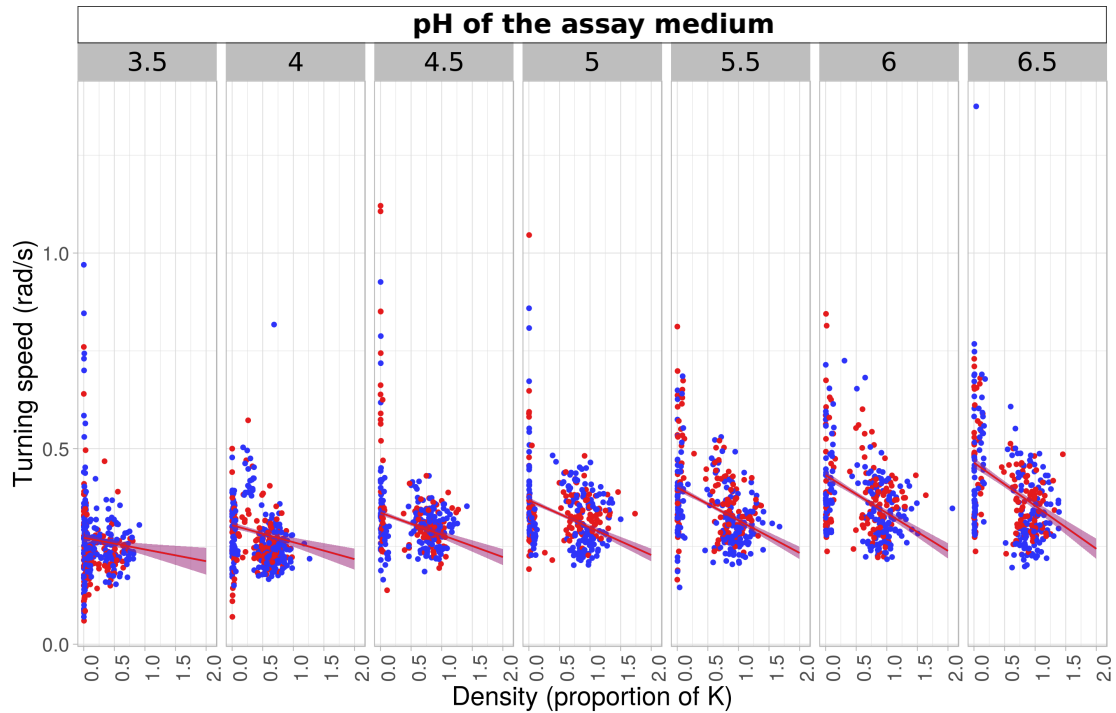


Figure S3.8: Cell turning speed plotted to the standardized population density (percentage of the population equilibrium density K). Dots show datapoints, and full lines and shaded areas the model predictions (means and 95 % confidence intervals). Blue dots, lines and shaded areas represent data and predictions from populations that expanded into uniform abiotic conditions during the range expansion experiment. Red dots, lines and shaded areas show data and predictions for populations that expanded into a gradient during the range expansion experiment. The different panels represent the pH values of the assay medium in which the traits were measured.

Table S3.25: Type III ANOVA table of the best model for evolution of cell turning speed, based on the BIC criterion.

	F-value	Degrees of freedom	Pr (>F)
--	---------	--------------------	---------

(Intercept)	9.535	1	0.002
pH of assay medium	395.909	1	<0.0001
Density (prop. of K)	4.941	1	0.026
pH of assay medium × Density (prop. of K)	24.277	1	<0.0001

Table S3.26: Summary table of the best model for evolution of cell turning speed, based on the BIC criterion.

	Value	Std.Error	DF	t-value	p-value
(Intercept)	0.049	0.016	2024	3.088	0.002
pH of assay medium	0.064	0.003	200	19.897	<0.0001
Density (prop. of K)	0.063	0.029	2024	2.223	0.026
pH of assay medium × Density (prop. of K)	-0.027	0.005	2024	-4.927	<0.0001

S.3.4.11 Dispersal rates

	Abiotic conditions	Reproduction	Gene flow	Mean percentage of dispersers
Treatment 1	“Uniform”	“Asexual”	“Absent”	6.00
Treatment 2	“Uniform”	“Asexual”	“Present”	4.98
Treatment 3	“Uniform”	“Sexual”	“Absent”	5.44
Treatment 4	“Uniform”	“Sexual”	“Present”	5.29
Treatment 5	“Gradient”	“Asexual”	“Absent”	3.22
Treatment 6	“Gradient”	“Asexual”	“Present”	2.49
Treatment 7	“Gradient”	“Sexual”	“Absent”	2.95
Treatment 8	“Gradient”	“Sexual”	“Present”	3.90

Table S3.27: Average dispersal rates (percentage of dispersers) for each of the eight treatment groups in the range expansion experiment.

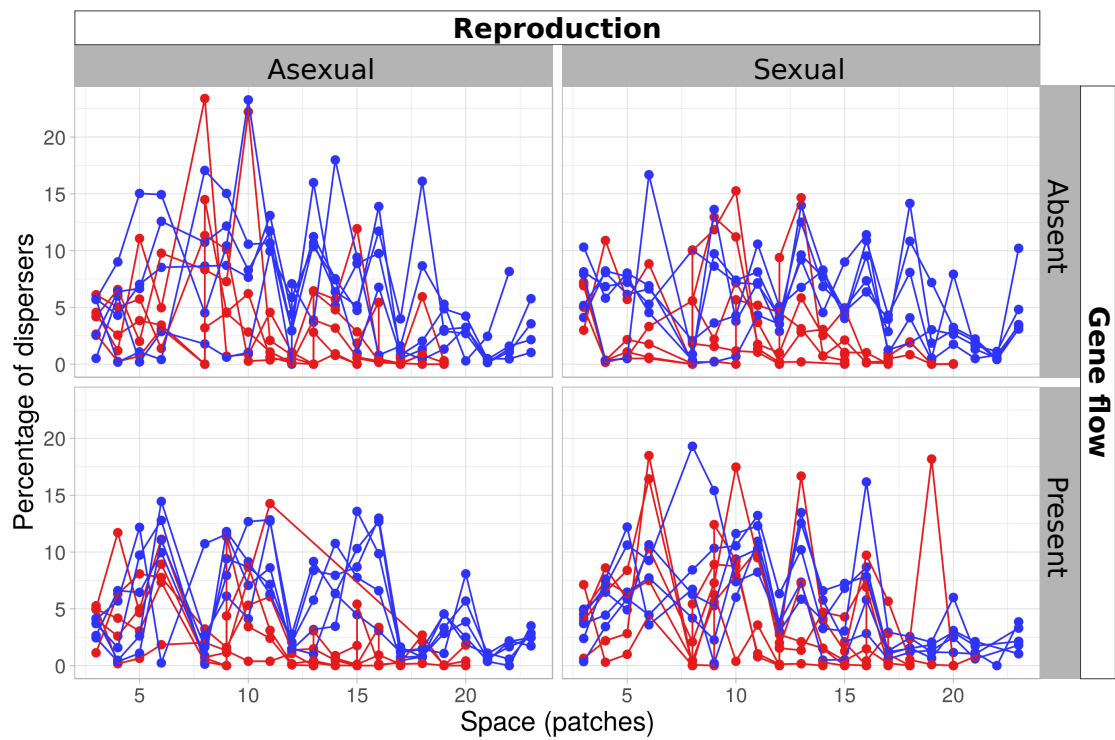


Figure S3.9: Dispersal rates (percentage of dispersers) plotted to the total distance expanded during range expansion. Blue dots and lines show data for populations expanding into uniform abiotic conditions, red dots and lines data for populations expanding into a gradient. Each line represents a distinct population over the course of the range expansion experiment.

Chapter S.4

Supplementary Material of Chapter 4

S.4.1 Video analysis script and parameters

```
#####  
# R script for analysing video files with BEMOVI (www.bemovi.info)  
rm(list=ls())  
# load package  
library(devtools)  
install_github("efronhofer/bemovi", ref="experimental")  
library(bemovi)  
  
#####  
# VIDEO PARAMETERS  
  
# video frame rate (in frames per second)  
fps <- 25  
# length of video (in frames)  
total_frames <- 500  
  
# measured volume (in microliter)  
measured_volume <- 34.4 # for Leica M205 C with 1.6 fold magnification,  
Sample height 0.5 mm and Hamamatsu Orca Flash 4  
  
# size of a pixel (in micrometer)  
pixel_to_scale <- 4.05 # for Leica M205 C with 1.6 fold magnification,  
Sample height 0.5 mm and Hamamatsu Orca Flash 4  
  
# specify video file format (one of "avi","cxd","mov","tiff")
```

```

# bemovi only works with avi and cxd. other formats are reformatted
# to avi below
video.format <- "cxd"

# setup
difference.lag <- 10
thresholds <- c(10,255) # don't change the second value
#thresholds <- c(50,255)

#####
# FILTERING PARAMETERS
# min and max size: area in pixels
particle_min_size <- 5
particle_max_size <- 1000

# number of adjacent frames to be considered for linking particles
trajectory_link_range <- 3
# maximum distance a particle can move between two frames
trajectory_displacement <- 16

# these values are in the units defined by the parameters above:
# fps (seconds),
#measured_volume (microliters) and pixel_to_scale (micrometers)
filter_min_net_disp <- 25
filter_min_duration <- 1
filter_detection_freq <- 0.1
filter_median_step_length <- 3

#####
# MORE PARAMETERS (USUALLY NOT CHANGED)

# set paths to ImageJ and particle linker standalone
IJ.path <- "/home/felix/bin/ImageJ"
to.particlelinker <- "/home/felix/bin/ParticleLinker"

# directories and file names
to.data <- paste(getwd(),"/",sep="")
video.description.folder <- "0_video_description/"
video.description.file <- "video_description.txt"
raw.video.folder <- "1_raw/"

```

```

particle.data.folder <- "2_particle_data/"
trajectory.data.folder <- "3_trajectory_data/"
temp.overlay.folder <- "4a_temp_overlays/"
overlay.folder <- "4_overlays/"
merged.data.folder <- "5_merged_data/"
ijmacs.folder <- "ijmacs/"

# RAM allocation
memory.alloc <- c(60000)

# RAM per particle linker instance
memory.alloc.perLinker <- c(10000)

#####
# VIDEO ANALYSIS

# identify particles
locate_and_measure_particles(to.data, raw.video.folder,
particle.data.folder,
difference.lag, thresholds, min_size = particle_min_size,
max_size = particle_max_size, IJ.path, memory.alloc)

# link the particles
link_particles(to.data, particle.data.folder, trajectory.data.folder,
linkrange = trajectory_link_range, disp = trajectory_displacement,
start_vid = 1, memory = memory.alloc,
memory_per_linkerProcess = memory.alloc.perLinker)

# merge info from description file and data
merge_data(to.data, particle.data.folder, trajectory.data.folder,
video.description.folder, video.description.file, merged.data.folder)

# load the merged data
load(paste0(to.data, merged.data.folder, "Master.RData"))

# filter data: minimum net displacement, their duration, the detection
#frequency and the median step length
trajectory.data.filtered <- filter_data(trajectory.data,
filter_min_net_disp, filter_min_duration, filter_detection_freq,
filter_median_step_length)

```

```
# summarize trajectory data to individual-based data
morph_mvt <- summarize_trajectories(trajectory.data.filtered,
calculate.median=F, write = T, to.data, merged.data.folder)

# get Sample level info
summarize_populations(trajectory.data.filtered, morph_mvt,
write=T, to.data, merged.data.folder, video.description.folder,
video.description.file, total_frames)

# create overlays for validation
create_overlays(trajectory.data.filtered, to.data,
merged.data.folder, raw.video.folder, temp.overlay.folder,
overlay.folder, 2048, 2048, difference.lag, type = "label",
predict_spec = F, IJ.path, contrast.enhancement = 1,
memory = memory.alloc)
```

S.4.2 Visual representation of experimental evolution phase

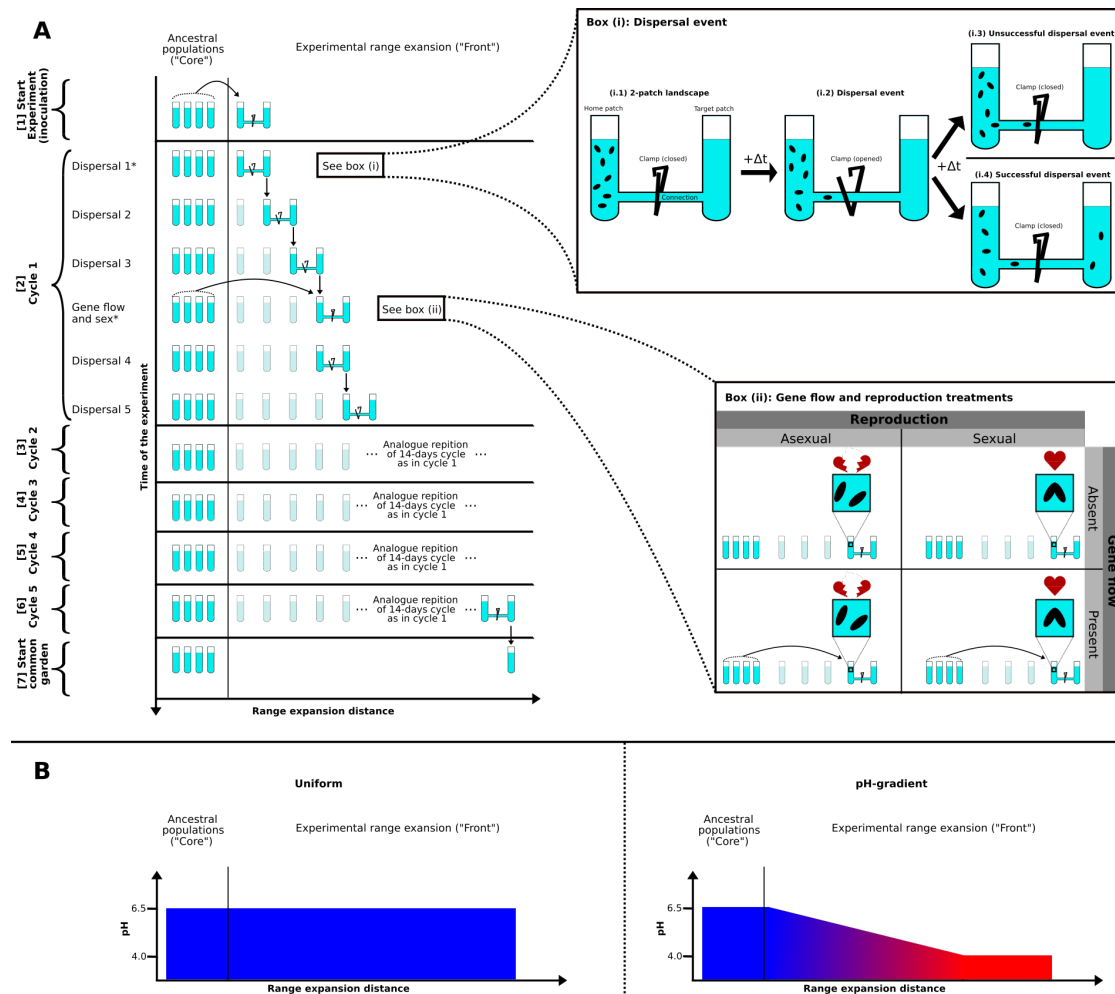


Figure S4.1: **Schematic representation of the experimental range expansion.** Adapted from Moerman et al. (2020b). Panel A shows the timeline of the experiment, with the y-axis depicting time, and the x-axis the distance by which populations expanded during range expansion. Box (i) shows in more detail the experimental approach involved in a dispersal step, and box (ii) the treatments related to gene flow and reproduction. Panel B shows the abiotic conditions experienced during range expansion into a pH-gradient or a uniform environment.

S.4.3 Nuclear separation media reagents

reagents of medium A

Reagent	Concentration	Amount/1 L
Sucrose	0.1 M	34.23 g
MgCl ₂ (*H ₂ O ₆)	2 mM	0.407 g
Gum arabic	4 %	40 g
Tris pH 7.5 (Tris base, with pH adjusted)	10 mM	1.211 g
Iodoacetamide	1mM	0.185 g
Butyric acid	10 mM	0.881 g / 0.918 µL

Table S4.1: Reagents required for the preparation of 1 L of to prepare medium A

reagents of nuclei was buffer

Reagent	Concentration	Amount/1 L
Sucrose	0.25 M	85.574 g
Tris pH 7.5 (Tris base, with pH adjusted)	10 mM	1.211 g
CaCl ₂	3 mM	0.441 g
MgCl ₂	1 mM	0.2033 g
Iodoacetamide	1mM	0.185 g
Butyric acid	10 mM	0.881 g / 0.918 µL

Table S4.2: Reagents required for the preparation of 1 L of nuclei wash buffer

Ingredients of SyBr-Green Tris-HCl

Reagent	Amount
10 mM Tris-HCl (pH 7.5)	50 mL
SyBr-Green 10.000X concentrated	50 µL

Table S4.3: Ingredients required for the preparation of the SyBr-Green Tris-HCl solution for nuclear staining

S.4.4 Read mapping statistics

Population	History	Reads	Mapped reads	Percentage mapped	Abiotic conditions	Gene flow	Reproduction
B2086.2	Ancestral	88538723	87177869	98.46	Ancestral	Ancestral	Ancestral
CU427.4	Ancestral	60231352	58955342	97.88	Ancestral	Ancestral	Ancestral
CU428.2	Ancestral	121454032	119887118	98.71	Ancestral	Ancestral	Ancestral
SB3539	Ancestral	55923710	54488844	97.43	Ancestral	Ancestral	Ancestral
EVO4	Evolved	151091447	148015322	97.96	pH-gradient	Present	Sexual
EVO5	Evolved	61936120	60664281	97.95	pH-gradient	Present	Sexual
EVO8	Evolved	66688733	65342004	97.98	pH-gradient	Present	Asexual
EVO9	Evolved	74980890	73779386	98.4	pH-gradient	Present	Asexual
EVO11	Evolved	81714042	79260522	97.00	pH-gradient	Absent	Sexual
EVO14	Evolved	145705318	142906377	98.08	pH-gradient	Absent	Sexual
EVO18	Evolved	58985398	57659400	97.75	pH-gradient	Absent	Asexual
EVO20	Evolved	65135354	63837265	98.01	pH-gradient	Absent	Asexual
EVO23	Evolved	120307664	116904548	97.17	Uniform	Present	Sexual
EVO24	Evolved	67309446	65539280	97.37	Uniform	Present	Sexual
EVO29	Evolved	113384019	111097232	97.98	Uniform	Present	Asexual
EVO30	Evolved	50504039	49125464	97.27	Uniform	Present	Asexual
EVO33	Evolved	104327400	101909411	97.68	Uniform	Absent	Sexual
EVO35	Evolved	73190459	71198417	97.28	Uniform	Absent	Sexual
EVO36	Evolved	62024246	60916336	98.21	Uniform	Absent	Asexual

EVO39		Evolved		78497531		75953004		96.76		Uniform		Absent		Asexual
-------	--	---------	--	----------	--	----------	--	-------	--	---------	--	--------	--	---------

Table S4.4: Read mapping statistics following mapping of the 2x150 bp paired end Illumina reads. For each of the ancestor clones and evolved populations, we list the total number of reads (Reads), the number of reads that mapped to the reference genome (Mapped reads), and the percentage of total reads that mapped to the reference genome (Percentage mapped reads).

S.4.5 Coverage statistics

Population	History	Mean coverage	St. Dev of coverage	Abiotic conditions	Gene flow	Reproduction
B2086.2	Ancestral	118.755	43.5969	Ancestral	Ancestral	Ancestral
CU427.4	Ancestral	81.2459	38.9025	Ancestral	Ancestral	Ancestral
CU428.2	Ancestral	161.785	48.7088	Ancestral	Ancestral	Ancestral
SB3539	Ancestral	199.782	53.2433	Ancestral	Ancestral	Ancestral
EVO4	Evolved	82.3705	39.575	pH-gradient	Present	Sexual
EVO5	Evolved	88.5749	40.4345	pH-gradient	Present	Sexual
EVO8	Evolved	100.868	40.7681	pH-gradient	Present	Asexual
EVO9	Evolved	107.539	47.8459	pH-gradient	Present	Asexual
EVO11	Evolved	193.385	56.6183	pH-gradient	Absent	Sexual
EVO14	Evolved	78.104	28.0777	pH-gradient	Absent	Sexual
EVO18	Evolved	86.7873	40.9995	pH-gradient	Absent	Asexual
EVO20	Evolved	158.747	55.3373	pH-gradient	Absent	Asexual
EVO23	Evolved	89.3272	43.8388	Uniform	Present	Sexual
EVO24	Evolved	150.726	46.9788	Uniform	Present	Sexual
EVO29	Evolved	66.8015	39.7007	Uniform	Present	Asexual
EVO30	Evolved	138.968	45.7587	Uniform	Present	Asexual
EVO33	Evolved	94.2837	41.5059	Uniform	Absent	Sexual
EVO35	Evolved	83.0331	37.2433	Uniform	Absent	Sexual
EVO36	Evolved	103.031	42.4438	Uniform	Absent	Asexual
EVO39	Evolved	73.0205	36.1424	Uniform	Absent	Asexual

Table S4.5: Genome coverage statistics after sequencing the populations using 2x150 bp paired end Illumina reads. For each of the ancestor clones and evolved populations, we list the mean coverage across the entire genome (Mean coverage) and the standard deviation in coverage across the entire genome (St. Dev of coverage).

S.4.6 Derived alleles in sequenced populations

Population	History	SNPs	INDELs	Transitions	Transversions	Transition/Transversion ratio	Abiotic conditions	Gene flow	Reproduction
B2086.2	Ancestral	19140	9328	8204	10981	0.7471	Ancestral	Ancestral	Ancestral
CU427.4	Ancestral	23201	7848	10088	13169	0.766	Ancestral	Ancestral	Ancestral
CU428.2	Ancestral	12983	9677	5293	7737	0.6841	Ancestral	Ancestral	Ancestral
SB3539	Ancestral	640765	80210	310239	332015	0.9344	Ancestral	Ancestral	Ancestral
EVO4	Evolved	8510	8302	3394	5154	0.6585	pH-gradient	Present	Sexual
EVO5	Evolved	23494	8944	10198	13349	0.764	pH-gradient	Present	Sexual
EVO8	Evolved	23306	10906	10057	13293	0.7566	pH-gradient	Present	Asexual
EVO9	Evolved	20477	9127	8829	11689	0.7553	pH-gradient	Present	Asexual
EVO11	Evolved	23168	11609	9869	13354	0.739	pH-gradient	Absent	Sexual
EVO14	Evolved	12011	12020	4769	7288	0.6544	pH-gradient	Absent	Sexual
EVO18	Evolved	24468	8811	10620	13896	0.7642	pH-gradient	Absent	Asexual
EVO20	Evolved	23600	8632	10721	13384	0.801	pH-gradient	Absent	Asexual
EVO23	Evolved	13277	9534	5455	7870	0.6931	Uniform	Present	Sexual
EVO24	Evolved	23136	9231	10036	13146	0.7634	Uniform	Present	Sexual
EVO29	Evolved	13264	10840	5447	7860	0.693	Uniform	Present	Asexual

EVO30	Evolved	24581	9730	10592	14041	0.7544	Uniform	Present	Asexual
EVO33	Evolved	14776	9452	6161	8667	0.7109	Uniform	Absent	Sexual
EVO35	Evolved	22484	9649	9777	12745	0.7671	Uniform	Absent	Sexual
EVO36	Evolved	25608	11874	10911	14745	0.74	Uniform	Absent	Asexual
EVO39	Evolved	25158	12406	10727	14492	0.7402	Uniform	Absent	Asexual

Table S4.6: Derived variants found after variant calling. For each of the ancestor clones and evolved populations, we list the number of SNPs that deviate from the reference genome (SNPs), the number of indels that deviate from the reference genome (INDELS), the number of transitions found among all derived SNPs (Transitions), the number of transversion found among all derived SNPS (Transversion) and the transition to transversion ratio. Note the high number of derived SNPs and indels for clone SB3539, as well as the noticeably higher transition to transversion ratio for this clone.

S.4.7 Principle component analysis on standing genetic variation

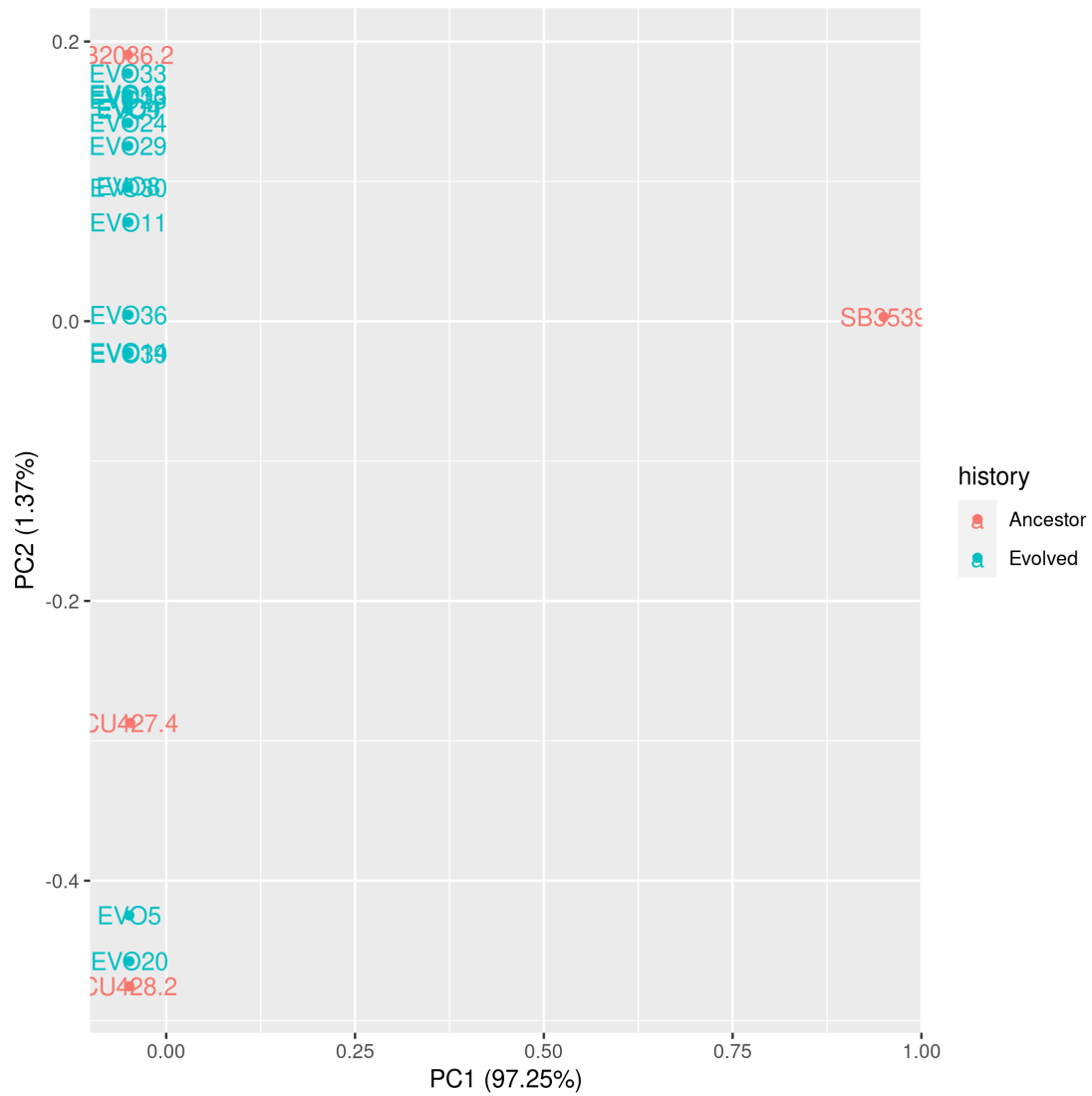


Figure S4.2: textbfStrong genetic divergence of clone SB3539. Principle component analysis, comparing allele frequencies for standing genetic variations for all 20 populations (4 ancestral clones and 16 evolved populations). Note that almost all variation is associated with PC1 (97.24 %), which corresponds to the highly divergent ancestral clone (SB3539).

S.4.8 Intrinsic growth rate of populations

ID	Abiotic conditions	Reproduction	Gene flow	r_0	r_0 change	Included in genetic analysis
EVO1	pH-gradient	Sexual	Present	0.0402	0.0627	no
EVO2	pH-gradient	Sexual	Present	0.0603	0.6496	no
EVO4	pH-gradient	Sexual	Present	0.0611	0.6700	yes
EVO5	pH-gradient	Sexual	Present	0.0637	0.7276	yes
EVO6	pH-gradient	Asexual	Present	0.0686	0.8355	no
EVO7	pH-gradient	Asexual	Present	0.0669	0.7990	no
EVO8	pH-gradient	Asexual	Present	0.0671	0.8029	yes
EVO9	pH-gradient	Asexual	Present	0.07073	0.8783	yes
EVO10	pH-gradient	Asexual	Present	0.0658	0.7747	no
EVO11	pH-gradient	Sexual	Absent	0.0705	0.8735	yes
EVO13	pH-gradient	Sexual	Absent	0.0670	0.8019	no
EVO14	pH-gradient	Sexual	Absent	0.0675	0.8120	yes
EVO18	pH-gradient	Asexual	Absent	0.0687	0.8366	yes
EVO20	pH-gradient	Asexual	Absent	0.0583	0.6000	yes
EVO21	Uniform	Sexual	Present	0.1033	0.0124	no
EVO22	Uniform	Sexual	Present	0.1077	0.0728	no
EVO23	Uniform	Sexual	Present	0.1178	0.2030	yes
EVO24	Uniform	Sexual	Present	0.1082	0.0802	yes
EVO25	Uniform	Sexual	Present	0.1079	0.0761	no
EVO26	Uniform	Asexual	Present	0.1206	0.2362	no
EVO27	Uniform	Asexual	Present	0.1086	0.0856	no
EVO28	Uniform	Asexual	Present	0.1116	0.1244	no
EVO29	Uniform	Asexual	Present	0.1222	0.2551	yes
EVO30	Uniform	Asexual	Present	0.1245	0.2823	yes
EVO31	Uniform	Sexual	Absent	0.1103	0.1075	no
EVO32	Uniform	Sexual	Absent	0.1073	0.0672	no
EVO33	Uniform	Sexual	Absent	0.1254	0.2930	yes
EVO34	Uniform	Sexual	Absent	0.1131	0.1443	no

EVO35	Uniform	Sexual	Absent	0.1161	0.1819	yes
EVO36	Uniform	Asexual	Absent	0.1115	0.1231	yes
EVO37	Uniform	Asexual	Absent	0.1029	0.0079	no
EVO38	Uniform	Asexual	Absent	0.0782	-0.3881	no
EVO39	Uniform	Asexual	Absent	0.1110	0.1162	yes
EVO40	Uniform	Asexual	Absent	0.1089	0.0888	no

Table S4.7: Phenotypic evolution of the evolved populations. For each of the evolved populations, we list the intrinsic growth rate (r_0), as well as the change in r_0 compared to the ancestral population (r_o change), calculated as the log (base 2) of the ratio between the intrinsic growth rate of the evolved population and the intrinsic growth rate of the ancestral population. The column "Included in genetic analysis" indicates whether the population was selected for sequencing or not.

S.4.9 Gene ontology Classification

Gene ontology term	Classification
1-phosphatidylinositol-3-kinase activity	Metabolism, activity and transport: Other carbohydrates
1-phosphatidylinositol-4-phosphate 3-kinase activity	Metabolism, activity and transport: Other carbohydrates
acetyl-CoA transport	Metabolism, activity and transport: Other carbohydrates
acetyl-CoA transporter activity	Metabolism, activity and transport: Other carbohydrates
acetyltransferase activity	Metabolism, activity and transport: Other carbohydrates
aromatic compound biosynthetic process	Metabolism, activity and transport: Other carbohydrates
aromatic compound catabolic process	Metabolism, activity and transport: Other carbohydrates
carbohydrate derivative biosynthetic process	Metabolism, activity and transport: Other carbohydrates
carbohydrate derivative catabolic process	Metabolism, activity and transport: Other carbohydrates
carbohydrate derivative metabolic process	Metabolism, activity and transport: Other carbohydrates
carbohydrate metabolic process	Metabolism, activity and transport: Other carbohydrates

carbohydrate phosphorylation	Metabolism, activity and transport: Other carbohydrates
carbohydrate transport	Metabolism, activity and transport: Other carbohydrates
carbohydrate transporter activity	Metabolism, activity and transport: Other carbohydrates
carbon-nitrogen ligase activity with glutamine as amido-N-donor	Metabolism, activity and transport: Other carbohydrates
carbon-nitrogen lyase activity	Metabolism, activity and transport: Other carbohydrates
carboxyl-O-methyltransferase activity	Metabolism, activity and transport: Other carbohydrates
carboxylic acid binding	Metabolism, activity and transport: Other carbohydrates
carboxylic acid biosynthetic process	Metabolism, activity and transport: Other carbohydrates
carboxylic acid transport	Metabolism, activity and transport: Other carbohydrates
carboxypeptidase activity	Metabolism, activity and transport: Other carbohydrates
cell wall macromolecule catabolic process	Metabolism, activity and transport: Other carbohydrates
cell wall macromolecule metabolic process	Metabolism, activity and transport: Other carbohydrates
cell wall organization or biogenesis	Metabolism, activity and transport: Other carbohydrates
cell wall polysaccharide metabolic process	Metabolism, activity and transport: Other carbohydrates
cellular aromatic compound metabolic process	Metabolism, activity and transport: Other carbohydrates
fatty acid biosynthetic process	Metabolism, activity and transport: Other carbohydrates
fatty-acyl-CoA transport	Metabolism, activity and transport: Other carbohydrates
galactokinase activity	Metabolism, activity and transport: Other carbohydrates
galactose metabolic process	Metabolism, activity and transport: Other carbohydrates
glutathione peroxidase activity	Metabolism, activity and transport:

glycerolipid biosynthetic process	Other carbohydrates Metabolism, activity and transport:
glycerolipid metabolic process	Other carbohydrates Metabolism, activity and transport:
glycerophospholipid biosynthetic process	Other carbohydrates Metabolism, activity and transport:
glycosaminoglycan catabolic process	Other carbohydrates Metabolism, activity and transport:
glycosaminoglycan metabolic process	Other carbohydrates Metabolism, activity and transport:
glycosyl compound biosynthetic process	Other carbohydrates Metabolism, activity and transport:
hemicellulose metabolic process	Other carbohydrates Metabolism, activity and transport:
heterocycle biosynthetic process	Other carbohydrates Metabolism, activity and transport:
heterocycle catabolic process	Other carbohydrates Metabolism, activity and transport:
heterocycle metabolic process	Other carbohydrates Metabolism, activity and transport:
heterocyclic compound binding	Other carbohydrates Metabolism, activity and transport:
hexose metabolic process	Other carbohydrates Metabolism, activity and transport:
hydrolase activity	Other carbohydrates Metabolism, activity and transport:
hydrolase activity acting on acid anhydrides	Other carbohydrates Metabolism, activity and transport:
hydrolase activity acting on acid anhydrides catalyzing transmembrane movement of substances	Other carbohydrates Metabolism, activity and transport:
hydrolase activity acting on acid anhydrides in phosphorus-containing anhydrides	Other carbohydrates Metabolism, activity and transport:
hydrolase activity acting on carbon-nitrogen (but not peptide) bonds	Other carbohydrates Metabolism, activity and transport:
hydrolase activity acting on ester bonds	Other carbohydrates Metabolism, activity and transport:

hydrolase activity acting on glycosyl bonds	Other carbohydrates Metabolism, activity and transport: Other carbohydrates
hydrolase activity hydrolyzing O-glycosyl compounds	Metabolism, activity and transport: Other carbohydrates
ligase activity forming carbon-sulfur bonds	Metabolism, activity and transport: Other carbohydrates
lipid biosynthetic process	Metabolism, activity and transport: Other carbohydrates
lipid localization	Metabolism, activity and transport: Other carbohydrates
lipid metabolic process	Metabolism, activity and transport: Other carbohydrates
lipid modification	Metabolism, activity and transport: Other carbohydrates
lipid particle	Metabolism, activity and transport: Other carbohydrates
lipid phosphorylation	Metabolism, activity and transport: Other carbohydrates
lipid storage	Metabolism, activity and transport: Other carbohydrates
lipid transport	Metabolism, activity and transport: Other carbohydrates
monocarboxylic acid biosynthetic process	Metabolism, activity and transport: Other carbohydrates
monosaccharide metabolic process	Metabolism, activity and transport: Other carbohydrates
organic acid binding	Metabolism, activity and transport: Other carbohydrates
organic acid biosynthetic process	Metabolism, activity and transport: Other carbohydrates
organic acid transmembrane transporter activity	Metabolism, activity and transport: Other carbohydrates
organic acid transport	Metabolism, activity and transport: Other carbohydrates
organic cyclic compound binding	Metabolism, activity and transport: Other carbohydrates
organic cyclic compound biosynthetic process	Metabolism, activity and transport: Other carbohydrates

organic cyclic compound catabolic process	Metabolism, activity and transport: Other carbohydrates
organic cyclic compound metabolic process	Metabolism, activity and transport: Other carbohydrates
organic hydroxy compound metabolic process	Metabolism, activity and transport: Other carbohydrates
organonitrogen compound catabolic process	Metabolism, activity and transport: Other carbohydrates
organophosphate biosynthetic process	Metabolism, activity and transport: Other carbohydrates
phosphoserine binding	Metabolism, activity and transport: Other carbohydrates
polysaccharide catabolic process	Metabolism, activity and transport: Other carbohydrates
polysaccharide metabolic process	Metabolism, activity and transport: Other carbohydrates
S-acyltransferase activity	Metabolism, activity and transport: Other carbohydrates
steroid metabolic process	Metabolism, activity and transport: Other carbohydrates
sterol metabolic process	Metabolism, activity and transport: Other carbohydrates
tetrapyrrole binding	Metabolism, activity and transport: Other carbohydrates
thioester transport	Metabolism, activity and transport: Other carbohydrates
transferase activity transferring acyl groups other than amino-acyl groups	Metabolism, activity and transport: Other carbohydrates
transferase activity transferring one-carbon groups	Metabolism, activity and transport: Other carbohydrates
xylan catabolic process	Metabolism, activity and transport: Other carbohydrates
xylan metabolic process	Metabolism, activity and transport: Other carbohydrates
covalent chromatin modification	Gene expression (transcription and translation)
exon-exon junction complex	Gene expression (transcription and translation)

histone acetylation	Gene expression (transcription and translation)
histone acetyltransferase activity	Gene expression (transcription and translation)
histone modification	Gene expression (transcription and translation)
Prp19 complex	Gene expression (transcription and translation)
transcription coactivator activity	Gene expression (transcription and translation)
transcription cofactor activity	Gene expression (transcription and translation)
transcription factor activity protein binding	Gene expression (transcription and translation)
transcription factor activity transcription factor binding	Gene expression (transcription and translation)
tRNA (cytosine-5-)-methyltransferase activity	Gene expression (transcription and translation)
tRNA (cytosine) methyltransferase activity	Gene expression (transcription and translation)
tRNA modification	Gene expression (transcription and translation)
tRNA threonylcarbamoyladenosine dehydratase	Gene expression (transcription and translation)
UFM1 activating enzyme activity	Gene expression (transcription and translation)
action potential	Ion transport and binding
anion transmembrane transport	Ion transport and binding
anion transmembrane transporter activity	Ion transport and binding
anion transport	Ion transport and binding
calcium ion binding	Ion transport and binding
cation binding	Ion transport and binding
cation channel activity	Ion transport and binding
cation transmembrane transport	Ion transport and binding
cation transmembrane transporter activity	Ion transport and binding
cation transport	Ion transport and binding
cation:sugar symporter activity	Ion transport and binding
cellular potassium ion transport	Ion transport and binding
copper ion transmembrane transport	Ion transport and binding

copper ion transmembrane transporter activity	Ion transport and binding
copper ion transport	Ion transport and binding
inorganic cation transmembrane transport	Ion transport and binding
inorganic cation transmembrane transporter activity	Ion transport and binding
inorganic ion transmembrane transport	Ion transport and binding
ion binding	Ion transport and binding
ion channel activity	Ion transport and binding
ion transmembrane transport	Ion transport and binding
ion transmembrane transporter activity	Ion transport and binding
ion transport	Ion transport and binding
iron ion binding	Ion transport and binding
metal ion binding	Ion transport and binding
metal ion transmembrane transporter activity	Ion transport and binding
metal ion transport	Ion transport and binding
monovalent inorganic cation transmembrane transporter activity	Ion transport and binding
monovalent inorganic cation transport	Ion transport and binding
organic anion transmembrane transporter activity	Ion transport and binding
organic anion transport	Ion transport and binding
potassium channel activity	Ion transport and binding
potassium ion transmembrane transport	Ion transport and binding
potassium ion transmembrane transporter activity	Ion transport and binding
potassium ion transport	Ion transport and binding
regulation of ion transmembrane transport	Ion transport and binding
regulation of ion transport	Ion transport and binding
solute:cation symporter activity	Ion transport and binding
solute:proton symporter activity	Ion transport and binding
sugar:proton symporter activity	Ion transport and binding
symporter activity	Ion transport and binding
transition metal ion binding	Ion transport and binding
transition metal ion transmembrane transporter activity	Ion transport and binding
transition metal ion transport	Ion transport and binding
voltage-gated cation channel activity	Ion transport and binding
voltage-gated ion channel activity	Ion transport and binding
voltage-gated potassium channel activity	Ion transport and binding
zinc ion binding	Ion transport and binding

membrane depolarization	Ion transport and binding
membrane depolarization during action potential	Ion transport and binding
active transmembrane transporter activity	Membrane functioning, transport and structure
bounding membrane of organelle	Membrane functioning, transport and structure
carboxylic acid transmembrane transport	Membrane functioning, transport and structure
channel activity	Membrane functioning, transport and structure
coated membrane	Membrane functioning, transport and structure
coated vesicle membrane	Membrane functioning, transport and structure
COPI-coated vesicle membrane	Membrane functioning, transport and structure
cytoplasmic vesicle membrane	Membrane functioning, transport and structure
endomembrane system	Membrane functioning, transport and structure
envelope	Membrane functioning, transport and structure
ER membrane protein complex	Membrane functioning, transport and structure
extrinsic component of membrane	Membrane functioning, transport and structure
gated channel activity	Membrane functioning, transport and structure
integral component of membrane	Membrane functioning, transport and structure
integral component of organelle membrane	Membrane functioning, transport and structure
integral component of peroxisomal membrane	Membrane functioning, transport and structure
integral component of plasma membrane	Membrane functioning, transport and structure
intracellular protein transmembrane import	Membrane functioning, transport and structure
intracellular protein transmembrane transport	Membrane functioning, transport and structure

intrinsic component of membrane	Membrane functioning, transport and structure
intrinsic component of organelle membrane	Membrane functioning, transport and structure
intrinsic component of peroxisomal membrane	Membrane functioning, transport and structure
intrinsic component of plasma membrane	Membrane functioning, transport and structure
macromolecule transmembrane transporter activity	Membrane functioning, transport and structure
membrane	Membrane functioning, transport and structure
membrane coat	Membrane functioning, transport and structure
membrane docking	Membrane functioning, transport and structure
membrane fusion	Membrane functioning, transport and structure
membrane organization	Membrane functioning, transport and structure
membrane part	Membrane functioning, transport and structure
membrane protein complex	Membrane functioning, transport and structure
microbody membrane	Membrane functioning, transport and structure
organelle inner membrane	Membrane functioning, transport and structure
organelle membrane	Membrane functioning, transport and structure
organelle membrane fusion	Membrane functioning, transport and structure
organic acid transmembrane transport	Membrane functioning, transport and structure
P-P-bond-hydrolysis-driven transmembrane transporter activity	Membrane functioning, transport and structure
passive transmembrane transporter activity	Membrane functioning, transport and structure
peroxisomal membrane	Membrane functioning,

plasma membrane	transport and structure Membrane functioning,
plasma membrane organization	transport and structure Membrane functioning,
plasma membrane part	transport and structure Membrane functioning,
primary active transmembrane transporter activity	transport and structure Membrane functioning,
protein channel activity	transport and structure Membrane functioning,
protein transmembrane transport	transport and structure Membrane functioning,
protein transmembrane transporter activity	transport and structure Membrane functioning,
regulation of membrane potential	transport and structure Membrane functioning,
regulation of transmembrane transport	transport and structure Membrane functioning,
secondary active transmembrane transporter activity	transport and structure Membrane functioning,
single-organism membrane fusion	transport and structure Membrane functioning,
substrate-specific channel activity	transport and structure Membrane functioning,
substrate-specific transmembrane transporter activity	transport and structure Membrane functioning,
sugar transmembrane transporter activity	transport and structure Membrane functioning,
transmembrane transport	transport and structure Membrane functioning,
transmembrane transporter activity	transport and structure Membrane functioning,
vacuolar membrane	transport and structure Membrane functioning,
vesicle membrane	transport and structure Membrane functioning,
voltage-gated channel activity	transport and structure Membrane functioning,

whole membrane	transport and structure Membrane functioning, transport and structure
amino acid transmembrane transport	Membrane functioning, transport and structure
amino acid transmembrane transporter activity	Membrane functioning, transport and structure
endomembrane system organization	Membrane functioning, transport and structure
carboxylic acid transmembrane transporter activity	Membrane functioning, transport and structure
membrane-bounded organelle	Membrane functioning, transport and structure
AP-type membrane coat adaptor complex	Membrane functioning, transport and structure
carbohydrate transmembrane transporter activity	Membrane functioning, transport and structure
non-membrane-bounded organelle	Membrane functioning, transport and structure
P-P-bond-hydrolysis-driven protein transmembrane transporter activity	Membrane functioning, transport and structure
phospholipid scramblase activity	Membrane functioning, transport and structure
phospholipid scrambling	Membrane functioning, transport and structure
ATP-dependent microtubule motor activity	Microtubules and cytoskeleton
ATP-dependent microtubule motor activity plus-end-directed	Microtubules and cytoskeleton
cytoplasmic microtubule organization	Microtubules and cytoskeleton
cytoskeletal part	Microtubules and cytoskeleton
cytoskeletal protein binding	Microtubules and cytoskeleton
cytoskeleton	Microtubules and cytoskeleton
cytoskeleton organization	Microtubules and cytoskeleton
equatorial microtubule organizing center	Microtubules and cytoskeleton
interphase microtubule nucleation by interphase microtubule organizing center	Microtubules and cytoskeleton
microtubule associated complex	Microtubules and cytoskeleton
microtubule binding	Microtubules and cytoskeleton
microtubule cytoskeleton	Microtubules and cytoskeleton

microtubule cytoskeleton organization	Microtubules and cytoskeleton
microtubule minus-end binding	Microtubules and cytoskeleton
microtubule motor activity	Microtubules and cytoskeleton
microtubule nucleation	Microtubules and cytoskeleton
microtubule nucleation by microtubule organizing center	Microtubules and cytoskeleton
microtubule organizing center part	Microtubules and cytoskeleton
microtubule polymerization	Microtubules and cytoskeleton
microtubule polymerization or depolymerization	Microtubules and cytoskeleton
microtubule-based movement	Microtubules and cytoskeleton
microtubule-based process	Microtubules and cytoskeleton
kinesin complex	Microtubules and cytoskeleton
inner mitochondrial membrane	
rotein complex	Mitochondrial functioning and oxidoreductase-reactions
integral component of mitochondrial inner membrane	Mitochondrial functioning and oxidoreductase-reactions
integral component of mitochondrial membrane	Mitochondrial functioning and oxidoreductase-reactions
intrinsic component of mitochondrial inner membrane	Mitochondrial functioning and oxidoreductase-reactions
intrinsic component of mitochondrial membrane	Mitochondrial functioning and oxidoreductase-reactions
mitochondrial envelope	Mitochondrial functioning and oxidoreductase-reactions
mitochondrial inner membrane	Mitochondrial functioning and oxidoreductase-reactions
mitochondrial inner membrane presequence translocase complex	Mitochondrial functioning and oxidoreductase-reactions
mitochondrial membrane	Mitochondrial functioning and oxidoreductase-reactions
mitochondrial membrane part	Mitochondrial functioning and oxidoreductase-reactions
mitochondrial part	Mitochondrial functioning and oxidoreductase-reactions

mitochondrial protein complex	Mitochondrial functioning and oxidoreductase-reactions
mitochondrial respiratory chain complex assembly	Mitochondrial functioning and oxidoreductase-reactions
mitochondrial respiratory chain complex III assembly	Mitochondrial functioning and oxidoreductase-reactions
mitochondrial respiratory chain complex III biogenesis	Mitochondrial functioning and oxidoreductase-reactions
mitochondrial translation	Mitochondrial functioning and oxidoreductase-reactions
mitochondrial transmembrane transport	Mitochondrial functioning and oxidoreductase-reactions
mitochondrial transport	Mitochondrial functioning and oxidoreductase-reactions
mitochondrion	Mitochondrial functioning and oxidoreductase-reactions
mitochondrion organization	Mitochondrial functioning and oxidoreductase-reactions
oxidation-reduction process	Mitochondrial functioning and oxidoreductase-reactions
oxidoreductase activity	Mitochondrial functioning and oxidoreductase-reactions
oxidoreductase activity acting on CH-OH group of donors	Mitochondrial functioning and oxidoreductase-reactions
oxidoreductase activity acting on paired donors with incorporation or reduction of molecular oxygen	Mitochondrial functioning and oxidoreductase-reactions
oxidoreductase activity acting on peroxide as acceptor	Mitochondrial functioning and oxidoreductase-reactions
protein import into mitochondrial matrix	Mitochondrial functioning and oxidoreductase-reactions
protein localization to mitochondrion	Mitochondrial functioning and oxidoreductase-reactions

protein targeting to mitochondrion	Mitochondrial functioning and oxidoreductase-reactions
respiratory chain complex III assembly	Mitochondrial functioning and oxidoreductase-reactions
oxidoreductase activity acting on the CH-OH group of donors NAD or NADP as acceptor	Mitochondrial functioning and oxidoreductase-reactions
gamma-tubulin complex	Mitochondrial functioning and oxidoreductase-reactions
intramolecular oxidoreductase activity transposing S-S bonds	Mitochondrial functioning and oxidoreductase-reactions
monooxygenase activity	Mitochondrial functioning and oxidoreductase-reactions
palmitoyltransferase activity	Mitochondrial functioning and oxidoreductase-reactions
ubiquinone-6 biosynthetic process	Mitochondrial functioning and oxidoreductase-reactions
ubiquinone-6 metabolic process	Mitochondrial functioning and oxidoreductase-reactions
cell division site	Mitosis, DNA repair and chromosome division
cell division site part	Mitosis, DNA repair and chromosome division
centrosome duplication	Mitosis, DNA repair and chromosome division
chromosomal part	Mitosis, DNA repair and chromosome division
chromosome	Mitosis, DNA repair and chromosome division
chromosome condensation	Mitosis, DNA repair and chromosome division
chromosome segregation	Mitosis, DNA repair and chromosome division
condensed chromosome	Mitosis, DNA repair and chromosome division
damaged DNA binding	Mitosis, DNA repair and chromosome division
DNA biosynthetic process	Mitosis, DNA repair and

DNA clamp loader activity	chromosome division Mitosis, DNA repair and chromosome division
DNA packaging	Mitosis, DNA repair and chromosome division
DNA packaging complex	Mitosis, DNA repair and chromosome division
DNA polymerase activity	Mitosis, DNA repair and chromosome division
DNA replication factor C complex	Mitosis, DNA repair and chromosome division
DNA-directed DNA polymerase activity	Mitosis, DNA repair and chromosome division
double-strand break repair via nonhomologous end joining	Mitosis, DNA repair and chromosome division
exit from Mitosis, Mitosis, DNA repair and chromosome division	
gamma-tubulin binding	Mitosis, DNA repair and chromosome division
gamma-tubulin small complex	Mitosis, DNA repair and chromosome division
leading strand elongation	Mitosis, DNA repair and chromosome division
mitotic chromosome condensation	Mitosis, DNA repair and chromosome division
mitotic nuclear division	Mitosis, DNA repair and chromosome division
mitotic sister chromatid segregation	Mitosis, DNA repair and chromosome division
mitotic spindle assembly	Mitosis, DNA repair and chromosome division
non-recombinational repair	Mitosis, DNA repair and chromosome division
nuclear chromosome segregation	Mitosis, DNA repair and chromosome division
nuclear division	Mitosis, DNA repair and chromosome division
protection from non-homologous end joining at telomere	Mitosis, DNA repair and

regulation of exit from Mitosis, Mitosis,
DNA repair and chromosome division
sister chromatid segregation

spindle pole

spindle pole body

telomere capping

telomere maintenance in response
to DNA damage

chromatin organization

interstrand cross-link repair

spindle assembly

tubulin binding

3'-5'-exoribonuclease activity

5'-nucleotidase activity

8-oxo-7,8-dihydroguanosine triphosphate
pyrophosphatase activity

ARF guanyl-nucleotide exchange factor activity

cyclic threonylcarbamoyladenosine
biosynthetic process

cysteine-type endopeptidase activity

cysteine-type peptidase activity

DNA topoisomerase type I activity

chromosome division

Mitosis, DNA repair and
chromosome division

Metabolism, activity and transport:
Nucleic acids

endonuclease activity	Metabolism, activity and transport: Nucleic acids
endonuclease activity active with either ribo- or deoxyribonucleic acids and producing 3'-phosphomonoesters	Metabolism, activity and transport: Nucleic acids
endoribonuclease activity	Metabolism, activity and transport: Nucleic acids
endoribonuclease activity producing 3'-phosphomonoesters	Metabolism, activity and transport: Nucleic acids
exonuclease activity	Metabolism, activity and transport: Nucleic acids
exonuclease activity active with either ribo- or deoxyribonucleic acids and producing 5'-phosphomonoesters	Metabolism, activity and transport: Nucleic acids
exoribonuclease activity	Metabolism, activity and transport: Nucleic acids
exoribonuclease activity producing 5'-phosphomonoesters	Metabolism, activity and transport: Nucleic acids
glutamate-tRNA ligase activity	Metabolism, activity and transport: Nucleic acids
glutamyl-tRNA aminoacylation	Metabolism, activity and transport: Nucleic acids
guanyl nucleotide binding	Metabolism, activity and transport: Nucleic acids
guanyl ribonucleotide binding	Metabolism, activity and transport: Nucleic acids
guanyl-nucleotide exchange factor activity	Metabolism, activity and transport: Nucleic acids
intracellular ribonucleoprotein complex	Metabolism, activity and transport: Nucleic acids
ncRNA metabolic process	Metabolism, activity and transport: Nucleic acids
ncRNA processing	Metabolism, activity and transport: Nucleic acids
nuclease activity	Metabolism, activity and transport: Nucleic acids

nucleic acid binding	Metabolism, activity and transport: Nucleic acids
nucleic acid metabolic process	Metabolism, activity and transport: Nucleic acids
nucleic acid phosphodiester bond hydrolysis	Metabolism, activity and transport: Nucleic acids
nucleobase-containing compound biosynthetic process	Metabolism, activity and transport: Nucleic acids
nucleobase-containing compound catabolic process	Metabolism, activity and transport: Nucleic acids
nucleobase-containing compound metabolic process	Metabolism, activity and transport: Nucleic acids
nucleoside biosynthetic process	Metabolism, activity and transport: Nucleic acids
nucleoside-triphosphatase activity	Metabolism, activity and transport: Nucleic acids
nucleoside-triphosphatase regulator activity	Metabolism, activity and transport: Nucleic acids
nucleotidase activity	Metabolism, activity and transport: Nucleic acids
nucleotide-sugar biosynthetic process	Metabolism, activity and transport: Nucleic acids
nucleotide-sugar metabolic process	Metabolism, activity and transport: Nucleic acids
purine nucleobase metabolic process	Metabolism, activity and transport: Nucleic acids
purine nucleoside biosynthetic process	Metabolism, activity and transport: Nucleic acids
purine ribonucleoside biosynthetic process	Metabolism, activity and transport: Nucleic acids
purine-containing compound biosynthetic process	Metabolism, activity and transport: Nucleic acids
purine-containing compound metabolic process	Metabolism, activity and transport: Nucleic acids

RNA metabolic process	Metabolism, activity and transport: Nucleic acids
RNA modification	Metabolism, activity and transport: Nucleic acids
RNA phosphodiester bond hydrolysis	Metabolism, activity and transport: Nucleic acids
RNA phosphodiester bond hydrolysis endonucleolytic	Metabolism, activity and transport: Nucleic acids
RNA polymerase II C-terminal domain binding	Metabolism, activity and transport: Nucleic acids
RNA polymerase II C-terminal domain phosphoserine binding	Metabolism, activity and transport: Nucleic acids
RNA splicing	Metabolism, activity and transport: Nucleic acids
RNA-3'-phosphate cyclase activity	Metabolism, activity and transport: Nucleic acids
RNA-DNA hybrid ribonuclease activity	Metabolism, activity and transport: Nucleic acids
rRNA metabolic process	Metabolism, activity and transport: Nucleic acids
rRNA processing	Metabolism, activity and transport: Nucleic acids
rRNA-containing ribonucleoprotein complex export from nucleus	Metabolism, activity and transport: Nucleic acids
all	Other
amidine-lyase activity	Other
anaphase-promoting complex binding	Other
binding	Other
biological process	Other
biological regulation	Other
catabolic process	Other
catalytic activity	Other
catalytic step 1 spliceosome	Other
cell	Other
cell part	Other
cell periphery	Other
cellular catabolic process	Other

cellular component	Other
cellular component assembly	Other
cellular component biogenesis	Other
cellular component organization	Other
cellular component organization or biogenesis	Other
cellular lipid metabolic process	Other
cellular localization	Other
cellular macromolecular complex assembly	Other
cellular macromolecule catabolic process	Other
cellular macromolecule localization	Other
cellular nitrogen compound catabolic process	Other
cellular nitrogen compound metabolic process	Other
cellular process	Other
cellular protein catabolic process	Other
cellular protein complex assembly	Other
cellular protein localization	Other
cellular response to DNA damage stimulus	Other
cellular response to stimulus	Other
coenzyme binding	Other
coenzyme transport	Other
coenzyme transporter activity	Other
cofactor binding	Other
cofactor transport	Other
cofactor transporter activity	Other
cytochrome complex assembly	Other
cytoplasm	Other
cytoplasmic part	Other
cytosol	Other
Elongator holoenzyme complex	Other
endoplasmic reticulum	Other
endoplasmic reticulum organization	Other
enzyme activator activity	Other
enzyme binding	Other
enzyme regulator activity	Other
establishment of localization	Other
establishment of localization in cell	Other
extracellular region	Other
extracellular region part	Other
extracellular space	Other
generation of precursor metabolites and energy	Other

Golgi apparatus	Other
Golgi apparatus part	Other
heme binding	Other
intracellular	Other
intracellular membrane-bounded organelle	Other
intracellular non-membrane-bounded organelle	Other
intracellular organelle	Other
intracellular organelle part	Other
intracellular part	Other
intracellular transport	Other
late endosome	Other
ligase activity	Other
localization	Other
macromolecular complex	Other
macromolecular complex assembly	Other
macromolecular complex binding	Other
macromolecular complex disassembly	Other
macromolecular complex subunit organization	Other
macromolecule catabolic process	Other
macromolecule localization	Other
macromolecule methylation	Other
maintenance of location	Other
maintenance of location in cell	Other
maintenance of protein location	Other
maintenance of protein location in cell	Other
metabolic process	Other
methylation	Other
methyltransferase activity	Other
microbody	Other
microbody part	Other
modification-dependent macromolecule	
catabolic process	Other
molecular function	Other
molecular function regulator	Other
molecular transducer activity	Other
motor activity	Other
movement of cell or subcellular component	Other
NAD binding	Other
nitrogen compound metabolic process	Other
O-methyltransferase activity	Other

organelle	Other
organelle assembly	Other
organelle envelope	Other
organelle fission	Other
organelle fusion	Other
organelle organization	Other
organelle part	Other
phosphorelay sensor kinase activity	Other
phosphotransferase activity	
nitrogenous group as acceptor	Other
positive regulation of catalytic activity	Other
positive regulation of hydrolase activity	Other
positive regulation of molecular function	Other
primary metabolic process	Other
pyrophosphatase activity	Other
receptor activity	Other
regulation of anatomical structure size	Other
regulation of biological process	Other
regulation of biological quality	Other
regulation of catalytic activity	Other
regulation of cell communication	Other
regulation of cellular component size	Other
regulation of cellular process	Other
regulation of hydrolase activity	Other
regulation of lipid metabolic process	Other
regulation of localization	Other
regulation of molecular function	Other
regulation of organelle organization	Other
regulation of response to stimulus	Other
regulation of transport	Other
response to stimulus	Other
response to stress	Other
S-adenosylmethionine-dependent	
methyltransferase activity	Other
single-organism biosynthetic process	Other
single-organism carbohydrate metabolic process	Other
single-organism cellular localization	Other
single-organism cellular process	Other
single-organism intracellular transport	Other
single-organism localization	Other

single-organism membrane organization	Other
single-organism metabolic process	Other
single-organism organelle organization	Other
single-organism process	Other
single-organism transport	Other
small molecule biosynthetic process	Other
small molecule metabolic process	Other
soluble NSF attachment protein activity	Other
structural constituent of ribosome	Other
structural molecule activity	Other
substrate-specific transporter activity	Other
supramolecular fiber organization	Other
transport	Other
transporter activity	Other
TRAPP complex	Other
TRAPPIII protein complex	Other
organic substance catabolic process	Other
organic substance metabolic process	Other
organic substance transport	Other
'de novo' AMP biosynthetic process	Metabolism, activity and transport: Nucleic acids
'de novo' IMP biosynthetic process	Metabolism, activity and transport: Nucleic acids
(S)-2-(5-amino-1-(5-phospho-D-ribosyl) imidazole-4-carboxamido) succinate AMP-lyase (fumarate-forming) activity	Metabolism, activity and transport: Nucleic acids
activation of GTPase activity	Metabolism, activity and transport: Nucleic acids
AMP biosynthetic process	Metabolism, activity and transport: Nucleic acids
AMP metabolic process	Metabolism, activity and transport: Nucleic acids
ATPase activity	Metabolism, activity and transport: Nucleic acids
ATPase activity coupled	Metabolism, activity and transport: Nucleic acids
ATPase activity coupled to movement of substances	Metabolism, activity and transport:

ATPase activity coupled to transmembrane movement of ions phosphorylative mechanism

ATPase activity coupled to transmembrane movement of substances

copper-transporting ATPase activity

GTP binding

GTPase activator activity

GTPase binding

GTPase regulator activity

IMP biosynthetic process

IMP metabolic process

N6-(1 2-dicarboxyethyl)AMP AMP-lyase (fumarate-forming) activity

positive regulation of GTPase activity

proton-transporting ATP synthase complex assembly

proton-transporting ATP synthase complex biogenesis

proton-transporting two-sector ATPase complex assembly

Rab GTPase binding

Ras GTPase binding

Nucleic acids

Metabolism, activity and transport:
Nucleic acids

regulation of GTPase activity	Metabolism, activity and transport: Nucleic acids
small GTPase binding	Metabolism, activity and transport: Nucleic acids
amino acid binding	Metabolism, activity and transport: Proteins and amino acids
amino acid transport	Metabolism, activity and transport: Proteins and amino acids
aminoglycan catabolic process	Metabolism, activity and transport: Proteins and amino acids
aminoglycan metabolic process	Metabolism, activity and transport: Proteins and amino acids
aspartate family amino acid metabolic process	Metabolism, activity and transport: Proteins and amino acids
aspartic-type endopeptidase activity	Metabolism, activity and transport: Proteins and amino acids
aspartic-type peptidase activity	Metabolism, activity and transport: Proteins and amino acids
clathrin adaptor complex	Metabolism, activity and transport: Proteins and amino acids
clathrin coat	Metabolism, activity and transport: Proteins and amino acids
endopeptidase activity	Metabolism, activity and transport: Proteins and amino acids
establishment of protein localization	Metabolism, activity and transport: Proteins and amino acids
establishment of protein localization to mitochondrion	Metabolism, activity and transport: Proteins and amino acids
establishment of protein localization to organelle	Metabolism, activity and transport: Proteins and amino acids
establishment of protein localization to peroxisome	Metabolism, activity and transport: Proteins and amino acids
establishment of protein localization to vacuole	Metabolism, activity and transport: Proteins and amino acids
exopeptidase activity	Metabolism, activity and transport: Proteins and amino acids

intein-mediated protein splicing	Metabolism, activity and transport: Proteins and amino acids
internal peptidyl-lysine acetylation	Metabolism, activity and transport: Proteins and amino acids
internal protein amino acid acetylation	Metabolism, activity and transport: Proteins and amino acids
intracellular protein transport	Metabolism, activity and transport: Proteins and amino acids
metalloexopeptidase activity	Metabolism, activity and transport: Proteins and amino acids
modification-dependent protein catabolic process	Metabolism, activity and transport: Proteins and amino acids
N-acetyltransferase activity	Metabolism, activity and transport: Proteins and amino acids
N-acyltransferase activity	Metabolism, activity and transport: Proteins and amino acids
NEDD8-specific protease activity	Metabolism, activity and transport: Proteins and amino acids
peptidase activity	Metabolism, activity and transport: Proteins and amino acids
peptidase activity acting on L-amino acid peptides	Metabolism, activity and transport: Proteins and amino acids
peptide N-acetyltransferase activity	Metabolism, activity and transport: Proteins and amino acids
peptide-lysine-N-acetyltransferase activity	Metabolism, activity and transport: Proteins and amino acids
peptide-methionine (S)-S-oxide reductase activity	Metabolism, activity and transport: Proteins and amino acids
peptidoglycan catabolic process	Metabolism, activity and transport: Proteins and amino acids
peptidoglycan metabolic process	Metabolism, activity and transport: Proteins and amino acids
peptidoglycan muralytic activity	Metabolism, activity and transport: Proteins and amino acids
peptidyl-glutamic acid modification	Metabolism, activity and transport: Proteins and amino acids
peptidyl-lysine acetylation	Metabolism, activity and transport:

peptidyl-lysine modification	Proteins and amino acids
phosphatidylinositol 3-kinase activity	Metabolism, activity and transport: Proteins and amino acids
phosphatidylinositol 3-kinase complex	Metabolism, activity and transport: Proteins and amino acids
phosphatidylinositol biosynthetic process	Metabolism, activity and transport: Proteins and amino acids
phosphatidylinositol kinase activity	Metabolism, activity and transport: Proteins and amino acids
phosphatidylinositol metabolic process	Metabolism, activity and transport: Proteins and amino acids
phosphatidylinositol phosphate kinase activity	Metabolism, activity and transport: Proteins and amino acids
phosphatidylinositol phosphorylation	Metabolism, activity and transport: Proteins and amino acids
phosphatidylinositol-3-phosphate biosynthetic process	Metabolism, activity and transport: Proteins and amino acids
phosphoprotein binding	Metabolism, activity and transport: Proteins and amino acids
protein acetylation	Metabolism, activity and transport: Proteins and amino acids
protein acylation	Metabolism, activity and transport: Proteins and amino acids
protein alkylation	Metabolism, activity and transport: Proteins and amino acids
protein binding	Metabolism, activity and transport: Proteins and amino acids
protein carboxyl O-methyltransferase activity	Metabolism, activity and transport: Proteins and amino acids
protein catabolic process	Metabolism, activity and transport: Proteins and amino acids
protein complex	Metabolism, activity and transport: Proteins and amino acids
protein complex assembly	Metabolism, activity and transport: Proteins and amino acids
protein complex binding	Metabolism, activity and transport: Proteins and amino acids

protein complex biogenesis

protein complex subunit organization

protein deubiquitination

protein disulfide isomerase activity

protein folding in endoplasmic reticulum

protein histidine kinase activity

protein import

protein insertion into ER membrane

protein insertion into membrane

protein localization

protein localization to organelle

protein localization to
pre-autophagosomal structure

protein localization to vacuole

protein maturation

protein methylation

protein methyltransferase activity

protein modification by
small protein conjugation

protein modification by small
protein conjugation or removal

Proteins and amino acids

Metabolism, activity and transport:

Proteins and amino acids

protein modification by small protein removal	Metabolism, activity and transport: Proteins and amino acids
protein oligomerization	Metabolism, activity and transport: Proteins and amino acids
protein phosphorylated amino acid binding	Metabolism, activity and transport: Proteins and amino acids
protein polyglutamylation	Metabolism, activity and transport: Proteins and amino acids
protein polymerization	Metabolism, activity and transport: Proteins and amino acids
protein processing	Metabolism, activity and transport: Proteins and amino acids
protein retention in Golgi apparatus	Metabolism, activity and transport: Proteins and amino acids
protein splicing	Metabolism, activity and transport: Proteins and amino acids
protein sumoylation	Metabolism, activity and transport: Proteins and amino acids
protein tag	Metabolism, activity and transport: Proteins and amino acids
protein targeting	Metabolism, activity and transport: Proteins and amino acids
protein targeting to vacuole	Metabolism, activity and transport: Proteins and amino acids
protein tetramerization	Metabolism, activity and transport: Proteins and amino acids
protein to membrane docking	Metabolism, activity and transport: Proteins and amino acids
protein transport	Metabolism, activity and transport: Proteins and amino acids
protein transporter activity	Metabolism, activity and transport: Proteins and amino acids
protein ubiquitination	Metabolism, activity and transport: Proteins and amino acids
protein ufmylation	Metabolism, activity and transport: Proteins and amino acids
protein-cysteine S-acyltransferase activity	Metabolism, activity and transport: Proteins and amino acids
protein-cysteine S-palmitoyltransferase activity	Metabolism, activity and transport: Proteins and amino acids

protein-DNA loading ATPase activity	Proteins and amino acids Metabolism, activity and transport: Proteins and amino acids
protein-L-isoaspartate (D-aspartate) O-methyltransferase activity	Metabolism, activity and transport: Proteins and amino acids
proteolysis	Metabolism, activity and transport: Proteins and amino acids
proteolysis involved in cellular protein catabolic process	Metabolism, activity and transport: Proteins and amino acids
small protein activating enzyme activity	Metabolism, activity and transport: Proteins and amino acids
SNARE complex disassembly	Metabolism, activity and transport: Proteins and amino acids
syntaxin binding	Metabolism, activity and transport: Proteins and amino acids
thiol-dependent ubiquitin-specific protease activity	Metabolism, activity and transport: Proteins and amino acids
thiol-dependent ubiquitinyl hydrolase activity	Metabolism, activity and transport: Proteins and amino acids
ubiquitin ligase complex	Metabolism, activity and transport: Proteins and amino acids
ubiquitin protein ligase activity	Metabolism, activity and transport: Proteins and amino acids
ubiquitin protein ligase binding	Metabolism, activity and transport: Proteins and amino acids
ubiquitin-dependent protein catabolic process	Metabolism, activity and transport: Proteins and amino acids
ubiquitin-dependent protein catabolic process via the N-end rule pathway	Metabolism, activity and transport: Proteins and amino acids
ubiquitin-like protein ligase activity	Metabolism, activity and transport: Proteins and amino acids
ubiquitin-like protein ligase binding	Metabolism, activity and transport: Proteins and amino acids
ubiquitin-like protein transferase activity	Metabolism, activity and transport: Proteins and amino acids
ubiquitin-like protein-specific protease activity	Metabolism, activity and transport: Proteins and amino acids

ubiquitin-protein transferase activator activity	Metabolism, activity and transport: Proteins and amino acids
ubiquitin-protein transferase activity	Metabolism, activity and transport: Proteins and amino acids
ubiquitin-protein transferase regulator activity	Metabolism, activity and transport: Proteins and amino acids
ubiquitinyl hydrolase activity	Metabolism, activity and transport: Proteins and amino acids
cleavage in ITS2 between 5.8S rRNA and LSU-rRNA of tricistronic rRNA transcript (SSU-rRNA 5.8S rRNA LSU-rRNA)	Ribosomal structure, activity and functioning
establishment of ribosome localization	Ribosomal structure, activity and functioning
ribonuclease activity	Ribosomal structure, activity and functioning
ribonuclease T2 activity	Ribosomal structure, activity and functioning
ribonucleoprotein complex	Ribosomal structure, activity and functioning
ribonucleoside biosynthetic process	Ribosomal structure, activity and functioning
ribosomal subunit export from nucleus	Ribosomal structure, activity and functioning
ribosome localization	Ribosomal structure, activity and functioning
ARF protein signal transduction	Signaling
inositol lipid-mediated signaling	Signaling
intracellular signal transduction	Signaling
phosphatidylinositol-mediated signaling	Signaling
phosphorelay signal transduction system	Signaling
protein kinase C-activating G-protein coupled receptor signaling pathway	Signaling
Ras protein signal transduction	Signaling
regulation of ARF protein signal transduction	Signaling
regulation of intracellular signal transduction	Signaling
regulation of Ras protein signal transduction	Signaling
regulation of signal transduction	Signaling
regulation of signaling	Signaling
regulation of small GTPase mediated signal transduction	Signaling
signal transducer activity	Signaling
signal transduction	Signaling
signal transduction by protein phosphorylation	Signaling
signaling	Signaling
signaling receptor activity	Signaling
single organism signaling	Signaling
small GTPase mediated signal transduction	Signaling

peroxidase activity	Vesicle structures
peroxisomal part	Vesicle structures
peroxisomal transport	Vesicle structures
peroxisome	Vesicle structures
peroxisome fission	Vesicle structures
peroxisome matrix targeting signal-1 binding	Vesicle structures
peroxisome organization	Vesicle structures
peroxisome targeting sequence binding	Vesicle structures
protein import into peroxisome matrix	Vesicle structures
protein import into peroxisome matrix docking	Vesicle structures
protein localization to peroxisome	Vesicle structures
protein targeting to peroxisome	Vesicle structures
regulation of peroxisome size	Vesicle structures
condensin complex	Vesicle structures
coated vesicle	Vesicle structures
COPI vesicle coat	Vesicle structures
COPI-coated vesicle	Vesicle structures
cytoplasmic vesicle	Vesicle structures
cytoplasmic vesicle part	Vesicle structures
endocytic vesicle	Vesicle structures
intracellular vesicle	Vesicle structures
phagocytic vesicle	Vesicle structures
phagocytosis	Vesicle structures
phagolysosome	Vesicle structures
phagolysosome assembly	Vesicle structures
phagosome maturation	Vesicle structures
phagosome-lysosome fusion	Vesicle structures
regulation of vesicle fusion	Vesicle structures
regulation of vesicle-mediated transport	Vesicle structures
vesicle	Vesicle structures
vesicle coat	Vesicle structures
vesicle fusion	Vesicle structures
vesicle organization	Vesicle structures
food vacuole	Vesicle structures
lysosome	Vesicle structures
lysosome organization	Vesicle structures
lysozyme activity	Vesicle structures
lytic vacuole	Vesicle structures
lytic vacuole organization	Vesicle structures
pexophagy	Vesicle structures

vacuolar part	Vesicle structures
vacuolar transport	Vesicle structures
vacuole	Vesicle structures
vacuole organization	Vesicle structures
CVT pathway	Vesicle structures
secondary lysosome	Vesicle structures

Table S4.8: Categorization of the enriched gene ontology terms. We list for each of the enriched gene ontology terms to which of the 13 broad categories we classified those terms to.

S.4.10 Model summary and Anova tables

S.4.10.1 Genetic changes on standing genetic variation

	χ^2	Df	Pr(> χ^2)
(Intercept)	3358.814	1	<0.001
Reproduction	0.265	1	0.601
Gene flow	0.026	1	0.873
Abiotic conditions	0.592	1	0.442
Cut-off	1101.998	1	<0.001
Reproduction×Gene flow	0.0002	1	0.990
Reproduction×Abiotic conditions	8.398	1	0.004
Gene flow×Abiotic conditions	0.317	1	0.573
Reproduction×Cut-off	102.306	1	<0.001
Gene flow×Cut-off	22.694	1	<0.001
Abiotic conditions×Cut-off	104.755	1	<0.001
Reproduction×Gene flow×Abiotic conditions	3.752	1	0.053
Reproduction×Gene flow×Cut-off	24.295	1	<0.001
Reproduction×Abiotic conditions×Cut-off	263.736	1	<0.001
Gene flow×Abiotic conditions×Cut-off	41.389	1	<0.001
Reproduction×Gene flow×Abiotic conditions×Cut-off	133.781	1	<0.001

Table S4.9: Type III Anova table for the best model describing allele frequency changes in standing genetic variation, based on BIC model comparisons. For each of the variables, we list the χ^2 value, the degrees of freedom (Df), and the significance (Pr> χ^2).

	Estimate	Std. Error	z value	Pr(> z)
(Intercept)	9.337	0.161	57.955	<0.001
Reproduction (Sexual)	-0.104	0.202	-0.515	0.607
Gene flow (Present)	0.033	0.209	0.160	0.873
Abiotic conditions (Gradient)	-0.156	0.202	-0.770	0.442
Cut-off	-10.891	0.328	-33.196	<0.001
Reproduction (Sexual) × Gene flow (Present)	-0.004	0.272	-0.013	0.990
Reproduction (Sexual) × Abiotic conditions (Gradient)	0.809	0.279	2.898	<0.001
Gene flow (present) × Abiotic conditions (Gradient)	0.154	0.273	0.563	0.573
Reproduction (Sexual) × Cut-off	3.575	0.353	10.115	<0.001
Gene flow (Present) × Cut-off	1.838	0.386	4.764	<0.001
Abiotic conditions (Gradient) × Cut-off	3.624	0.354	10.235	<0.001
Reproduction (Sexual) × Gene flow (Present) × Abiotic conditions (Gradient)	-0.731	0.377	-1.937	0.053
Reproduction (Sexual) × Gene flow (Present) × Cut-off	-2.136	0.433	-4.929	<0.001
Reproduction (Sexual) × Abiotic conditions (Gradient) × Cut-off	-7.686	0.473	-16.240	<0.001
Gene flow (Present) × Abiotic conditions (Gradient) × Cut-off	-2.815	0.437	-6.433	<0.001
Reproduction (Sexual) × Gene flow (Present) × Abiotic conditions (Gradient) × Cut-off	6.686	0.578	11.566	<0.001

Table S4.10: Summary table for the best model describing allele frequency changes in standing genetic variation, based on BIC model comparisons. We list the estimates for the variables (Estimate), the standard error of the estimate (Std. Error), the z-value, and the probability that the estimate is different from 0 ($\text{Pr}(>|z|)$).

S.4.10.2 Genetic changes through *De novo* mutation

	χ^2	Df	Pr(> χ^2)
(Intercept)	347.748	1	<0.001
Reproduction	13.567	1	<0.001
Cut-off	693.055	1	<0.001
Reproduction \times Cut-off	18.696	1	<0.001

Table S4.11: Type III Anova table for the best model describing genetic change through *de novo* mutation, based on BIC model comparisons. For each of the variables, we list the χ^2 value, the degrees of freedom (Df), and the significance (Pr> χ^2).

	Estimate	Std. Error	DF	t-value	p-value
(Intercept)	1700.632	91.197	126	18.648	<0.001
Reproduction (Sexual)	475.052	128.971	14	3.683	0.003
Cut-off	-1968.292	74.766	126	-26.326	<0.001
Reproduction (Sexual) \times Cut-off	-457.188	105.735	126	-4.324	<0.001

Table S4.12: Summary table for the best model describing genetic change through *de novo* mutation, based on BIC model comparisons. We list the estimates for the variables (Estimate), the standard error of the estimate (Std. Error), the z-value, and the probability that the estimate is different from 0 (Pr>|z|).

S.4.10.3 Fitness changes: evolution of population growth rate

	DF	χ^2 -value	Pr (> χ^2)
(Intercept)	1	11.42	0.006
Reproduction	1	6.44	0.027
Gene flow	1	8.09	0.016
Abiotic conditions	1	299.16	<0.0001
Reproduction \times Gene flow	1	14.36	0.003
Residuals	11		

Table S4.13: Type III Anova table for the best model describing the change of intrinsic population growth rate, according to the AICc model comparisons. For each of the variables, we list, the degrees of freedom (Df) the χ^2 value, and the significance (Pr> χ^2).

	Estimate	Std. Error	t value	Pr(> t)
(Intercept)	0.127	0.038	3.379	0.006
Reproduction (Sexual)	0.121	0.048	2.539	0.028

Gene flow (Present)	0.136	0.048	2.844	0.016
Abiotic conditions (Gradient)	0.583	0.034	17.296	<0.001
Reproduction (Sexual) × Gene flow (Present)	-0.256	0.067	-3.789	0.003

Table S4.14: Type III Anova table for the best model describing the change of intrinsic population growth rate, according to the AICc model comparisons. We list the estimates for the variables (Estimate), the standard error of the estimate (Std. Error), the degrees of freedom (DF), the t-value, and the probability that the estimate is different from 0 ($\text{Pr}>|t|$).

S.4.11 Association between genetic change through *de novo* mutation and fitness change.

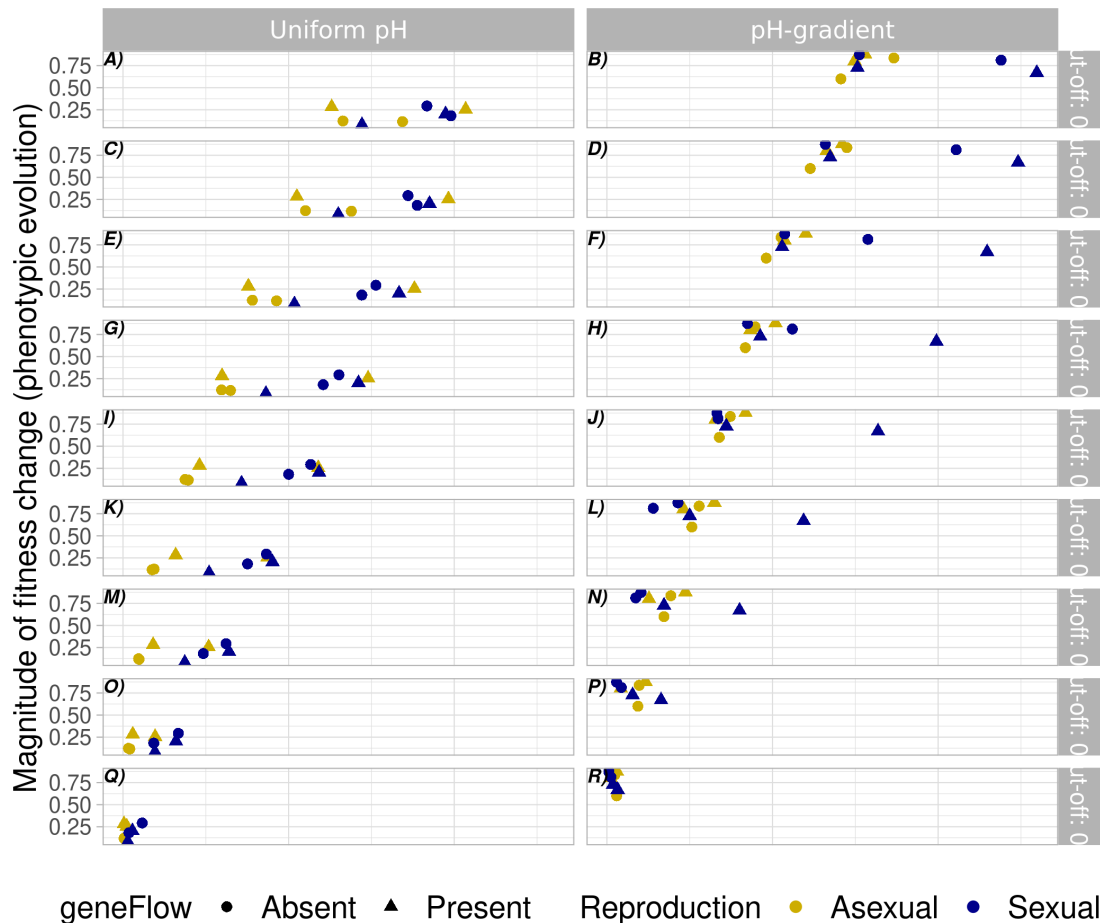


Figure S4.3: **No association between fitness change and number of *de novo* mutations.** Association between change in fitness and rate of molecular change (number of *de novo* mutations). The y-axis shows phenotypic evolution in terms of the log ratio of growth rate change ($\log_2(r_0$ of evolved population / r_0 of ancestral population)). The x-axis shows the number of *de novo* mutations detected in the populations. The left subplots show the data for populations expanding into a uniform environment, and the right subplots for populations expanding into a pH-gradient. Horizontal subplots show the data for different cut-off values for the minimal frequency of *de novo* mutations. Each circle within a subplot represents a single population, with colour representing the mode of reproduction (yellow=asexual, blue=sexual) and shape representing gene flow (circle=gene flow absent, triangle=gene flow present).

S.4.12 Genes involved in adaptive evolution through genetic change on standing variation

S.4.12.1 Analysis of genetic changes on standing variation: general adaptation

	Gene ID	Gene function	Populations
1	TTHERM_00721820	Leishmanolysin family protein	16
2	TTHERM_00672030	Transmembrane protein, putative	16
3	TTHERM_00896100	FAD-dependent pyridine nucleotide-disulfide oxidoreductase	16
4	TTHERM_00263480	Cyclic nucleotide-binding domain protein	16
5	TTHERM_001186268	Kinase domain protein	15
6	TTHERM_00283160	ABC transporter C family protein	15
7	TTHERM_00129550	Surface protein	15
8	TTHERM_00641320	Transmembrane protein, putative	15
9	TTHERM_00355140	Transmembrane protein, putative	15
10	TTHERM_00809310	Type A von willebrand factor domain protein	15
11	TTHERM_00942900	Transmembrane protein, putative	15
12	TTHERM_00115540	Zinc finger lsd1 subclass family protein	15
13	TTHERM_00702240	Tubulin-tyrosine ligase family protein	15
14	TTHERM_01466260	Zinc finger lsd1 subclass family protein	14
15	TTHERM_01054360	Uncharacterized protein	14
16	TTHERM_00218220	Uncharacterized protein	14
17	TTHERM_01576270	Kinase domain protein	14
18	TTHERM_000252299	Uncharacterized protein	14
19	TTHERM_00490570	Uncharacterized protein	14
20	TTHERM_01335240	Uncharacterized protein	14
21	TTHERM_00895950	Zinc finger, LSD1 subclass family protein, putative	14
22	TTHERM_00467340	Uncharacterized protein	13
23	TTHERM_00615940	Dienelactone hydrolase family protein	13
24	TTHERM_000660229	Cyclic nucleotide-binding domain protein	13
25	TTHERM_01368730	Transmembrane protein, putative	13
26	TTHERM_001076853	Uncharacterized protein	13
27	TTHERM_000740571	Uncharacterized protein	13
28	TTHERM_00783190	Uncharacterized protein	13
29	TTHERM_00158130	Uncharacterized protein	13
30	TTHERM_000713618	Kinase domain protein	12
31	TTHERM_001287957	Kinase domain protein	12

32	TTHERM_00243960	Transmembrane protein, putative	12
33	TTHERM_00564050	Transmembrane protein, putative	12
34	TTHERM_001230180	Transmembrane protein, putative	12
35	TTHERM_001250061	Cation channel family protein	12
36	TTHERM_00317270	Transmembrane protein, putative	12
37	TTHERM_00130070	Tetratricopeptide repeat protein	12
38	TTHERM_00129530	REJ domain protein	12
39	TTHERM_00378920	Transmembrane protein, putative	12
40	TTHERM_000222205	Transmembrane protein, putative (Fragment)	12
41	TTHERM_00161670	Cation channel family protein	12
42	TTHERM_00538520	Transmembrane protein, putative	12
43	TTHERM_00070830	Cyclic nucleotide-binding domain protein	12

Table S4.15: Genes for which we observed changes in allele frequency associated with general adaptation during range expansion, ordered by the number of populations for which we observed allele frequency changes in the specified genes. For each gene, we list the gene identifier (Gene ID), the function associated with the gene, and the number of populations in which we observed significant allele frequency changes for the gene.

S.4.12.2 Analysis of genetic changes on standing variation: gradient-specific adaptation

Gene ID	Gene function
TTHERM_001431570	Cell surface immobilization antigen
TTHERM_00526520	Response regulator receiver domain protein
TTHERM_000526679	Dpy-30 motif protein
TTHERM_00526750	Cyclic nucleotide-binding domain protein
TTHERM_00526960	Uncharacterized protein
TTHERM_00526990	SIR2 family histone deacetylase, putative
TTHERM_00495910	Uncharacterized protein
TTHERM_00918480	Uncharacterized protein
TTHERM_000676909	Cyclic nucleotide-binding domain protein (Fragment)
TTHERM_000678048	Kinase domain protein
TTHERM_00678480	Latrophilin/CL-like GPS domain protein
TTHERM_002653394	Cyclic nucleotide-binding domain protein (Fragment)
TTHERM_01496780	Serine/Threonine kinase domain protein (Fragment)
TTHERM_01131800	Tetratricopeptide repeat protein
TTHERM_001284707	Kinase domain protein (Fragment)
TTHERM_01697320	Kinase domain protein (Fragment)
TTHERM_000645801	Transmembrane protein, putative
TTHERM_00842500	U1 small nuclear ribonucleoprotein A
TTHERM_01324740	Cyclic nucleotide-binding domain protein
TTHERM_001325754	Kinase domain protein
TTHERM_000726249	Cation channel family protein
TTHERM_00726490	Uncharacterized protein
TTHERM_00904020	Uncharacterized protein
TTHERM_00905060	Uncharacterized protein
TTHERM_00688320	Zinc finger transcription factor sma protein, putative

TTHERM_002653480	Uncharacterized protein (Fragment)
TTHERM_00941510	Serine/Threonine kinase domain protein
TTHERM_00941610	Zinc finger lsd1 subclass family protein
TTHERM_01515340	Kinase domain protein
TTHERM_001449010	Kinase domain protein (Fragment)
TTHERM_01107380	Transmembrane protein, putative
TTHERM_01889100	Kinase domain protein
TTHERM_01165190	Regulator of chromosome condensation RCC1 protein (Fragment)
TTHERM_01165250	Kinase domain protein
TTHERM_00864900	Kinase domain protein
TTHERM_01008670	Transmembrane protein, putative
TTHERM_01008680	Uncharacterized protein
TTHERM_01311210	Uncharacterized protein
TTHERM_000326869	C1-like domain protein, putative
TTHERM_00327030	IQ calmodulin-binding motif protein
TTHERM_00327310	Transmembrane protein, putative
TTHERM_00332170	Amine-terminal domain cyclin
TTHERM_002653514	Transmembrane protein, putative
TTHERM_002653515	Transmembrane protein, putative (Fragment)
TTHERM_000851660	Protein kinase
TTHERM_00790580	Serine/Threonine kinase domain protein
TTHERM_00790660	Cyclic nucleotide-binding domain protein
TTHERM_00790680	Endo-1,4-beta-xylanase xylA, putative
TTHERM_00790690	Uncharacterized protein
TTHERM_00971900	Transmembrane protein, putative
TTHERM_01232200	Uncharacterized protein
TTHERM_01232250	Uncharacterized protein
TTHERM_001232265	Cyclic nucleotide-binding domain protein
TTHERM_001651030	Uncharacterized protein

TTHERM_01114210	Uncharacterized protein (Fragment)
TTHERM_01390270	Kinase domain protein
TTHERM_01392280	Kinase domain protein, putative
TTHERM_00711790	ATPase, histidine kinase-, DNA gyrase B
TTHERM_00711850	Uncharacterized protein
TTHERM_00713260	Uncharacterized protein
TTHERM_00713280	Transmembrane protein, putative
TTHERM_01093490	MIR domain protein
TTHERM_01525430	Kinase domain protein
TTHERM_001354239	Uncharacterized protein
TTHERM_01732490	von willebrand factor type A domain protein
TTHERM_01220450	Uncharacterized protein
TTHERM_00697230	Cyclic nucleotide-binding domain protein
TTHERM_00697080	Plant dual-specificity MAP kinase kinase family domain protein
TTHERM_00695680	IQ calmodulin-binding motif protein
TTHERM_001363590	Uncharacterized protein
TTHERM_01243410	Transmembrane protein, putative
TTHERM_01489720	Kinase domain protein (Fragment)
TTHERM_001489730	Transmembrane protein, putative
TTHERM_01645010	Uncharacterized protein
TTHERM_001571179	Uncharacterized protein (Fragment)
TTHERM_001615779	Transmembrane protein, putative
TTHERM_001287953	Kinase domain protein, putative
TTHERM_00723300	Uncharacterized protein
TTHERM_00723330	MFS transporter
TTHERM_00723630	Thioredoxin and glutathione reductase family protein
TTHERM_001400689	Cyclic nucleotide-binding domain protein
TTHERM_00684550	Serine/Threonine kinase domain protein
TTHERM_00686010	EF hand protein

TTHERM_001257658	Kinase domain protein (Fragment)
TTHERM_001259661	Kinase domain protein, putative
TTHERM_001259662	Kinase domain protein
TTHERM_000465070	Cyclic nucleotide-binding domain protein
TTHERM_00467250	Dynein_AAA_lid domain-containing protein
TTHERM_00239160	Transmembrane protein, putative
TTHERM_00241480	ABC transporter B family protein
TTHERM_00242360	Transmembrane protein, putative
TTHERM_01573200	Cyclic nucleotide-binding domain protein
TTHERM_00715690	Uncharacterized protein
TTHERM_00615890	Uncharacterized protein
TTHERM_00615940	Dienelactone hydrolase family protein
TTHERM_00616610	Transmembrane protein, putative
TTHERM_00616630	Transmembrane protein, putative
TTHERM_00299600	Tubulin-tyrosine ligase family protein
TTHERM_00300150	REJ domain protein
TTHERM_00300170	Transmembrane protein, putative
TTHERM_001224670	Tetratricopeptide repeat protein
TTHERM_00532220	Leucyl-tRNA synthetase protein
TTHERM_000532408	Cation channel family protein
TTHERM_01406900	Kinase domain protein
TTHERM_002653492	Cyclic nucleotide-binding domain protein (Fragment)
TTHERM_000703469	Uncharacterized protein
TTHERM_00703990	BTB And carboxy-terminal kelch protein
TTHERM_001151573	Protein kinase
TTHERM_000455680	Transmembrane protein, putative
TTHERM_00459360	EGF-like domain protein
TTHERM_000823849	CRAL/TRIO domain protein
TTHERM_00659000	Transmembrane protein, putative

TTHERM_00243690	Transmembrane amino acid transporter protein
TTHERM_00245820	Tetratricopeptide repeat protein
TTHERM_01662070	Kinase domain protein
TTHERM_001662070	Kinase domain protein
TTHERM_00732640	60S ribosomal protein L13/L16
TTHERM_00732660	Transmembrane protein, putative
TTHERM_00732760	D-alanyl-D-alanine carboxypeptidase family protein
TTHERM_00732770	Uncharacterized protein
TTHERM_01100430	Transmembrane protein, putative
TTHERM_01100470	Uncharacterized protein
TTHERM_001574229	Uncharacterized protein
TTHERM_000691839	Transmembrane protein, putative
TTHERM_01466260	Zinc finger lsd1 subclass family protein
TTHERM_001466260	Zinc finger lsd1 subclass family protein
TTHERM_00571710	Tetratricopeptide repeat protein
TTHERM_00569500	Guanine nucleotide exchange factor
TTHERM_01587460	Regulator of chromosome condensation RCC1 protein (Fragment)
TTHERM_001085711	Transmembrane protein, putative
TTHERM_00655270	Phosphatidylinositol 3-and 4-kinase
TTHERM_000655322	Uncharacterized protein
TTHERM_00655870	Polypyrimidine tract-binding protein
TTHERM_00655930	Kelch motif protein
TTHERM_00656080	Nucleotidyl transferase family protein
TTHERM_000939049	Cyclic nucleotide-binding domain protein, putative
TTHERM_01434640	Translation initiation factor eIF-5A family protein
TTHERM_00492320	Uncharacterized protein
TTHERM_00492410	Transmembrane protein, putative
TTHERM_00494410	Uncharacterized protein
TTHERM_00494480	Uncharacterized protein

TTHERM_00529650	DUF4201 domain-containing protein
TTHERM_00530270	ASH domain-containing protein
TTHERM_00353280	Adenosylhomocysteinase (EC 3.3.1.1)
TTHERM_000351139	Heat shock-binding protein 70, ER luminal protein
TTHERM_001372842	Oxalate/formate antiporter protein (Fragment)
TTHERM_00579250	Transmembrane protein, putative
TTHERM_00579300	Transmembrane protein, putative
TTHERM_00951800	ABC transporter C family protein
TTHERM_01044570	Polycystin cation channel protein
TTHERM_000630737	Cyclic nucleotide-binding domain protein, putative
TTHERM_000630669	Cyclic nucleotide-binding domain protein, putative
TTHERM_00630610	Response regulator receiver domain protein
TTHERM_000630029	Kinase domain protein
TTHERM_00630030	Glycoside hydrolase family 38 amine-terminal domain protein
TTHERM_00629770	Transmembrane protein, putative
TTHERM_001089079	Transmembrane protein, putative
TTHERM_001090198	Transmembrane protein, putative
TTHERM_01090200	Transmembrane protein, putative
TTHERM_00433560	Serine/Threonine kinase domain protein
TTHERM_00431380	Uncharacterized protein
TTHERM_00431340	EEIG1/EHBP1 protein amine-terminal domain protein
TTHERM_00429720	Adenylate/guanylate cyclase domain protein
TTHERM_00429690	Cyclic nucleotide-binding domain protein
TTHERM_01533610	Transmembrane protein, putative
TTHERM_001338459	Transmembrane protein, putative
TTHERM_01338500	Cyclic nucleotide-binding domain protein
TTHERM_01156760	Kinase domain protein
TTHERM_01156890	Oxalate/formate antiporter protein, putative (Fragment)
TTHERM_00420850	Uncharacterized protein

TTHERM_01245620	Kinesin motor catalytic domain protein
TTHERM_000622658	Transmembrane protein, putative
TTHERM_01474480	Kinase domain protein
TTHERM_01474490	Carrier protein
TTHERM_00822190	Transmembrane protein, putative
TTHERM_000989520	Kinase domain protein
TTHERM_00787420	Myxococcus cysteine-rich repeat protein
TTHERM_00566830	Uncharacterized protein
TTHERM_000566889	Uncharacterized protein
TTHERM_00859280	Kinesin motor catalytic domain protein
TTHERM_00859330	SIR2 family transcriptional regulator
TTHERM_01277450	Kinase domain protein (Fragment)
TTHERM_01277470	Uncharacterized protein
TTHERM_01277530	Cation channel family protein
TTHERM_001277531	Cation channel family protein
TTHERM_00933160	PH domain protein
TTHERM_01109790	Uncharacterized protein
TTHERM_01027580	Uncharacterized protein
TTHERM_01027670	Dynein heavy chain 1, axonemal protein
TTHERM_002653518	Uncharacterized protein (Fragment)
TTHERM_01230160	Kinase domain protein
TTHERM_001230169	Uncharacterized protein
TTHERM_00721280	Cyclic nucleotide-binding domain protein
TTHERM_00721370	GRASP55/65 family protein
TTHERM_01181980	Transmembrane protein, putative
TTHERM_01182010	Kinase domain protein
TTHERM_002653469	Kinase domain protein (Fragment)
TTHERM_01285860	Uncharacterized protein
TTHERM_01285880	Uncharacterized protein

TTHERM_00486110	Transmembrane protein, putative
TTHERM_01054360	Uncharacterized protein
TTHERM_000898192	Kinase domain protein, putative
TTHERM_00149170	Cation channel family protein
TTHERM_00149670	Uncharacterized protein
TTHERM_01413110	Uncharacterized protein (Fragment)
TTHERM_01414130	Transmembrane protein, putative
TTHERM_000316109	AMP-binding enzyme family protein
TTHERM_00316200	Transmembrane protein, putative
TTHERM_00316880	Transmembrane protein, putative
TTHERM_00318780	PH domain protein
TTHERM_00774860	Uncharacterized protein
TTHERM_00777070	Protein phosphatase 1 regulatory subunit 7
TTHERM_00304320	Zinc finger lsd1 subclass family protein
TTHERM_000304329	Zinc finger lsd1 subclass family protein
TTHERM_00309880	Ku70/Ku80 beta-barrel domain protein, putative
TTHERM_00409040	Tetratricopeptide repeat protein
TTHERM_00411410	Transmembrane protein, putative
TTHERM_00956490	Transmembrane protein, putative
TTHERM_01295350	Cyclic nucleotide-binding domain protein
TTHERM_01495770	Uncharacterized protein (Fragment)
TTHERM_01476540	REJ domain protein
TTHERM_00216030	Uncharacterized protein
TTHERM_00216110	ATPase, histidine kinase-, DNA gyrase B
TTHERM_000218559	Transmembrane protein, putative
TTHERM_000220708	Protein kinase
TTHERM_00470560	Cyclic nucleotide-binding domain protein
TTHERM_00935420	Kinase domain protein
TTHERM_00937650	Kinase domain protein

TTHERM_000797791	Cyclic nucleotide-binding domain protein
TTHERM_000799209	Uncharacterized protein
TTHERM_00891270	Transmembrane protein, putative
TTHERM_00959810	Kinase domain protein
TTHERM_00912290	Dynein heavy chain 2, putative
TTHERM_00916430	ABC transporter family protein
TTHERM_00663930	Transmembrane protein, putative
TTHERM_00663820	Oxalate/formate antiporter family transporter
TTHERM_00660310	Kinase domain protein
TTHERM_00666890	Transmembrane protein, putative
TTHERM_00586810	Zinc finger lsd1 subclass family protein
TTHERM_000590238	Uncharacterized protein
TTHERM_00138560	Inositol 1,4,5-trisphosphate receptor type 3
TTHERM_00136200	Transmembrane protein, putative
TTHERM_00131260	MFS transporter
TTHERM_01121610	Kinase domain protein, putative
TTHERM_00628350	Transmembrane protein, putative
TTHERM_000627299	Transmembrane protein, putative
TTHERM_00627230	Myb-like DNA-binding domain protein
TTHERM_000627099	Kinase domain protein
TTHERM_01213900	Serine/Threonine kinase domain protein
TTHERM_00388560	EF-hand pair protein
TTHERM_00249790	Cation-transporting ATPase (EC 7.2.2.-)
TTHERM_00251050	Kinase domain protein
TTHERM_00251120	Uncharacterized protein
TTHERM_00252280	Uncharacterized protein
TTHERM_000252388	Cation channel family protein
TTHERM_00253469	Transmembrane protein, putative
TTHERM_000255649	Ataxin-2 amine-terminal region family protein

TTHERM_00255680	Uncharacterized protein
TTHERM_00256740	Transmembrane protein, putative
TTHERM_01211840	Kinase domain protein
TTHERM_00581840	MORN repeat protein
TTHERM_00582380	AMP-binding enzyme family protein
TTHERM_00717660	Cation channel family protein
TTHERM_00717670	Cation channel family protein
TTHERM_00462820	Kinase domain protein, putative
TTHERM_001161050	Kinase domain protein
TTHERM_00285260	Type A von willebrand factor domain protein
TTHERM_000286805	Transmembrane protein, putative
TTHERM_00290640	Leishmanolysin family protein, putative
TTHERM_00292200	Transmembrane protein, putative
TTHERM_00998800	ABC transporter C family protein
TTHERM_001421350	Uncharacterized protein
TTHERM_000341290	Kinase domain protein, putative
TTHERM_00343580	Transmembrane protein, putative
TTHERM_00344110	Surface protein with EGF domain and furin-like repeat protein, putative
TTHERM_00344130	Surface protein with EGF domain and furin-like repeat protein, putative
TTHERM_000751040	Kinase domain protein
TTHERM_00753290	Amine-terminal region of chorein, A TM vesicle-mediated sorter
TTHERM_000753301	Transmembrane protein, putative
TTHERM_000753449	Transmembrane protein, putative
TTHERM_00277360	Kinase domain protein
TTHERM_000277588	Uncharacterized protein
TTHERM_00279971	Kinase domain protein
TTHERM_00283300	F-box protein
TTHERM_00283340	Uncharacterized protein
TTHERM_00283580	REJ domain protein

TTHERM_000284229	Transmembrane protein, putative
TTHERM_01312310	Uncharacterized protein (Fragment)
TTHERM_001312320	Transmembrane protein, putative
TTHERM_01312370	Transmembrane protein, putative
TTHERM_00954390	Transmembrane protein, putative
TTHERM_01046960	Kinase domain protein
TTHERM_01461130	Kinase domain protein
TTHERM_01087810	Transmembrane protein, putative
TTHERM_01087820	Transmembrane protein, putative
TTHERM_01087860	Uncharacterized protein
TTHERM_01009810	REJ domain protein
TTHERM_01009860	Leishmanolysin family protein
TTHERM_001009993	Transmembrane protein, putative
TTHERM_000335848	PAS domain S-box protein
TTHERM_00476560	Rab-GAP TBC domain-containing protein
TTHERM_00481240	Cation channel family protein
TTHERM_00483430	Uncharacterized protein
TTHERM_00193480	CLASP amine-terminal protein
TTHERM_00194630	Uncharacterized protein
TTHERM_00195950	Cation channel family protein
TTHERM_01469350	Kinase domain protein (Fragment)
TTHERM_01368730	Transmembrane protein, putative
TTHERM_00862730	Kinase domain protein
TTHERM_00862740	Transporter family ABC domain protein
TTHERM_000862770	Kinase domain protein
TTHERM_01081620	Uncharacterized protein
TTHERM_01081630	Transmembrane protein, putative
TTHERM_00758930	AMP-binding enzyme family protein
TTHERM_001076869	Transmembrane protein, putative

TTHERM_00979950	Leishmanolysin family protein
TTHERM_000488184	Dynein motor region D1 hydrolytic ATP-binding site protein
TTHERM_000490579	Uncharacterized protein
TTHERM_00490650	Transmembrane protein, putative
TTHERM_00490660	Endonuclease/exonuclease/phosphatase family protein
TTHERM_00491010	Transmembrane protein, putative
TTHERM_00491190	Transmembrane protein, putative
TTHERM_000491227	Transmembrane protein, putative
TTHERM_000491228	Transmembrane protein, putative
TTHERM_00188740	Cyclic nucleotide-binding domain protein
TTHERM_00190658	SIT4 phosphatase-associated protein
TTHERM_000191018	Cyclic nucleotide-binding domain protein
TTHERM_00191530	Cyclic nucleotide-binding domain protein
TTHERM_000648673	Ubiquitin family protein
TTHERM_000129899	Uncharacterized protein
TTHERM_000128319	Amylo-alpha-1,6-glucosidase
TTHERM_000818428	Uncharacterized protein
TTHERM_000819632	Kinase domain protein
TTHERM_00878190	Transmembrane protein, putative
TTHERM_000275799	Tetratricopeptide repeat protein
TTHERM_000073142	Uncharacterized protein
TTHERM_00075780	Uncharacterized protein
TTHERM_000075819	Transmembrane protein, putative
TTHERM_00077010	Transmembrane protein, putative
TTHERM_00077280	Kinase domain protein, putative
TTHERM_00077470	Cyclic nucleotide-binding domain protein
TTHERM_000077478	Cyclic nucleotide-binding domain protein
TTHERM_00079679	MFS transporter, putative
TTHERM_001397459	Kinase domain protein, putative

TTHERM_000382129	Kinase domain protein
TTHERM_00382170	Cation channel family protein
TTHERM_00641270	Uncharacterized protein
TTHERM_00641320	Transmembrane protein, putative
TTHERM_00644670	Cyclic nucleotide-binding domain protein
TTHERM_000644779	Cyclic nucleotide-binding domain protein
TTHERM_000506970	Tetratricopeptide repeat protein
TTHERM_00515260	Kinase domain protein, putative
TTHERM_00519770	TNFR/NGFR cysteine-rich region family protein
TTHERM_00672030	Transmembrane protein, putative
TTHERM_00672250	Uncharacterized protein
TTHERM_000672288	Kinase domain protein
TTHERM_00675560	Tc5 transposase DNA-binding domain protein
TTHERM_00675710	Cation channel family protein
TTHERM_00675720	RAP domain protein
TTHERM_01327890	Kinase domain protein
TTHERM_01328900	Transmembrane protein, putative
TTHERM_01328940	Transmembrane protein
TTHERM_01335330	Uncharacterized protein
TTHERM_00522080	D-alanyl-D-alanine carboxypeptidase family protein
TTHERM_00522890	Uncharacterized protein
TTHERM_000523058	EF hand protein
TTHERM_000225939	Uncharacterized protein
TTHERM_00227020	Cytochrome P450 family monooxygenase
TTHERM_00227090	Uncharacterized protein
TTHERM_00227100	Uncharacterized protein
TTHERM_000227559	Kinase domain protein
TTHERM_00398130	Small GTP-binding domain protein
TTHERM_000399159	Small GTP-binding domain protein

TTHERM_00654110	Transmembrane protein, putative
TTHERM_00653900	Protein kinase
TTHERM_00030330	Uncharacterized protein
TTHERM_00030470	Tetratricopeptide repeat protein
TTHERM_00031620	Cyclic nucleotide-binding domain protein
TTHERM_00035140	Cyclic nucleotide-binding domain protein
TTHERM_00035180	Acetoacetate decarboxylase, putative
TTHERM_00037250	TNFR-Cys domain-containing protein
TTHERM_00037430	ABC transporter transmembrane region family protein
TTHERM_00040370	Uncharacterized protein
TTHERM_002653471	Uncharacterized protein
TTHERM_000770889	Transmembrane protein, putative
TTHERM_000770900	Cation channel family protein
TTHERM_000770911	Cation channel family protein
TTHERM_00772000	Uncharacterized protein
TTHERM_00424520	Transmembrane protein, putative
TTHERM_00426390	Uncharacterized protein
TTHERM_00833680	Uncharacterized protein
TTHERM_00833830	EF hand protein
TTHERM_00746850	Transmembrane protein, putative
TTHERM_00746860	Uncharacterized protein
TTHERM_00746890	Uncharacterized protein
TTHERM_01119390	Kinase domain protein
TTHERM_01119400	Kinase domain protein
TTHERM_01119540	DNA-directed RNA polymerase
TTHERM_01256580	Zinc finger transcription factor sma protein, putative
TTHERM_01256640	Oxalate/formate antiporter protein
TTHERM_001442802	Uncharacterized protein
TTHERM_01442810	Tetratricopeptide repeat protein (Fragment)

TTHERM_000927011	Uncharacterized protein
TTHERM_00927310	Uncharacterized protein
TTHERM_01399600	Transmembrane protein, putative
TTHERM_01329990	Kinase domain protein
TTHERM_000448979	Transmembrane protein, putative
TTHERM_00449070	Uncharacterized protein
TTHERM_00450990	Cyclin-dependent kinase-like Serine/Threonine kinase family protein
TTHERM_00296020	Transmembrane protein, putative
TTHERM_00294770	Serine/Threonine kinase domain protein
TTHERM_00293290	BRCT domain-containing protein
TTHERM_001365637	Kinase domain protein
TTHERM_00320000	Uncharacterized protein
TTHERM_00320020	ABC transporter C family protein
TTHERM_001398493	Kinase domain protein
TTHERM_01646010	Uncharacterized protein (Fragment)
TTHERM_01640980	Kinase domain protein (Fragment)
TTHERM_00094160	Alpha/beta superfamily hydrolase
TTHERM_000086966	Leishmanolysin family protein
TTHERM_00085030	Transmembrane protein, putative
TTHERM_00083590	Cation channel family protein
TTHERM_00083350	Uncharacterized protein
TTHERM_00355100	Dynein heavy chain
TTHERM_00355210	Transmembrane protein, putative
TTHERM_00355610	Transmembrane protein, putative
TTHERM_00355920	Chorein_N domain-containing protein
TTHERM_00357130	Transmembrane protein, putative
TTHERM_00357150	Zinc finger lsd1 subclass family protein
TTHERM_01137150	Uncharacterized protein
TTHERM_01052950	Uncharacterized protein

TTHERM_01053050	Eukaryotic aspartyl protease
TTHERM_00095610	Transmembrane protein, putative
TTHERM_00099960	Transmembrane protein, putative
TTHERM_000100047	Transmembrane protein, putative
TTHERM_00100080	Transmembrane protein, putative
TTHERM_00102640	Transmembrane protein, putative
TTHERM_000105389	Transmembrane protein, putative
TTHERM_00805860	Uncharacterized protein
TTHERM_00807930	AMP-binding enzyme family protein
TTHERM_00809200	Cation channel family protein
TTHERM_000809289	Cyclic nucleotide-binding domain protein
TTHERM_00809450	SLEI family protein
TTHERM_00393140	Uncharacterized protein
TTHERM_00783190	Uncharacterized protein
TTHERM_01321560	REJ domain protein
TTHERM_01321580	Adenosine/AMP deaminase family protein, putative
TTHERM_002653496	Transmembrane protein, putative
TTHERM_00834900	Kinase domain protein, putative
TTHERM_00835060	Zinc carboxypeptidase family protein
TTHERM_000835379	Cyclic nucleotide-binding domain protein
TTHERM_00835520	Transmembrane protein, putative
TTHERM_001423407	Transmembrane protein, putative
TTHERM_00592720	14-3-3 family epsilon domain protein
TTHERM_000598670	Transmembrane protein, putative
TTHERM_001356321	Kinase domain protein
TTHERM_01550950	Uncharacterized protein
TTHERM_01550970	von willebrand factor type A domain protein
TTHERM_000735291	Translation initiation factor eIF-5A family protein
TTHERM_001663099	Kinase domain protein

TTHERM_00142220	Transmembrane protein, putative
TTHERM_00706290	Cyclic nucleotide-binding domain protein
TTHERM_00706350	Cation channel family transporter
TTHERM_01481590	von willebrand factor type A domain protein
TTHERM_01481600	Kinase domain protein
TTHERM_01481610	Cyclic nucleotide-binding domain protein (Fragment)
TTHERM_000942629	Kinase domain protein
TTHERM_000577308	Transmembrane protein, putative
TTHERM_00577240	50S ribosomal protein L1P
TTHERM_00576640	Transmembrane protein, putative
TTHERM_000109280	Transmembrane protein, putative
TTHERM_000109324	Kinase domain protein
TTHERM_00115530	Zinc finger lsd1 subclass family protein
TTHERM_00115540	Zinc finger lsd1 subclass family protein
TTHERM_000123759	Kinase domain protein
TTHERM_00124050	Uncharacterized protein
TTHERM_00601850	Uncharacterized protein
TTHERM_00602900	Cell surface immobilization antigen
TTHERM_00602930	Cell surface immobilization antigen
TTHERM_00606950	Cell surface immobilization antigen
TTHERM_00606960	Cell surface immobilization antigen
TTHERM_00607140	Tyrosine kinase family protein
TTHERM_00610559	Two component regulator propeller family protein
TTHERM_000610559	Two component regulator propeller family protein
TTHERM_00613650	Uncharacterized protein
TTHERM_001482651	Kinase domain protein
TTHERM_01018270	Uncharacterized protein
TTHERM_01018400	Serine/Threonine kinase domain protein
TTHERM_01018480	Uncharacterized protein

TTHERM_01050420	Endo-1,4-beta-xylanase xylA, putative
TTHERM_001050449	Tetratricopeptide repeat protein
TTHERM_01050480	Tetratricopeptide repeat protein
TTHERM_00559710	Zinc finger, C3HC4 type (RING finger) protein
TTHERM_000559911	Transmembrane protein, putative
TTHERM_00561600	ABC transporter family protein
TTHERM_000562812	Uncharacterized protein
TTHERM_00633420	Uncharacterized protein
TTHERM_00635770	ABC transporter family protein
TTHERM_01332100	Uncharacterized protein
TTHERM_00974100	Regulator of chromosome condensation (RCC1) protein
TTHERM_00974150	DnaJ carboxy-terminal domain protein
TTHERM_001412048	Kinase domain protein
TTHERM_001412049	Cyclic nucleotide-binding domain protein
TTHERM_01217210	Plasma-membrane choline transporter
TTHERM_00161670	Cation channel family protein
TTHERM_000161279	EF-hand domain-containing protein
TTHERM_00161120	Transmembrane protein, putative
TTHERM_00158220	Uncharacterized protein
TTHERM_000157849	Transmembrane protein, putative
TTHERM_000155258	Transmembrane protein, putative
TTHERM_00372660	Transmembrane protein
TTHERM_01021950	Kinase domain protein, putative
TTHERM_01023060	Transmembrane protein, putative
TTHERM_01025120	PAS domain S-box protein
TTHERM_001026159	Cyclic nucleotide-binding domain protein (Fragment)
TTHERM_001026242	Uncharacterized protein
TTHERM_001563108	Uncharacterized protein
TTHERM_01564120	Kinase domain protein (Fragment)

TTHERM_01445950	Kinase domain protein
TTHERM_00550730	Protein phosphatase 2c
TTHERM_000550767	Cation channel family protein
TTHERM_00551040	Hydrocephalus-inducing protein
TTHERM_00551130	Uncharacterized protein
TTHERM_00551170	Transmembrane protein, putative
TTHERM_00551190	Transmembrane protein, putative
TTHERM_00554220	Transmembrane protein, putative
TTHERM_000259339	Uncharacterized protein
TTHERM_00259549	Sell domain protein
TTHERM_00259620	Uncharacterized protein
TTHERM_000259629	Uncharacterized protein
TTHERM_00260770	Serine/Threonine kinase domain protein
TTHERM_00263290	SF-assemblin/beta giardin family protein
TTHERM_00265190	Response regulator receiver domain protein
TTHERM_001504069	Kinase domain protein (Fragment)
TTHERM_01504070	Regulator of chromosome condensation (RCC1) protein, putative
TTHERM_01504080	Transmembrane protein, putative
TTHERM_01297410	Transmembrane protein, putative
TTHERM_01246730	Uncharacterized protein
TTHERM_000963272	Kinase domain protein
TTHERM_01204220	Transmembrane protein, putative
TTHERM_00162860	Uncharacterized protein
TTHERM_00170310	Tubulin-tyrosine ligase family protein
TTHERM_00170530	Transmembrane protein, putative
TTHERM_00171610	Kinase domain protein
TTHERM_00180930	Fibronectin-binding protein A, amine-terminal protein
TTHERM_00181110	Uncharacterized protein
TTHERM_000185509	Uncharacterized protein

TTHERM_00186030	Uncharacterized protein
TTHERM_00810450	Uncharacterized protein
TTHERM_00812920	Eukaryotic membrane protein (Cytomegalovirus gH-receptor) family protein, putative
TTHERM_00813030	Uncharacterized protein
TTHERM_01138320	Uncharacterized protein
TTHERM_001405859	Transmembrane protein, putative
TTHERM_00001310	Uncharacterized protein
TTHERM_00001370	Uncharacterized protein
TTHERM_000002618	Transmembrane protein, putative
TTHERM_00006270	WD domain, G-beta repeat protein
TTHERM_00008700	Cyclic nucleotide-binding domain protein
TTHERM_00011350	Transmembrane protein, putative
TTHERM_00011840	Chromosome condensation regulator RCC1 repeat protein
TTHERM_000011939	Transmembrane protein
TTHERM_00012990	Vacuolar sorting protein 9, VPS9 domain protein
TTHERM_00013610	Transmembrane protein, putative
TTHERM_000014929	Kinesin motor domain protein
TTHERM_00016050	Cleft lip and palate transmembrane protein
TTHERM_00016580	Uncharacterized protein
TTHERM_000019714	Oxalate/formate antiporter protein
TTHERM_00024050	Elongator complex protein 1
TTHERM_00024080	ABC transporter family protein
TTHERM_001577289	Transmembrane protein, putative (Fragment)
TTHERM_00538500	WD domain, G-beta repeat protein
TTHERM_00538520	Transmembrane protein, putative
TTHERM_000538595	WD domain, G-beta repeat protein
TTHERM_00538690	WD domain, G-beta repeat protein
TTHERM_000538712	Transmembrane protein, putative
TTHERM_00538850	SET domain protein

TTHERM_01558020	Kinase domain protein
TTHERM_01558040	Kinase domain protein, putative
TTHERM_01268140	Transmembrane protein, putative
TTHERM_001270201	Transmembrane protein, putative
TTHERM_00069530	Uncharacterized protein
TTHERM_00066870	Transmembrane protein, putative
TTHERM_00062690	Transmembrane protein, putative
TTHERM_00360330	Kinase domain protein
TTHERM_00361360	Kinase domain protein
TTHERM_00361380	Amidase
TTHERM_00361560	Kinase domain protein
TTHERM_00361640	Kinase domain protein
TTHERM_00361720	RNA 3'-terminal phosphate cyclase
TTHERM_00363150	Transmembrane protein, putative
TTHERM_00364290	Uncharacterized protein
TTHERM_00365370	IPT/TIG domain protein
TTHERM_00418470	EF-hand protein
TTHERM_00418030	Transmembrane protein, putative
TTHERM_000415819	Uncharacterized protein
TTHERM_00414340	Transmembrane protein, putative
TTHERM_000885891	Transmembrane protein, putative
TTHERM_00197780	Permease family protein
TTHERM_000197789	Kinase domain protein
TTHERM_00197820	Two component regulator propeller family protein
TTHERM_000198011	Kinase domain protein
TTHERM_00198130	Transmembrane protein, putative
TTHERM_000198489	Transmembrane protein, putative
TTHERM_00202830	Zinc finger, C3HC4 type (RING finger) protein
TTHERM_00202850	Transmembrane protein, putative

TTHERM_000213644	Kinase domain protein
TTHERM_001234350	Cyclic nucleotide-binding domain protein, putative
TTHERM_001236361	Uncharacterized protein
TTHERM_00699790	REJ domain protein
TTHERM_00701050	Right-handed beta helix region protein
TTHERM_00701200	Uncharacterized protein
TTHERM_00702270	Kinase domain protein (Fragment)
TTHERM_000866469	Kinase domain protein
TTHERM_000872599	Uncharacterized protein
TTHERM_00549590	Transmembrane protein, putative
TTHERM_00548050	Cyclic nucleotide-binding domain protein
TTHERM_01013200	Uncharacterized protein
TTHERM_01013280	Transmembrane protein, putative
TTHERM_001293243	Tetratricopeptide repeat protein
TTHERM_01058760	Uncharacterized protein
TTHERM_001060771	Kinase domain protein
TTHERM_01060790	Uncharacterized protein
TTHERM_02084560	Uncharacterized protein (Fragment)
TTHERM_002653511	Uncharacterized protein (Fragment)
TTHERM_01984390	Surface protein (Fragment)
TTHERM_02548190	Kinase domain protein (Fragment)

Table S4.16: Genes for which we observed changes in allele frequency associated with gradient-specific adaptation during range expansion. For each gene, we list the gene identifier (Gene ID), and the function associated with the gene.

S.4.13 Genes involved in adaptive evolution through *de novo* mutation.

To identify the functions of those genes in which *de novo* mutations preferentially occurred, we focused on mutations associated with general adaptations and mutations associated with gradient-specific adaptations.

We considered a *de novo* mutation as being associated with a general adaptation if it occurred in at least 75 % (12/16) of our evolved populations, independent of reproductive mode, gene flow, or the presence of a pH-gradient.

We considered a mutation to be associated with the presence or absence of a pH-gradient if it had a high prevalence in populations expanding into a pH-gradient and a low prevalence in populations expanding into a uniform environment, or vice versa. To identify such mutations, we first created a list with all genes with at least one *de novo* mutation in at least one evolved population. We then scored every evolved population and each of these genes for the presence of mutations. Specifically, for each gene we assigned a value of zero to a population if the gene harboured no mutations in this population, or a value of one if the gene harboured one or more mutations. We then summed these scores separately for the evolved populations expanding into a pH-gradient, and for the populations expanding into a uniform environment to obtain a prevalence of mutations for each class of populations. This prevalence can assume values between zero (no population harbours a mutation in the gene) and eight (all populations do). Finally, we calculated the absolute difference between these prevalences, to obtain a metric for the discrepancy in mutation prevalence between populations that had expanded into a pH-gradient, and populations that had expanded into a uniform environment. We then ranked genes by their difference in this prevalence, and focused on genes for which the absolute difference in prevalence was five or larger. These are genes in which mutations occurred in at least five more populations that had expanded into a pH-gradient than in populations that had expanded into a uniform environment, or vice versa. We discuss the biological functions of these high-discrepancy genes.

S.4.13.1 Analysis of *de novo* mutations: general adaptations

We found in total 66 genes for which we found mutations in at least 75 % of the evolved populations (12 or more out of 16 populations). Out of these 66 genes, 26 were genes coding for kinase domain proteins or protein kinases. Kinases proteins constitute a fairly large proportion (approximately 3.8 %) of the *T. thermophila* proteome (Eisen et al., 2006), yet this alone is not enough to explain the high proportion (39.4 %) of kinase proteins we found in this dataset. Although kinase domain proteins were clearly the most represented group in the dataset, we found three other gene functions for which there were common mutations. Specifically, we found common mutations in nine genes

coding for transmembrane proteins, five genes coding for cyclic nucleotide-binding domain proteins, and two genes coding for translation initiation factors (a full list of all common mutations can be found in Table S4.17).

	Gene ID	Populations	Gene function
1	TTHERM_001170561	16	Kinase domain protein
2	TTHERM_001234350	16	Cyclic nucleotide-binding domain protein, putative
3	TTHERM_001260714	16	Kinase domain protein
4	TTHERM_001360490	16	Kinase domain protein (Fragment)
5	TTHERM_00698620	16	Kinase domain protein
6	TTHERM_00954200	16	Chitobiosyldiphosphodolichol beta-mannosyltransferase
7	TTHERM_01156750	16	Kinase domain protein
8	TTHERM_000736509	15	Uncharacterized protein
9	TTHERM_000741704	15	Uncharacterized protein
10	TTHERM_000796721	15	Kinase domain protein
11	TTHERM_001051830	15	Kinase domain protein
12	TTHERM_001412049	15	Cyclic nucleotide-binding domain protein
13	TTHERM_01237380	15	Kinase domain protein, putative
14	TTHERM_01736560	15	Kinase domain protein (Fragment)
15	TTHERM_000359190	14	Kinase domain protein
16	TTHERM_000829471	14	Uncharacterized protein
17	TTHERM_001031291	14	Cyclic nucleotide-binding domain protein, putative
18	TTHERM_001055426	14	Kinase domain protein
19	TTHERM_001159975	14	Cyclic nucleotide-binding domain protein
20	TTHERM_001270201	14	Transmembrane protein, putative
21	TTHERM_00133420	14	Uncharacterized protein
22	TTHERM_001494742	14	Uncharacterized protein (Fragment)
23	TTHERM_00361430	14	Uncharacterized protein
24	TTHERM_00949690	14	Uncharacterized protein
25	TTHERM_01165250	14	Kinase domain protein
26	TTHERM_01393310	14	Translation initiation factor eIF-5A family protein

27	TTHERM_00011350	13	Transmembrane protein, putative
28	TTHERM_000213629	13	Kinase domain protein
29	TTHERM_00028650	13	C2 domain-containing protein
30	TTHERM_00047700	13	Ubiquitin carboxyl-terminal hydrolase
31	TTHERM_000630029	13	Kinase domain protein
32	TTHERM_000901705	13	Transmembrane protein, putative
33	TTHERM_000903901	13	Uncharacterized protein
34	TTHERM_000964361	13	Kinase domain protein
35	TTHERM_00102640	13	Transmembrane protein, putative
36	TTHERM_001257659	13	Kinase domain protein
37	TTHERM_001577290	13	Kinase domain protein (Fragment)
38	TTHERM_00309970	13	Ankyrin domain protein
39	TTHERM_00678280	13	Transmembrane protein, putative
40	TTHERM_00797960	13	Phospholipid-transporting ATPase (EC 7.6.2.1)
41	TTHERM_00927140	13	Uncharacterized protein
42	TTHERM_00951920	13	Chitinase-like protein cluster protein
43	TTHERM_00965380	13	Cyclic nucleotide-binding domain protein
44	TTHERM_00991600	13	Translation initiation factor eIF-5A family protein
45	TTHERM_01246690	13	Kinase domain protein
46	TTHERM_01491730	13	Kinase domain protein, putative
47	TTHERM_01504080	13	Transmembrane protein, putative
48	TTHERM_000220708	12	Protein kinase
49	TTHERM_000538595	12	WD domain, G-beta repeat protein
50	TTHERM_000891310	12	Uncharacterized protein
51	TTHERM_001054400	12	Uncharacterized protein (Fragment)
52	TTHERM_001412048	12	Kinase domain protein
53	TTHERM_00227700	12	Transmembrane protein, putative
54	TTHERM_00405390	12	Kinesin motor catalytic domain protein
55	TTHERM_00782120	12	Uncharacterized protein

57	TTHERM_01074590	12	Translation initiation factor eIF-5A family protein
58	TTHERM_01119420	12	Kinase domain protein
59	TTHERM_01211820	12	Kinase domain protein
60	TTHERM_01312370	12	Transmembrane protein, putative
61	TTHERM_01323720	12	Transmembrane protein, putative
62	TTHERM_01465220	12	Kinase domain protein
63	TTHERM_01496780	12	Serine/Threonine kinase domain protein (Fragment)
64	TTHERM_01500990	12	Transporter/monovalent cation: proton antiporter-1 (CPA1) family protein
65	TTHERM_01644000	12	Kinase domain protein

Table S4.17: Genes for which we observed mutations associated with general adaptation during range expansion, ordered by the number of populations for which we observed mutations in the specific gene. For each gene, we list the gene ID, the gene function associated with the gene and the number of populations in which we observed mutations in this specific gene.

384

S.4.13.2 Analysis of *de novo* mutations: gradient-specific adaptations

We found a total of 47 genes with large differences in the prevalence of mutations between populations expanding into a gradient and populations expanding into a uniform environment. Out of these 47 genes, genes coding for transmembrane proteins were most common (ten out of 47 genes; 21.28 %). Next most common were genes encoding kinase domains (eight out of 47 genes), genes encoding cyclic nucleotide binding proteins (two out of 47 genes) and genes encoding zinc finger proteins (two out of 47 genes). A full list of all gradient-specific mutations can be found in Table S4.18.

	Gene ID	Gene function	Gradient populations	Uniform populations	Absolute difference in prevalence
1	TTHERM_00782110	Transmembrane protein, putative	1	7	6
2	TTHERM_002141639	Transmembrane protein, putative	7	2	5
3	TTHERM_001147151	Uncharacterized protein	1	6	5
4	TTHERM_001230169	Uncharacterized protein	1	6	5
5	TTHERM_00554430	Uncharacterized protein	1	6	5
6	TTHERM_00673500	UvrD/REP helicase family protein	1	6	5
7	TTHERM_000782169	Uncharacterized protein	0	5	5
8	TTHERM_000951751	Uncharacterized protein	0	5	5
9	TTHERM_00129390	Cation channel family protein	5	0	5
10	TTHERM_001412048	Kinase domain protein	4	8	4
11	TTHERM_001117341	Uncharacterized protein	3	7	4
12	TTHERM_00912220	Transmembrane protein, putative	3	7	4
13	TTHERM_01050420	Endo-1,4-beta-xylanase xylA, putative	3	7	4
14	TTHERM_000019704	Cyclic nucleotide-binding domain protein	2	6	4
15	TTHERM_000252299	Uncharacterized protein	2	6	4
16	TTHERM_000956510	Tetrapolypeptide repeat protein	2	6	4
17	TTHERM_001250149	Transmembrane protein, putative	2	6	4

18	TTHERM_001537659	Transmembrane protein, putative (Fragment)	6	2	4
19	TTHERM_00263580	Cyclic nucleotide-binding domain protein	2	6	4
20	TTHERM_00734070	Transmembrane protein, putative	6	2	4
21	TTHERM_01256580	Zinc finger transcription factor sma protein, putative	2	6	4
22	TTHERM_001102662	Kinase domain protein	1	5	4
23	TTHERM_00122240	Uncharacterized protein	5	1	4
24	TTHERM_001318490	Kinase domain protein	5	1	4
25	TTHERM_001470377	Oxalate/formate antiporter protein	1	5	4
26	TTHERM_001542773	Uncharacterized protein (Fragment)	1	5	4
27	TTHERM_00158430	Serine/Threonine kinase domain protein	1	5	4
28	TTHERM_00187130	Phospholipase (EC 3.1.4.4)	5	1	4
29	TTHERM_00252280	Uncharacterized protein	1	5	4
30	TTHERM_00283350	Uncharacterized protein	1	5	4
31	TTHERM_00491190	Transmembrane protein, putative	1	5	4
32	TTHERM_00702240	Tubulin-tyrosine ligase family protein	5	1	4
33	TTHERM_01378930	Kinase domain protein	5	1	4
34	TTHERM_01445950	Kinase domain protein	5	1	4
35	TTHERM_01600640	REJ domain protein (Fragment)	1	5	4
36	TTHERM_000539021	Transmembrane protein, putative	0	4	4
37	TTHERM_00071100	WD domain, G-beta repeat protein	0	4	4
38	TTHERM_000860562	Transmembrane protein, putative	4	0	4
39	TTHERM_001222475	Uncharacterized protein	4	0	4
40	TTHERM_00129020	Transmembrane protein, putative	4	0	4
41	TTHERM_001318501	Kinase domain protein	0	4	4
42	TTHERM_00158480	Serine/Threonine kinase domain protein	4	0	4
43	TTHERM_00219430	Uncharacterized protein	0	4	4
44	TTHERM_002653371	Uncharacterized protein	0	4	4
45	TTHERM_00479090	Zinc finger, lsd1 subclass family protein	0	4	4
46	TTHERM_00954360	WW domain protein	4	0	4

47 | TTHERM_01546850 |

Uncharacterized protein

| 4 | 0 | 4

Table S4.18: Genes for which we observed mutations associated with gradient-specific adaptation during range expansion, ordered by the number of populations for which we observed mutations in the specific gene. For each gene, we list the gene identifier, the gene function associated with the gene, and the number of populations in which we observed mutations in this specific gene

S.4.14 Cochran-Mantel-Haenszel test

S.4.14.1 Pairing of populations

Comparison number	Population 1 (Gradient)	Population 2 (Uniform)	Gene flow	Reproduction
1	EVO4	EVO23	Present	Sexual
2	EVO5	EVO24	Present	Sexual
3	EVO8	EVO29	Present	Asexual
4	EVO9	EVO30	Present	Asexual
5	EVO11	EVO33	Absent	Sexual
6	EVO14	EVO35	Absent	Sexual
7	EVO18	EVO36	Absent	Asexual
8	EVO19	EVO39	Absent	Asexual

Table S4.19: All population comparisons used in the Cochran-Mantel-Haenszel test to identify differential selection in populations expanding into a uniform environment and populations expanding into a gradient.